DISS. ETH NO. 23987

Southern Ocean response
to recent changes in surface freshwater fluxes

A thesis submitted to attain the degree of

DOCTOR OF SCIENCES of ETH ZURICH

(Dr. sc. ETH Zurich)

presented by

F. ALEXANDER HAUMANN

M. Sc. in Physics and Climate Science, Universiteit Utrecht

born on May 28th, 1984

citizen of Germany

accepted on the recommendation of

Prof. Dr. Nicolas Gruber, examiner

Prof. Dr. Gerald H. Haug, co-examiner

Dr. Matthias Münnich, co-examiner

Prof. Dr. Michael P. Meredith, co-examiner

2016

Summary

Earth's climate bears a close relation to the vertical exchange of water masses in the global ocean. This relation originates from the transport of heat, carbon, and nutrients with the subduction and upwelling of water masses. The majority of this vertical exchange occurs in the Southern Ocean, where carbon- and nutrient-rich deep waters re-surface. To date, the mechanisms, which control long-term changes in this upwelling, are not firmly established. Both changes in either surface winds or surface freshwater fluxes could hypothetically alter the upwelling. Strong meridional gradients in the surface wind field propel a surface divergence that pulls waters from the deep. This process is facilitated by a marginally stable vertical density stratification, which is mainly set up by salinity and therefore by surface freshwater fluxes. So far, the exploration of stratification changes has been limited by the availability of observational freshwater flux data and by their poor representation in climate models. In this dissertation, I investigate recent changes in surface freshwater fluxes and their effect on the hydrography, circulation, as well as the vertical exchange of heat and carbon in the Southern Ocean. A particular focus of this thesis is on yet unconstrained freshwater fluxes which originate from the seasonal formation and melting of sea ice.

In the first part of this thesis, I provide the first comprehensive data set of annual freshwater fluxes arising from the formation, transport, and melting of sea ice in the Southern Ocean over the time period from 1982 to 2008. For this purpose, I combine numerous satellite, in-situ, and reanalysis data of sea-ice concentration, thickness, and drift. The resulting freshwater flux estimates reveal that 410 ± 110 mSv (1 mSv $= 10^3$ m^3 s^{-1}) of freshwater are removed and added to the surface waters by the formation and melting of sea ice each year. Compared to the available data of the atmospheric and land-ice freshwater fluxes, sea ice provides the dominant freshwater flux in the seasonally ice-covered region of the Southern Ocean. Most of the sea ice forms in the coastal ocean; and 130 ± 30 mSv of this sea ice are transported towards the sea-ice edge, where it melts. Thereby, it increases the salinity in coastal and bottom waters and lowers the open-ocean surface and intermediate water salinity. This northward transport of freshwater has increased by $20\pm10\%$ over the observational period, which corresponds to a freshening of -0.02 ± 0.01 g kg^{-1} per decade in the open-ocean waters. From this analysis, I conclude that the increased northward transport of freshwater by sea ice explains the majority of the observed freshening of the open-ocean waters. In fact, ocean salinity data shows that the largest freshening signal coincides with the region of largest increased sea-ice melting in the Pacific sector.

In order to better understand the ocean's response to changing freshwater fluxes, I am using the newly derived sea-ice–ocean freshwater fluxes to constrain a regional ocean circulation model in the second part of this thesis. By perturbing the model with the observed recent changes in these fluxes, I find that the increased northward sea-ice transport could also be responsible for most of the observed surface cooling in the Southern Ocean that occurred over recent decades, despite global warming. The model simulations suggest that this cooling originates from a freshening and enhanced surface density stratification in the upwelling region that delays and shoals the deep winter-time mixing. As a consequence, the total heat capacity of the mixed layer decreases and less warm deep water enters the surface layer, which results in a surface cooling and sub-surface warming. Moreover, about 25% less carbon-dioxide (CO_2) is released to the atmosphere from the upwelling region. This response can be explained, on the one hand, by the surface cooling that increases the solubility of CO_2 in seawater and, on the other hand, by reduction in upwelling. The reduced CO_2 release is opposed by a reduced subduction of CO_2 into Antarctic Intermediate Water and Subantarctic Mode Water due to the increasing stratification. These findings suggest that the increased surface density stratification could explain why the Southern Ocean carbon sink has not saturated but has rather strengthened over recent decades, despite increasing surface winds.

In conclusion, the insights gained from my dissertation point towards much higher sensitivity of the upwelling in the Southern Ocean to changes in the sea-ice freshwater fluxes than previously assumed. My combined analyses of observational data and model experiments elucidate that sea ice effectively re-shovels freshwater from the lower overturning cell to the upper overturning cell and thereby increases the meridional and vertical salinity and density gradients in the Southern Ocean. In the long-term, changes in this system could alter the atmospheric CO_2 concentration and therefore the global climate. A potential warming of the sea-ice region in the future could reverse the changes observed over recent decades and enhance the release of CO_2 from the ocean to the atmosphere, which might amplify global warming. In contrast, in colder glacial climates, increased sea-ice formation could reduce the upwelling of carbon-rich waters to the surface ocean and lower the atmospheric CO_2 concentrations. This interpretation of my results is in line with the hypothesis that past glacial–interglacial variations in the global atmospheric CO_2 concentration could originate from changes in the Southern Ocean density stratification.

Zusammenfassung

Der vertikale Austausch von Wassermassen im globalen Ozean hat einen grossen Einfluss auf das Klima der Erde, da das Absinken und Aufsteigen der Wassermassen Wärme, Kohlenstoff und Nährstoffe zwischen dem tiefen und oberflächennahen Ozean umverteilt. Diese Umverteilung findet vorwiegend im Südpolarmeer statt, wo kohlenstoff- und nährstoffhaltiges Tiefenwasser an die Oberfläche kommt. Bis heute sind die Ursachen von längerfristigen Veränderungen dieses Auftriebs noch nicht fest etabliert. Diese könnten entweder von Veränderungen der oberflächennahen Winde oder des Süsswassereintrags hervorgerufen werden. Starke meridionale Gradienten in den Winden treiben das Oberflächenwasser in dieser Region auseinander und sorgen für den Auftrieb des Wassers aus der Tiefe. Dieser Prozess wird durch eine nur geringfügig stabile Dichteschichtung der Wassersäule erleichtert, welche über den Salzgehalt des Wassers und somit durch den Süsswassereintrag bestimmt wird. Die Erforschung von Veränderungen in der Dichteschichtung wurde bis jetzt weitgehend von einem Mangel an Beobachtungsdaten von Süsswasserflüssen und deren Unsicherheiten in Simulationen mit Klimamodellen eingeschränkt. In dieser Doktorarbeit untersuche ich kürzliche Veränderungen im Süsswassereintrag und deren Einfluss auf die Hydrographie, die Zirkulation und den vertikalen Austausch von Kohlenstoff und Wärme im Südpolarmeer. Dabei ist der weitgehend unbestimmte Beitrag von Süsswasserflüssen des sich jahreszeitlich bildenden und abschmelzenden Meereises ein zentrales Thema.

Der erste Teil dieser Arbeit beschreibt den ersten umfassenden Datensatz von jährlichen Süsswasserflüssen, die durch die Bildung, den Transport und das Abschmelzen von Meereis zwischen 1982 und 2008 entstanden sind. Dieser beruht auf verschiedene Satellitenmessungen, bodennahe Beobachtungen und Reanalysedaten von Meereiskonzentration, -dicke und -drift. Die daraus resultierenden Abschätzungen zeigen auf, dass jährlich 410 ± 110 mSv (1 mSv $= 10^3$ m^3 s^{-1}) Süsswasser durch das Bilden und Abschmelzen von Meereis dem Oberflächenozean entzogen und wieder hinzugefügt werden. Im Vergleich zum Süsswassereintrag aus der Atmosphäre oder vom Landeis der Antarktis, formt Meereis somit die Hauptkomponente der Süsswasserflussbilanz in der Meereisregion. Das meiste Meereis bildet sich in Küstennähe, wovon 130 ± 30 mSv zur Meereiskante nach Norden transportiert werden, wo das Eis abschmilzt, dabei erhöht es den Salzgehalt des küstennahen Ozeans und des sich dort bildenden Bodenwassers und reduziert den Salzgehalt des Oberflächen- und Zwischenwassers im offenen Ozean. Dieser Nordwärtstransport von Meereis hat über den Beobachtungszeitraum um $20\pm10\%$ zugenommen, was einer Reduk-

tion des Salzgehaltes im offenen Ozean um -0.02 ± 0.01 g kg^{-1} pro Dekade entspricht. Aus dieser Analyse ziehe ich die Schlussfolgerung, dass sich durch den erhöhten Nordwärtstransport von Süsswasser durch das Meereis der grösste Teil der beobachteten Salzgehaltsabnahme im offenen Ozean erklären lässt, welche im Pazifischen Teil des Südpolarmeeres am stärksten ist, wo auch die grösste Zunahme im Süsswassereintrag durch das Meereis stattgefunden hat.

Um die Reaktion des Ozeans auf Veränderungen im Süsswassereintrag vom Meereis zu untersuchen, verwende ich im zweiten Teil meiner Doktorarbeit den neuen Datensatz um ein regionales Ozeanzirkulationsmodell anzutreiben. Eine Veränderung der Meereissüsswasserflüsse im Modell um den beobachteten Wert zeigt, dass die Zunahme im Nordwärtstransport vom Meereis auch für eine Abkühlung des Oberflächenwassers in die vergangenen Jahrzehnte verantwortlich sein könnte, die in dieser Region trotz der globalen Erwärmung festgestellt wurde. Die Abkühlung in der Modellsimulation ist die Folge einer verstärkten Dichteschichtung in der Auftriebsregion, welche die tiefe Mischung der Wassermassen in den Wintermonaten zeitlich verzögert und abflacht. Daraus resultiert eine veringerte Wärmekapazität der gemischten Schicht und ein verringertes Eindringen von Wärme in die oberen Schichten, was eine oberflächennahe Abkühlung und eine Erwärmung unterhalb der Oberfläche zur Folge hat. Zusätzlich nimmt die Freisetzung von Kohlenstoffdioxid (CO_2) in die Atmosphäre in der Auftriebsregion um ungefähr 25% ab. Diese Abnahme kann zum einen durch die verstärkte Löslichkeit von CO_2 im kühleren Oberflächenwasser und zum anderen durch einen geringeren Auftrieb erklärt werden. Diesem Prozess wirkt eine verringerte Aufnahme von CO_2 mit dem Antarktischen und Subantarktischen Zwischenwasser durch die verstärkte Dichteschichtung entgegen. Diese Erkenntnisse zeigen auf, dass eine verstärkte Dichteschichtung erklären könnte, wieso trotz einer Zunahme der Westwinde über die letzten Jahrzehnte keine Sättigung, sondern eher eine Verstärkung der CO_2-Aufnahme des Südpolarmeeres in Beobachtungsdaten zu erkennen ist.

Abschliessend lässt sich die Erkenntnis ableiten, dass der Tiefenwasserauftrieb im Südpolarmeer wesentlich stärker auf Süsswasserflussveränderungen vom Meereis reagiert als zuvor angenommen. Die Analysen von Beobachtungsdaten und Modellexperimenten veranschaulichen, dass Meereis Süsswasser von der unteren in die obere Ozeanzirkulationszelle umverteilt und dabei die meridionalen und vertikalen Salz- und Dichtegradienten im Ozean verstärkt. Auf längeren Zeitskalen könnten Veränderungen in diesem System den atmosphärischen CO_2-Gehalt und somit das globale Klima beeinflussen. Eine mögliche zukünftige Erwärmung der Meereisregion hätte eine Umkehr der hier beschriebenen Veränderungen zur Folge, was zu einer verstärkten Freisetzung von CO_2 in die Atmosphäre und einer Verstärkung der globalen Klimaerwärmung führen könnte. Im Gegensatz dazu könnte eine erhöhte Meereisbildung während Eiszeiten den Auftrieb von kohlenstoffhaltigem Tiefenwasser an die Oberfläche reduziert und somit zu einer tieferen CO_2-Konzentration in der Atmosphäre geführt haben. Diese Interpretation meiner Resultate stimmt mit der Hypothese überein, dass die Schwankungen der globalen atmosphärischen CO_2-Konzentration zwischen Eiszeiten und Warmzeiten durch Veränderungen in der Dichteschichtung des Südpolarmeeres bedingt werden.

Contents

Chapter 1

Introduction

In 1984, three pioneering studies (Knox and McElroy, 1984; Sarmiento and Toggweiler, 1984; Siegenthaler and Wenk, 1984) suggested that the polar oceans have played the most critical role for regulating carbon dioxide (CO_2) concentrations in the Earth's atmosphere over the past thousands of years, prior to any human influence. Ever since, the climate research community has built overwhelming evidence that this connection between the atmospheric CO_2 concentrations and polar oceans stems from the Southern Ocean (Toggweiler, 1999; Sigman et al., 2010). The rationale behind this hypothesis is that this region acts as the major pathway for deep ocean waters to rise to the surface (Talley, 2013), fueling the surface ocean with large amounts of dissolved carbon and nutrients (Marinov et al., 2006). These upwelled waters provide a natural source of CO_2 to the atmosphere (Gruber et al., 2009) and nutrients for the global marine biological production (Sarmiento et al., 2004). However, it is not just this upwelling of deep waters in this region that is important for the climate system, but also the subduction of newly formed water masses that ventilate most of the interior ocean (Ganachaud and Wunsch, 2000; DeVries and Primeau, 2011). This subduction process buffers perturbations that occur in the surface climate, such as human-induced climate change (IPCC, 2013), by taking up anthropogenic CO_2 (Sarmiento et al., 1998; Caldeira and Duffy, 2000; Sabine et al., 2004; Gruber et al., 2009) and heat (Gille, 2002; Levitus et al., 2012; Purkey and Johnson, 2013; Frölicher et al., 2015; Morrison et al., 2015) from the atmosphere. Due to these profound influences on the global carbon cycle and the surface energy balance, the upwelling and subduction of waters in the Southern Ocean are thought to be key elements to understand past, current, and future changes of the global climate.

In this chapter, I will describe the link between changes in the global carbon cycle and Earth's surface climate (section 1.1), followed by a discussion of the role of ocean circulation in altering both the carbon cycle and the surface energy balance (section 1.2). Then, I will describe why the ocean circulation and density stratification in the Southern Ocean might be critically linked to surface freshwater fluxes (section 1.3) and why this system might be very sensitive to changes in global climate (section 1.4). Finally, I will formulate my objectives (section 1.5), and outline the chapters of this thesis (section 1.6).

1.1 Atmospheric carbon dioxide & the global surface climate

The Earth's surface temperature is tightly coupled to the atmospheric CO_2 concentration (Pierre-humbert, 2011). This relation stems from the absorption of long-wave radiation by atmospheric CO_2, which is the second most important greenhouse gas—next to atmospheric water vapor. Using Stefan-Boltzmann's law for a black body, one finds that the natural atmospheric greenhouse effect rises the Earth's mean surface temperature by roughly $33°$ C and that roughly one third of this effect can be attributed to atmospheric CO_2 (Sarmiento and Gruber, 2006), making the Earth a habitable planet. Therefore, the anthropogenic perturbation and natural variations of the atmospheric CO_2 concentration can strongly alter the global surface climate, as I will briefly describe in this section.

1.1.1 Anthropogenic perturbation

Through fossil fuel burning and land-use change, human activity has increased the atmospheric CO_2 concentrations since pre-industrial times (Figure 1.1) to a current mean level of about 403 ppm (June, 2016, after removing the seasonal cycle; http://www.esrl.noaa.gov/gmd/ccgg/trends/global.html). Small air bubbles trapped in the East-Antarctic ice sheet show that such high atmospheric CO_2 concentrations have not occurred over at least the last 800,000 years (EPICA
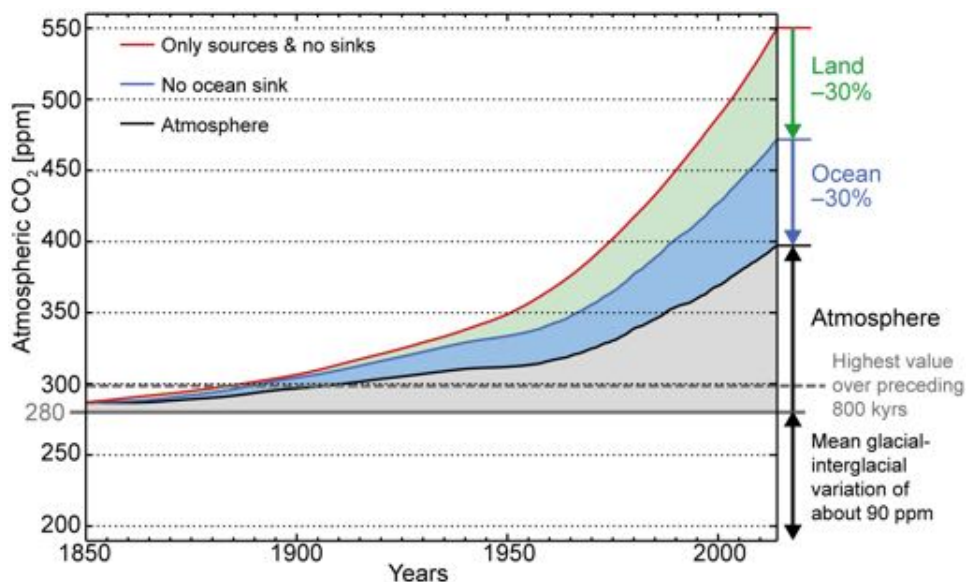
Figure 1.1   Changes in the global carbon cycle 1850–2014: The black curve shows the increase in atmospheric CO_2 concentration. The colored curves show the atmospheric CO_2 concentration equivalent if there were only anthropogenic sources but no sinks (red) and if there was no ocean sink (blue). The land sink is indicated in light green and the ocean sink in light blue shading. The land sink is computed from the residual after subtracting the ocean and atmosphere from the total emissions. Data stems from the Global Carbon Budget (Le Quéré et al., 2015) and from the observed atmospheric CO_2 concentration after 1980 (Dlugokencky & Tans, NOAA/ESRL, www.esrl.noaa.gov/gmd/ccgg/trends, Ballantyne et al., 2012).

community members et al., 2004; IPCC, 2013). The current atmospheric CO_2 concentration is about 44% higher compared to the pre-industrial level (about 280 ppm, Figure 1.1) and this increase led to an increase of the radiative forcing, dominating the observed temperature rise of about 0.85° C over the past 130 years (Hansen et al., 2010; IPCC, 2013). Earth System Models (ESMs) suggest that even if anthropogenic atmospheric CO_2 emissions would stall, warming could continue over centuries (Frölicher et al., 2014). However, the atmospheric growth rate of CO_2 has been accelerating over recent decades, reaching an average growth of about 2.1 ppm per year over the past decade (Le Quéré et al., 2015).

Figure 1.2a illustrates that the actual anthropogenic emissions of CO_2 are considerably larger than the growth rate of atmospheric CO_2. In fact, the anthropogenic emissions of about 10 Pg of carbon per year over the last decade (Le Quéré et al., 2015) have been stronger than any reconstructed natural carbon release rate to the atmosphere over the past 66 million years (Figure 1.2a;
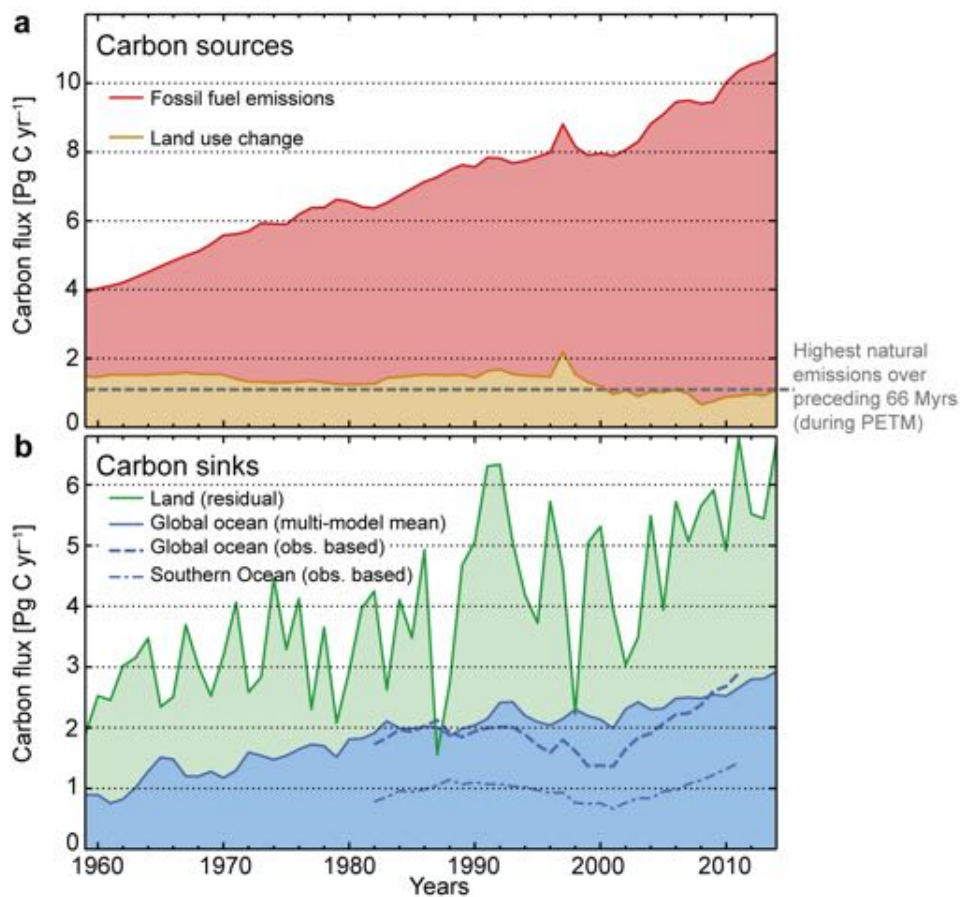
Figure 1.2 Sources and sinks of anthropogenic carbon 1959–2014: (a) Anthropogenic carbon emissions from fossil fuel burning (red) and land use change (orange) from the global carbon budget (Le Quéré et al., 2015). The estimate of the natural emissions during the Palaeocene-Eocene Thermal Maximum is given as a comparison (PETM; Zeebe et al., 2016). **(b)** Land (green; residual) and ocean sinks (blue; multi-model mean) for anthropogenic carbon from the Global Carbon Budget (Le Quéré et al., 2015). The dased line shows an observation based estimate from Landschützer et al. (2015a) for the global ocean sink (corrected as described by Landschützer et al. (2014b) to obtain the anthropogenic contribution) and the dash-dotted line the Southern Ocean sink (Landschützer et al., 2015b, scaled according to the global correction).

Zeebe et al., 2016). The current release rate is about one order of magnitude higher than estimates for the Palaeocene-Eocene Thermal Maximum (PETM; Zeebe et al., 2016)—a strong warming period which is often compared to the current global warming (Zachos et al., 2001). Thus, the anthropogenic perturbation forces the Earth's carbon cycle into unprecedented rapid changes. The carbon cycle responds with a rapid increase of the uptake of carbon by the land and the ocean, which took up about 60% of the emitted carbon between 1850 and 2014 (Figure 1.1; Sabine et al., 2004; Le Quéré et al., 2015). Without these sinks, the atmospheric CO_2 concentration would have reached 550 ppm in 2014 (Figure 1.1).

About 30% of the anthropogenic emission since pre-industrial times were taken up by the ocean, and another 30% by the land (Figure 1.1; Sabine et al., 2004; Le Quéré et al., 2015). Both the strength of the anthropogenic sources as well as the overall strength of the sinks have been gradually increasing (Figure 1.2; Khatiwala et al., 2009). However, in contrast to the anthropogenic sources, the sinks reveal large variability over time with periods of stronger and weaker uptake (Le Quéré et al., 2009). These variations result from variations in the surface climate. In particular, the land sink undergoes large interannual variability, which is largely driven by El Niño Southern Oscillation (ENSO; Zeng et al., 2005). The multi-model mean of the ocean sink from the Global Carbon Budget (Le Quéré et al., 2015) exhibits much less variability. However, new observationally constrained estimates show that also the ocean sink undergoes large variability on decadal time scales (Landschützer et al., 2015b,a), especially in the Southern Ocean (Figure 1.2b), which dominates the overall global uptake of anthropogenic CO_2 from the atmosphere (see section 1.3; see also Mikaloff Fletcher et al., 2006; Gruber et al., 2009; Khatiwala et al., 2009). Thus, variations in the global surface climate can alter the rate at which anthropogenic CO_2 is taken up by the ocean and land.

Global models suggest that in the long-term the link between climatic changes and the global carbon cycle induces a positive feedback, which accelerates the projected global warming over the 21st century and beyond (Cox et al., 2000; Friedlingstein et al., 2001, 2006). This feedback is induced by a reduction of the efficiency at which both the land and the ocean take up anthropogenic CO_2 as the climate is warming. In particular, the projected future uptake of anthropogenic carbon by the land decreases; eventually turning the land into a carbon source (Cao and Woodward, 1998; Stocker et al., 2013). This change in the land sink results in the ocean becoming the dominant sink in the long-term (Cox et al., 2000; Randerson et al., 2015). However, the ocean sink will probably also weaken over time, which is mostly a result of positive feedbacks from ocean acidification, surface ocean warming, and changes in mixing and transport (see section 1.2; Manabe and Stouffer, 1993; Sarmiento et al., 1995; Sarmiento and Le Quéré, 1996; Sarmiento et al., 1998; Joos et al., 1999; Gruber, 2011; Stocker, 2015). These feedbacks between the carbon sinks and global climate have been identified as a key challenge in climate research in order to understand the dissipation of anthropogenic carbon perturbations in the climate system and to make reliable estimates of future climatic changes (IPCC, 2013; Ilyina and Friedlingstein, 2016).

1.1.2 Natural fluctuations

While the above considerations are concerned with the addition of anthropogenic CO_2 to the atmosphere that drives an increase of the global surface temperature, Earth's history shows that, conversely, variations in surface temperature can also drive changes in the atmospheric CO_2 concentration. This relation becomes evident from synchronously varying atmospheric CO_2 (EPICA community members et al., 2004; Lüthi et al., 2008) and Antarctic surface temperatures over the last glacial cycles (Figure 1.3; Petit et al., 1999; EPICA community members et al., 2004; Jouzel et al., 2007; Parrenin et al., 2013). The coincidence of these variations with the Earth's orbital eccentricity suggests that the solar radiation received by the Earth surface paces these variations (Hays et al., 1976), even though this causal link has been debated (Saltzman et al., 1984; Wunsch and Ferrari, 2004; Huybers and Wunsch, 2005). In any case, changes in direct solar forcing would be largely insufficient to change the surface temperature by the reconstructed amplitude (Imbrie et al., 1993). Thus, most of the observed amplitude must result from internal feedbacks in the climate system (Köhler et al., 2010).
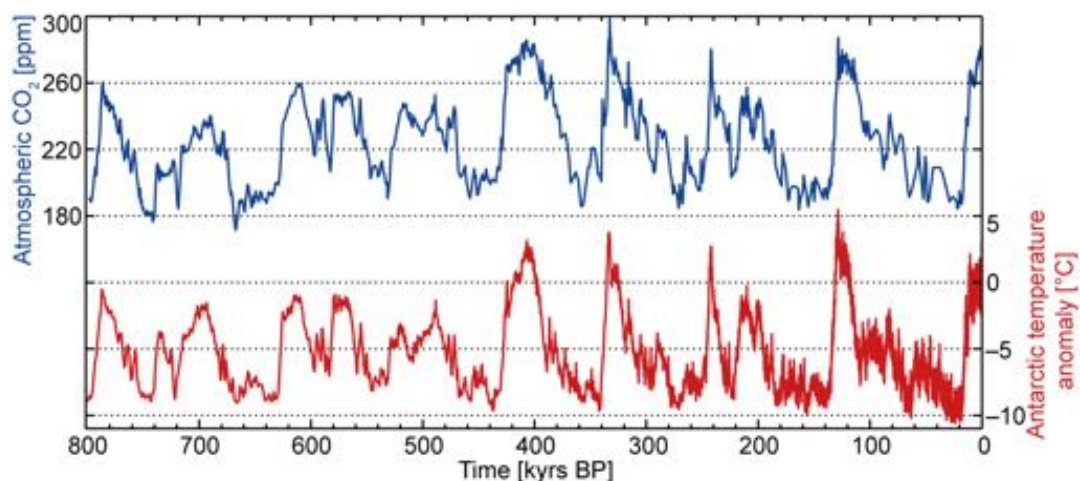
Figure 1.3 Glacial-interglacial variations of atmospheric CO_2 and temperature: The blue line shows the variations of atmospheric CO_2 over the past 800,000 years as measured in Antarctic ice cores (EPICA community members et al., 2004; Lüthi et al., 2008). The red line shows the Antarctic surface temperature anomalies with respect to the past 1,000 years that were inferred from deuterium in the ice cores (Petit et al., 1999; EPICA community members et al., 2004; Jouzel et al., 2007; Parrenin et al., 2013).

For a long time the theory prevailed that these changes are associated with the growth and decay of the northern hemisphere ice sheets that would lead, among other changes, to large changes in the surface albedo (Imbrie and Imbrie, 1980; Oerlemans, 1980; Abe-Ouchi et al., 2013). Shackleton (2000) challenged this perspective, arguing that the proxy for ice sheet volume, which is derived from the oxygen isotopic composition ($\delta^{18}O$) of deep-sea sediments and ice cores, lags the proxies for the Antarctic surface temperatures, as well as the atmospheric CO_2 concentration and orbital eccentricity. As the latter three quantities appear to be in phase, he concludes that the amplitude of the glacial-interglacial variations could be explained by carbon-cycle feedbacks

rather than northern hemisphere ice-sheet feedbacks. A more recent compilation of surface temperature proxies (Shakun et al., 2012) supports such a theory, because it shows that the global mean temperature lags both atmospheric CO_2 and Antarctic surface temperatures during the last deglaciation. This suggests a southern-hemisphere driven change in the carbon cycle as a predominant cause for the deglaciation. Yet, large uncertainties exist in both the magnitude and timing of all these proxy data sets, exacerbating arguments related to the phasing and location of these changes.

Results with a simplified model by Berger et al. (1993) suggest that a change in atmospheric CO_2 of 80 to 100 ppm during the last four glacial cycles (Figures 1.1 and 1.3; Petit et al., 1999) can only explain about one third of the temperature variation, when indirect effects such as the associated water vapor feedback are included. Current state-of-the-art ESMs suggest that this small response is probably an underestimation of the warming resulting from the CO_2 increase. Using the estimated long-term climate feedback parameter from these model simulations of about $0.8 \, \mathrm{W \, m^{-2} \, K^{-1}}$ (Andrews et al., 2015), the equilibrium temperature change resulting from glacial-interglacial CO_2 variations and related indirect effects would be about $2.5°$ C. Such a simplified consideration thus suggests that more than half of the last deglacial global mean temperature rise (about $3.5°$ C; Shakun et al., 2012) could be related to the atmospheric CO_2 rise. However, the climate feedback parameter varies widely among different models and long-term responses from ice sheets are not included in these ESMs, leading to no conclusive answer on whether a southern hemisphere carbon-cycle feedback or a northern hemisphere ice-sheet feedback would trigger deglaciations.

Despite these contrasting views on the causes for the global temperature changes during glacial-interglacial changes, the ice core records clearly reveal that a warming of the climate system during deglaciations leads to a natural rise of atmospheric CO_2, with strong positive feedbacks in the global climate system that amplified the global warming. This lesson from Earth's history leads to concerns that the anthropogenic induced climate change might be considerably amplified over many centuries not only due to the anthropogenic perturbation itself, as outlined in section 1.1.1, but also due to positive feedbacks with the natural carbon cycle. Consequently, it is an urgent matter to understand why the atmospheric CO_2 has been increasing at all during deglaciations in order to better understand the response of the natural carbon cycle to future changes in the surface temperature.

1.2   The importance of ocean circulation for global climate: A Southern Ocean perspective

The ocean circulation redistributes heat, carbon, and nutrients between low and high latitudes and between the surface and the deep ocean. Thereby, it regulates the regional and global surface climate. In this section, I will briefly discuss the influence of this circulation on the global carbon cycle and the surface energy balance from a perspective of both a natural system and the anthropogenic perturbation of this system. This discussion will elucidate the critical role played by the Southern Ocean in the climate system.

1.2.1   Global overturning circulation

The circulation of ocean waters on a global scale is driven by a modification of the seawater density through surface heat and freshwater fluxes as well as by surface winds. The densest and deepest waters of the global ocean are formed in high-latitudes, where a strong loss of buoyancy occurs; namely in the north Atlantic (North Atlantic Deep Water, NADW) and around the coast of the Antarctic continent (Antarctic Bottom Water, AABW). These water masses sink to the abyssal ocean and spread to lower latitudes. They are then brought back towards surface by upwelling in the Southern Ocean (Toggweiler and Samuels, 1995; Gnanadesikan, 1999; Marshall and Speer, 2012; Morrison et al., 2015) and vertical mixing in low latitudes (Munk, 1966; Munk and Wunsch, 1998; Ganachaud and Wunsch, 2000; Wunsch and Ferrari, 2004). A second major type of sub-surface water masses, namely Antarctic Intermediate Water (AAIW) and Subantarctic Mode Water (SAMW), is subducted to intermediate depth in sub-polar regions of the Southern Ocean, ventilating the global low-latitude thermocline. All these deep, intermediate, and surface waters are intertwined (Schmitz, 1995, 1996; Talley, 2013) to constitute a global-scale overturning circulation (Gordon, 1986a,b; Broecker, 1987, 1991; Lumpkin and Speer, 2007).

The dominant role of the Southern Ocean in this circulation manifests itself in the fraction of global water masses that is ventilated through the Southern Ocean. Up to 80% of subducted NADW and AABW re-surface through transport and mixing in the Southern Ocean (Talley, 2013). Watson et al. (2013) argue that roughly 20 to 30% of this upwelling is caused by cross-density (diapycnal) mixing and the remainder through isopycnal mixing and transport. However, not only the upwelling is dominated by the Southern Ocean, but also around 65% of global sub-surface waters originate from the surface waters of this region through the subduction of AABW, AAIW, and SAMW (DeVries and Primeau, 2011).

The return time scale for water parcels participating in the global overturning circulation is on the order of 1,000 years (Broecker and Peng, 1982). This time scale is largely governed by slow, counter-gradient, upward mixing of bottom waters in deep northern Pacific (Munk, 1966).

However, the time scales at which the global overturning circulation interacts with global climate is much shorter (Weaver et al., 1991; Delworth et al., 1993; Ganopolski and Rahmstorf, 2001; Cunningham et al., 2007; Park and Latif, 2008). This shorter time scale is owing to relatively faster variations in some upwelling and subduction processes, which are on the order of years to several decades for NADW (Weaver et al., 1991; Delworth et al., 1993; Cunningham et al., 2007) and AAIW/SAMW (Santoso and England, 2004; Naveira Garabato et al., 2009; Sallée et al., 2010a; Kwon, 2013) and possibly even centuries in the high-latitude Southern Ocean (incl. AABW formation; Latif et al., 2013; Martin et al., 2013). On these time scales the interaction of overturning circulation with the surface climate occurs through the meridional and vertical advection of heat, salt, and carbon and through related changes in the air-sea fluxes.

As the subduction of water masses in both hemispheres occurs on time scales equivalent to the anthropogenic perturbation, concerns have been raised that the upwelling and subduction in the higher latitudes might change in future (Stocker and Schmittner, 1997; Toggweiler and Russell, 2008; Meredith et al., 2012; Waugh, 2014), potentially altering the ability of the ocean to take up anthropogenic carbon and excess heat (Manabe and Stouffer, 1993; Sarmiento et al., 1998; Stocker, 2015). A major difference that exists between the subduction of water masses in the northern and southern hemisphere is that water masses subducted in the northern hemisphere stem from the surface waters of the low latitudes, whereas those subducted in the Southern Ocean have been upwelled from the deep ocean. Thus, the waters that are subducted in the Southern Ocean have not yet seen the anthropogenic perturbation and have a much larger potential to buffer this perturbation. The rate at which this buffering of variations in the surface climate by the Southern Ocean waters occurs depends on the rate of upwelling and subduction or the surface residence time of these waters (see section 1.3).

1.2.2   Ocean carbon pumps

The ocean contains 60 times more carbon than the atmosphere and most of this carbon is stored in the form of dissolved inorganic carbon (DIC) in the deep ocean (Sarmiento and Gruber, 2006). At the surface the concentration of DIC is about 15% lower than in the deep ocean. This gradient comes about mostly due to gravitational sinking of biologically produced matter out of the sunlit, euphotic layer (upper about 100 m) into deeper layers—a process referred to as export production. As illustrated in Figure 1.4 (following Heinze et al., 1991; IPCC, 2013), this biological pump can be split into processes associated with the export of particulate organic carbon (POC), the soft-tissue pump, and the export of biogenic calcium carbonate ($CaCO_3$), the carbonate or hard-tissue pump.

The soft-tissue pump is the major biological process that is responsible for the surface to the deep ocean gradient in DIC (Sarmiento and Gruber, 2006). It is driven by the formation of organic matter through photosynthesis by marine phytoplankton. During this process the phytoplankton

takes up dissolved carbon and nutrients from the seawater to build organic matter. The net biological uptake of CO_2 resulting from production and respiration by phytoplankton is referred to as net primary production (NPP). The total amount of NPP is limited by the availability of light and nutrients. Some phytoplankton and zooplankton species form calcareous shells that consist of mineral $CaCO_3$. Thereby they do not only extract DIC from the seawater but also lower the seawater alkalinity (Alk). The latter is defined through the excess of bases over acids. A lower Alk leads to a release of CO_2 to the atmosphere. Consequently, while the soft-tissue pump leads to a net uptake of CO_2 from the atmosphere, the carbonate pump leads to a net release to the atmosphere (Figure 1.4) .

The organic detritus that sinks out of the surface layer is to a large extent remineralized by heterotrophic organisms at intermediate depth (Figure 1.4). Only a small fraction of the NPP sinks further into the deep ocean (Suess, 1980). Kwon et al. (2009) argue that the depth at which the bulk of the organic carbon is remineralized, the remineralization depth, significantly influences the atmospheric CO_2 levels, underpinning the importance of this sinking processes. The line of thought behind this relation is that the deeper the carbon sinks into the ocean, the longer is its return period to the surface (Primeau, 2005). If we consider an extreme condition where no carbon is exported to depth, i.e., in absence of a vertical DIC gradient, simplified model experiments show that the atmospheric CO_2 concentration could be roughly 150 ppm higher (Gruber and Sarmiento, 2002). Even though this case is unrealistically extreme, it demonstrates that a change in the vertical gradient could substantially alter the atmospheric CO_2 levels. The carbonate pump also leads to vertical DIC gradients, but plays a secondary role. One key difference of this mechanism to the soft-tissue pump is that $CaCO_3$ is dissolved much deeper in the water column and that a much larger fraction is buried in the sediment as compared to the particulate organic carbon. Thus, it becomes an important process on time scales longer than a few hundred years (Broecker, 1987; Sarmiento et al., 1988; Archer et al., 2000; Sigman and Boyle, 2000).

The major physical processes in the ocean that influence the carbon cycle are vertical transport and mixing of dissolved carbon and nutrients. They counteract vertical gradients induced by the carbon pumps through their tendency to restore a homogenous distribution of tracers in the ocean. Upwelling in the Southern Ocean returns nutrients to the surface (Marinov et al., 2006). However, not all nutrients are consumed in the Southern Ocean surface waters and are subducted again with AAIW and SAMW. These nutrient-rich waters then feed into the low-latitude thermocline waters, where they can be mixed to the surface and fuel biological production (Sarmiento et al., 2004). Model experiments show that about 75% of the total biological production in the low-latitudes (north of 30° S) can be explained by the provision of nutrients through the Southern Ocean, and if it were not for the ocean circulation, biological production in the global surface ocean would diminish (Sarmiento et al., 2004). Therefore, the return path of nutrients through the ocean circulation to the surface closes the major biogeochemical loop in the global ocean (bold white in Figure 1.4).
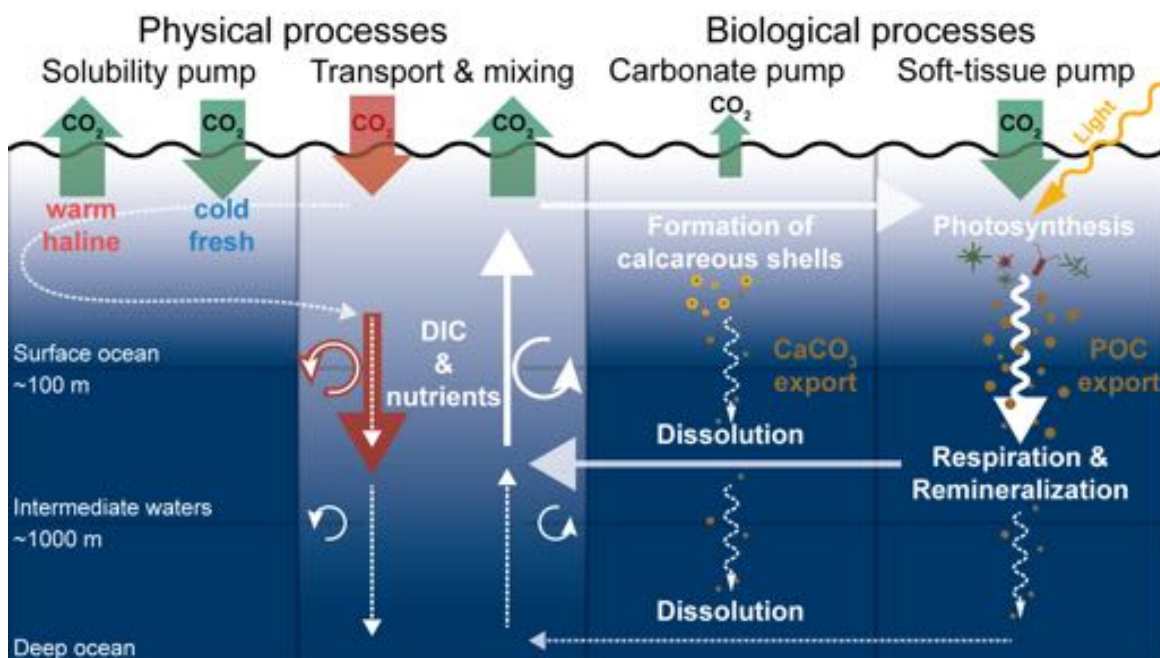
Figure 1.4   Cycling of carbon in the ocean: Physical and biological processes responsible for the vertical exchange of carbon between the deep and surface ocean (Heinze et al., 1991; IPCC, 2013). Soft-tissue pump: Photosynthetic production of organic matter, gravitational sinking, and heterotrophic remineralization of particulate organic carbon (POC). Carbonate pump: Biogenic formation of calcareous shells consisting of mineral calcium carbonate ($CaCO_3$), gravitational sinking, and dissolution. Physical processes: Vertical mixing and transport of dissolved inorganic carbon (DIC) and nutrients, as well as changes in solubility of carbon dioxide (CO_2) in seawater due to variations in temperature and salinity. All processes affect the air–sea gas exchange of CO_2 (green). In red: The major pathway of anthropogenic CO_2 into the ocean.

The mixing and transport of subsurface waters into the surface ocean bring not only nutrients but also DIC to the surface. This process counteracts the biologically produced vertical DIC gradient in the ocean. Thus, the vertical DIC gradient could either be altered by a change in mixing and transport or by biological productivity (Sarmiento et al., 1988). The sum of these two effects is often referred to as the efficiency of the biological pump (Sarmiento and Gruber, 2006). A very efficient biological pump occurs in the low latitudes due to the almost complete use of nutrients. The opposite, i.e., a low efficiency of the biological pump, occurs in high latitudes due to a reduced usage of nutrients (Gruber and Sarmiento, 2002). Since the production in low latitudes is largely nutrient-limited, the rate at which nutrients are provided through the high-latitudes ultimately determines the productivity in the global ocean (Sarmiento and Toggweiler, 1986). Thus, the high-latitudes provide the major control on the exchange of carbon between the atmosphere and the deep ocean either through changing the upwelling or changing the high-latitude productivity (Toggweiler, 1999; Sigman and Boyle, 2000). In a natural system, an increased vertical exchange in high-latitudes would lead to rise in atmospheric CO_2 while a decrease would lower atmospheric CO_2 (Knox and McElroy, 1984; Sarmiento and Toggweiler, 1984; Siegenthaler and Wenk, 1984). Therefore, physical processes associated with ocean transport and mixing have a large potential to alter the atmospheric CO_2 concentration on time-scales of decades to several centuries.

A third mechanism that substantially alters the vertical DIC gradient is associated with the solubility of CO_2 in seawater depending on its temperature and salinity (Figure 1.4). Surface cooling or freshening lead to an uptake of CO_2 from the atmosphere and warming or salinification lead to the contrary. Thus, waters that are transported towards higher latitudes and cool take up carbon (Gruber et al., 2009). As these waters are the source for deep and bottom waters, the solubility pump acts together with the ocean circulation to remove DIC from the surface ocean, especially in the North Atlantic (Sarmiento and Gruber, 2006). In contrast, the waters that upwell in equatorial regions gain heat and thus lose carbon to the atmosphere as a result of the solubility pump (Gruber et al., 2009). For example, water masses that are subducted to the thermocline depth in the relatively cold Southern Ocean, i.e., AAIW and SAMW, are upwelled to the surface in the very warm equatorial regions leading to substantial release of carbon due to a lower solubility. These effects resulting from the solubility, especially in response to temperature changes, can be as large as effects resulting from the soft-tissue pump or transport and mixing of DIC to the surface. Consequently, in combination with surface ocean physical or biological processes, ocean transport and mixing can effectively remove DIC and also dissolved organic carbon from the surface ocean (Figure 1.4).

The sum of all physical and biogeochemical effects on the air–sea CO_2 flux as displayed in Figure 1.4 is referred to as gas-exchange pump (Sarmiento and Gruber, 2006). Often the single contributions of each pump strongly oppose each other leading to a small net gas-exchange. For example, in a natural system (without anthropogenic influence), the upwelling in the Southern Ocean leads to an over-saturation of the seawater partial pressure of CO_2 (pCO_2) with respect to the atmosphere and thus to an out-gassing of CO_2 from the surface ocean (Figure 1.4; Mikaloff Fletcher et al., 2007; Gruber et al., 2009). This effect is partly compensated by a change in solubility due to the surface cooling and freshening and by biological productivity (Takahashi et al., 2002; Wang and Moore, 2012; Dufour et al., 2013; Hauck et al., 2013). The latter two effects become stronger towards lower latitudes of the Southern Ocean, gradually changing the surface ocean from a net source to a net sink of CO_2 (Mikaloff Fletcher et al., 2007; Gruber et al., 2009; Takahashi et al., 2009). In a natural (i.e., unperturbed) system, carbon is released from the ocean to the atmosphere in the Southern Ocean and in equatorial regions and taken up by the ocean in mid-latitudes and high northern latitudes (Mikaloff Fletcher et al., 2007; Gruber et al., 2009).

The spatial and temporal variations of the air–sea exchange mainly depend on the variations of the surface ocean pCO_2 since CO_2 in the atmosphere is well-mixed and thus rather uniform. Yet, the ultimate flux not only depends on the pCO_2 gradient but is also determined by the gas transfer coefficient, which depends on the wind speed and sea-ice concentration (Wanninkhof and McGillis, 1999; Butterworth and Miller, 2016). In order for the surface ocean pCO_2 to equilibrate with the atmosphere, it takes about six months to one year depending on the wind speed and the thickness of the surface layer (Sarmiento and Gruber, 2006). Yet, on longer time scales than one year the gradient in pCO_2, and thus the surface ocean pCO_2, dominates variations in the surface

flux (Landschützer et al., 2015b). The human induced increase in atmospheric pCO_2 offsets the long-term balance between the ocean and the atmosphere, leading to an average under-saturation of the surface ocean pCO_2 with respect to the atmosphere, which is the primary driver for the invasion of anthropogenic CO_2 into the ocean (red in Figure 1.4; Gruber et al., 2004). Thus, the larger the increase in the atmospheric pCO_2 is, the larger is the uptake by the ocean.

In order to sustain the surface ocean under-saturation and the effectiveness of the ocean carbon uptake, the anthropogenic carbon needs to be removed from the ocean surface and exported into the ocean interior. Recently, Bopp et al. (2015) suggested that vertical mixing is the major pathway for anthropogenic CO_2 to be exported from the surface ocean at the base of the mixed layer—a process which accounts for about 65% of the total subduction in their model. These results are overall consistent with findings by Dufour et al. (2013), who argue that vertical mixing is the major component of the surface mixed layer carbon budget in the Southern Ocean. However, below the surface mixed layer vertical mixing rapidly decreases, which would inhibit the carbon to be subducted into deeper layers. Reconstructions of the invasion of anthropogenic carbon into the subsurface ocean suggest that transport (i.e., advection) with NADW, AAIW and SAMW provides a major pathway for anthropogenic carbon to intermediate depths (Sabine et al., 2004; Mikaloff Fletcher et al., 2006; Gruber et al., 2009; Khatiwala et al., 2013). Thus, both vertical mixing and transport are likely critical components for the ocean uptake of anthropogenic CO_2 (red in Figure 1.4). Due to inhibited gas exchange by sea ice and dilution with deep water, AABW contains comparably little anthropogenic carbon, despite large formation rates (Poisson and Chen, 1987).

As I described earlier (section 1.2.1), the typical time-scale for subduction of surface waters is of the order of several years to decades, whereas the time-scale associated with the gas-exchange is much shorter. Thus, the ocean transport and mixing is the rate limiting factor for anthropogenic carbon uptake (Sarmiento et al., 1992). Without these subduction mechanisms, the ocean carbon sink would saturate in the long-term and the rate of uptake would slow down. Global model simulations show that the deep ocean ventilation through mixing and transport is reduced in a warming climate. Broecker (1997), and Stocker and Schmittner (1997) suggest that a decrease in the overturning circulation in the North Atlantic with global warming reduces the anthropogenic CO_2 uptake and amplifies global warming. For the Southern Ocean, Manabe and Stouffer (1993) and Sarmiento et al. (1998) suggest that an increased vertical density stratification strongly reduces the subduction of anthropogenic CO_2 due to increased warming and surface freshening, acting as a positive feedback on global warming (see also section 1.4).

A change in ocean mixing and transport would not only affect the subduction of anthropogenic CO_2 but could also alter the upwelling of DIC-rich waters in the Southern Ocean and thus alter the natural carbon cycle (Le Quéré et al., 2007; Pérez et al., 2013). A decrease in upward mixing and transport with global warming due to increased stratification would thus lead to a decrease in natural surface DIC, allowing the ocean to take up more CO_2 from the atmosphere.

Such a natural negative feedback on the upwelling could outweigh the positive feedback on the subduction rates, especially on shorter time scales of a few decades (Gruber et al., 2004). Because these two contrasting feedbacks associated with ocean mixing and transport are probably the strongest feedbacks between global warming and the carbon cycle in the long-term (Gruber et al., 2004) and their exact magnitude in projections with global climate models is still rather uncertain (Orr et al., 2001; Doney et al., 2004; Majkut et al., 2014; Kessler and Tjiputra, 2016), it is critical to better understand Southern Ocean circulation and stratification changes that are associated with a warming climate. Several other feedbacks may alter the long-term diminution of anthropogenic CO_2 in the ocean. An obvious positive feedback is related to a change in the solubility pump. The solubility of CO_2 in the surface ocean would decrease in a warming climate, leading to a reduction in the uptake. Other feedbacks include changes in the ocean chemistry and biology, which are discussed in detail by Gruber et al. (2004).

1.2.3   Ocean heat uptake

Due to its high heat capacity, the ocean buffers short-term fluctuations in the surface temperature and acts as an important regulator for the surface climate. Through the ocean circulation it redistributes the heat around the globe (Talley, 2003)—sometimes also in unexpected ways. The largest ocean heat gain occurs in the tropics, where the surface receives the largest amount of radiation, and the largest heat loss occurs in the high latitudes. However, surprisingly most of the heat is lost from the surface ocean in the high-latitude northern hemisphere (Ganachaud and Wunsch, 2000; Stammer et al., 2004), even though a much larger surface ocean area is exposed to the colder atmosphere in the southern hemisphere high-latitudes. This paradox can be explained through the ocean circulation. The heat that is gained in the tropics is mostly transport northward with the surface ocean currents (MacDonald and Wunsch, 1996; Ganachaud and Wunsch, 2000; Trenberth et al., 2001). After losing a large amount of heat to the atmosphere, NADW sinks in the north Atlantic and is transported southward at depth. On its way, it diffuses some of the heat in the deep ocean. In the Southern Ocean these water masses surface south of the Polar Front (PF), where surface temperatures are substantially colder than the temperature of NADW. Thus, a portion of the heat that these water masses originally gained in the tropics is also lost in the Southern Ocean surface waters. However, this heat has not been transported to the high-latitude Southern Ocean directly by surface waters, but by taking a detour through the North Atlantic and the deep ocean.

In the Southern Ocean, a fraction of the upwelled waters experiences a very large heat loss close to the Antarctic coast where the surface water is exposed to a very cold atmosphere in open water areas in the sea ice, called coastal polynyas. This heat loss leads to the formation of the densest and deepest water mass globally: the AABW (Jacobs et al., 1985; Orsi et al., 1999; Jacobs, 2004). Even though the rate of heat loss in the Antarctic coastal polynyas is very high, the

surface area through which the heat loss occurs is rather small. In the other high-latitude areas, heat exchange is largely inhibited by the presence of sea ice, which acts as an isolating layer between the ocean and the atmosphere (Maykut and Untersteiner, 1971). Thus, the total amount of heat lost to the atmosphere is much larger when transforming the warm surface waters from low latitudes to NADW then when transforming NADW to AABW. Another fraction of the upwelled deep waters in the Southern Ocean is transported northward. At first, they lose heat to the atmosphere. However, after crossing the PF, they start gaining heat again as the atmosphere becomes warmer than the ocean surface towards lower latitudes. Until they are subducted as AAIW and SAMW, these waters take up a substantial amount of heat and transport it to intermediate depths. In consequence, apart from the tropical regions, this region of AAIW and SAMW subduction is the second most important region for surface ocean heat gain (Stammer et al., 2003, 2004).

Changes in this heat redistribution through changes in ocean circulation could critically affect the global climate especially in the northern hemisphere where the largest meridional heat transport occurs. For example, it has been suggested that changes in the Atlantic Meridional Overturning Circulation (AMOC) are responsible for several abrupt changes in the northern hemisphere surface temperatures (Clark et al., 2002; Rahmstorf, 2002). Similarly, a slowdown of the AMOC with global warming could actually lead to reduced sub-polar cooling in the northern hemisphere (Rahmstorf et al., 2015).

While changes in the meridional heat transport affect the regional climate, the vertical transport of heat into the deep ocean can effectively delay the man-made surface warming globally. About 90% of the excess heat in the Earth's climate system since the 1950s went into heating the ocean (Levitus et al., 2001, 2012). Roemmich et al. (2012) suggest that even before that time the ocean took up excess heat at a similar rate. Thus, without this heat uptake through the ocean the global surface warming would have been substantially larger (Stocker, 2015). This uptake of heat by the global ocean has been increasing in concert with the global surface temperatures with about half of the total uptake occurring over the last two decades (Gleckler et al., 2016).

Similarly to the invasion of the anthropogenic CO_2 into the sub-surface ocean (section 1.1), the heat enters the ocean through the subduction of water masses from the surface. This subduction of heat seems to be dominated by the Southern Ocean (Durack et al., 2014; Roemmich et al., 2015; Frölicher et al., 2015; Cummins et al., 2016). Global climate models suggest that about 75% of the total global heat uptake since pre-industrial time occurred in this region (Frölicher et al., 2015). This uptake is largely driven by a subduction and northward transport of the heat by AAIW and SAMW (Cummins et al., 2016; Morrison et al., 2016). However, models also show a very large spread of the rate and patterns of subduction, which is a major concern for reducing uncertainties in projected future global warming (Boé et al., 2009; Cheng et al., 2016; Frölicher et al., 2015). Changes have not only occurred in relation to the subduction of AAIW and SAMW, but also the abyssal Southern Ocean (AABW) shows a long-term warming over recent decades (Purkey and Johnson, 2013). Overall, a potential future change in subduction of excess heat in

the Southern Ocean through changes in mixing and transport could critically accelerate or delay global warming in the future. Consequently, it is an urgent matter to reduce the uncertainty in projections with global climate models by understanding the mechanisms that lead to changes in mixing, transport, and air–sea fluxes.

1.3   Upwelling & subduction in the Southern Ocean

In the discussion on the role of ocean circulation for the ocean carbon and heat uptake in section 1.2, I illustrated the major importance of the upwelling and subduction for long-term changes in the climate system, both from a perspective of natural variability and the anthropogenic perturbation of the climate system. I also highlighted that most of the global ocean is ventilated through the Southern Ocean. Assuming that this ventilation happens mostly through the surface waters (upper 100 m) in an area south of a region somewhere between the SAF and STF (Figure 1.5), one obtains a residence time of about 3 to 6 years (using a total formation rate of all water masses of about 40 Sverdrup (Sv) = $40 \cdot 10^6$ m^3 s^{-1} (Talley, 2013)). However, much of the upwelling and subduction is not uniform but much more localized, e.g., to the region of Drake Passage, and depends on surface mixing and advection processes (Sallée et al., 2010a). A potentially smaller surface area through which ventilation typically occurs would imply a much shorter residence time that might even be less than a year (Viglione and Thompson, 2016). During this time, the water masses exchange heat, freshwater, and dissolved constituents with the atmosphere, the sea ice, and the land ice. The signature that is imprinted by this exchange is then carried to the sub-surface (Iudicone et al., 2011). I will discuss the processes leading to this enormous turn-over rate in the Southern Ocean in section 1.3.1 and the special role of surface freshwater fluxes that are the focus of my thesis in section 1.3.2.

1.3.1   Circulation & water masses

The Southern Ocean connects the three major global ocean basins, namely the Pacific, Atlantic, and Indian Ocean (Figure 1.5). The exchange rate between the Pacific and the Atlantic through the Southern Ocean (Drake Passage) amounts to a net eastward transport of about 140 Sv (Meredith et al., 2011b; Naveira Garabato et al., 2014; Koenig et al., 2014) and the one between the Indian Ocean and the Pacific (south of Australia) to about 150 Sv (Ganachaud and Wunsch, 2000; Naveira Garabato et al., 2014). This vast inter-basin exchange opposes a very weak exchange north of the Southern Ocean of about 10 Sv in the Indonesian Throughflow and about 1 Sv through the Bering Strait (Ganachaud and Wunsch, 2000; Stammer et al., 2003).

The strong and deep-reaching eastward transport of water in the Southern Ocean is represented by the Antarctic Circumpolar Current (ACC), which consists of several filaments of peak transport (Sokolov and Rintoul, 2009a, see Figure 1.5). These jets are associated with frontal regions of strong across-flow gradients in ocean properties, particularly in temperature, that are traditionally divided into the southern ACC front, the Polar Front (PF), and the Subantarctic Front (SAF; Orsi et al., 1995; Rintoul and Naveira Garabato, 2013). The dynamics of this current are rather complex and differ from other ocean currents. Its zonal transport is mainly set up by a meridional density gradient that is induced by Ekman divergence in the south of the ACC and

the surface buoyancy forcing (Olbers et al., 2004; Hogg, 2010). The resulting horizontal density gradient at each geopotential level leads to a geostrophic flow to the east. The direct eastward momentum forcing by the wind only plays a minor role. Standing and transient eddies transfer the zonal momentum to the ocean floor, where it is thought to be compensated by bottom form stress. These mesoscale eddies form from baroclinic instabilities of the zonal flow and act not only to transfer momentum to depth but also to exchange heat and tracers in a meridional direction across the frontal region and the ACC (Dufour et al., 2015; Frenger et al., 2015), which shield the high-latitude and thus the deep ocean from the low-latitude surface ocean. This meridional exchange and thus the dynamics of the ACC are closely linked to the meridional overturning circulation in the Southern Ocean. Yet, the total ACC transport seems not to be very sensitive to changes in the surface wind stress as well as to changes in the eddy field (Meredith et al., 2004; Böning et al., 2008), as the energy of an increased momentum flux almost entirely propagates to the mesoscale rather than increasing the mean flow; a process which is known as eddy saturation (Hallberg and Gnanadesikan, 2006; Meredith and Hogg, 2006; Meredith et al., 2012).

The isopycnal surfaces in the Southern Ocean ascend towards the pole (Figure 1.5). This ascent results from a combination of surface wind and buoyancy forcing (Rintoul and Naveira Garabato, 2013). Strong westerly winds drive water masses to the north at the surface through Ekman transport, leading to a divergence south of the maximum wind stress and to a convergence north of the maximum wind stress. The surface divergence south of the PF leads to upwelling of waters from below and lifts the isopycnal surfaces (Toggweiler and Samuels, 1993; Döös and Webb, 1994; Toggweiler and Samuels, 1995; Gnanadesikan, 1999). The northward Ekman transport to the north is balanced by a southward transport in the deep ocean. By analyzing hydrographic data from the Southern Ocean, Sverdrup (1933) and Deacon (1937) already noticed the existence of such a wind-driven upper circulation cell. More recently, surface buoyancy forcing was found to critically contribute to this overturning circulation as well (Speer et al., 2000; Marshall and Radko, 2003; Olbers et al., 2004; Morrison et al., 2011). As the upwelled waters are transported to lower latitudes at the surface, buoyancy is gained due to a net surface warming and freshening, making these waters lighter. This meridional gradient in the buoyancy forcing results in a meridional density gradient in the ocean, which is reflected by the upward tilt of the isopycnal surface from north to south. Model simulations show that a substantial fraction of the upper overturning cell can be attributed to this buoyancy gain (Olbers et al., 2004; Morrison et al., 2011). While the surface momentum and buoyancy forcing act to steepen the isopycnals, the eddy field that results from the baroclinic instabilities flattens them through a net southward transport of heat and thus density. This eddy-induced transport counter-acts the mean wind- and buoyancy-driven transport, resulting in residual overturning circulation with a more complex vertical structure (Karsten et al., 2002; Marshall and Radko, 2003; Marshall and Speer, 2012). While most of the mean transport occurs at the surface and in the deep ocean, the eddy-induced transport acts at the surface and intermediate depth. Therefore, in contrast to the ACC transport, it has been shown that the magnitude and structure of the meridional overturning circulation is sensitive to changes in the wind

stress and the eddy field (Meredith et al., 2012).

Close to the Antarctic coast, strong easterly winds drive the westward transport of the Antarctic Coastal Current (Fahrbach et al., 1992; Schröder and Fahrbach, 1999; Dong et al., 2016, blue in Figure 1.5). The peak transport occurs at the continental shelf break and is associated with strong gradients in temperature and tracers, referred to as the Antarctic Slope Front (Jacobs, 1991). The easterly winds also drive an onshore surface Ekman transport and a subsurface eddy-induced transport of warmer deep waters onto the continental shelf (Ito and Marshall, 2008; Stewart and Thompson, 2013; Thompson et al., 2014). The waters that are upwelled to the Antarctic Surface Waters (AASW) and transported southward onto the continental shelf lose buoyancy through cooling making these waters much denser. After a complex modification of the water masses along the Antarctic coast, which involves interaction with the sea ice, land ice, and atmosphere (Orsi et al., 1999, 2002; Jacobs, 2004; Snow et al., 2016), these dense shelf waters mix with NADW and CDW and flow northward following the ocean floor as AABW. This return flow compensates for the onshore convergence created by the combined southward Ekman and eddy transport above. This overturning circulation forms the lower circulation cell in the Southern Ocean, which is responsible for ventilating large parts of the abyssal global ocean.

In a zonal mean, upwelling and subduction form together a double-celled meridional overturning circulation in the Southern Ocean (Gordon, 1986b; Sloyan and Rintoul, 2001b; Lumpkin and Speer, 2007; Marshall and Speer, 2012, see Figure 1.5). The upper cell is associated with a buoyancy gain and the lower cell with a buoyancy loss with respect to the upwelled water masses (Speer et al., 2000). The ratio between the amount of the upwelled water that enters the upper cell to feed the low latitude thermocline versus the amount that enters the lower cell to be subducted to the abyssal ocean essentially depends on the processes acting on the Southern Ocean surface waters south of the SAF, i.e. in the Polar Frontal Zone and the Antarctic Zone. In the interior ocean within the Southern Ocean and at lower latitudes the upper and lower circulation cells are eventually connected through diapycnal mixing processes between AABW and NADW in the Atlantic and between AABW and CDW in the Pacific and Indian Ocean (Gordon, 1986b; Talley, 2013). Gordon (1986b) estimated that the lower and upper cells are associated with an overturning of about 30 Sv and 20 Sv, respectively. These estimates broadly agree with newer, more confined estimates by Talley (2013), who estimates a net AABW formation of about 29 Sv and a net AAIW and SAMW formation of about 13 Sv. Estimates in literature range between 12 Sv and 21 Sv for the transformation from upwelling waters to AAIW and SAMW and between 10 Sv to 50 Sv for the transformation of NADW and CDW to AABW (Rintoul and Naveira Garabato, 2013, and references therein). Part of the large uncertainty associated with the lower cell stems from the uncertainty in the rate of mixing and entrainment of NADW and CDW into AABW (Rintoul and Naveira Garabato, 2013).

The meridional overturning circulation arising from the zonal mean consists in reality of large circumpolar variations of upwelling and subduction. AABW is predominantly formed in
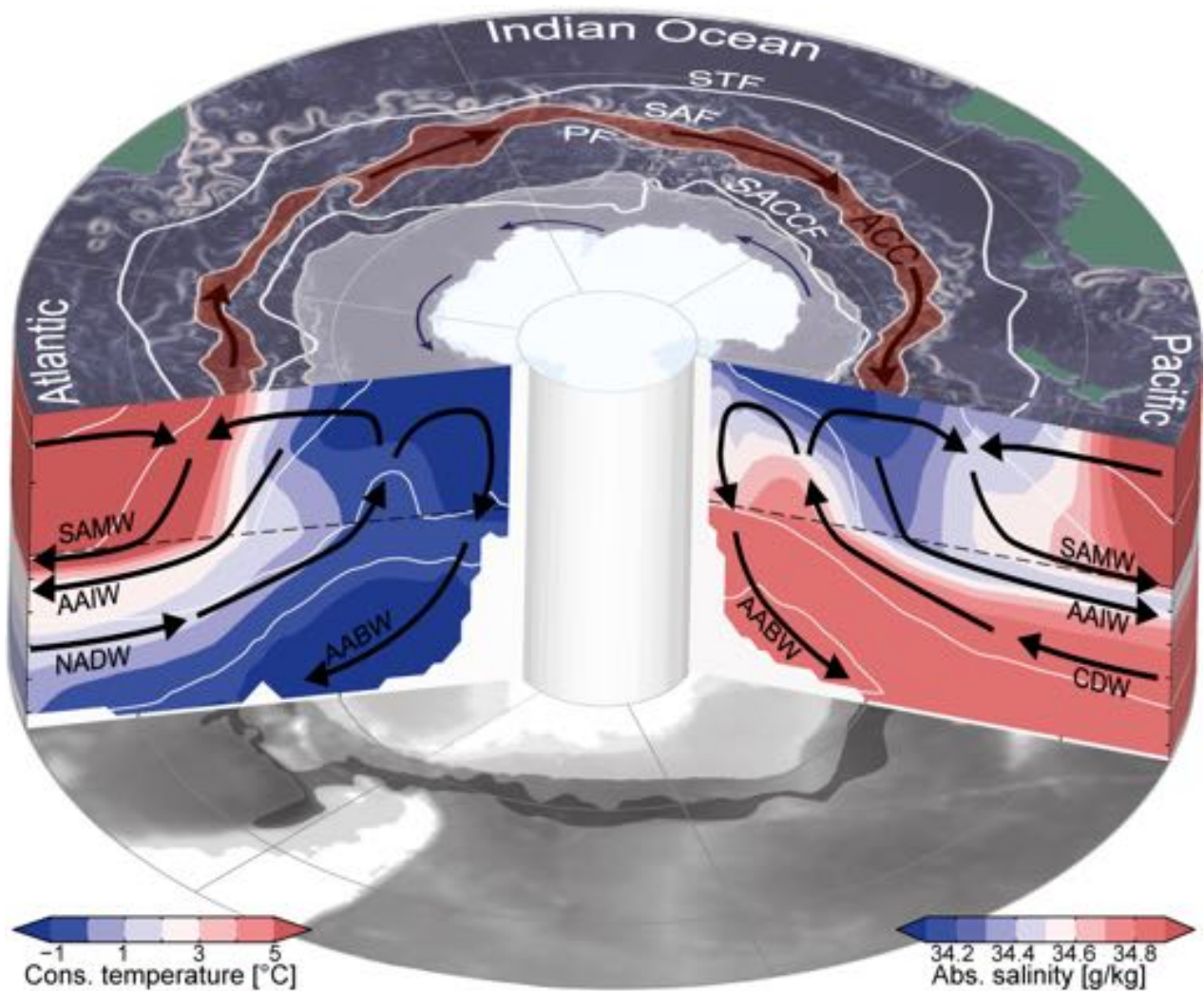
Figure 1.5 Southern Ocean circulation, water masses, and stratification: The top shows the main fronts (STF: Subtropical front, SAF: Subantarctic Front, PF: Polar Front, SACCF: Southern ACC Front; white; Orsi et al., 1995), the Antarctic Circumpolar Current (ACC; red), the Antarctic Coastal Current (blue), the winter sea-ice extent (September; gray), and ocean velocity (background). The left cross-section shows the mean Atlantic conservative temperature and the right cross-section the mean Pacific absolute salinity (Ingleby and Huddleston, 2007). The white contours show the corresponding isopycnals (from top to bottom: $\sigma_0 = 25.8$, $\sigma_0 = 26.6$, $\sigma_0 = 27.4$, $\sigma_0 = 27.8$, $\gamma = 28.27$). The black arrows in the cross-sections schematically illustrate the overturning circulation and water masses (AABW: Antarctic Bottom Water, NADW: North Atlantic Deep Water, CDW: Circumpolar Deep Water, AAIW: Antarctic Intermediate Water, SAMW: Subantarctic Mode Water).

the high-latitude embayments of the Weddell and Ross Seas, and along the Adélie coast (Orsi et al., 1999; Jacobs, 2004; Williams et al., 2010), but other formation sides around the Antarctic continent have been identified as well (e.g. Ohshima et al., 2013). AABW forms from NADW and denser CDW classes, because they upwell further south than the lighter CDWs from the Pacific and Indian Ocean (Talley, 2013). NADW that enters the Southern Ocean in the Atlantic basin is not transported directly into the high-latitude Atlantic but is, instead, circulated around the Southern Ocean with the ACC until it surfaces close to the continental shelf (pers. comm. L. Talley and J. Sarmiento).

Lighter CDW, referred to as Upper Circumpolar Deep Water (UCDW), returns to the Southern Ocean from the Pacific and Indian Ocean and lies above the NADW and Lower Circumpolar Deep Water (LCDW). Therefore, it upwells further north, in the region between the seasonal sea-ice zone and the Polar Front. However, upwelling of UCDW into the AASW occurs not uniformly in time and space and depends on topographic features, eddy-induced mixing, local Ekman divergence, and surface mixed-layer processes (Morrison et al., 2011; Sallée et al., 2010a). Very little is currently known on the actual upwelling processes, magnitude, and variability. Large parts of the upwelled water masses are subducted again as AAIW, which forms south of the SAF, after being transformed by surface buoyancy fluxes during the northward transport. Strong mixing and cabbeling are important components of this AAIW formation process (Iudicone et al., 2008, 2011; Urakawa and Hasumi, 2012). It occurs predominately in the south-eastern Pacific and south-western Atlantic (England et al., 1993; Talley, 1996; Sloyan and Rintoul, 2001a; Saenko et al., 2003; Iudicone et al., 2007; Sallée et al., 2010a; Hartin et al., 2011). Thus, AAIW is imprinted by the buoyancy forcing further downstream in the South Pacific where the water masses considerably freshen, resulting in a pronounced salinity minimum at intermediate depth north of the SAF (England et al., 1993; Iudicone et al., 2007; Hartin et al., 2011). Another fraction of the the upwelled waters is transported across the SAF at the surface layers by northward Ekman transport. In this Subantarctic Zone between the Subtropical Front (STF) and the SAF, SAMW forms through a convergence of waters from the north (Subtropical waters) and south (Iudicone et al., 2008, 2011; Cerovečki and Mazloff, 2016). The subduction of SAMW occurs mostly over large parts of the Pacific sector and in the south-eastern Indian Ocean (Sallée et al., 2010a).

1.3.2   Stratification & surface freshwater fluxes

The close connection between the deep ocean and surface waters in the Southern Ocean arises mainly from the relatively low vertical density stratification. Whereas the low latitudes are strongly stratified by temperature (thermocline), surface cooling of the polar ocean induces statically unstable conditions. However, a strong supply of freshwater to this region counteracts the destabilizing temperature effects by lightening the Southern Ocean surface waters. As the polar ocean's temperature is close to the freezing point, the contribution of the vertical temperature structure to the density stratification is drastically reduced and the salinity structure dominates the surface ocean stratification. This effect is owing to a non-linear dependence of the seawater density on temperature and salinity (Haug et al., 1999; Sigman et al., 2004). A typical vertical profile in the high-latitude Southern Ocean (south of the Polar Front) is characterized by a very fresh surface layer that is warm in summer and cold in winter (upper 50 m to 100 m). As the cold winter temperatures destabilize the water column, the surface waters mix deeper. The resulting cold sub-surface temperature minimum that arises in the annual mean profile is referred to as Winter Water (WW). This layer is slightly more saline than the surface water but still fresher than the underlying deep water. Below the WW both salinity and temperature considerably increase

(halocline) as one enters the upwelling deep waters (Gordon and Huber, 1984, 1990; Gordon, 1991; Martinson, 1990, 1991). Thus, unlike most of the global ocean, the high-latitude Southern Ocean's vertical stability is dominated by the salinity profile and with a marginally stable density stratification.

Because the marginal stability of the Southern Ocean surface waters is driven by salinity, changes in surface freshwater fluxes might implicate crucial changes in its vertical stability and, consequently, its overturning circulation, mixed layer depth, and water masses. Therefore, I will focus on the buoyancy forcings induced by freshwater fluxes and their effects on stratification and overturning circulation in this thesis. Surface freshwater fluxes in the Southern Ocean consist of atmospheric freshwater fluxes from evaporation (E) and precipitation (P), glacial meltwater fluxes from the Antarctic continent that are induced either by under ice-shelf melting or by ice-berg calving, and freshwater fluxes from the formation, transport, and melting of sea ice. Additionally, freshwater in the ocean is redistributed through ocean circulation and mixing.

The net atmospheric flux (P−E) is a freshwater source for the ocean almost everywhere over the Southern Ocean as precipitation exceeds evaporation. It is generally high north of 60°S and decreases towards the continent. An exception, however, is the south-east Pacific where fluxes increase towards the coastal regions of the Bellingshausen and Amundsen Seas, specifically at the western coast of the Antarctic Peninsula (Tietäväinen and Vihma, 2008). This zonal asymmetry in the atmospheric freshwater flux is caused by a spiraling of the freshwater distribution from more northern latitudes in the western Atlantic towards more southern latitudes in the eastern Pacific. Papritz et al. (2014) show that this pattern stems from the strong precipitation that is associated with extra-tropical cyclones and fronts that move along a spiraling storm-track. Atmospheric freshwater supply is lowest in the southern Ross and Weddell Seas due to a large influence of dry and cold continental air-masses from Antarctica. As a consequence, from an ocean perspective, most coastal regions experience only a small buoyancy gain from atmospheric freshwater, and the positive buoyancy forcing in regions of the PF and further north is substantial. While the patterns of the atmospheric freshwater fluxes over the Southern Ocean are understood rather well, the exact magnitude of these fluxes is highly uncertain and varies strongly among different reanalysis products (Bromwich et al., 2011; Nicolas and Bromwich, 2011).

The overall net accumulation of freshwater over the Antarctic continent (about 2'600 Gt per year or 82 mSv; Lenaerts et al., 2016) is balanced by freshwater input into the Southern Ocean in coastal regions either through under ice shelf melt or calving of ice bergs (about 2'780 Gt per year or 88 mSv; Depoorter et al., 2013; Rignot et al., 2013). An imbalance exists between the total melting and the accumulation due to increased grounding line fluxes (Rignot et al., 2008; Shepherd et al., 2012) over recent decades. The largest basal ice-shelf melting fluxes are found along the coasts of the Bellingshausen and Amundsen Seas where the continental shelf is narrow and the relatively warm CDW intrudes on the shelf (Martinson and McKee, 2012; Cook et al., 2016). Only very little freshwater is added overall to the ocean by surface runoff, since temper-

atures are too cold at the ice-shelf surface. However, this process might be important locally or also on larger scales under a warming future climate. Roughly half of the total freshwater input from the ice sheet to the Southern Ocean occurs through ice-berg melting (Depoorter et al., 2013; Rignot et al., 2013). These icebergs are typically transported westward with the coastal current and only about 40% of them drift to lower latitudes (Silva et al., 2006). The combined effect of basal melting and iceberg melting provide a major source of freshwater to the coastal region affecting sea-ice and AABW formation (Hellmer, 2004; Martin and Adcroft, 2010; Stössel et al., 2015; Merino et al., 2016).

The seasonal cycle of melting and freezing of the surface ocean redistributes freshwater vertically in the sea-ice covered regions. In winter-time, the colder and more saline waters induced by the brine rejection are heavier and mix deeper in the water column than the fresher and warmer summer-time waters. In the course of several seasonal cycles this process can lead to a stable vertical salinity stratification (Martinson et al., 1981; Goosse and Zunz, 2014). Such a process was suggested to be an important contributor to the characteristic haloclines in both the northern (Aagaard et al., 1981; Aagaard and Carmack, 1989) and southern high latitudes (Martinson et al., 1981; Fahrbach et al., 1994; Goosse et al., 1999; Goosse and Zunz, 2014), yet observational evidence is sparse. A first attempt to derive basin-wide freshwater fluxes from sea ice to the ocean is provided by Tamura et al. (2011), using atmospheric re-analysis data. They conclude that the sea-ice fluxes might exceed regionally the atmospheric flux by one order of magnitude and that, in coastal regions, it is slightly larger than the glacial melt water flux. However, a lack of observational data to constrain these products as well as their methodology induce a very large uncertainty. More recently, Abernathey et al. (2016) also suggest such a dominance of the sea-ice freshwater fluxes in the surface freshwater balance by assimilating ocean observational data with an ocean circulation model.

Sea ice in the Southern Ocean is very dynamic and a strong drift of the thin seasonal sea ice occurs all around the Antarctic continent as a response to the southerly and easterly winds, and ocean currents. Along East Antarctica and the southern coast of the Bellingshausen and Amundsen Seas, easterly winds drive the sea ice along the continent with a small on-shore component due to the Ekman drift. In the Weddell and Ross Seas, however, it is exported northward due to southerly winds and the cyclonicity of the gyres (Emery et al., 1997; Haumann, 2011). It forms in the coastal polynya regions affecting AABW formation by brine rejection (Jacobs et al., 1985; Zwally et al., 1985; Toggweiler and Samuels, 1995; Duffy and Caldeira, 1997; Duffy et al., 1999). After being transported to the north, it melts along the ice edge adding freshwater to the surface ocean. This freshwater redistribution could considerably affect the stratification and upwelling north of the continental shelf, as well as the occurrence of open ocean convection (Gordon and Taylor, 1975; Martinson, 1991; Fahrbach et al., 1994; Timmermann et al., 2001). It is not only this local effect that might be important, but it might also considerably influence AAIW and SAMW through cross-frontal Ekman and eddy transport of freshwater (Rintoul and England, 2002). In fact, numerous modeling studies suggested that AAIW, SAMW and AABW could only be repre-

sented quasi-realistically in models if they included the meridional transport of sea ice (England, 1992; Saenko and Weaver, 2001; Saenko et al., 2002; Komuro and Hasumi, 2003; Santoso and England, 2004; Ogura, 2004; Kirkman and Bitz, 2011; Abernathey et al., 2016). However, in many current global climate models this process is not well represented (England, 1992; Uotila et al., 2014; Lecomte et al., 2016), providing a potential contribution to their large biases in the Southern Ocean water-mass structure (Downes et al., 2010, 2011; Heuzé et al., 2013, 2015; Sallée et al., 2013b).

The net freshwater input over the Southern Ocean is balanced by a northward export of freshwater by AAIW and SAMW, a southward salt flux with the mean circulation (Wijffels, 2001; Talley, 2008), and a southward eddy flux (Meijers et al., 2007). Actually, the largest global meridional freshwater transport by the ocean occurs between the Southern Ocean and the southern hemisphere subtropics (Stammer et al., 2004). Interestingly, this is opposite to the meridional heat transport that is dominated by the northern hemisphere (section 1.2.3). This large redistribution of the freshwater with the ocean circulation is represented by a large tongue of minimum salinity at intermediate depth, a key characteristic of AAIW and SAMW.

Multiple studies show that the freshwater fluxes and their partitioning are strongly variable in space and time. Timmermann et al. (2001) suggest that the sea-ice freshwater export from the south-western Weddell Sea is almost twice as large as the atmospheric flux and that it balances the inflow of freshwater from the atmosphere, glacial melt water, and oceanic advection. Using $\delta^{18}O$ and salinity, Jacobs et al. (1985) argue that these different freshwater components indeed tend to balance in the high-latitude embayments of the Ross and Weddell Seas. Meredith et al. (2013) use $\delta^{18}O$ and salinity measurements along the west coast of the Antarctic Peninsula and found that the net atmospheric and glacial waters are the dominant fluxes. In the open Southern Ocean north the sea-ice edge, Ren et al. (2011) make a first attempt to derive a freshwater budget for the mixed layer. They found that the sea-ice contribution is comparable to the ocean advection and atmospheric fluxes. In sum, all these studies suggest that the cryospheric freshwater fluxes from land or sea ice are critical to understand the freshwater balance of the Southern Ocean.

Each of the freshwater components is sensitive to changes in the surface climate. The net atmospheric freshwater flux to the Southern Ocean is expected to increase in a warming climate and decrease in a cooling climate (Trenberth et al., 2011; Durack et al., 2012; Knutti and Sedláček, 2013). Similarly, one expects glacial meltwater input to increase in a warming climate in the long-term due to increased basal melting and break-ups of ice shelves (Golledge et al., 2015). With sea ice this relation seems more difficult: a warming surface climate potentially reduces the amount of sea-ice formation and a retreat of the northern ice edge. This could lead to a reduction in both the vertical and horizontal salinity distribution in the ocean. The latter effect is complicated by the role of changes in surface winds in redistributing the sea ice around the Antarctic continent. Thus, there are probably compensating effects between the freshwater fluxes in a warming climate, with potentially increasing atmospheric and glacial freshwater fluxes and hypothetically decreasing

sea-ice freshwater fluxes. These effects could be additionally complicated by regional variations in the warming of the surface climate (see section 1.4.1).

To date, there is no consensus either on the total magnitude of the surface freshwater fluxes over the Southern Ocean, on the contribution of each freshwater flux component, or on their spatial and temporal variations (Speer et al., 2012; Bourassa et al., 2013). This gap of knowledge is mostly owing to sparse observations in this region, providing a major limitation to our understanding of Southern Ocean surface processes and hinders the improvement of current global climate models. The representation of the Southern Ocean water mass structure and circulation is very sensitive to the surface freshwater fluxes and the vertical mixing of freshwater (England, 1992; Timmermann and Beckmann, 2004; Kjellsson et al., 2015; Stössel et al., 2015). Gordon (2016) argues that in the near future advances in satellite-based estimates of the ocean sea-surface salinity will greatly improve our understanding of the magnitude and variability of freshwater fluxes. However, in order to distinguish the contributions of the different sources, other methods will be required.

1.4   Recent changes in the Southern Ocean

The previous sections of this chapter illustrated that upwelling and subduction in the Southern Ocean might change in response to changes in the surface forcing on time scales of decades to centuries, and even glacial cycles, with important implications for the global climate. Therefore, it is extremely important to better understand the response of the Southern Ocean to changes in the surface forcing. For this purpose, I will focus in this thesis on the most recent changes, as these changes are much better constrained by observations as opposed to simulations of the past and future with global climate models or past changes inferred from proxy data. This discussion will reveal that many of the observed changes in the Southern Ocean and Antarctica are rather surprising and puzzling in the context of a warming global climate. A better understanding of the processes at work over recent decades will then help to better constrain past and future changes, as I will outline at the end of this thesis (chapter 6). In this section, I will first describe recent changes in the Southern Ocean surface climate (1.4.1), which will be followed by a discussion on the impact of these changes on upwelling and subduction (1.4.2), and the carbon uptake (1.4.3).

1.4.1   Changes in the surface climate

One of the key features of changes in the Southern Ocean surface climate over recent decades are changes in the atmospheric circulation. These changes are reflected in a reconstructed long-term shift of the Southern Annular Mode (SAM) index to more positive phases (Marshall, 2003; Abram et al., 2014). The SAM is largely measure of meridional gradients in sea-level pressure and its recent increase thus reflects a strengthening of the zonal geostrophic winds close to the surface. Model simulations consistently suggest that such an intensification and a poleward shift of the westerly winds over the Southern Ocean is a response to stratospheric ozone depletion and greenhouse gas increase (Arblaster and Meehl, 2006; Son et al., 2008; Thompson et al., 2011; Lee and Feldstein, 2013).

While the SAM index provides a measure for zonal mean circulation changes in the atmosphere, it does not allow to study zonal variations and spatial patterns in circulation changes. However, atmospheric reanalysis suggests that these changes were asymmetric in a zonal direction (Turner et al., 2009; Bromwich et al., 2011; Haumann et al., 2014). This zonal asymmetry incorporates a significant deepening of the Amundsen Sea Low (ASL), which induced a southerly wind anomaly over the Ross and Amundsen Seas and a northerly wind anomaly in the Antarctic Peninsula region and the adjacent ocean, mostly over the Bellingshausen Sea. At the same time the deepening and expansion of the ASL induces a slight northward shift of the westerly winds in the Pacific sector, while they moved southward in the other sectors. The influence of the anthropogenic forcing on the observed ASL trend over recent decades has been debated. In climatological mean state the circulation around the Antarctic continent is not perfectly annular either

with large interannual to decadal variations in the zonal symmetry. Sea-level pressure variations in the ASL region are associated with quasi-stationary, planetary wave-number 1 and 2 patterns (van Loon and Jenne, 1972; Carril and Navarra, 2001; Yuan and Martinson, 2001; Turner et al., 2016). Their variability is directly linked to changes in the tropical Pacific (Ding et al., 2011; Schneider et al., 2012b; Meehl et al., 2016) and Atlantic (Li et al., 2014; Simpkins et al., 2014). Thus, the observed long-term trend in the ASL could be related to multi-decadal variations in the tropical Pacific and Atlantic (Li et al., 2014; Meehl et al., 2016), especially in light of the prevailing La Niña conditions over the recent decade (Landschützer et al., 2015b). On the other hand, the long-term decrease of the surface pressure in the ASL region is also consistent with the anthropogenic forcing (Neff et al., 2008; Turner et al., 2009; Hosking et al., 2013; Haumann et al., 2014; Raphael et al., 2016, see chapter A for a more in-depth discussion).

Both the zonally symmetric (i.e., westerly wind) and asymmetric (i.e., primarily meridional wind) changes of the atmospheric circulation are considered the prime drivers of the observed changes in the Southern Ocean and Antarctic surface climate over recent decades. As I will describe in the remainder of this section, many of the observed changes can be linked to zonally asymmetric changes in the atmospheric circulation.

Despite global warming, much of the high-latitude Southern Ocean surface has cooled during the satellite era (since 1979), especially in the Pacific sector (Fan et al., 2014; Armour et al., 2016). A series of very recent studies (Ferreira et al., 2015; Armour et al., 2016; Kostov et al., 2016; Seviour et al., 2016) suggests that this cooling or delayed warming of the Southern Ocean surface is an initial response of the sea-surface temperature (SST) to an increase in westerly winds. It is proposed that these winds increase the northward transport of cold polar surface waters through Ekman transport (Thompson et al., 2011). Yet, several other potential explanations exist. One of them is that an increased surface ocean stratification that is observed over large regions in the high-latitudes (de Lavergne et al., 2014) could inhibit the mixing of warmer CDW into the surface layer and lead to a long-term cooling (Zhang, 2007; Bintanja et al., 2013; Goosse and Zunz, 2014; Pauling et al., 2016). Another potential explanation is that the zonally asymmetric circulation changes in the atmosphere lead to a more intense meridional exchange of heat between the cold Antarctic continent and the warmer air over the open Southern Ocean, which would effectively cool the open ocean region especially in the Pacific sector (Haumann, 2011; Papritz et al., 2015; Landschützer et al., 2015b; Raphael et al., 2016). In addition, an expansion or retreat of Antarctic sea ice in relation to changes in meridional winds induces positive ice–albedo and surface heat flux feedbacks that lead to anomalies in the SST (Haumann et al., 2014). In summary, the absence of recent decadal warming in large parts of the Southern Ocean surface has not yet been fully understood, which is also owing to problems in global climate models to reproduce these changes.

An absence of decadal warming has also been recorded over the Antarctic continent over the satellite era (Jones et al., 2016; Smith and Polvani, 2016) and even since pre-industrial times

(Abram et al., 2016; Smith and Polvani, 2016). However, a significant warming occurred along the coastal regions of the Antarctic Peninsula, and the Bellingshausen and Amundsen Seas (Jacobs et al., 2012; Schmidtko et al., 2014). This warming probably results from an increased upwelling of CDW onto the continental shelf (Cook et al., 2016) leading to an accelerated melting of the ice shelves in this region (Pritchard et al., 2012; Paolo et al., 2015). The increased upwelling of CDW onto the shelf can be directly linked to an increasing alongshore (mostly easterly) winds in this region (Spence et al., 2014), which are in turn part of an increasing cyclonic atmospheric circulation in the ASL region.

Antarctic sea ice has been expanding moderately over the satellite era (Comiso and Nishio, 2008). This expansion is the result of multiple opposing regional trends, with an increasing sea-ice cover mostly in the Ross Sea and decreasing sea-ice cover in the Antarctic Peninsula region and the Bellingshausen and Amundsen Seas (Stammerjohn et al., 2008). These regional changes have been related to regional changes in the meridional winds, with stronger southerly winds pushing the sea-ice edge northward through increasing ice drift in the Ross Sea and stronger northerly winds in the Antarctic Peninsula region advecting warmer maritime air masses that melt the ice (Haumann, 2011; Holland and Kwok, 2012; Haumann et al., 2014). Thus, the observed sea-ice changes can be directly related to zonally asymmetric changes in the atmospheric circulation. The question whether or not these changes are a forced response or induced by multi-decadal variability is directly linked to the question if the zonal asymmetry in the atmospheric circulation is a forced response (Turner et al., 2009; Haumann et al., 2014; Hobbs et al., 2016). Currently, it is not possible to confidently answer this question since not only the sign and pattern of the forced response but also the magnitude and pattern of the natural variability in global climate models disagree with the observed changes (Haumann et al., 2014) and observed changes seem to short to fully capture the natural variability of the system (Hobbs et al., 2016; Jones et al., 2016). While the regional sea-ice cover indeed undergoes large decadal variations that superimpose a long-term trend (Haumann, 2011), a recent review by Hobbs et al. (2016) suggests that regional trends over the satellite era in the Ross Sea exceed natural variability in all CMIP5 models in the warm season. This observation is confirmed by a most recent sea-ice reconstruction that suggests that the increase in the sea-ice cover in the Ross Sea is unprecedented over the past three centuries (Thomas and Abram, 2016). Thus, it is possible that there is an anthropogenic influence on the recent sea-ice changes around Antarctica (Haumann et al., 2014).

The changes in the cryosphere, that I described above, induced pronounced changes in the Southern Ocean freshwater balance. Large amounts of additional glacial meltwater entered the coastal ocean of the Amundsen Sea over the last two decades (Sutterley et al., 2014; Paolo et al., 2015), freshening the waters of the continental shelf in this region and in the Ross Sea (Jacobs et al., 2002; Jacobs and Giulivi, 2010). Also the sea-ice changes potentially induce large changes in the surface freshwater balance over large regions of the Southern Ocean coastal and open ocean. However, this contribution has not been adequately quantified yet. Changes in the third surface freshwater flux component, the atmospheric freshwater flux (P-E), are highly uncertain and most

reliable estimates from atmospheric reanalysis do not show significant changes in the atmospheric flux over the Southern Ocean (Bromwich et al., 2011; Nicolas and Bromwich, 2011). However, simulations with global climate models suggest a long-term increase of the excess precipitation over the Southern Ocean with global warming (Knutti and Sedláček, 2013), consistent with an observed decrease in surface salinity over recent decades (Durack et al., 2012).

De Lavergne et al. (2014) suggest that the increased freshening observed over much of the high-latitude Southern Ocean surface waters acted to increase the vertical density stratification. This would imply a reduction in vertical mixing. However, the increased wind-driven mixing, especially in the Polar Frontal Zone, could have acted to deepen the surface mixed layer (Sallée et al., 2010b). Global climate models have generally large biases in the surface mixed-layer depth and tend to simulate a shoaling that is associated with a surface warming (Sallée et al., 2013a).

1.4.2   Changes in ocean circulation & hydrography

In contrast to the surface ocean, much of the Southern Ocean subsurface waters have been warming over recent decades. This warming is most pronounced in the region of AAIW subduction (Gille, 2002; Böning et al., 2008; Schmidtko and Johnson, 2012), suggesting an increased heat uptake by AAIW that is expected with global warming (Cai et al., 2010; Armour et al., 2016). In contrast, some of the warming has also been related to a potential poleward shift of the ACC (Böning et al., 2008; Gille, 2008; Meijers et al., 2011). However, these shifts in the ACC can only explain parts of the subsurface warming in the Atlantic and Indian Ocean sectors, as there are strong regional variations similar to the atmospheric circulation changes (Sokolov and Rintoul, 2009b; Meijers et al., 2011). AAIW did not only warm, but it also significantly freshened over recent decades, with most of the freshening occurring in the Pacific sector (Wong et al., 1999; Böning et al., 2008; Helm et al., 2010; Schmidtko and Johnson, 2012). This freshening has been attributed to changes in the atmospheric freshwater flux, even though simulated changes by global climate models appear to be largely insufficient to explain the recent freshening of AAIW (Wong et al., 1999; Helm et al., 2010).

An additional contribution to the subsurface warming and freshening might be an increased subduction of AAIW and SAMW, even though such a contribution has been debated (Böning et al., 2008). Observational evidence for changes in subduction rates has been very difficult to obtain. Yet, using chlorofluorocarbon (CFC) and sulfur hexafluoride (SF6), Waugh et al. (2013) and Waugh (2014) suggest an increase in AAIW and SAMW subduction due to an increase in westerly winds. This finding is somewhat in conflict with the finding by Helm et al. (2011) that the dissolved oxygen content in AAIW decreased, which could mean that the subduction decreased. Thus, even though there is some evidence for changes in the overturning circulation, there is yet no consensus.

A warming and freshening is also present in the other major water mass that is subducted in the Southern Ocean, AABW (Jullion et al., 2013; Purkey and Johnson, 2013). The freshening of the AABW has been attributed to the increased glacial meltwater from the Antarctic continent that freshens the continental shelf waters (Jacobs et al., 2002; Jacobs and Giulivi, 2010; Purkey and Johnson, 2013; Nakayama et al., 2014). The source of the AABW warming has been less well understood. One potential contribution might be the increased advection of warmer CDW onto the shelf of the Bellingshausen and Amundsen Seas (Schmidtko et al., 2014; Spence et al., 2014). However, AABW is not formed in this region, but rather in the high-latitude embayments of the Weddell and Ross Seas. A more likely explanation is that AABW warming would be related to changes in the gyre circulation or changes in the subduction rates (Meredith et al., 2011a). Using CFCs and SF6, Purkey et al. (2016, Ocean Sciences Meeting) argue that AABW production in the Ross Sea might have decreased. Such a decrease in AABW subduction might occur due to an increased surface buoyancy from glacial meltwater (Williams et al., 2016).

While the potential of changes in Southern Ocean upwelling and subduction to modulate the global climate in the long-term is renowned (sections 1.2 and 1.3), the driving processes are less evident and have been a major incentive to explore the Southern Ocean. To date, two prevailing views on these driving processes exist: A number of studies (Toggweiler and Samuels, 1995; Toggweiler et al., 2006; Russell et al., 2006; Toggweiler and Russell, 2008; Anderson et al., 2009; Sigmond et al., 2011) put forward the theory that long-term changes in the vertical exchange are largely induced by the wind-driven overturning circulation. However, at the dawn of high-resolution ocean circulation models, the response of the overturning circulation to changes in the surface wind field was found to be somewhat less sensitive, i.e. a higher southward eddy transport compensates for at least part of the increased surface northward Ekman transport (Hallberg and Gnanadesikan, 2006; Farneti et al., 2010; Meredith et al., 2012). Indeed, more recent studies show that the eddy kinetic energy in the Southern Ocean increased with increasing winds over recent decades (Hogg et al., 2015; Patara et al., 2016). Such an increased eddy activity could potentially also increase the tracer transport through isopycnal mixing.

An alternative hypothesis is that the vertical mixing and transport in the Southern Ocean can be altered by changes in the vertical density stratification (Hasselmann, 1991; Manabe and Stouffer, 1993; Francois et al., 1997; Sarmiento et al., 1998; Sigman et al., 2004). More recently, this theory found support by conceptual considerations and simple models that the vertical exchange is sensitive to changes in the surface buoyancy fluxes, i.e., the alteration of the surface density through surface heat and freshwater fluxes (Watson and Naveira Garabato, 2006; Morrison et al., 2011; Ferrari et al., 2014; Watson et al., 2015; Sun et al., 2016). Since the density stratification in the Southern Ocean is set up by salinity (section 1.3.2), there are reasonable grounds to believe that surface freshwater fluxes might be a critical controlling factor of changes in upwelling and subduction in the Southern Ocean. Much of the discussion on the influence of changes in surface buoyancy forcing has so far been around past or future changes, but given the potential strong changes in the surface freshwater fluxes over recent decades (section 1.4.1), they might

have influenced changes in upwelling and subduction over recent decades.

1.4.3   Carbon uptake changes

Ultimately, I turn the discussion of changes in the Southern Ocean to changes in the carbon uptake. Due to the anthropogenic increase in atmospheric pCO_2, the Southern Ocean turned from a net carbon source to a net carbon sink (Hoppema, 2004; Gruber et al., 2009) with seasonal outgassing of natural CO_2 that is overcompensated by a seasonal uptake of anthropogenic CO_2 (Hauck et al., 2013; Landschützer et al., 2014b). The subduction of CO_2 with AAIW and SAMW in the Southern Ocean is the most important sink for anthropogenic CO_2 in the global ocean (see Figure 1.1, and section 1.1.1). Multiple concerns have been raised that this sink could weaken with global warming and could have weakened already over recent decades.

One concern is that an acceleration of the upper overturning cell in response to increasing westerly winds could saturate the Southern Ocean carbon sink by upwelling more DIC-rich waters into the surface layer. This argument arose from inverse estimates and modeling studies that seemed to confirm a saturation of the carbon sink over past decades and the upcoming century due to winds (Le Quéré et al., 2007; Lovenduski et al., 2007, 2008; Lovenduski and Ito, 2009; Lenton et al., 2009, 2013; Hauck et al., 2013). Using a model of higher resolution, Dufour et al. (2013) argue that about one third of the outgassing from enhanced Ekman pumping is compensated by enhanced southward eddy transport. This value of eddy compensation might be even larger if one used an even higher resolution than $0.5°$. They further argue that it is actually not only the response of the Ekman pumping that is important for enhanced outgassing under stronger winds but even more so the enhanced mixing at the base of the mixed layer.

Very recent observational studies show that contrary to expectations, the Southern Ocean carbon sink actually strengthened again over the last decade despite a continued strengthening of the westerly winds (Fay et al., 2014; Landschützer et al., 2015b; Munro et al., 2015; Tagliabue and Arrigo, 2016). These studies illustrate that the Southern Ocean carbon sink is much more complex than previously thought. A first long-term observation-based estimate of surface CO_2 fluxes over the Southern Ocean by Landschützer et al. (2015b) shows that the carbon uptake undergoes a large decadal variability with an apparent saturation in the 1990s and a strengthening in the 2000s. They argue that this variability is induced by decadal changes in the zonal asymmetry of the atmospheric circulation, which is consistent with decadal variations found in other variables of the surface climate, such as temperature (Yuan and Yonekura, 2011; Yeo and Kim, 2015; Turner et al., 2016), ACC transport (Meredith et al., 2004, 2011b), and water-mass formation (Santoso and England, 2004; Naveira Garabato et al., 2009; Sallée et al., 2010a; Kwon, 2013). Yet another interesting observation in the longer-term record of surface CO_2 fluxes is that the Southern Ocean carbon sink did not saturate over the past 30 years but actually increased its strength according to what is expected from the increase of atmospheric pCO_2 alone (Landschützer et al., 2015b). This

raises the questions if other mechanisms are at work in the long-term that counter-act a potential saturation due to increasing winds.

Another factor that could alter the carbon uptake by the Southern Ocean is a changing stratification of the surface layer. Even before concerns regarding the effect of changes in winds were raised, simulations with global climate models led to the concern that an increased stratification due to a surface warming in the areas of the subduction could inhibit the uptake of anthropogenic CO_2 (Manabe and Stouffer, 1993; Sarmiento et al., 1998; Bernardello et al., 2014a,b). This reduction in the models occurs largely due to a stabilization of the surface mixed layer and an associated reduced mixing into the subsurface layers from where isopycnal transport could subduct the carbon into deeper layers, i.e. an isolation of the surface layer from the outcropping isopycnals (Caldeira and Duffy, 2000). This hypothesis is in stark contrast to the perception of changes in the natural carbon cycle between glacial–interglacial cycles. It is thought that a warming climate during deglaciations is associated with a decrease in stratification in the high-latitudes and that this decreased stratification actually leads to an increased release of CO_2 to the atmosphere rather than an increased uptake (Francois et al., 1997; Toggweiler, 1999; Sigman and Boyle, 2000; Watson and Naveira Garabato, 2006; Skinner et al., 2010).

The key difference between the two scenarios above is that the former is concerned with changes in the uptake of anthropogenic CO_2 from the atmosphere during the subduction process and the latter with the release of CO_2 to the atmosphere during the upwelling of DIC-rich waters. Consequently, the essential question is where and when an increase in stratification occurs and if the decrease in the outgassing or the decrease in the uptake dominates. Mikaloff Fletcher et al. (2007) and Matear and Lenton (2008) conclude that a reduction in outgassing of natural CO_2 would overwhelm the reduction in uptake of anthropogenic CO_2 leading to a net strengthening of the CO_2 uptake by the Southern Ocean under increased stratification. Nevertheless, before this question can be answered, one has to understand the factors that alter the stratification of the Southern Ocean (section 1.3.2) and how stratification changes alter the pathway of carbon into the Southern Ocean. An answer to this question seems even more pressing when considering that physical changes in the Southern Ocean were found to be very sensitive to the surface freshwater forcing (Hogg, 2010; Morrison et al., 2011; Kjellsson et al., 2015; Stössel et al., 2015) and that these physical changes induce the largest uncertainty in the present and future CO_2 uptake by the ocean, apart from the uncertainty in future emissions (Doney et al., 2004; Hewitt et al., 2016; Kessler and Tjiputra, 2016; Nevison et al., 2016).

1.5   Objectives & approach

After building the case that changes in surface freshwater fluxes might be critical in driving changes in Southern Ocean overturning and stratification and thus might cause changes in the global carbon cycle and surface energy balance, I will formulate the goals of this thesis in this section. **The overarching goal of my thesis is to better understand the sensitivity of the Southern Ocean stratification, circulation, and carbon uptake to changes in the surface freshwater forcing with a focus on the effect of sea-ice changes.**

(1) Very little is known on the type and magnitude of freshwater fluxes in the Southern Ocean. While estimates exist for both the atmospheric freshwater fluxes and the glacial freshwater fluxes and their changes (sections 1.3.2 and 1.4.1), freshwater fluxes from sea ice to the ocean are largely unconstrained. I here intend to quantify surface freshwater fluxes associated with sea-ice formation, transport, and melting and their changes over recent decades. For this purpose, I will derive sea-ice–ocean freshwater fluxes from currently available satellite, in-situ, and reanalysis data and estimate their uncertainties.

(2) The new sea-ice–ocean freshwater flux estimates will allow me to directly compare the individual surface freshwater flux components in the Southern Ocean. I will base the comparison on freshwater flux estimates from atmospheric reanalysis data and estimates of glacial meltwater. Despite potentially large remaining uncertainties, I aim to assess the relative contribution of the freshwater fluxes and their changes to the Southern Ocean salinity distribution. For this purpose, I will use both simple box model considerations and a regional ocean circulation model (ROMS).

(3) The latter involves the goal to set up a model for the Southern Ocean that simulates present-day stratification and circulation as accurately as possible. Therefore, I will use a realistic geographic setting and constrain the model by the observation-based surface fluxes from the atmosphere, and from the sea and land ice.

(4) While the response of the Southern Ocean to changes in the surface wind forcing has been extensively studied (section 1.4.2 and 1.3.1), its response to changes in surface freshwater fluxes has received less attention even though idealized model experiments (Morrison et al., 2011; Watson et al., 2015) and ocean proxy data (Adkins et al., 2002; Sigman et al., 2004) suggest a high sensitivity. This is mostly owing to previously unconstrained surface freshwater fluxes as well as poorly performing models. Using the advances from objectives 1 through 4, I will perform sensitivity experiments with the model to study the response of stratification, temperature, and circulation to changes in the freshwater forcing.

(5) Finally, I will run the model coupled to a biogeochemistry-ecosystem-circulation (BEC) model, to better understand the response of the Southern Ocean carbon release and uptake

in response to changing surface freshwater fluxes and compare this response to the response to the surface wind changes.

I hypothesize that freshwater fluxes associated with sea-ice formation, transport, and melting are a key factor in redistributing salt in the Southern Ocean vertically and horizontally, and thereby establishing the characteristic halocline. An increase in the sea-ice fluxes would lead to an enhanced salt redistribution that strengthens the halocline. Enhanced sea-ice fluxes would result from either a surface cooling or enhanced offshore winds and vice versa. As the sea-ice forms around the Antarctic coast and melts a along the ice edge, an increased flux would make the lower circulation cell, i.e. AABW, saltier and the upper circulation cell, i.e. AAIW and SAMW, fresher. This process would not only strengthen the surface halocline, but it would also enhance the salinity gradient between the deep and the surface ocean. Therefore, the surface waters would decouple from the deep ocean due to a shoaling of the overturning circulation and a reduction of the mixing of deep water into the surface layer. Such a reduced mixing of deep waters into the surface layer would hypothetically lead to a surface cooling, subsurface warming in the open ocean, and an enhanced uptake of carbon by the Southern Ocean mainly through reduced outgassing. These hypotheses seem consistent with some of the observed changes over recent decades (section 1.4). Thus, sea-ice freshwater fluxes might have contributed to some of these changes. In terms of carbon fluxes, a recent increase in stratification might have acted to maintain an efficient uptake of anthropogenic carbon over recent decades despite increasing winds by suppressing the upwelling of carbon-rich deep waters.

1.6   Thesis structure

Apart from the introduction chapter, this thesis consists of four main chapters, a synthesis chapter, and an appendix:

Chapter 2 provides estimates of sea-ice freshwater fluxes due to ice formation, transport, and melting and their changes over the period 1982 through 2008. I provide an estimate of their contribution to the ocean salinity distribution in the Southern Ocean by using a simple box model. This chapter was published as:

Haumann, F. A., N. Gruber, M. Münnich, I. Frenger, S. Kern (2016): Sea-ice transport driving Southern Ocean salinity and its recent trends. *Nature*, 537(7618):89–92. doi:10.1038/nature19101.

Chapter 3 describes the regional ocean circulation model (ROMS) used for chapters 4 and 5 in detail. I will provide an overview on challenges that one faces and considerations to make when modeling the Southern Ocean. I will describe both the physical and biogeochemical components of the model, the model domain and topography, as well as the model forcing at the surface and lateral boundaries. Moreover, in this chapter, I will provide a discussion of the model initialization, spin-up, and drift and a detailed evaluation of the model's mean state using observational data. Parts of this chapter will be published in a condensed form as part of chapter 4.

Chapter 4 examines the impact of changes in surface freshwater fluxes on the Southern Ocean hydrography and circulation. I will perform sensitivity experiments with ROMS by perturbing the different surface freshwater flux components and compare the response to changes induced by the surface momentum fluxes. These perturbations will correspond in terms of their spatial pattern and magnitude to the recently observed changes. I will then assess the resulting changes in salinity, temperature, stratification, and overturning circulation. This will elucidate whether freshwater fluxes could be responsible for some of the observed changes in the Southern Ocean. I will specifically focus on the changes induced by sea-ice–ocean freshwater fluxes. This chapter is in preparation for *Journal of Climate*.

Chapter 5 explores the response of the Southern Ocean CO_2 uptake to the observation-based changes in sea-ice–ocean freshwater fluxes. I will contrast these changes in terms of spatial patterns, and magnitude with changes induced by the surface wind stress that have been the focus of many previous studies. Then, I will contextualize these model-based findings in the light of the recent observation-based estimates of CO_2 fluxes in the Southern Ocean to better understand the observed changes. This chapter is in preparation for a peer-reviewed journal.

Chapter 6 synthesizes the questions that are addressed in each chapter of the this thesis. I will summarize the main findings and conclusions and discuss the limitations arising from the approach. Then, I will relate my findings to the broader picture of the interaction between the ocean circulation, the carbon cycle, and the global climate. This involves implications for the future of the Southern Ocean carbon and heat uptake and for glacial–interglacial variations in

the climate. Finally, I will provide some recommendations for future research activities and for potential improvements in global climate models that could reduce the large uncertainty in their representation of Southern Ocean processes.

Appendix chapter A addresses the question whether the recently observed zonally asymmetric changes in the atmospheric circulation and Antarctic sea ice could be induced by human activity in the form of stratospheric ozone depletion and greenhouse gas increase or are simply a result of multi-decadal natural variations. This question directly relates to the question if the processes described in this thesis are of anthropogenic origin and if they can be expected to continue in future. This chapter was published as:

Haumann, F. A., D. Notz and H. Schmidt (2014): Anthropogenic influence on recent circulation-driven Antarctic sea-ice changes. *Geophysical Research Letters*, 41(23):8429–8437. doi: 10.1002/2014GL061659.

In the course of this thesis, I made additional and directly related contributions to the studies by Stössel et al. (2015) and Landschützer et al. (2015b) that are not included as chapters.

Chapter 2

Sea-ice transport driving Southern Ocean salinity and its recent trends[*]

F. Alexander Haumann[1,2], Nicolas Gruber[1,2], Matthias Münnich[1], Ivy Frenger[1,3], Stefan Kern[4]

[1]Environmental Physics, Institute of Biogeochemistry and Pollutant Dynamics, ETH Zürich, Zürich, Switzerland

[2]Center for Climate Systems Modeling, ETH Zürich, Zürich, Switzerland

[3]Biogeochemical Modelling, GEOMAR Helmholtz Centre for Ocean Research Kiel, Kiel, Germany

[4]Integrated Climate Data Center - ICDC, Center for Earth System Research and Sustainability, University of Hamburg, Hamburg, Germany

Abstract

Recent salinity changes in the Southern Ocean (Wong et al., 1999; Jacobs et al., 2002; Böning et al., 2008; Helm et al., 2010; Durack et al., 2012; Purkey and Johnson, 2013; de Lavergne et al., 2014) are among the most prominent signals in the global ocean, yet their underlying causes have not been firmly established (Wong et al., 1999; Böning et al., 2008; Helm et al., 2010; Purkey and Johnson, 2013). Here, we propose that trends in northward transport of Antarctic sea ice are a major contributor to these changes. Using satellite observations supplemented by sea-ice reconstructions, we estimate that the wind-driven (Holland and Kwok, 2012; Haumann et al., 2014) northward freshwater transport by sea ice increased by 20±10% between 1982 and 2008. The strongest and most robust increase occurred in the Pacific sector coinciding with the largest observed salinity changes (Helm et al., 2010; Durack et al., 2012). We estimate that the additional freshwater for the entire northern sea-ice edge entails a freshening rate of -0.02 ± 0.01 g kg^{-1} per decade in open ocean surface and intermediate waters, similar to the observed freshening (Wong et al., 1999; Jacobs et al., 2002; Böning et al., 2008; Helm et al., 2010; Durack et al., 2012). The enhanced rejection of salt near the coast of Antarctica associated with stronger sea-ice export counteracts regionally the freshening of continental shelf (Jacobs et al., 2002; Jacobs and Giulivi, 2010; Nakayama et al., 2014) and newly formed bottom waters (Purkey and Johnson, 2013) due to the increasing addition of glacial meltwater (Paolo et al., 2015). Although the data sources underlying our results have substantial uncertainties, regional analyses (Drucker et al., 2011) and independent data from an atmospheric reanalysis support our conclusions. Our finding that northward sea-ice freshwater transport is a key determinant of the Southern Ocean salinity distribution also in the mean state further underpins the importance of the sea-ice induced freshwater flux. Through its influence on the oceans density structure (Sigman et al., 2010), this process has critical consequences for the global climate by affecting the deep-to-surface ocean exchange of heat, carbon, and nutrients (Sigman et al., 2010; Ferrari et al., 2014; Frölicher et al., 2015; Landschützer et al., 2015b).

2.1 Article

Observations of salinity in the Southern Ocean over the last decades have revealed a substantial, wide-spread freshening in both coastal (Jacobs and Giulivi, 2010; Hellmer et al., 2011) and open ocean surface waters (Jacobs et al., 2002; Durack et al., 2012) as well as in the water masses sourced from these regions (Wong et al., 1999; Böning et al., 2008; Helm et al., 2010; Purkey and Johnson, 2013). In particular, Antarctic Intermediate Water (AAIW) and Subantarctic Mode Water (SAMW) freshened at a rate between -0.01 and -0.03 g kg^{-1} per decade during the second half of the 20th century (Wong et al., 1999; Böning et al., 2008; Helm et al., 2010). In the Pacific and Indian Ocean sectors, continental shelf waters and Antarctic Bottom Water (AABW) also freshened substantially (Jacobs et al., 2002; Jacobs and Giulivi, 2010; Purkey and Johnson, 2013), while in the Atlantic this freshening was smaller (Purkey and Johnson, 2013; Hellmer et al., 2011). These salinity changes have been attributed to increased surface freshwater fluxes, stemming either from enhanced Antarctic glacial melt (Jacobs et al., 2002; Jacobs and Giulivi, 2010; Purkey and Johnson, 2013; Nakayama et al., 2014; Paolo et al., 2015) or from increased atmospheric freshwater fluxes, as a result of an excess of precipitation over evaporation (Wong et al., 1999; Durack et al., 2012). Glacial meltwater (Paolo et al., 2015) most likely freshened coastal waters in the Amundsen and Ross Seas (Jacobs et al., 2002; Jacobs and Giulivi, 2010; Nakayama et al., 2014), but the freshening signal in AABW, which is formed in this region, is much smaller than expected (Purkey and Johnson, 2013). In contrast, in the open Southern Ocean, increases in the atmospheric freshwater flux as simulated by global climate models appear to be largely insufficient to explain the recent freshening of AAIW (Wong et al., 1999; Helm et al., 2010).

Changes in northward sea-ice transport could possibly contribute to the wide-spread salinity changes in the Southern Ocean (Holland and Kwok, 2012). This process acts as a lateral conveyor of freshwater by extracting freshwater from the coastal regions around Antarctica where sea ice forms and releasing it at the northern sea-ice edge where sea ice melts (Figure 2.1; Saenko et al., 2002; Komuro and Hasumi, 2003; Kirkman and Bitz, 2011). Despite substantial wind-driven changes in sea-ice drift over the last few decades (Holland and Kwok, 2012; Haumann et al., 2014), this contribution has not been quantified yet. Here, we suggest that surface freshwater fluxes induced by a stronger northward sea-ice transport are a major cause for the observed salinity changes in recent decades. The large contribution of freshwater transport by sea ice to the salinity trends is corroborated by our finding that this process plays a key role for the climatological mean salinity distribution.

Our conclusions are based on basin-scale estimates of annual net sea-ice-ocean freshwater fluxes and annual northward transport of freshwater by sea ice over the period 1982 through 2008. Further evidence in support is provided by our assessment of atmospheric reanalysis data (Dee et al., 2011) and results from another regional study (Drucker et al., 2011). We derived the sea-
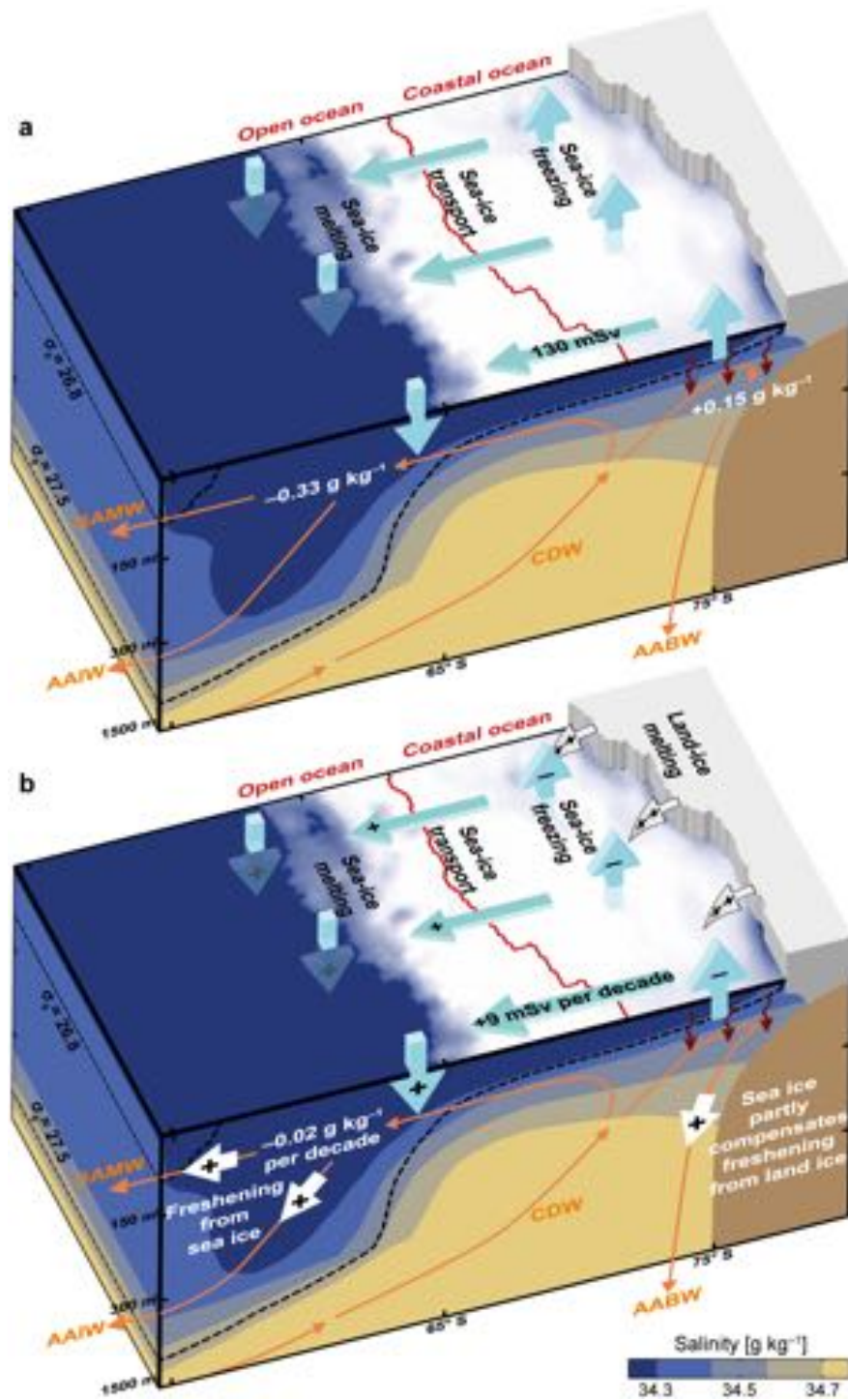
Figure 2.1   Effect of northward sea-ice freshwater transport on Southern Ocean salinity:
Schematic cross-section illustrating the effect of northward sea-ice freshwater transport (blue arrows) on (**a**) mean ocean salinity and (**b**) on the trends over the period 1982 through 2008 (section 2.2.11). The red line separates the open and coastal ocean regions. The increasing sea-ice transport freshened the open ocean and, by leaving the salt behind in the coastal region (red curved arrows), compensated for part of the freshening by enhanced glacial meltwater input (gray arrows). White arrows indicate the freshening effect from both sea ice and land ice. Positive fluxes are defined downward or northward. The background shows mean salinity (in color) and density (dashed black lines) separating Circumpolar Deep Water (CDW) from Antarctic Intermediate Water (AAIW) and Subantarctic Mode Water (SAMW). Orange arrows: ocean circulation; AABW: Antarctic Bottom Water.

ice related freshwater fluxes by combining sea-ice concentration, drift, and thickness data and by using a mass-balance approach of the sea-ice volume divergence and local change (section 2.2.5). The analyzed sea-ice concentration stems from satellite observations (Meier et al., 2013b, section 2.2.2, Figure 2.5) and its thickness from a combination of satellite data (Kurtz and Markus, 2012) and a model-based sea-ice reconstruction that assimilates satellite data (Massonnet et al., 2013, section 2.2.3, Figure 2.6). The sea-ice volume divergence was computed from satellite-based sea-ice drift vectors (Fowler et al., 2013b, section 2.2.4, Figures 2.7 and 2.8) and sea-ice volume. From the resulting sea-ice volume budget, we finally estimated the freshwater equivalents of local annual sea-ice-ocean fluxes due to freezing and melting and annual lateral sea-ice transport (sections 2.2.5 and 2.2.6).

Uncertainties in these derived freshwater flux products are substantial (section 2.2.8). A major challenge arises from the need to combine sea-ice drift estimates from different satellites in order to estimate trends. We addressed potential inhomogeneities and biases by vigorous data quality control, several corrections, and considering different time periods (section 2.2.7). A second challenge is associated with the relatively limited number of observations of sea-ice thickness. These uncertainties plus the observationally constrained range of the other input quantities entered our error estimates of the final freshwater flux product (Tables 2.1 and 2.2). In the Atlantic sector, uncertainties associated with the mean sea-ice thickness distribution dominate the uncertainty, while in the Pacific sector, uncertainties are mostly caused by uncertainties in sea-ice drift.

Our analysis reveals large trends in the meridional sea-ice freshwater transport in the Southern Ocean between 1982 and 2008 (Figures 2.1b and 2.2c) affecting the regional sea-ice-ocean freshwater fluxes (Figure 2.2d). The annual northward sea-ice freshwater transport of 130 ± 30 mSv (1 milli-Sverdrup = 10^3 m^3 s^{-1} $\approx$ 31.6 Gt yr^{-1}; Figure 2.2a; Table 2.1) from the coastal to the open ocean region strengthened by $+9\pm5$ mSv per decade (Table 2.2). Here, the coastal ocean refers to the region between the Antarctic coast and the zero sea-ice-ocean freshwater flux line, and the open ocean is the region between the zero sea-ice-ocean freshwater flux line and the sea-ice edge (Figure 2.2b). The increased northward transport caused, on average, an additional extraction of freshwater from the coastal ocean of -40 ± 20 mm yr^{-1} per decade and an increased addition to the open ocean region of $+20\pm10$ mm yr^{-1} per decade.

The overall intensification occurred primarily in the Pacific sector where we find a vigorous northward freshwater transport trend of $+14\pm5$ mSv per decade. The trends in this sector are the most robust ones (Table 2.3). Over the whole period, this change in the Pacific sector corresponds to an increase of about 30% with respect to the climatological mean in the entire Southern Ocean (Table 2.1). Largest trends occurred locally in the high-latitude Ross Sea (Figure 2.2d), where our estimated trends agree well with a previous study (Drucker et al., 2011, section 2.2.9). The increase in the Pacific sector is partly compensated for by small decreases in the Atlantic and Indian Ocean sectors. We reach similar conclusions when we consider only the satellite data
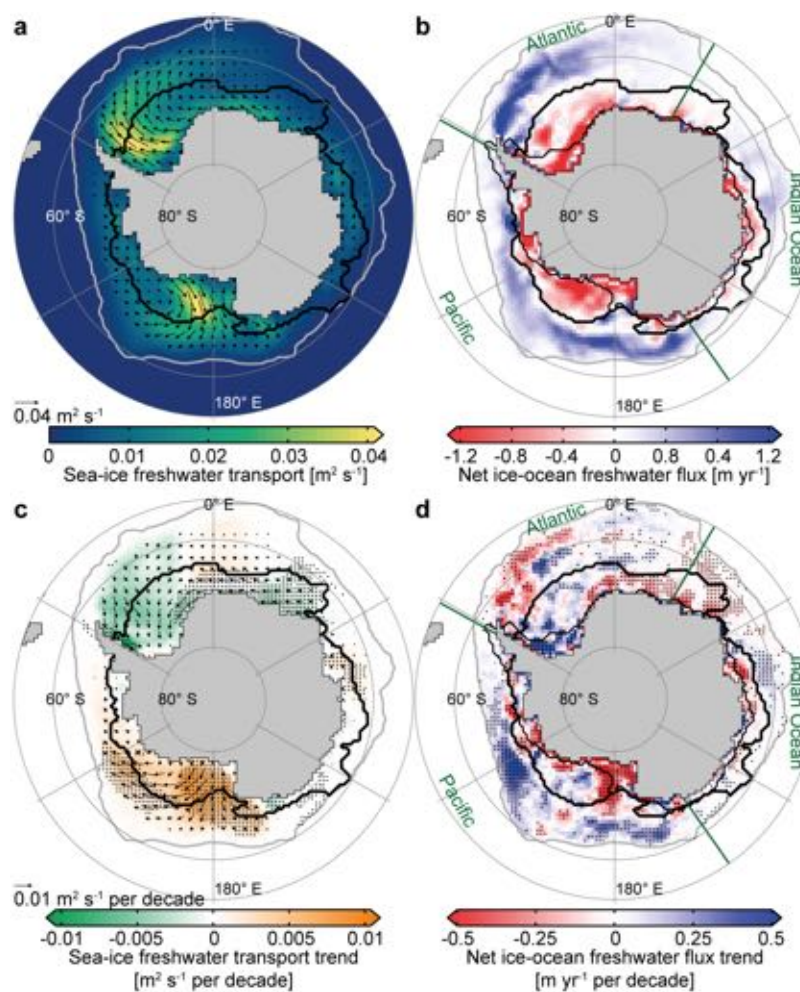
Figure 2.2   Mean state and trends of net annual freshwater fluxes associated with sea ice over the period 1982 through 2008: (**a**) Mean sea ice induced freshwater transport. (**b**) Mean net sea-ice-ocean freshwater flux. (**c, d**) Linear trends of northward sea-ice freshwater transport (c) and net sea-ice-ocean freshwater flux from freezing and melting (d). Stippled trends are significant at the 90% level (section 2.2.8). Arrows: (a) mean and (c) trend of the annual transport vectors; thick black lines: zero sea-ice-ocean freshwater flux line dividing the coastal from the open ocean regions; thin black lines: continental shelf (1000-m isobath); gray lines: sea-ice edge (1% sea-ice concentration); green lines: basin boundaries.

from 1992 through 2004, i.e., the period when they are least affected by potential inhomogeneities (Table 2.3).

The reason for the observed northward sea-ice freshwater transport and its recent trends is the strong southerly winds over the Ross and Weddell Seas, which persistently blow cold air from Antarctica over the ocean, pushing sea ice northward (Haumann et al., 2014). The winds over the Ross Sea considerably strengthened in recent decades, possibly due to a combination of natural, multi-decadal variability, changes in greenhouse gases, and stratospheric ozone depletion (Haumann et al., 2014). These changes in southerly winds induced regional changes in northward sea-ice drift (Holland and Kwok, 2012; Haumann et al., 2014), which are responsible for the sea-ice freshwater transport trends (sections 2.2.3, 2.2.6, and 2.2.10). This relation between the atmospheric circulation and sea-ice drift changes enabled us to independently esti-

mate the sea-ice drift anomalies using sea-surface pressure gradients along latitude bands from
atmospheric reanalysis data (Dee et al., 2011, section 2.2.10). Comparing the resulting northward
sea-ice transport anomalies to the satellite-based estimates across the same latitude bands, results
in a similar overall trend (Figure 2.3). Thus, this alternative approach not only corroborates our
estimated long-term trend, but it also suggests that any remaining inhomogeneities in the sea-ice
drift data due to changes in the satellite instruments are comparably small after applying multiple
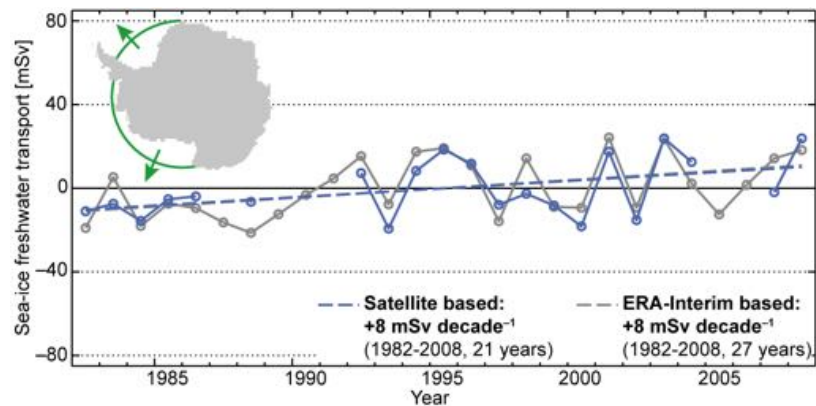corrections (sections 2.2.4 and 2.2.7).

**Figure 2.3 Time series of annual northward sea-ice freshwater transport anomalies across
latitude bands:** The underlying sea-ice drift data are based on two independent data sources, i.e.,
the corrected NSIDC satellite data (blue; only consistent years) and zonal sea-level pressure gradi-
ents from ERA-Interim data (gray; section 2.2.10). Dashed lines show the respective linear regres-
sions. Inserted map shows the latitude bands in the Atlantic (69.5° S) and Pacific (71° S) sectors.

To assess how the changing sea-ice-ocean freshwater flux (Figure 2.2d) affected the salinity in
the Southern Ocean, we assumed that the additional freshwater in the open ocean region entered
AAIW and SAMW formed from upwelling Circumpolar Deep Waters (CDW; Abernathey et al.,
2016; Talley, 2013, section 2.2.11). We find that our freshwater flux trends imply a freshening at
a rate of -0.02 ± 0.01 g kg^{-1} per decade in the surface waters that are transported northward and
form AAIW and SAMW (Figure 2.1b). Thus, the sea-ice freshwater flux trend could account for
a substantial fraction of the observed long-term freshening in these water masses (Wong et al.,
1999; Böning et al., 2008; Helm et al., 2010). The strong sea-ice-ocean freshwater flux trends
in the Pacific sector (Figure 2.2d) spatially coincide with the region of largest observed surface
freshening (Figure 2.12; Jacobs et al., 2002; Durack et al., 2012) and can explain also the stronger
freshening of the Pacific AAIW as compared to that of the Atlantic (Wong et al., 1999; Helm et al.,
2010). A more quantitative attribution of the observed salinity trends to the freshwater transport
trends is beyond the scope of our study because the observed freshening trends stem from different
time periods, and have strong regional variations and large uncertainties themselves (Wong et al.,
1999; Böning et al., 2008; Helm et al., 2010). However, our data show that changes in northward
sea-ice freshwater transport induce salinity changes of comparable magnitude to the observed
trends.

Our estimates in coastal regions (Figure 2.2d) also help to explain the observed salinity

changes in AABW (Purkey and Johnson, 2013), which is sourced from this region. Additional glacial meltwater from West Antarctica (Paolo et al., 2015) strongly freshened the continental shelf in the Ross and Amundsen Seas over recent decades (Jacobs et al., 2002; Jacobs and Giulivi, 2010; Nakayama et al., 2014, Figure 2.1b). However, the observed freshening in Pacific and Indian Ocean AABW was found to be much smaller than expected by this additional glacial meltwater (Purkey and Johnson, 2013). Our data suggests that the freshening induced by the increasing glacial meltwater is substantially reduced by a salinification from an increased sea-ice to ocean salt flux over the continental shelf in the Pacific sector. This salt flux trend corresponds to a freshwater equivalent of -10 ± 3 mSv per decade, resulting from an increasing northward sea-ice export from this region of enhanced sea-ice formation (Figure 2.2c-d). In contrast, over the continental shelf in the Atlantic sector, our data suggests a decreasing sea-ice to ocean salt flux, corresponding to a freshwater equivalent of $+6\pm3$ mSv per decade, which may have contributed to the observed freshening of the newly formed Atlantic AABW (Purkey and Johnson, 2013) and the north-western continental shelf waters (Hellmer et al., 2011).

The large contribution of trends in sea-ice freshwater transport to recent salinity changes in the Southern Ocean is in line with the dominant role that sea ice plays for the surface freshwater budget in the seasonal sea-ice zone (Tamura et al., 2011) and for the global overturning circulation (Saenko et al., 2002; Komuro and Hasumi, 2003; Kirkman and Bitz, 2011; Abernathey et al., 2016) in the mean state. The freshwater equivalent of the total Southern Ocean sea-ice melting flux (Figure 2.4a) is as large as 460 ± 100 mSv (Table 2.1). On an annual basis, the vast majority of this melting flux is supported by the freezing of seawater of -410 ± 110 mSv, with the remaining flux arising from snow-ice formation (Massom et al., 2001, section 2.2.3). Most of the sea ice is produced in the coastal region (-320 ± 70 mSv), but only about 60% of the sea ice also melts there. The rest, i.e., 130 ± 30 mSv is being exported to the open ocean (Figure 2.4c). These mean estimates agree well with an independent study carried out in parallel to this study (Abernathey et al., 2016), which is based on the assimilation of Southern Ocean salinity and temperature observations (section 2.2.9).

The process of northward freshwater transport by sea ice effectively removes freshwater from waters entering the lower oceanic overturning cell, in particular AABW, and adds it to the upper circulation cell, especially AAIW (Figure 2.1a). Hereby, the salinity difference between these two water masses and thus the meridional and vertical salinity gradients increase. In steady state, the northward sea-ice freshwater transport of 130 ± 30 mSv implies a salinity modification of $+0.15\pm0.06$ g kg^{-1} and -0.33 ± 0.09 g kg^{-1} in waters entering the lower and upper cell, respectively (section 2.2.11). The latter suggests that sea-ice freshwater transport accounts for the majority of the salinity difference between upwelling CDW and the exiting AAIW. We estimated that the salinification from sea ice in waters entering the lower circulation cell is compensated for by glacial meltwater and by an excess precipitation over evaporation in this region at about equal parts, agreeing with the very small salinity difference between CDW and AABW (section 2.2.11).
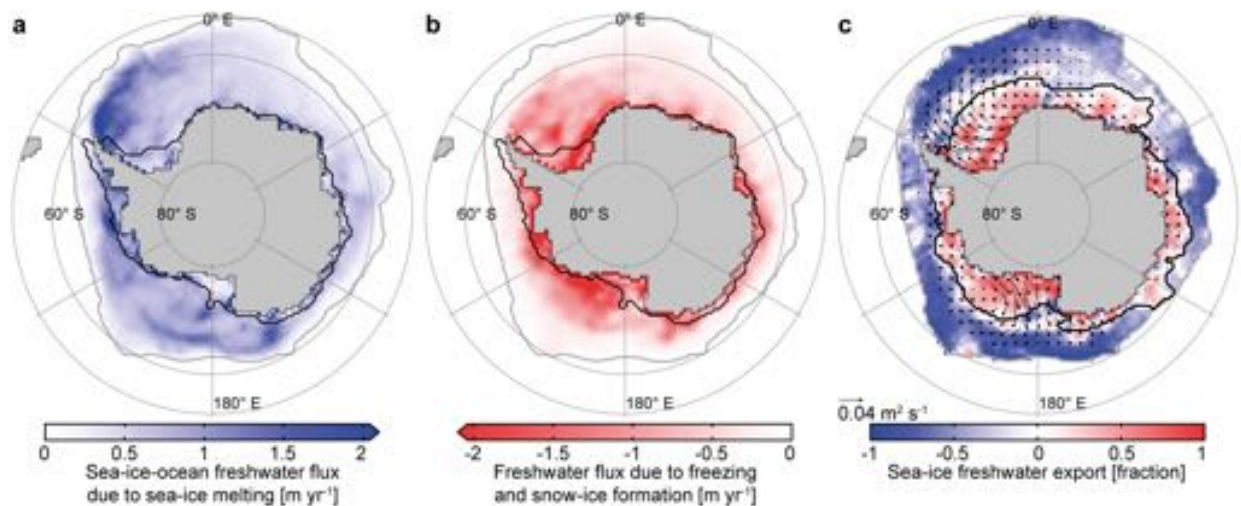
Figure 2.4   Mean annual sea-ice related freshwater fluxes associated with melting, freezing, and transport over the period 1982 through 2008: (**a**) Sea-ice-ocean freshwater flux due to melting. (**b**) Freshwater flux associated with freezing and snow-ice formation. (**c**) Fraction of freshwater exported relative to local freezing flux (red) and imported relative to the local melting flux (blue) due to sea-ice induced freshwater transport (arrows). Black and gray lines as in Figure 2.2.

Because salinity dominates the density structure in polar oceans (Sigman et al., 2010), our findings imply that sea-ice transport is a key factor for the vertical and meridional density gradients in the Southern Ocean and their recent changes (Figure 2.1). This interpretation is consistent with the observation that large areas of the upper Southern Ocean not only freshened but also stratified in recent decades (de Lavergne et al., 2014). Increased stratification potentially hampers the mixing of deeper, warmer, and carbon-rich waters into the surface layer and thus could increase the net uptake of CO_2 (Sigman et al., 2010; Frölicher et al., 2015; Landschützer et al., 2015b). Consequently, our results suggest that Antarctic sea-ice freshwater transport, through its influence on ocean stratification and the carbon cycle, is more important for changes in global climate (Sigman et al., 2010; Ferrari et al., 2014) than has been appreciated previously. This implication of our findings for the climate system stresses the urge to better constrain spatial patterns as well as temporal variations of sea-ice-ocean fluxes by reducing uncertainties in observations of drift, thickness, and snow cover of Antarctic sea ice.

2.2 Methods

2.2.1 Data

Satellite-derived sea-ice concentration stems from the Climate Data Record (CDR, version 2; 1980 to 2009; http://dx.doi.org/10.7265/N55M63M1; Meier et al., 2013b) that comprises data from the NASA Team algorithm (NTA; Cavalieri and Parkinson, 2008) and the Bootstrap algorithm (BA; version 2; Comiso, 1986), as well as a merged data set. Sea-ice thickness data stems from a reconstruction with the ocean-sea-ice model NEMO-LIM2 (1980 to 2009; Massonnet et al., 2013), from the laser altimeter ICESat-1 (2003 to 2008; http://seaice.gsfc.nasa.gov; Kurtz and Markus, 2012), as well as from ship-based observations (ASPeCt; 1980 to 2005; http://aspect. antarctica.gov.au; Worby et al., 2008). Satellite-derived sea-ice drift stems from the National Snow and Ice Data Center (NSIDC, version 2; 1980 to 2009, http://nsidc.org/data/nsidc-0116; Fowler et al., 2013b) and is corrected by drifting buoy data (1989 to 2005; Schwegmann et al., 2011). We used an alternative sea-ice drift product for the uncertainty estimation (1992 to 2003; http://rkwok.jpl.nasa.gov; Kwok et al., 1998; Kwok, 2005). Additionally, we used daily atmospheric sea-level pressure, surface air temperature, and 10-m wind speed from the ERA-Interim reanalysis (1980 to 2009; http://apps.ecmwf.int; Dee et al., 2011). We provide a detailed description of the data processing in the corresponding sections below.

2.2.2 Sea-ice concentration

We used all three sea-ice concentration products available from the CDR (Meier et al., 2013b, section 2.2.1). If any of the grid points in either the merged, NTA, or BA product shows 0% sea-ice concentration, all products are set to 0% sea-ice concentration. We used a first order conservative remapping method from the Climate Data Operators (CDO, 2015, version 1.6.8) to interpolate the sea-ice concentration to the sea-ice drift grid. The BA performs superior compared to the NTA around Antarctica as the NTA underestimates sea-ice concentrations by 10% or more (Figures 2.5a-b; Comiso et al., 1997; Meier et al., 2013b). Therefore, we primarily used the BA product. However, BA potentially underestimates sea-ice concentration in presence of thin sea ice and leads (Comiso et al., 1997; Meier et al., 2013b). Therefore, we used the merged product that should be more accurate in these regions (Meier et al., 2013b) to estimate the uncertainties. Generally, sea-ice concentration is the best constrained of the three sea-ice variables. Its contribution to the climatological mean flux uncertainty is below 1% (Table 2.1). To obtain the uncertainty in the freshwater flux trends, we additionally used the NTA because differences in the Antarctic sea-ice area trends between the BA and NTA have been reported (Eisenman et al., 2014). Differences between the BA and NTA sea-ice concentration trends range from 10% to 20% relative to the actual trend (Figures 2.5c-d). The associated uncertainties in the spatially integrated sea-ice
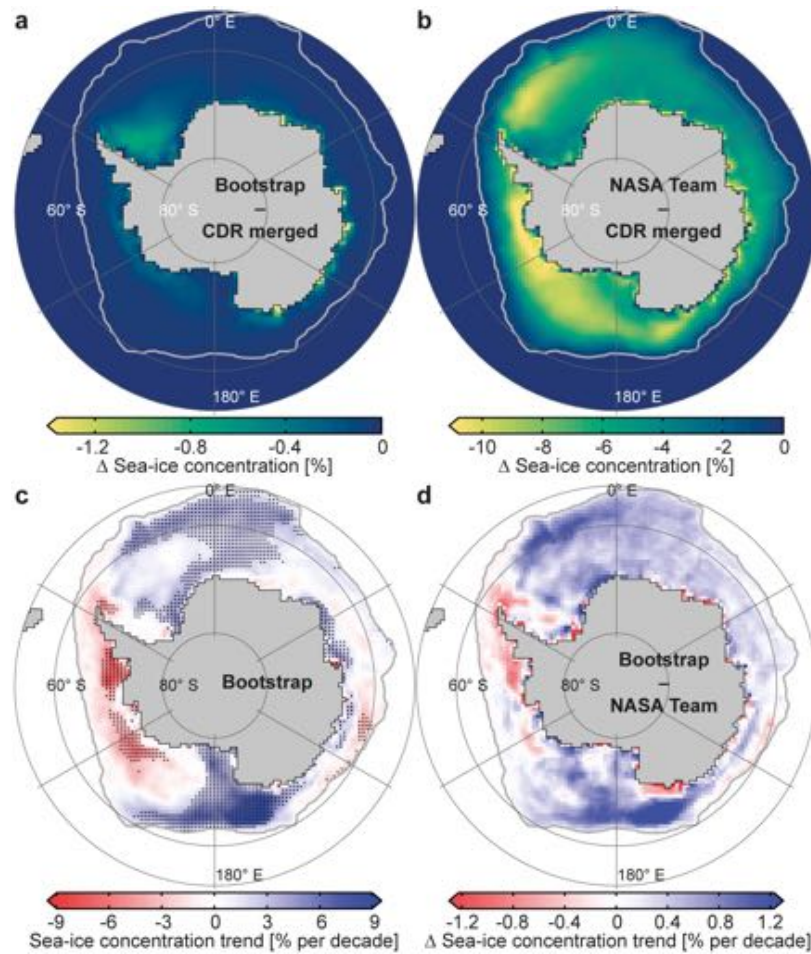
freshwater flux trends are about 10% (Table 2.2).

Figure 2.5   Uncertainties and trends in Antarctic sea-ice concentration over the period 1982 through 2008: (**a**) Bootstrap (BA) minus CDR merged data. (**b**) NASA Team (NTA) minus CDR merged data. (**c**) Decadal trends of the BA sea-ice concentration. Stippled trends are statistically significant (at least 90% level). (**d**) Decadal trends of Bootstrap minus NASA Team data. The thick gray line marks the mean sea-ice edge (1% sea-ice concentration).

2.2.3   Sea-ice thickness

Sea-ice thickness data spanning our entire analysis period do not exist, mostly owing to challenges in remote sensing of Antarctic sea-ice thickness (Kern and Spreen, 2015). Therefore, we used a sea-ice thickness reconstruction (Massonnet et al., 2013, section 2.2.1) from a model that assimilated the observed sea-ice concentration. Through the assimilation, the model constrained air-sea heat fluxes, improving the spatial and temporal variability of sea-ice thickness. The model did not assimilate sea-ice thickness observations themselves. Sea-ice thickness, as we use it here, is not weighted with sea-ice concentration and does not include the snow layer.

The reconstruction overestimates the sea-ice thickness in the central Weddell and Ross Seas and underestimates it in some coastal regions compared to the ICESat-1 (Kurtz and Markus, 2012) and ASPeCt (Worby et al., 2008) data sets (section 2.2.1; Figure 2.6). To compare the different

sea-ice thickness data sets, we interpolated the reconstruction, ICESat-1, and ASPeCt data to the sea-ice drift grid using CDO (2015) distance-weighted averaging. For our best estimate of the sea-ice freshwater fluxes, we applied a weighted bias correction to the reconstruction using the spatially gridded version of the ICESat-1 data (see below). Both the ICESat-1 and ASPeCt data sets are potentially biased low, particularly in areas with thick or deformed sea ice (Worby et al., 2008; Kwok and Maksym, 2014; Kern and Spreen, 2015; Williams et al., 2015), where we found the largest differences between these two data sets and the uncorrected reconstruction. Thus, the thicker sea ice in the Weddell Sea in the uncorrected reconstruction might yet be realistic, especially when considering alternative ICESat-1 derived estimates for this region (Kern and Spreen, 2015; Yi et al., 2011; Kern et al., 2016). To capture the full uncertainty range associated with the mean sea-ice thickness distribution, we used the difference between the uncorrected reconstruction and the ICESat-1 data. Uncertainties in sea-ice thickness dominate the climatological freshwater flux uncertainties in the Atlantic and Indian Ocean sectors, ranging from 10% to 35%, and are also substantial in all other regions and for the overall trends (Tables 2.1 and 2.2).

For the correction of the mean sea-ice thickness distribution, we first calculated relative differences to ICESat-1 whenever data were available. Then, we averaged all differences that were within two standard deviations over time. We applied this average, relative bias correction map to the data at each time step. To ensure that local extremes were not exaggerated, we used weights. Weights were one for a sea-ice thickness of 1.2 m, i.e., the full bias correction was applied, and decreased to zero for sea-ice thicknesses of 0.2 m and 2.2 m, i.e., no bias correction was applied. We derived these thresholds empirically to reduce biases with respect to the non-gridded ICESat-1 and ASPeCt data (Figure 2.6). Trends in the reconstruction remain largely unaffected by the bias correction (comparing Figure 2.6a and the original trend by Massonnet et al. (2013)).

Local extremes in the sea-ice thickness reconstruction, caused by ridging events, are most likely inconsistent with the observed sea-ice drift and would lead to unrealistic short-term variations in our final fluxes. However, when considering net annual melting and freezing fluxes and averages over large areas these variations cancel. To reduce the noise in our data set, we filtered extremes with a daily sea-ice thickness anomaly larger than 2 m with respect to the climatological seasonal cycle, representing only 0.1% of all data points. These and other missing grid points (in total 2.6%) were interpolated by averaging the neighboring grid points. We also calculated our sea-ice freshwater fluxes based on the unfiltered data and included these fluxes in our uncertainty estimate.

Snow-ice formation due to flooding and refreezing (Massom et al., 2001; Maksym and Markus, 2008) is part of the estimated sea-ice thickness. As snow-ice forms partly from the atmospheric freshwater flux and not from the ocean alone, it could lead to an overestimation of the total ocean to sea-ice freshwater flux due to freezing. The amount of snow-ice formation is highly uncertain (Massom et al., 2001; Maksym and Markus, 2008) but within the uncertainty of the sea-ice thickness. To account for this process, we reduced the freezing fluxes according to snow-ice formation
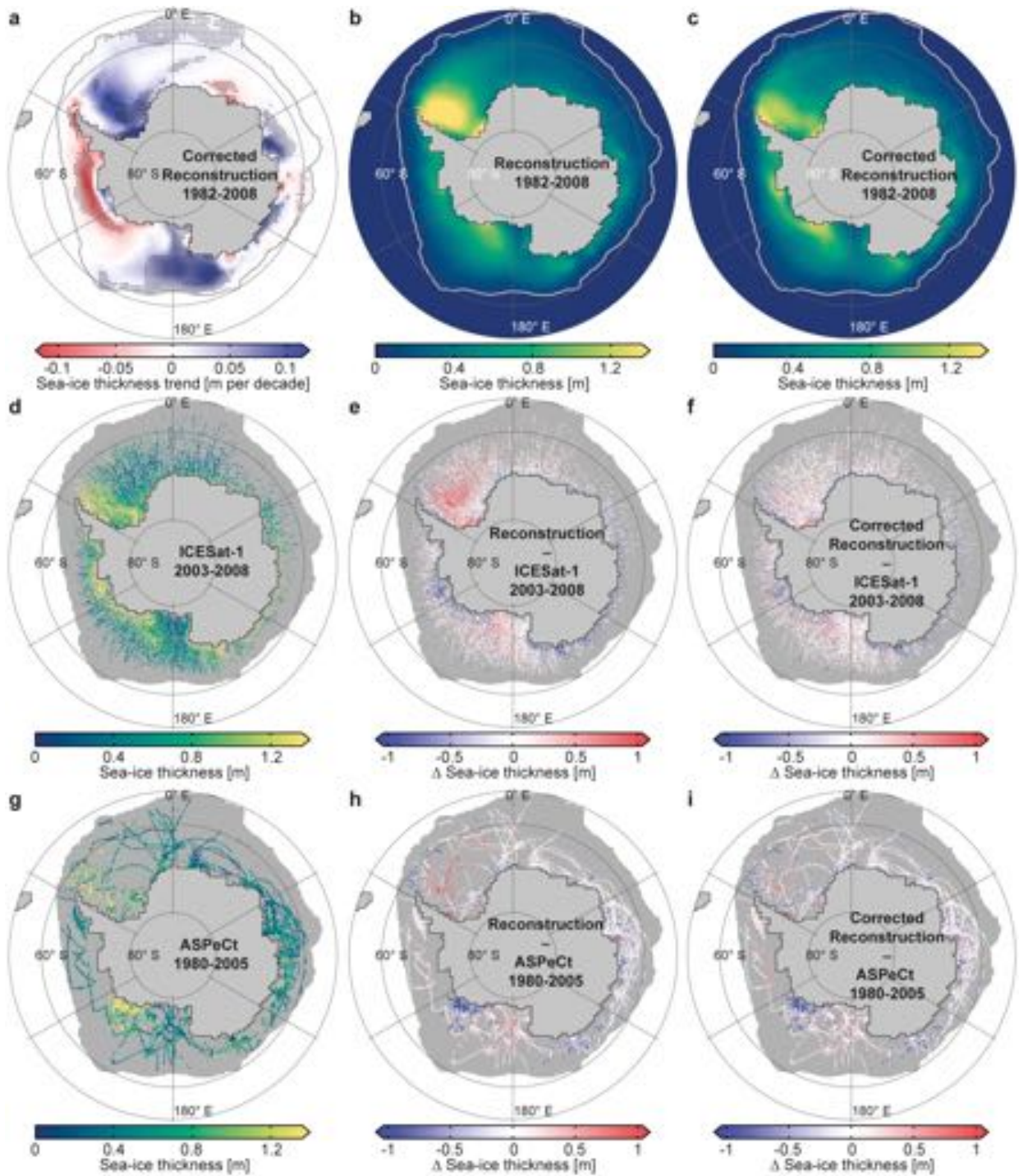
Figure 2.6   Mean, trend, and uncertainty of Antarctic sea-ice thickness: (**a**) Decadal trends of the corrected reconstruction (1982–2008). Stippled trends are statistically significant (at least 90% level). (**b**) Mean of the reconstruction (1982–2008). (**c**) Mean of the corrected reconstruction (1982–2008). (**d**) Mean of the non-gridded ICESat-1 data (2003–2008, 13 campaigns). (**e**) Reconstruction minus non-gridded ICESat-1 data (2003–2008). (**f**) Corrected reconstruction minus non-gridded ICESat-1 data (2003–2008). (**g**) Mean of the ASPeCt data (1980–2005). (**h**) Reconstruction minus ASPeCt data (1980–2005). (**i**) Corrected reconstructions minus ASPeCt data (1980–2005). The thick gray line marks the mean sea-ice edge (1% sea-ice concentration). Differences are based on data when both respective products were available. Data points without data in the sea-ice covered region are gray shaded in d–i.

estimates from the reviewed literature (Massom et al., 2001). In the Atlantic, Indian Ocean, and Pacific sectors, we applied approximate snow-ice formation rates of 8±8%, 15±15%, and 12±12% of the freezing flux, respectively (Massom et al., 2001). In the entire Southern Ocean, the amount of snow that is transformed to ice would thus amount to about 50 mSv, or about 35% of the suggested atmospheric freshwater flux onto Antarctic sea ice (Abernathey et al., 2016).

Trends in sea-ice thickness (Figure 2.6a) are highly uncertain but broadly agree among different modeling studies (Massonnet et al., 2013; Zhang, 2014; Holland, 2014). To show that our results are robust with respect to the less certain trends or short-term variations in sea-ice thickness, we compared our estimated transport trends across the latitude bands (equation 2.3) with a sensitivity analysis, where we kept the sea-ice thickness constant. The resulting transport trends across the latitude bands of about 6 mSv per decade in the Atlantic sector and about +11 mSv per decade in the Pacific sector are still within our estimated uncertainty (Table 2.2). Most of the sea-ice thickness trends (Figure 2.6a) occur either north (Pacific sector) or south (Atlantic sector) of the zero freshwater flux line or latitude bands. Thus, the trend in sea-ice thickness does not considerably affect the northward sea-ice freshwater transport trend. However, the mean sea-ice thickness uncertainty at the zero freshwater flux line is the largest contributor to the overall northward sea-ice freshwater transport trend (Table 2.2).

2.2.4   Sea-ice drift

We used the gridded version of the NSIDC (Fowler et al., 2013b, section 2.2.1) sea-ice drift data set. In the Antarctic, it is based on five passive microwave sensors (Emery et al., 1995, 1997) and the Advanced Very High Resolution Radiometer (AVHRR; Maslanik et al., 1997) data (Figure 2.8). Two studies validated this data set with buoy data in the Weddell Sea (Schwegmann et al., 2011, 1989 through 2005) and around East Antarctica (Heil et al., 2001, 1985 to 1997). There is a very high correlation between the buoy and the satellite data on large temporal and spatial scales, i.e., monthly and regional, and a strongly reduced agreement on smaller scales, i.e., daily and local (Heil et al., 2001; Schwegmann et al., 2011). The satellite-derived sea-ice drift underestimates the sea-ice velocity given by the buoys by 34.5% (Schwegmann et al., 2011), i.e., faster drift velocities have a larger bias (Sumata et al., 2014). The bias is smaller for the meridional (26.3%) than for the zonal drift (Schwegmann et al., 2011). We here corrected for these low biases by multiplying the drift velocity with the correction factor (1.357) that corresponds to the meridional drift bias (Schwegmann et al., 2011). We argue that the meridional component of the bias is the better estimate in the central sea-ice region, which is the key region for our results. Here, the drift is mainly meridional. The larger biases are observed in the swift, mostly zonal drift along the sea-ice edge causing the larger zonal biases. The spatial dependence of the bias and our correction imply that larger biases and uncertainties remain in our final product around the sea-ice edge.

We further processed this bias-corrected drift data. First, we removed all data flagged as

bad in the product. Second, we removed any data with sea-ice concentrations below 50%, closer than 75 km to the coast (Schwegmann et al., 2011), or with a spurious, exact value of zero. Our results are not sensitive to this filtering but it reduces the spatial and temporal noise. After these modifications, about 75% of all grid cells covered by sea ice had an associated drift vector.
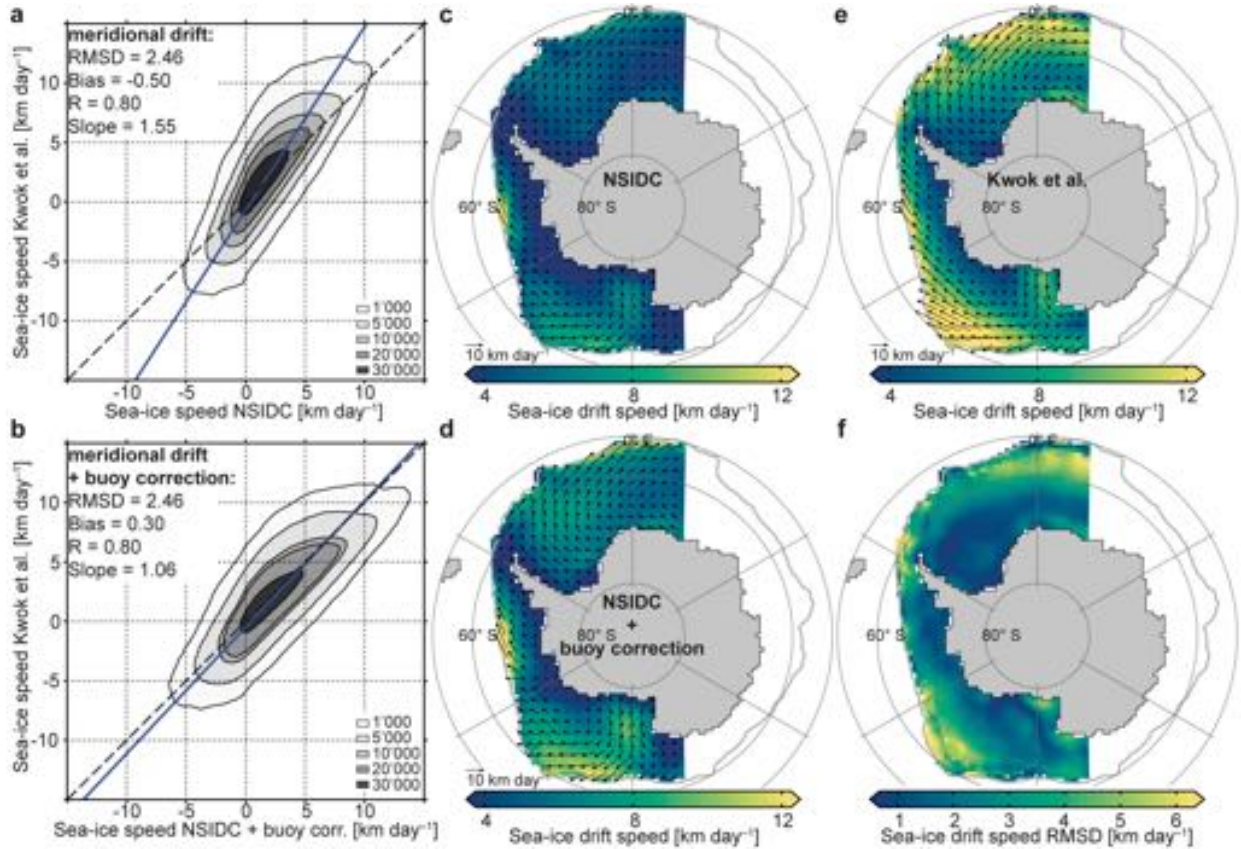

Figure 2.7   Sea-ice drift speed comparison between the NSIDC and Kwok et al. data for the period 1992 to 2003: (**a, b**) Low-pass filtered, 21-day running mean, (a) original and (b) bias-corrected daily meridional NSIDC sea-ice drift speed compared to the low-pass filtered daily meridional Kwok et al. data. Contours mark the number of grid boxes and the blue line marks the fitted least squares linear regression line. (**c-e**) Mean sea-ice drift speed of the (c) original and (d) bias-corrected NSIDC, and (e) Kwok et al. sea-ice drift speed. Arrows denote the drift vectors. (**f**) Root-mean-square differences between the annual mean bias-corrected NSIDC and Kwok et al. sea-ice drift speed. The thick gray line in c-f marks the mean sea-ice edge (1% sea-ice concentration). Data points were compared when both data sets were available.

We compared both the original and the bias-corrected data to a partly independent product by Kwok et al. (1998) and Kwok (2005). We interpolated these data onto our grid using CDO (2015) distance weighted averaging and applied the same 21-day running mean as for the NSIDC sea-ice drift data. We compared sea-ice drift vectors whenever both data sets were available and sea-ice concentrations were larger than 50%. Figure 2.7 shows the meridional drift components prior (a) and after applying the bias correction factor from the buoy data (b). We find that the agreement between the two data sets is much higher after the corrections. Compared to the original NSIDC sea-ice drift data set, the largest improvement occurs in the slope: 1.06 compared to 1.55. Root-mean-square differences and the linear correlation coefficient remain identical and the absolute bias is reduced by 0.2 km/day. Correlation coefficients between the two data sets are 0.8 for both

the zonal and meridional drift component. The spatial patterns of the mean annual sea-ice drift speed (Figures 2.7c-e) illustrate the improvement in agreement between the two data sets after the application of the bias correction but confirm that considerable differences remain at the sea-ice edge. These differences lead to a relatively high root-mean-square difference of the annual mean sea-ice drift speed in these regions (Figure 2.7f). However, in the central sea-ice packthe region that is crucial for our resultsthe root-mean-square differences are much smaller.

Our bias-corrected sea-ice drift speeds are typically slightly lower (about 9% to 19%) than those by Kwok et al. but considerably higher than in the uncorrected NSIDC data (about 26%, see above). We used these differences between the data sets to estimate the uncertainties induced by sea-ice drift on the final product (Δu in Tables 2.1 and 2.2): First, we re-computed all fluxes by correcting the original NSIDC data with correction factors derived from the Kwok et al. data (1.82 or 45% for the zonal drift, and 1.55 or 35% for the meridional drift) instead of the buoy-derived correction factor. This way, we also accounted for an uncertainty in the drift direction. Then, we averaged the deviations between our best estimate and the Kwok et al. based estimate with those between our best estimate and using the uncorrected and unfiltered NSIDC data. Uncertainties from sea-ice drift in the freshwater fluxes are about 20%. They considerably contribute to the final freshwater flux uncertainty and our trend uncertainties in all regions.

2.2.5   Sea-ice-ocean freshwater flux

We estimated annual net sea-ice-ocean freshwater fluxes over the period 1982 through 2008 by calculating the local sea-ice volume change and divergence (Holland and Kwok, 2012; Haumann, 2011). From this, we derived, through a mass balance, the local freshwater fluxes F (m^3 s^{-1}) from the sea ice to the ocean due to freezing and melting on a daily basis:

$$F = -C_{fw} \left(\frac{\partial(A\,c\,h)}{\partial t} + \nabla \cdot (A\,c\,h\,\vec{u}) \right). \tag{2.1}$$

The four variables c, h, $\vec{u}$, and A denote the sea-ice concentration, thickness, drift velocity, and grid-cell area, respectively. The factor C_{fw} converts the sea-ice volume flux to a freshwater equivalent (Ohshima et al., 2014):

$$C_{fw} = \frac{\rho_{ice}(1 - s_{ice}/s_{sw})}{\rho_{fw}}. \tag{2.2}$$

Here, ρ_{ice}, s_{ice}, s_{sw}, and ρ_{fw} are sea-ice density (925 kg m^{-3}; Timco and Frederking, 1996), sea-ice salinity (6 g kg^{-1}; Vancoppenolle et al., 2009), reference seawater salinity (34.7 g kg^{-1}; Talley, 2013), and freshwater density (1000 kg m^{-3}), respectively.

Annual sea-ice freshwater fluxes were computed from the daily fluxes from March to February of the next year (i.e., March 1982 to February 2009), which corresponds to the annual freezing

Table 2.1 **Mean and uncertainties of annual sea-ice freshwater fluxes over the period 1982 through 2008**

	Flux [mSv]	Δt [mSv]	ΔA [mSv]	Δc [mSv]	Δh [mSv]	Δu [mSv]	ΔC_{fw} [mSv]
Southern Ocean:							
Transport	+130 ±30	±0	±5	±0	±16	±25	±6
Net open ocean	+130 ±30	±0	±5	±0	±16	±25	±6
Net coastal ocean	−130 ±30	±0	±5	±0	±14	±26	±6
Net continental shelf	−60 ±20	±0	±0	±0	±8	±13	±3
Total melting	+460 ±100	±37	–	±1	±74	±49	±23
Total freezing	−410 ±110	±37	–	±1	±73	±50	±23
Atlantic sector:							
Transport	+60 ±20	±0	±1	±0	±13	±11	±3
Net open ocean	+60 ±20	±0	±1	±0	±13	±11	±3
Net coastal ocean	−50 ±20	±0	±1	±0	±14	±9	±3
Net continental shelf	−20 ±5	±0	±0	±0	±2	±4	±1
Total melting	+180 ±40	±13	–	±0	±25	±21	±9
Total freezing	−160 ±40	±13	–	±0	±25	±19	±9
Indian Ocean sector:							
Transport	+10 ±5	±0	±1	±0	±4	±2	±1
Net open ocean	+10 ±5	±0	±1	±0	±4	±2	±1
Net coastal ocean	−10 ±6	±0	±1	±0	±4	±4	±1
Net continental shelf	−10 ±4	±0	±0	±0	±3	±2	±0
Total melting	+70 ±30	±7	–	±0	±24	±5	±4
Total freezing	−70 ±30	±7	–	±0	±24	±6	±4
Pacific sector:							
Transport	+60 ±20	±0	±2	±0	±9	±12	±3
Net open ocean	+60 ±20	±0	±2	±0	±9	±12	±3
Net coastal ocean	−60 ±20	±0	±2	±0	±9	±13	±3
Net continental shelf	−30 ±9	±0	±0	±0	±6	±6	±2
Total melting	+200 ±50	±17	–	±0	±43	±23	±10
Total freezing	−180 ±60	±17	–	±0	±43	±24	±10

Positive numbers indicate a freshwater flux into the ocean or northward transport (1 mSv = 10^3 m^3 s^{-1}). The final uncertainty estimate (95% confidence level) stems from the uncertainties in the filtering of high-frequency temporal noise (Δt), variations of the zero freshwater flux line (ΔA), sea-ice concentration (Δc), sea-ice thickness (Δh), sea-ice drift (Δu), and the freshwater conversion factor (ΔC_{fw}), respectively. See Figure 2.11 for definition of regions.

and melting cycle of sea ice in the Southern Ocean (Haumann, 2011). Remaining imbalances between, e.g., the open and coastal ocean of the Atlantic sector (Tables 2.1 and 2.2) are due to multi-year sea ice in the coastal region. We performed all calculations on the grid of the sea-ice drift data (Fowler et al., 2013b) and averaged all data products over three by three grid boxes resulting in a nominal resolution of 75 km. To obtain the zero freshwater flux contour line, we averaged the climatological fluxes over nine by nine grid boxes. To estimate melting and freezing fluxes, we separately summed up positive and negative daily fluxes over a year (Figures 2.4a and b). As temporal fluctuations accumulate when only adding positive or negative values, noise can lead to an overestimation of these fluxes. Therefore, each of the sea-ice variables (c, h, and $\vec{u}$)

were low-pass filtered using a 21-day running mean.

Table 2.2   Decadal trends of annual sea-ice freshwater fluxes and their uncertainties over the period 1982 through 2008

	Flux [mSv dec^{-1}]	Δs_e [mSv dec^{-1}]	Δt [mSv dec^{-1}]	ΔA [mSv dec^{-1}]	Δc [mSv dec^{-1}]	Δh [mSv dec^{-1}]	Δu [mSv dec^{-1}]	ΔC_{fw} [mSv dec^{-1}]
Southern Ocean:								
Transport	+**9** ±5	±3.2	±0.3	±1.1	±0.8	±3.0	±1.9	±0.5
Net open ocean	+**10** ±5	±3.5	±0.4	±1.1	±0.8	±3.0	±2.0	±0.5
Net coastal ocean	−**10** ±5	±3.5	±0.2	±1.1	±0.7	±3.3	±1.1	±0.5
Net continental shelf	−**3** ±2	±1.8	±0.0	±0.0	±0.1	±0.8	±0.1	±0.1
Atlantic sector:								
Transport	−4 ±5	±4.3	±0.1	±0.7	±0.1	±1.4	±0.7	±0.2
Net open ocean	−4 ±5	±4.4	±0.1	±0.7	±0.1	±1.4	±0.7	±0.2
Net coastal ocean	+6 ±6	±5.7	±0.1	±0.7	±0.0	±0.6	±1.8	±0.3
Net continental shelf	+**6** ±3	±2.5	±0.0	±0.0	±0.0	±0.6	±1.6	±0.3
Indian Ocean sector:								
Transport	−1 ±1	±1.3	±0.0	±0.2	±0.1	±0.3	±0.2	±0.0
Net open ocean	−1 ±1	±1.3	±0.0	±0.2	±0.1	±0.3	±0.2	±0.0
Net coastal ocean	−**3** ±2	±0.9	±0.0	±0.2	±0.1	±1.1	±0.7	±0.1
Net continental shelf	+**2** ±1	±0.9	±0.1	±0.0	±0.1	±0.3	±0.4	±0.1
Pacific sector:								
Transport	+**14** ±5	±3.4	±0.2	±0.6	±0.7	±1.3	±2.8	±0.7
Net open ocean	+**14** ±5	±3.4	±0.3	±0.5	±0.7	±1.2	±2.9	±0.7
Net coastal ocean	−**13** ±5	±3.6	±0.2	±0.5	±0.6	±1.9	±2.3	±0.7
Net continental shelf	−**10** ±3	±2.6	±0.1	±0.0	±0.2	±1.2	±1.8	±0.5

Positive numbers indicate a freshwater flux trend into the ocean or a northward transport trend (1 mSv dec^{-1} = 10^3 m^3 s^{-1} per decade). The final uncertainty estimate (95% confidence level) stems from the standard error of the slope of the regression line (Δs_e), filtering of high-frequency temporal noise (Δt), variations of the zero freshwater flux line (ΔA), sea-ice concentration (Δc), sea-ice thickness (Δh), sea-ice drift (Δu), and the freshwater conversion factor (ΔC_{fw}), respectively. Bold numbers indicate a significance of at least a 90% confidence level. See Figure 2.11 for definition of regions.

2.2.6   Sea-ice freshwater transport

The total northward sea-ice volume transport (m^3 s^{-1}) between the coastal and open ocean region equals the spatial integral of the divergence term in (equation 2.1) in either of the two regions (Gauss's Theorem). We chose the open ocean region since there is considerable zonal exchange between the Indian Ocean and Atlantic sectors (Figure 2.2a) in the coastal region, influencing the sector based estimates. In the open ocean, this effect is negligible. We used this approach for the reported transport estimates (Tables 2.1-2.3 and Figures 2.9a-c).

To demonstrate that our main findings are robust on a basin-scale, and not influenced by small scale noise and local uncertainties, we also calculated the northward sea-ice freshwater transport

across the latitude bands 69.5° S in the Atlantic sector and 71° S in the Pacific sector (Figure 2.3). To this end, we averaged sea-ice concentration, thickness, and meridional drift (c_n, h_n, and v_n) in 1° longitude segments (n) along these latitudes and calculated the local freshwater transport T_n (m^3 s^{-1}):

$$T_n = C_{fw} \, c_n \, h_n \, v_n \, \Delta l_n. \tag{2.3}$$

Here Δl_n denotes the length of the latitude increment n along the boundary and C_{fw} is defined in (equation 2.2). Both sectors together show an annual northward freshwater transport of 100±30 mSv with an increase of +8±5 mSv per decade over the period 1982 to 2008 (Figure 2.9d and Figure 2.3). This compares well with the mean (120±30 mSv) and trend (+9±5 mSv per decade) of our spatially integrated sea-ice-ocean fluxes in the Pacific and Atlantic (Figures 2.9b-c). We calculated the spatial pattern of the sea-ice freshwater transport $\vec{f}$ (m^2 s^{-1}) as displayed in Figures 2.2a and c through:

$$\vec{f} = C_{fw} \, c \, h \, \vec{u}. \tag{2.4}$$

2.2.7 Time-series homogenization

Our analysis and earlier studies (Haumann et al., 2014; Olason and Notz, 2014) revealed major temporal inhomogeneities in the NSIDC sea-ice drift data set at the transitions between satellite sensors (Figure 2.8). We argue that these temporal inhomogeneities are linked to the unavailability of the 85/91 GHz channels and sparser data coverage in the earlier years. The drift speed before 1982 appears underestimated, which is to some extent mitigated by AVHRR data thereafter. From 1982 to 1986, the drift speed is consistent but has a low bias. The drift ramps up in 1987, when the 85 GHz channels became available, and decreases again between 1989 and 1991, when these channels degraded (Wentz, 1991). A final sudden decrease occurs from 2005 to 2006 when 85 GHz data were not used. We used wind speed data over the sea ice from ERA-Interim (Dee et al., 2011, section 2.2.1) as an independent data source and scaled it to the sea-ice drift velocity for comparison (Figures 2.8b). The scaling factor stems from the consistent years in the period 1988 to 2008 and varies in space and with season (Thorndike and Colony, 1982; Kimura, 2004). This analysis supports our argument that the sea-ice drift speed is underestimated when the higher resolution 85/91 GHz channels were not available. We note that the meridional drift seems less sensitive to these inhomogeneities than the total drift, which might be related to a higher data availability in the central sea-ice pack and is consistent with the lower biases found in the meridional sea-ice drift.

The spurious increase of the sea-ice velocity would affect our estimated trends if they were not taken into account (Figures 2.9 and 2.10). Thus, we corrected the annual divergence (equation 2.1) and lateral transport (equations 2.3 and 2.4) for the sensor-related temporal inconsistencies as follows: We excluded the inconsistent years 1980 and 1981, 1987, 1989 to 1991, 2005, and 2006 from the analysis. To homogenize the years 1982 to 1986 with the years 1988 to 2008, i.e.,
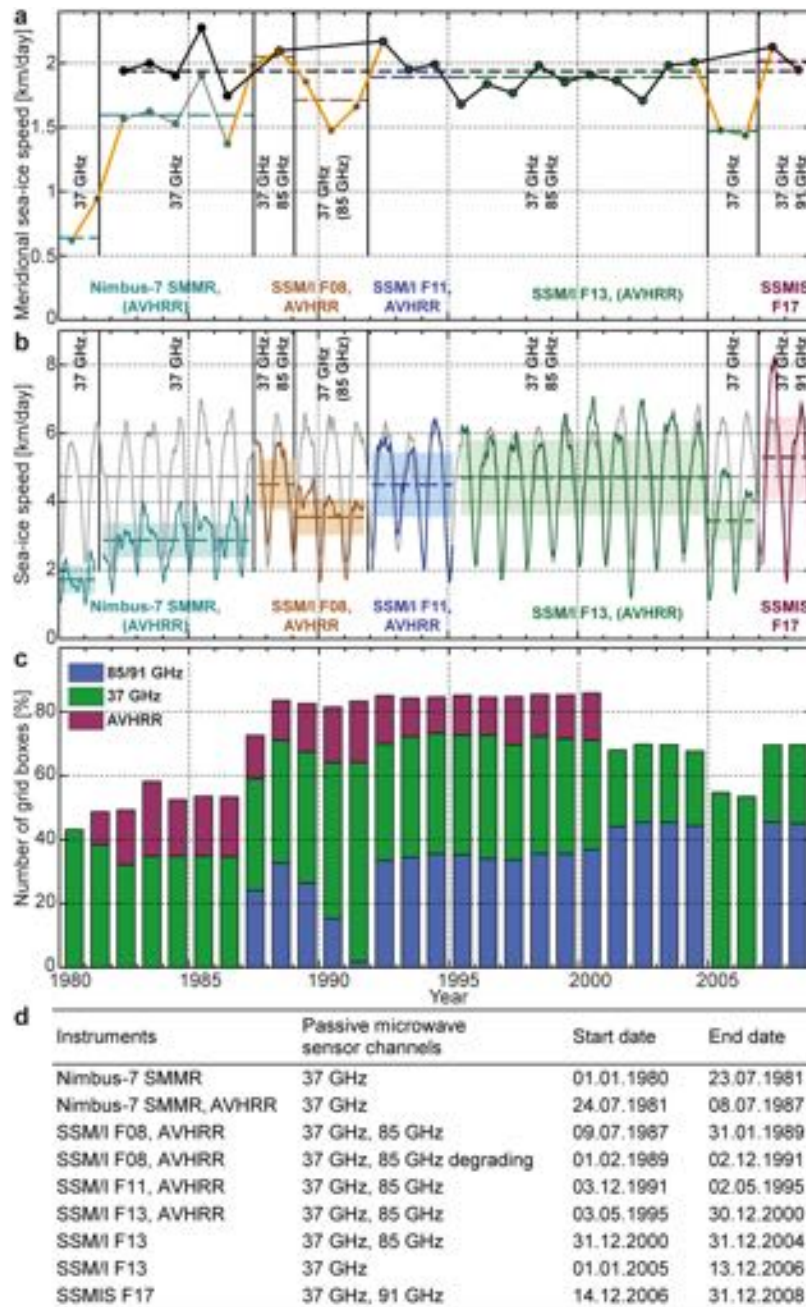
Figure 2.8 Temporal inhomogeneities in the NSIDC satellite sea-ice drift data: (**a**) Annual mean meridional sea-ice drift speed averaged over the entire sea-ice area (sea-ice concentration >50%). Thick orange lines: spurious trends due to changes in underlying data; black: data corrected for inconsistencies and used in this study (1982 to 2008). (**b**) Low-pass filtered (91-day running mean) sea-ice drift speed averaged over the entire sea-ice area (sea-ice concentration >50%). Gray: reduced wind speed from ERA-Interim using a reduction factor from the period 1988 to 2008. (a-b) In color: uncorrected data for each respective underlying satellite instrument combination; dashed lines: mean over the respective period; black vertical lines: periods of the same underlying channels. Text denotes the sensors and the frequency of the microwave radiometer channels used. (**c**) Fraction of sea-ice covered grid boxes with at least one drift vector observation in a 21-day window and a 75 by 75 km grid box using the non-gridded NSIDC drift data. Colors indicate the contribution of each sensor and channel. (**d**) Different combinations of instruments and passive microwave sensor channels and the related periods underlying the NSIDC sea-ice drift data.
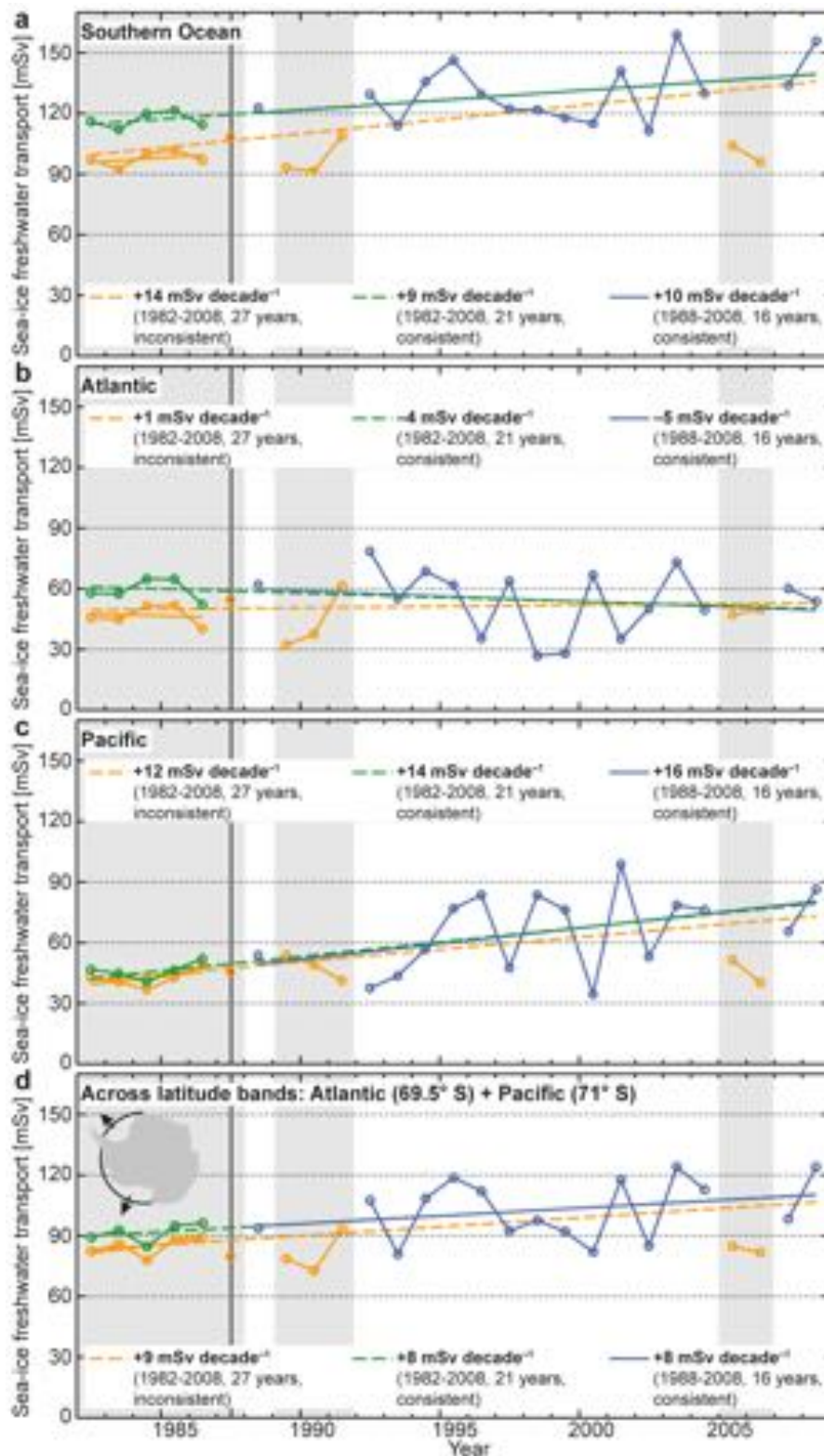
Figure 2.9 Time series and regions of annual northward sea-ice freshwater transport: Transport from the coastal ocean to the open ocean region in the (**a**) Southern Ocean (**b**) Atlantic sector (**c**) Pacific sector. (**d**) Across latitude bands in the Atlantic (69.5° S) and Pacific (71° S) sectors. Orange: not accounting for inhomogeneities; blue: homogeneous years only; green: homogenized time series. Corrected or removed years are shaded in gray. Straight lines show the linear regressions for the periods 1982 to 2008 (dashed orange and green), 1982 to 1986 (solid orange), and 1988 to 2008 (homogeneous years only; solid blue).

remove the spurious trend in 1987, we first calculated linear regression lines prior and after 1987 at each grid point. Then, we added the differences between the end (1986) and start (1988) points of the regression lines to all years prior to 1987, i.e., assuming a zero change in the year 1987. Fitting regressions prior and past spurious jumps is a common procedure to homogenize climate data (Peterson et al., 1998; Aguilar et al., 2003). Here, we used a linear regression that serves the purpose of computing long-term trends in the time series.
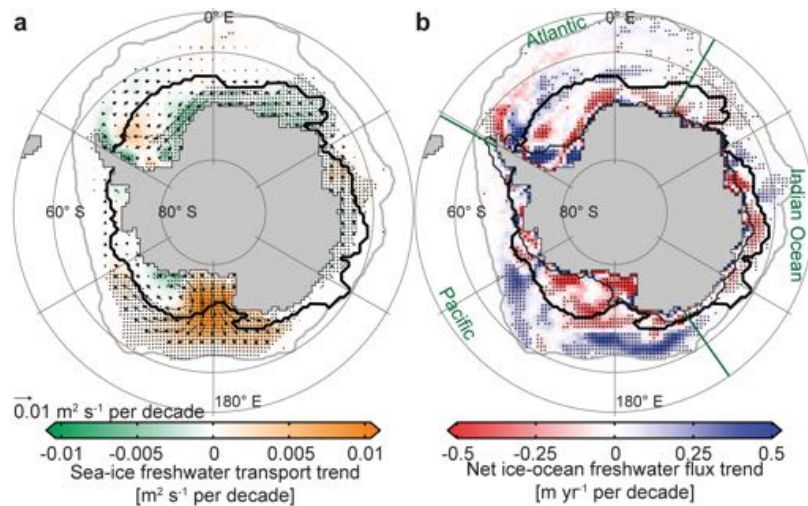
Figure 2.10   Trends of net annual freshwater fluxes associated with sea ice over the period 1982 through 2008 if temporal inhomogeneities in the sea-ice drift data were not considered: Linear trends of (**a**) meridional sea-ice freshwater transport and (**b**) net sea-ice-ocean freshwater flux from freezing and melting. Arrows (a) denote the trend of the annual transport vectors. Stippled trends are significant at the 90% level. Thick black lines: zero sea-ice-ocean freshwater flux line used to divide the coastal from the open ocean regions; thin black lines: continental shelf (1000-m isobath); gray lines: sea-ice edge (1% sea-ice concentration); green lines: basin boundaries.

To estimate the sensitivity of the trends in northwards sea-ice freshwater transport to uncertainties associated with the offset correction before 1987 (orange and green, Figure 2.9), we performed a Monte Carlo analysis by varying the offset and estimating the resulting trends. We generated 10^4 normally distributed offsets around our best guess (about 19 ± 5 mSv for the entire Southern Ocean; Table 2.3). The standard deviation of this distribution was chosen to match the offset uncertainty that arises from the root-mean-square errors of the trends in each of the two time intervals 1982 to 1986 and 1988 to 2008. For each of these generated offsets, we then estimated the trends and their significance (Table 2.3). For both the entire Southern Ocean and the Pacific sector, all sampled offsets yield a positive northward sea-ice freshwater transport trend. All trends for the Pacific sector and 92% for the entire Southern Ocean are positive and at the same time significant. Thus, our trend results are insensitive to uncertainties in the applied homogenization at the 90% confidence level. The posterior uncertainty shows that the uncertainty associated with the offset has no noticeable effect on the total uncertainty range, i.e., is smaller than ±1 mSv per decade.

Table 2.3   Sensitivity of northward sea-ice freshwater transport trend to time periods and homogenization

	Southern Ocean	Atlantic sector	Indian Ocean sector	Pacific sector
1992–2004: Flux trend [mSv dec^{-1}]	+4 ±9	−12 ±11	**−5** ±3	**+21** ±10
1992–2008: Flux trend [mSv dec^{-1}]	**+11** ±8	−5 ±9	−2 ±2	**+17** ±8
1982–2004: Flux trend [mSv dec^{-1}]	**+8** ±5	−6 ±5	−1 ±1	**+15** ±6
1982–2008: Flux trend [mSv dec^{-1}]	**+9** ±5	−4 ±5	−1 ±1	**+14** ±5
1982–2008 Monte Carlo analysis:				
Flux offset before 1987 [mSv]	+19 ±5	+13 ±7	+3 ±2	+4 ±5
Probability for trend of same sign [%]	100	92	78	100
Probability for significant trend of same sign [%]	92	26	9	100
Posterior trend uncertainty [mSv dec^{-1}]	±5	±6	±2	±5

Positive numbers indicate a northward freshwater transport trend (1 mSv dec^{-1} = 10^3 m^3 s^{-1} per decade). Bold numbers indicate a significance of the trend of at least a 90% confidence level. The Monte Carlo analysis is performed for 10^4 normally distributed sample offsets. Uncertainties (95% confidence level) stem from the standard error of the slope of the regression line and the data uncertainty. See Figure 2.11 for definition of regions.

2.2.8   Uncertainty estimation

Uncertainties of local (grid-point based) fluxes and time scales shorter than one year are probably large, due to potential inconsistencies between the data sets on such scales and an amplification of the uncertainties by the spatial and temporal differentiations in (equation 2.1). Integrating these terms in space and time greatly reduces these uncertainties (Tables 2.1 and 2.2). We estimated uncertainties in our product that are associated with the underlying input variables c, h, and $\vec{u}$ by using their observationally constrained range from different data sources, including the applied corrections and filtering as described in the corresponding sections. Additionally, we used an averaging period of 31 days, instead of 21 days, and, for trends only, an estimate without a running-mean filter, to obtain uncertainty estimates associated with temporal noise (Δt). The results confirmed that only the annual melting or freezing fluxes, but not the net annual fluxes, are sensitive to the low-pass filtering as in the latter product the noise is averaged out. The sensitivity of the spatially integrated values to variations of the zero freshwater flux line is estimated by

varying the smoothing radius from two to six grid boxes (ΔA). The uncertainty associated with the constant conversion factor (ΔC_{fw}; equation 2.2) is about 5% when using a realistic range of values (Timco and Frederking, 1996; Vancoppenolle et al., 2009; Talley, 2013). For the trends only, we computed the standard error of the slope from the variance of the residuals around the regression line (Δs_e; Santer et al., 2000). The total uncertainty for both the climatological mean and the trends was estimated by calculating the root-mean-square of the individual contributions. This analysis shows that in the Atlantic and Indian Ocean sectors both the uncertainties in the climatology and trends (Tables 2.1 and 2.2) are dominated by uncertainties in the sea-ice thickness. In contrast, the uncertainty in sea-ice drift dominates the uncertainty in the Pacific sector. We tested the significance of the trends with a t-test, accounting for the fact that only 21 out of 27 years were used and for a lag-one auto-correlation (Santer et al., 2000). To indicate the significance of the trends at grid-point level (Figures 2.2c-d and Figure 2.10), at which the data uncertainties are unknown, the local root-mean-square of the variance of the residuals was artificially increased by 40%, approximately corresponding to our data uncertainty estimate in Table 2.2. The quality of our data directly at the coastline and around the sea-ice edge is reduced due to the limited quality and quantity of the underlying observations in these regions.

2.2.9   Sea-ice freshwater flux evaluation

A modeling study by Abernathey et al. (2016), carried out in parallel to this study, calculated freshwater fluxes associated with sea-ice formation, melting, and transport in the Southern Ocean State Estimate (SOSE). This model assimilates a large amount of observational data and optimizes surface fluxes. They estimated an annual sea-ice-ocean freshwater flux due to sea-ice formation of -360 mSv over the entire Southern Ocean, which is within our estimated range of -410 ± 110 mSv. Moreover, they estimated that the combined annual sea-ice-ocean freshwater flux due to sea-ice and snow melting is about 500 mSv. Thus, in their estimate a total of 140 mSv of snow accumulated on the sea ice. Our estimates partly include snow accumulation on sea ice, because part of the sea-ice thickness results from snow-ice formation, which we estimated to be about -50 mSv (section 2.2.3). However, the snow layer on top of the sea ice is not included in our estimate of the freshwater flux due to sea-ice melting of 460 ± 100 mSv. Abernathey et al. (2016) estimate that the lateral sea-ice freshwater transport from the density class of CDW to AAIW and SAMW amounts to 200 mSv in the period between 2005 and 2010. Their estimate slightly differs from our estimated transport from the coastal to the open ocean that ranges between about 140 mSv and 160 mSv in 2007 and 2008 (Figure 2.9). The reasons might be the slightly different regions and that their estimate also includes the transport of the snow layer on top of the sea ice.

Given the reduced confidence in the local fluxes (e.g. sea-ice production in coastal polynyas), it is reassuring that our data agree within our estimated range of uncertainty with previous estimates of mean fluxes for some larger coastal polynya regions (Tamura et al., 2008; Ohshima et al.,

2013). Our confidence is higher for fluxes integrated over larger regions such as the high-latitude Ross and Weddell Seas (Figure 2.11). Here our estimates are in close agreement with previous studies as discussed in the following.
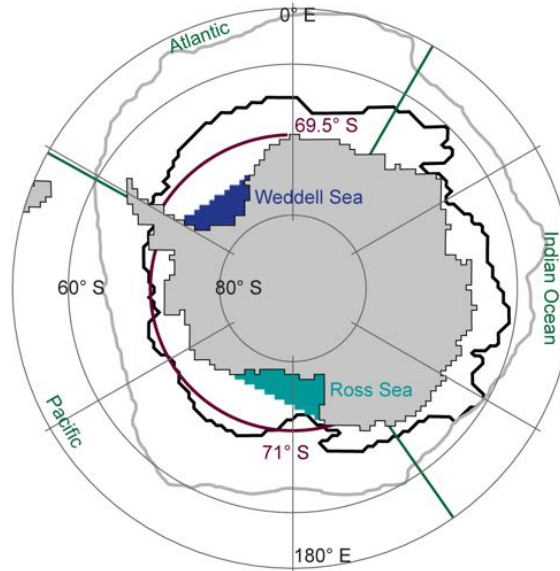

Figure 2.11   Regions used for evaluation of the sea-ice freshwater fluxes: Turquoise shading: area south of the coastal Ross Sea flux gate (Drucker et al., 2011; Kwok, 2005; Comiso et al., 2011); dark blue shading: area south of the coastal Weddell Sea flux gate (Drucker et al., 2011); purple lines: 69.5° S latitude band in the Atlantic sector and 71° S latitude band in the Pacific sector; black line: smoothed mean zero sea-ice-ocean freshwater flux line dividing the coastal and open ocean regions; thick gray line: mean sea-ice edge (1% sea-ice concentration); green lines: basin boundaries.

In the Ross Sea, we estimated that the northward transport from the coastal region across a flux gate between Land Bay and Cape Adare (turquoise area in Figure 2.11; Kwok, 2005) is 23±5 mSv, increasing by about 30% (or +7±4 mSv) per decade in the period 1992 to 2008. Based on the same passive microwave data but using a different algorithm for retrieving the sea-ice motion data, Kwok (2005) and Comiso et al. (2011) found a mean sea-ice area flux across this flux gate of about 10^6 km^2 between March and November in the periods 1992 to 2003 (Kwok, 2005) and 1992 and 2008 (Comiso et al., 2011), respectively. Using an approximated mean sea-ice thickness (0.6 m; Comiso et al., 2011; Drucker et al., 2011) and the conversion factor (equation 2.2), this corresponds to a mean northward freshwater transport of about 19 mSv. In close agreement with our estimate, these studies found an increase of 30% per decade (about +6 mSv per decade). Using sea-ice motion from the Advanced Microwave Scanning Radiometer-EOS (AMSR-E), Drucker et al. (2011) estimated that the mean sea-ice area flux between April and October (2003 to 2008) across the same flux gate is about $9.3 \cdot 10^5$ km^2 corresponding to a freshwater transport of about 23 mSv. Based on the same data but using an alternative approach (Martin et al., 2007), they found that the total sea-ice production in all Ross Sea polynyas together was about 737 km^3 between April and October (2003 to 2008), corresponding to a sea-ice-ocean freshwater flux of −31 mSv. This estimate is similar to the total production of about −36±7

mSv south of the flux gate in our data set, because most of the sea-ice production of this region occurs in the polynyas (Drucker et al., 2011). Using passive microwave data, the Drucker et al. (2011) found an increase of the production in the Ross Sea polynyas of 28% per decade between 1992 and 2008. A modeling study by Assmann and Timmermann (2005) found a net annual sea-ice-ocean freshwater flux due to melting and freezing of -27 mSv on the continental shelf in the Ross Sea, which is in agreement with our estimate of -23 ± 5 mSv. They also found a long-term (unquantified, see their Figure 9b) decrease of the net annual sea-ice-ocean freshwater flux over the Ross Sea continental shelf in the period 1963 to 2000, which is qualitatively in line with our results.

In the Weddell Sea, the northward sea-ice area flux across a flux gate close to the 1000-m isobaths (blue area in Figure 2.11) has been found to be $5.2\cdot10^5$ km^2 based on AMSR-E data between April and October (2003 to 2008; Drucker et al., 2011). Using an approximated mean sea-ice thickness (0.75 m; Drucker et al., 2011) and the conversion factor (equation 2.2), this corresponds to a mean northward freshwater transport of about 16 mSv. This agrees well with our estimate of an annual northward transport of 16 ± 4 mSv for the same years and the same region. Similar to the Ross Sea, the production in the major polynyas of the Weddell Sea was estimated (Drucker et al., 2011). However, in the Weddell Sea, a large fraction of the sea-ice transported across the flux gate is not produced in the coastal polynyas (Drucker et al., 2011), i.e., we cannot directly compare our large-scale estimate to the sea-ice production in the polynyas. In the same study, based on passive microwave data, Drucker et al. (2011) found a small, but insignificant long-term decrease of the sea-ice production in the Weddell Sea polynyas between 1992 and 2008, which is qualitatively consistent with our findings in the Atlantic sector. For a much larger area in the Weddell Sea, a modeling study by Timmermann et al. (2001) estimated an annual northward sea-ice freshwater transport of about 34 mSv and another observational study by Harms et al. (2001), mostly based on moorings and wind speed, estimated that this flux is as large as about 38 ± 15 mSv. These estimates agree well with our finding of an annual northward freshwater transport of 41 ± 18 mSv across the $69.5°$ S latitude band, which is approximately their considered transect.

2.2.10   Sea-ice freshwater transport based on ERA-Interim data

To support our findings, we quantified changes in sea-ice motion induced by changes geostrophic winds (Thorndike and Colony, 1982; Kottmeier and Sellmann, 1996; Harms et al., 2001; Kimura, 2004) from daily ERA-Interim (Dee et al., 2011) sea-level pressure and surface air temperature (section 2.2.1). We averaged the data over $1°$ longitudinal segments along the previously defined latitude bands (Figure 2.3), computed 21-day running means, and smoothed the data spatially over 7 longitude bins. Then, we calculated the sea-level pressure gradients along the latitude bands and used these together with the atmospheric surface density to estimate geostrophic winds normal to

the latitude bands (Thorndike and Colony, 1982; Kottmeier and Sellmann, 1996). From these, we calculated the sea-ice drift speed using a drift-to-wind-speed ratio of 0.016, derived from drifting buoys in the central Weddell Sea (Thorndike and Colony, 1982; Kottmeier and Sellmann, 1996). This parameter is strongly variable in space and time, which is a major uncertainty in the resulting sea-ice drift. Nevertheless, it provides an average estimate for the mostly free drifting sea ice in the central Antarctic sea-ice pack (Thorndike and Colony, 1982; Kottmeier and Sellmann, 1996).

The resulting northward sea-ice freshwater transport (equation 2.3) is independent in terms of the sea-ice drift but not in terms of the sea-ice concentration and thickness. We used anomalies (at each 1° increment) since the absolute values of the local transport are likely biased by local influences of ocean currents and sea-ice properties. The resulting total annual anomalies of the northward sea-ice freshwater transport agree well in terms of variability and long-term trend with the transport anomalies based on the satellite sea-ice drift (+8 mSv per decade; Figure 2.3). These estimates do not suffer from the temporal inhomogeneities that we identified in the satellite sea-ice drift data (section 2.2.7).

2.2.11   Sea-ice contribution to ocean salinity

We determined the evolution of ocean salinity s (g kg^{-1}) in response to a given surface freshwater flux F (m^3 s^{-1}) from a combination of mass and salt balances. The mass balance for a given, well-mixed ocean surface box of volume V and density ρ reads:

$$\frac{d\rho V}{dt} = \rho_{in}Q_{in} + \rho_{fw}F - \rho Q_{out}, \tag{2.5}$$

where Q_{in} and Q_{out} (m^3 s^{-1}) are the volume fluxes of seawater in or out of the box, ρ_{in} (kg m^{-3}) is the respective density. In a steady state, the above equation 2.5 yields:

$$\rho_{in}Q_{in} = \rho Q_{out} - \rho_{fw}F. \tag{2.6}$$

The corresponding salt balance reads:

$$\rho V \frac{ds}{dt} = \rho_{in}Q_{in}s_{in} - \rho Q_{out}s. \tag{2.7}$$

We assumed the same constant source water salinity $s_{in} = s_{sw}$ and freshwater density ρ_{fw} as in equation 2.2, and used a constant reference density ($\rho = 1027$ kg m^{-3}). Moreover, we used the formation rate of the modified water mass as the volume flux of seawater out of the surface box ($Q_{out} = Q$). Then, substituting equation 2.6 in 2.7 yields:

$$\rho V \frac{ds}{dt} = (\rho Q - \rho_{fw}F)s_{sw} - \rho Qs. \tag{2.8}$$

In a steady state, this results in an equation that describes the modified salinity s:

$$\rho Q s = (\rho Q - \rho_{fw} F) s_{sw}. \tag{2.9}$$

Using $s = s_{sw} + \Delta s$, where Δs is the salinity difference between the source and modified water masses, equation 2.9 reduces to:

$$\Delta s = -\frac{\rho_{fw} s_{sw} F}{\rho Q}. \tag{2.10}$$

We used net water-mass transformation rates (Q) of 29 Sv between CDW and AABW and 13 Sv between CDW and AAIW/SAMW (Talley, 2013). Figure 2.1a illustrates the results and shows the zonal mean ocean salinity and density distribution (Ingleby and Huddleston, 2007) for comparison.

Assuming that $+130\pm30$ mSv of freshwater enter CDW through northward sea-ice freshwater transport, the salinity modification (according to equation 2.10) is -0.33 ± 0.09 g kg^{-1}. The uncertainty includes a ±2 Sv uncertainty in the water-mass formation rate. In observations, the salinity difference between CDW and AAIW and SAMW ranges from about -0.3 to -0.5 g/kg (Talley, 2013). Thus, northward freshwater transport by sea-ice could explain the majority of the salinity modification, consistent with very recent findings (Abernathey et al., 2016) and a mixed-layer salinity budget (Ren et al., 2011).

Similarly, we calculated the contribution of -130 ± 30 mSv of freshwater removed from coastal regions due to northward sea-ice transport to the salinity modification (equation 2.10) between CDW and AABW, obtaining an increase of $+0.15\pm0.06$ g kg^{-1}. The uncertainty includes a ±7 Sv uncertainty in AABW formation. However, observed salinity differences between the CDW and AABW are generally small or even of opposite sign (Jacobs, 2004). This is the result of a compensating effect between a sea-ice driven salinification and a freshening from glacial and atmospheric freshwater. Freshwater fluxes from land ice through basal and iceberg melting are about $+46\pm6$ mSv and $+42\pm5$ mSv, respectively (Depoorter et al., 2013). Assuming that roughly 60% of the icebergs melt in the coastal regions (Silva et al., 2006), a total of about $+70$ mSv are added from the land ice to the coastal ocean, corresponding to a freshening of about -0.08 g kg^{-1} or a compensation of the sea-ice freshwater flux of about 55% in AABW. We estimated from the ERA-Interim atmospheric reanalysis data (Dee et al., 2011) that the net atmospheric freshwater flux in the coastal region is about $+80$ mSv, corresponding to a freshening of about -0.09 g kg^{-1}. The resulting net salinity change in coastal waters from sea-ice, atmospheric, and land-ice freshwater fluxes is almost zero (-0.02 g kg^{-1}). Such a compensation of the freshwater fluxes in coastal regions was noticed previously (Jacobs et al., 1985; Timmermann et al., 2001). We note that large regional variations of these fluxes have been reported (Meredith et al., 2010; Depoorter et al., 2013).

To estimate the temporal salinity changes at the surface and in newly formed AAIW and SAMW, we assumed a constant water-mass formation rate Q, and that the freshwater flux and

ocean salinity consist of a climatological value plus a time-dependent perturbation ($\overline{F} + F'$ and $\overline{s} + s'$, respectively). Then, equation 2.8 yields:

$$\rho V \frac{ds'}{dt} = \rho Q s_{sw} - \rho_{fw} s_{sw} \overline{F} - \rho Q \overline{s} - \rho_{fw} s_{sw} F' - \rho Q s'. \tag{2.11}$$

As the climatological fluxes are in steady state, the first three terms on the right side in equation 2.11 cancel according to equation 2.9, resulting in:

$$\rho V \frac{ds'}{dt} = -\rho_{fw} s_{sw} F' - \rho Q s'. \tag{2.12}$$

We approximated the freshwater-flux perturbation by our estimated trend ($F' = at$), and rearranged the terms resulting in a first order linear differential equation:

$$\frac{ds'}{dt} + \frac{Q}{V} s' = -\frac{\rho_{fw} s_{sw} a}{\rho V} t. \tag{2.13}$$

Integration in time yields an expression for the time-dependent evolution of the salinity perturbation:

$$s' = -\frac{\rho_{fw} s_{sw} a}{\rho Q} \left(t - \frac{V}{Q} + \frac{V}{Q} e^{-\frac{Q}{V} t} \right). \tag{2.14}$$

To obtain an estimate of the salinity trend at a given time t, we substituted equation 2.14 into 2.13:

$$\frac{ds'}{dt} = \frac{\rho_{fw} s_{sw} a}{\rho Q} \left(e^{-\frac{Q}{V} t} - 1 \right). \tag{2.15}$$

The equilibrium response of the system, i.e., the long-term trend after several years of perturbation is:

$$\lim_{t \to \infty} \frac{ds'}{dt} = -\frac{\rho_{fw} s_{sw} a}{\rho Q}. \tag{2.16}$$

Using our estimated sea-ice freshwater transport trend of $+9\pm5$ mSv per decade and a water-mass formation rate as above, we obtained an equilibrium freshening rate of -0.023 ± 0.014 g kg^{-1} per decade (green in Figure 2.12b), which is valid for sufficiently large Qt/V.

Figure 2.12b (purple and blue; using equation 2.14) shows that if we assumed that the trend started in 1982, there would be a delayed response lowering the mean salinity trend estimate depending on V. We thus tested the sensitivity of the trend to V, which corresponds to the upper 150 m between the zero sea-ice-ocean freshwater flux line and the Subantarctic Front (Figure 2.12a Orsi et al., 1995), which is the source region of AAIW. The circumpolar V of about $5 \cdot 10^6$ km^3 results in a mean salinity trend (using equation 2.14) of -0.014 ± 0.008 g kg^{-1} per decade between 1982 and 2008 (purple). However, AAIW formation does not occur in a circumpolar belt but mostly in the south-eastern Pacific and south-western Atlantic, i.e., on either side of Drake Passage (England et al., 1993; Talley, 1996; Sloyan and Rintoul, 2001a; Iudicone et al., 2007; Hartin et al., 2011). Assuming that most of the water is modified in this region and further downstream in the South Pacific (England et al., 1993; Iudicone et al., 2007; Hartin et al., 2011),
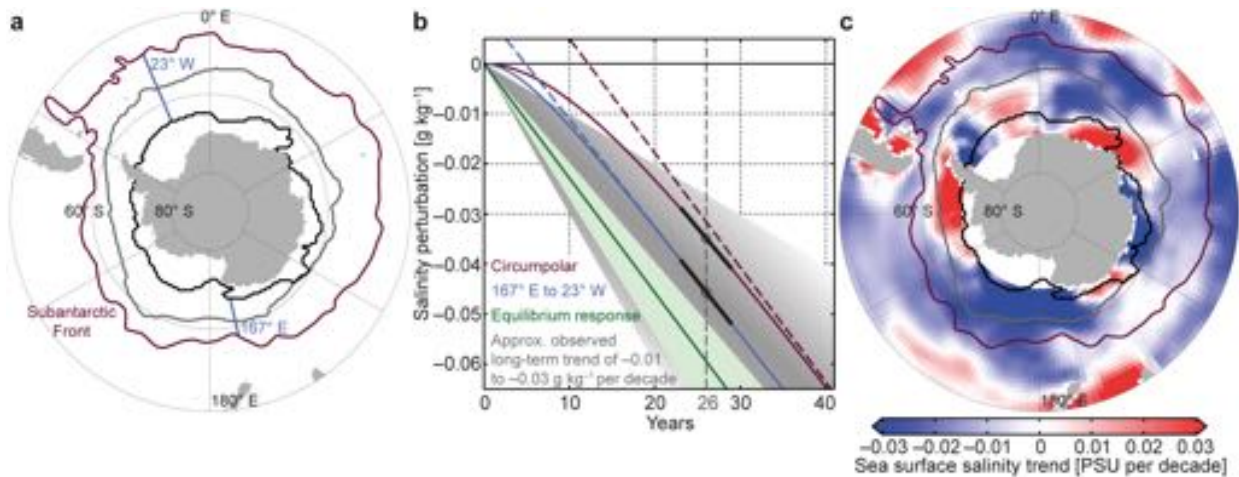
Figure 2.12   Contribution of sea-ice freshwater flux trends to ocean salinity: (**a**) Map showing the regions used for the estimation of salinity changes due to sea-ice freshwater fluxes. Blue lines: sector important for AAIW formation (167 E to 23 W); purple line: Subantarctic Front (Orsi et al., 1995); black line: smoothed mean zero freshwater flux line dividing the coastal and open ocean regions; thick gray line: mean sea-ice edge (1% sea-ice concentration). (**b**) Salinity response to a freshwater flux perturbation using the long-term equilibrium response (green) and using a delayed response starting in 1982 for a circumpolar reference volume (5×10^6 km^3; purple), or for the region of most AAIW formation (2×10^6 km^3; blue). Dashed lines: respective asymptotic equilibrium response; black lines: respective current trends; gray shading: approximate observed long-term trend in AAIW (Wong et al., 1999; Böning et al., 2008; Helm et al., 2010). (**c**) Observed long-term sea-surface salinity trends. Data from Durack et al. (2012); Durack and Wijffels (2010, http://www.cmar.csiro.au/oceanchange; 1950 to 2000)).

we estimated a second, somewhat smaller V of about $2 \cdot 10^6$ km^3 (blue). The sea-ice freshwater transport trend into this reference volume is about $+8 \pm 5$ mSv per decade (Figures 2.2c-d), resulting in a mean salinity trend (using equation 2.14) of -0.018 ± 0.010 g kg^{-1} per decade (blue). Since a certain amount of freshwater is transported eastward, out of this sector (blue), the mean trend of the delayed response lies somewhere in between the estimates based on the two different reference volumes (blue and purple).

It is unlikely that the trend started exactly in 1982. Thus, the actual salinity response will fall between our estimated delayed response and the equilibrium response. For the range of values in the discussion above, the deviations of the freshening rate due to effects of delay and variations in reference volume are much smaller than the actual magnitude of the trend itself. We thus conclude that the overall mean freshening rate of newly formed AAIW and the surface waters advected northward across the Subantarctic Front into SAMW due to the changes in sea-ice freshwater transport is about -0.02 ± 0.01 g kg^{-1} per decade (Figure 2.1b).

Data availability: Sea-ice freshwater fluxes leading to the main conclusions are publicly available (doi:10.16904/8).

Maksym (2016) wrote a *Nature* News & Views article about this research article (available online: doi:10.1038/537040a).

Chapter 3

A regional model of the Southern Ocean*

From an oceanographic perspective, the Southern Ocean is probably the most challenging region to model. This challenge manifests itself in the relatively poor performance of many state-of-the-art ocean circulation models in the Southern Ocean. In this region, global climate models exhibit their largest biases and inter-model disagreements. Among these issues in the models are the representation of ocean water masses (Downes et al., 2010, 2011; Heuzé et al., 2013, 2015; Sallée et al., 2013b), ocean circulation (Meijers et al., 2012; Downes and Hogg, 2013; Farneti et al., 2015), surface ocean mixed layer (Sallée et al., 2013a), sea-ice cover (Turner et al., 2013; Mahlstein et al., 2013; Haumann et al., 2014), surface fluxes (Majkut et al., 2014; Frölicher et al., 2015; Kessler and Tjiputra, 2016), and atmospheric circulation (Swart and Fyfe, 2012; Bracegirdle et al., 2013; Hosking et al., 2013). These issues do not only occur in the simulated mean states, but are also pronounced in the models' simulated responses to changes in the climate system. Since the Southern Ocean plays a pivotal role in the climate system (chapter 1), the relatively large inter-model spread and biases induce large uncertainties in future projections and our understanding of past changes. To better understand the sensitivity of the Southern Ocean to changes in the climate system, I here intend to obtain a model that reproduces the present-day Southern Ocean's water mass structure and circulation as closely as possible and is constrained by fluxes at the boundaries (section 3.5). Nevertheless, biases will remain and have to be considered carefully (section 3.7). Changes in the climate system can then be imposed on the model by varying the boundary conditions (chapters 4 and 5).

In many respects the requirements for a model of the Southern Ocean region differ from the rest of the globe. One particular reason is its unique topographic setting without zonal boundaries, large meridional gradients, and relatively weak vertical gradients. This setting induces strong flows and high levels of baroclinic instabilities. Global climate models typically do not resolve the resulting meso-scale turbulent flow. More recently, eddy-resolving ocean components have

---

*Parts of this chapter are part of a manuscript in preparation for Journal of Climate (see chapter 4)

been investigated in coupled global climate models (e.g. Dufour et al., 2015; Morrison et al., 2016) at a high computational cost. In order to reduce the computational cost, I will here apply a regional model described in section 3.1, with enhanced spatial resolution in higher latitudes (section 3.4). However, regional models have the challenge that they are influenced by the lateral boundary conditions, which have to be chosen and implemented carefully (section 3.5.5). Another major challenge stems from the generally weak or even inverted vertical gradients in temperature, salinity, and density in the Southern Ocean. They often violate a general assumption in ocean circulation models that horizontal motions are much larger than vertical motions and therefore fully rely on the parameterization of vertical processes rather than effectively solving the vertical equations of motion and transport (Griffies et al., 2000a). Such parameterizations of the surface and bottom boundary layers, as well as convective processes can hence induce large biases if they are not accurately adapted for the use in the Southern Ocean. They must be able to deal with a very large amplitude of the seasonal cycle that ranges between very stable conditions and shallow mixed layers in summer and marginally stable or unstable conditions and deep mixed layers in winter. I will discuss these issues in section 3.2.

Due to the weak stratification and the very thin isolating sea-ice layer that separates the cold atmosphere from the relatively warmer ocean, small inaccuracies in either the atmosphere, ocean, or sea ice can lead to strong amplifications of biases (e.g. Goosse et al., 1999; Goosse and Fichefet, 1999; Stössel et al., 2002, 2011, 2015; Timmermann and Beckmann, 2004; Mathiot et al., 2012; Kjellsson et al., 2015). Prescribing the surface fluxes rather than using a coupled model, can alleviate some of these problems (e.g. Treguier et al., 2010; Downes et al., 2015). Yet, the atmospheric fluxes are poorly constrained due to the limited availability of observational data especially in the sea-ice region (Speer et al., 2012; Bourassa et al., 2013), also leading to large biases in forced simulations. Biases induced by the forcing can be further reduced by an assimilation of ocean and sea-ice observational data (Mazloff et al., 2010; Cerovečki et al., 2011; Massonnet et al., 2013; Barth et al., 2015). In this study, I will use a novel approach and prescribe all surface fluxes, i.e. the atmospheric (section 3.5.1), sea-ice (section 3.5.2), and land-ice (section 3.5.3) forcing. This approach has the advantage of strongly constraining the model and, at the same time, enables to study the ocean response to changes in the prescribed forcing, which is the purpose of this thesis. However, it also implies that feedbacks in the system cannot be studied and that long-term changes are dependent on the forcing.

First, this chapter deals with the numerical representation of physical (sections 3.1, and 3.2) and biogeochemical (section 3.3) processes in the model. Then, I will describe the model domain, topography, and spatial grid (section 3.4), which is followed by a description of the forcing at surface and lateral boundaries (section 3.5) and by a description of model initialization, spin-up, and drift (section 3.6). Finally, I will provide a detailed evaluation of the model's mean state using observational data (section 3.7) and a summary of the current state of the model (section 3.8).

3.1   The Regional Ocean Modeling System (ROMS)

In this thesis, I model the Southern Ocean using the regional, forced, ocean circulation model ROMS (Regional Ocean Modeling System; Shchepetkin and McWilliams, 2003, 2005, 2009a). It numerically solves the set of primitive equations that describes the physics of the ocean (cf. Cushman-Roisin and Beckers, 2011), consisting of the mass and momentum budgets, the equation of state for seawater, and conservation equations for tracers such as temperature and salinity. These equations are discretized in an orthogonal, curvilinear coordinate system in the horizontal direction and a stretched, terrain-following coordinate system in the vertical direction (Song and Haidvogel, 1994; Shchepetkin and McWilliams, 2003, 2005).

ROMS originates from many previous advances in terrain-following models. Among the predecessors of ROMS (Shchepetkin and McWilliams, 2005) are the Princeton Ocean Model (POM; Blumberg and Mellor, 1987), the S-coordinate Primitive Equation Model (SPEM; Haidvogel et al., 1991; Haidvogel and Beckmann, 1999), and the S-Coordinates Rutgers University Model (SCRUM; Song and Haidvogel, 1994). Compared to these models, Shchepetkin and McWilliams (2005) advanced the mode-splitting and time-stepping (see also section 3.1.2). These advances allow for much larger time steps and thus ROMS is computationally much more efficient than its predecessors and can be used for larger scale, high-resolution applications.

There are multiple versions of ROMS that are supported by different institutes. The version that I am using in this thesis is the UCLA-ETH version and "ROMS" always refers to this version if not explicitly stated otherwise. This version includes most recent developments of the original UCLA version (Marchesiello et al., 2003; Shchepetkin and McWilliams, 2003, 2005, 2011; McWilliams et al., 2009; Lemarié et al., 2012b; Shchepetkin, 2015) as well as some complementary routines developed or coupled at ETH Zürich. The latter developments include the coupling of ROMS to biogeochemical-ecological models such as the nitrogen based Nutrient-Phytoplankton-Zooplankton-Detritus (NPZD) model (Gruber et al., 2006), and the Biological Elemental Cycling (BEC) model (Moore et al., 2004; Jin et al., 2008; Moore et al., 2013; Yang and Gruber, 2016, see section 3.3 for details). In this chapter, I will describe some further developments that are necessary to apply ROMS in the Southern Ocean (see sections 3.2, 3.5.2, 3.5.3, 3.5.1).

So far, ROMS has mostly been used to study coastal systems (e.g. Gruber et al., 2006, 2011; Lachkar and Gruber, 2011, 2013; Turi et al., 2014, 2016; Frischknecht et al., 2015). In the Southern Ocean, Byrne et al. (2014) applied ROMS in the South Atlantic region. This application showed that ROMS reproduces complex dynamical features of the Southern Ocean reasonably well. However, these simulations were only run on very short temporal and smaller spatial scales and are thus strongly controlled by the initial and boundary conditions. So, they essentially differ from the application in my thesis.

A number of studies have been carried out with the Rutgers version of ROMS (Shchepetkin and McWilliams, 2005; Haidvogel et al., 2008; Shchepetkin and McWilliams, 2009b) in the Southern Ocean by Dinniman et al. (2003, 2007, 2011, 2012). They showed that the model is able to reproduce a realistic circulation on the continental shelf regions in the Ross Sea (Dinniman et al., 2007, 2011) and the western side of the Antarctic Peninsula (Dinniman et al., 2011). Yet, these studies are very regional as well and confined to the shelf region. Some larger scale studies were carried out with the Bremerhaven Regional Ice Ocean Simulations model (BRIOS; Beckmann et al., 1999), which is a descendent of SPEM and therefore related to ROMS. BRIOS simulates a realistic water-mass structure and sea-ice cover in the Weddell (Beckmann et al., 1999; Timmermann et al., 2001; Schodlok et al., 2002) and Ross Seas (Assmann and Timmermann, 2005), providing reasonable grounds to believe that realistic large-scale applications in the Southern Ocean can be achieved with a terrain-following coordinate model.

3.1.1   Terrain-following coordinate system

The vertical coordinate system of ROMS is the pivotal difference to other commonly used ocean circulation models, i.e. z-level or isopycnal coordinates, and characterizes most of the advantages and disadvantages compared to these other models (Chassignet et al., 2000; Griffies et al., 2000a; Willebrand et al., 2001). Thus, in the following, I will first review the implications of using a terrain-following vertical coordinate system for modeling the Southern Ocean as a whole.

Terrain-following coordinate systems have historically been developed in ocean circulation models to study coastal regions. This is owing to their advantage of having an increasing vertical resolution as the water column shoals (Figure 3.2). In the high-latitude Southern Ocean, the high vertical resolution of the continental shelf waters and the natural representation of terrain-following, density-driven bottom flows allows, in principal, for a realistic production of AABW in such coordinate systems (Beckmann et al., 1999; Timmermann et al., 2001, 2002; Schodlok et al., 2002; Assmann and Timmermann, 2005; Rodehacke et al., 2007). In z-level models, i.e. in most global climate models, an accurate representation of AABW is a key issue. Often, they form only little or no AABW on the continental shelf or unrealistically produce AABW through open-ocean deep convection (Doney and Hecht, 2002; Heuzé et al., 2013), which leads to strong deviations in the Southern Ocean hydrography and circulation (Heuzé et al., 2013; Stössel et al., 2015). More recently, overflow parameterizations are developed to resolve such issues in z-level models (Chassignet et al., 2014; Snow et al., 2015). Isopycnal models only accurately represent AABW if the reference density is set deep enough (about 2000 m; Chassignet et al., 2003). As a consequence, models with terrain-following coordinates, such as ROMS, should in principle be ideal to study the formation of AABW and should provide an accurate representation of the deep-ocean water masses in the Southern Ocean, if a realistic surface forcing and surface mixing scheme were provided.

While having advantages that favor the representation of coastal regions and AABW formation in a terrain-following coordinate system, there are major disadvantages or challenges that have historically prevented the ocean modeling community from applying such models to large scales such as the deep-ocean basins and decadal to centenial time-scales (Barnier et al., 1998; Chassignet et al., 2000; Griffies et al., 2000a; Willebrand et al., 2001). The apparent challenges mostly arise from the stretching and tilting of the vertical coordinates as moving from the shallow coastal regions to the deeper ocean interior. These challenges, and approaches to mitigate them, have also been pointed out in a few existing basin-wide applications of ROMS in the Atlantic (Haidvogel et al., 2000) and the Pacific (Marchesiello et al., 2009; Lemarié et al., 2012b) and need consideration when modeling the Southern Ocean basin.

One major challenge is that, as the ocean gets deeper towards the interior basin, the vertical resolution in the surface ocean mixed layer decreases leading to a poorer representation of surface processes (Griffies et al., 2000a; Shchepetkin, 2005). In ROMS, this problem has partly been mitigated by introducing vertical stretching functions that enhance the resolution towards the surface and result in so-called vertical S-coordinates (Song and Haidvogel, 1994; Haidvogel and Beckmann, 1999; Haidvogel et al., 2000; Shchepetkin and McWilliams, 2003). An accurate representation of surface mixed layer processes in the Southern Ocean is sensitive to the vertical resolution at the surface and therefore to the choice of these stretching functions (see sections 3.4.2 and 3.7).

Several other challenges arise from the crossing of the terrain-following vertical coordinates with geopotential and isoneutral surfaces. On larger temporal and spatial scales, this interference can lead to numerical errors in the pressure gradients and the advection and diffusion of tracers. In small, regional domains this is less of a problem because water masses are renewed at the open boundary. However, in basin scale applications and over long-term integrations, as I attempt here, this effect can induce model drift and a degradation of the ocean interior water masses (Barnier et al., 1998; Marchesiello et al., 2009; Lemarié et al., 2012b). In ROMS, the pressure gradient errors have largely been mitigated by new numerical schemes (Shchepetkin and McWilliams, 2003). The second problem is that the crossing between vertical coordinate system with isoneutrals causes numerical, dianeutral mixing induced by higher order, diffusive tracer advection schemes, referred to as spurious mixing (Marchesiello et al., 2009). Such an advection scheme, i.e. a third-order upwind-biased advection scheme, is used in ROMS (Shchepetkin and McWilliams, 1998).

There are several ways one can mitigate spurious mixing to an acceptable level: One possible option is to reduce the angle between the vertical coordinates and the isoneutrals by smoothing of the topography with the drawback of losing realism. Another option is to increase resolution, which reduces errors associated with the finite differencing but increases the computational cost. A third option is to numerically split a hyperdiffusive part from the actual advection and rotate it in an isoneutral direction (Marchesiello et al., 2009; Lemarié et al., 2012b,a). The latter new

development is implemented in ROMS but requires more testing and is currently not compatible with the version I use in this thesis. Instead, I mitigate spurious mixing and pressure gradient errors by applying a more extensive topographic smoothing (section 3.4.3), and using a higher resolution than previous basin-scale applications (Marchesiello et al., 2009; Lemarié et al., 2012b, section 3.4.1). However, future efforts should be made to use the isoneutral advection scheme in this model setup and other basin-wide application of ROMS (Lemarié et al., 2012b).

In z-level models, numerical pressure gradient errors are not an issue as the isosurfaces of the model grid mostly align with geopotential surfaces. However, spurious diapycnal mixing can be problematic in z-level models (Griffies et al., 2000b), especially in higher latitudes due to the sloping isoneutrals in these regions, leading to a degradation of both AABW and AAIW in the interior ocean. A good representation of interior water masses in the Southern Ocean that is not influenced by spurious mixing can be obtained using isopycnal models (Hallberg and Gnanadesikan, 2006). However, their resolution decreases as stratification weakens, which is the disadvantage of using isopycnal models in the Southern Ocean.

3.1.2   Momentum & tracer equations

In the horizontal, the state variables in ROMS are staggered on an Arakawa-C grid. As a consequence, all tracers are situated in the center of the grid cell and the velocity components on the respective grid cell edges (Arakawa and Lamb, 1977; Haidvogel and Beckmann, 1999; Griffies et al., 2000a). The horizontal momentum equations in ROMS are solved in a split-explicit time-stepping scheme (Shchepetkin and McWilliams, 2005, 2009a), which separates the faster barotropic mode from the slower baroclinic mode. Thus, the model calculates the evolution of the depth-integrated flow, i.e. the barotropic mode, at a much faster time step (here chosen as 70 times the slow time step) than the vertical deviations from the barotropic flow, i.e. the baroclinic mode, and all other processes. The baroclinic momentum and tracer equations are advanced in time using a leap-frog predictor sub-step followed by a third-order accuracy Adams-Moulton corrector sub-step. Mode coupling only occurs for the corrector sub-step (Shchepetkin and McWilliams, 2005, 2009a).

ROMS has a free surface (Shchepetkin and McWilliams, 2005); hence it is able to resolve the evolution of the surface elevation and the barotropic gravity waves, which are about two orders of magnitude faster than the baroclinic waves (Griffies et al., 2000a). This approach has several advantages over the rigid-lid and implicit free-surface methods (Killworth et al., 1991; Griffies et al., 2000a; Shchepetkin and McWilliams, 2005): Among these are a better numerical stability and flow characteristics over rough topography, a straightforward implementation of the input of freshwater, and computational efficiency.

The formulation of the vertical momentum equation assumes hydrostatic balance (cf. Cushman-

Roisin and Beckers, 2011). Even though the hydrostatic approximation is commonly used in ocean circulation models, it is clearly a disadvantage in applications in the Southern Ocean. Here, due to the low static stability, the water-mass structure and circulation are sensitive to vertical motions like coastal (Jacobs et al., 1985; Ohshima et al., 2013; Gordon et al., 2015) and open-ocean convection (Gordon, 1991; Martinson, 1991; Marshall and Schott, 1999) or small-scale salt plumes from the formation of sea ice (Duffy and Caldeira, 1997; Duffy et al., 1999; Nguyen et al., 2009). All these processes should ideally be represented in a model of the Southern Ocean and have to be parameterized in a hydrostatic model (cf. section 3.2).

Kanarska et al. (2007) developed a non-hydrostatic version of ROMS. However, this version is computationally more expensive and requires a much higher vertical resolution. Additionally, it has not yet been extensively validated in realistic oceanographic studies and many additional numerical challenges arise from the implementation that might introduce new numerical errors. Consequently, I am not yet able to apply this non-hydrostatic version to a basin-wide study of the Southern Ocean.

3.1.3 Equation of state

As most models in geophysical fluid dynamics, ROMS makes use of the Boussinesq approximation, which states that deviations of density around a reference density ρ_0 (here I chose $\rho_0 = 1027 \, \text{kg m}^{-3}$) are small (cf. Cushman-Roisin and Beckers, 2011). This approximation entails the assumption of sea-water incompressibility. Yet, there is an exception implemented in ROMS to reduces errors in the mode splitting due the Boussinesq approximation. This correction is done by accounting for the compression induced by vertical pressure changes in the barotropic mode (option "SPLIT_EOS"; Shchepetkin and McWilliams, 2009a, 2011). Consequently, ROMS provides an intermediate solution of using all the numerical advantages resulting from the Boussinesq approximation and correcting for the major errors associated with this assumption (Dukowicz, 2001). Despite these simplifications of density effects, ROMS calculates the full, non-linear equation of state (Jackett and Mcdougall, 1995; Shchepetkin and McWilliams, 2003, 2011). It should be noted that this version does not correspond to the newest formulation of the equation of state (TEOS10, IOC, SCOR, and IAPSO, 2010). The resulting *in situ* density enters the calculation of the pressure gradient, the barotropic mode, the static stability, the surface buoyancy forcing (Shchepetkin and McWilliams, 2011), and the double diffusion (Large et al., 1994).

Particularly important to my study is an accurate representation of the equation of state in the calculation of the static stability (see section 1.3.2). Several stability effects result from the non-linearity of the equation of state in the Southern Ocean: Firstly, the density stratification is much more sensitive to salinity changes at low temperatures (Sigman et al., 2004; de Boer et al., 2007). Secondly, non-linearity effects like thermobaricity and cabbeling are important factors for water-mass transformation (McDougall, 1987; Stewart et al., 2016). McPhee (2003) argues that

thermobaricity, i.e. the pressure dependence of the thermal expansion coefficient, might be an important trigger for convective events in the the Southern Ocean. Cabbeling, i.e. the mixing of two water parcels of the same density but with different temperature and salinity and a heavier resulting density, is thought to be an important factor for the formation of AAIW and SAMW (Iudicone et al., 2008; Urakawa and Hasumi, 2012). However, whether or not such effects are accurately represented in ROMS does not only depend on the formulation of the equation of state in the model but also on the formulation of mixing and convective processes (McDougall, 1987; Ilicak et al., 2012). Nevertheless, a future update of the equation of state to the newest and most accurate formulation (TEOS10, IOC, SCOR, and IAPSO, 2010) might improve the representation of water masses in the model.

3.2   Mixing processes

Numerical models of the ocean generally resolve the ocean circulation and variations of properties on large temporal and spatial scales. Processes that cannot be resolved in these models are often parameterized. The most critical unresolved processes are sub-grid-scale turbulence occurring in the vertical (sections 3.2.2 and 3.2.1) and horizontal (section 3.2.3) , as well as vertical convection due to static instabilities. Other commonly parameterized mixing processes are double diffusion or internal wave breaking (section 3.2.1). In ROMS, vertical mixing processes are parameterized through K-theory (cf. Stull, 1988). This first-order closure scheme suggested by Large et al. (1994) approximates mixing processes through the product of the vertical gradient of momentum and tracers and the corresponding local eddy viscosity and diffusivity coefficients. Eddy diffusivity coefficients are calculated separately for temperature and for salt and all other tracers. This mixing scheme treats the oceanic surface and bottom boundary layer (section 3.2.2) and mixing in the ocean interior (section 3.2.1) separately.

As my thesis focuses on the relation between stratification and vertical exchange of tracers, an accurate representation of processes associated with mixing are critical. On the one hand, they determine the exchange of tracers such as carbon and nutrients between the surface and subsurface ocean (Gargett, 1991; Bopp et al., 2015). On the other hand, mixing processes determine the transformation of water masses in the Southern Ocean, i.e. the upwelling of CDW and the subduction of AABW, AAIW, and SAMW, and consequently the ventilation of the subsurface ocean (Orsi et al., 1999; Sloyan and Rintoul, 2001a; Jacobs, 2004; Iudicone et al., 2008; Urakawa and Hasumi, 2012). Consequently, it is an important contributor to the overturning circulation (Sloyan and Rintoul, 2001b; Lumpkin and Speer, 2007; Ito and Marshall, 2008; Marshall and Speer, 2012). Surface and subsurface mixing processes are also essential for setting up the typical hydrographic structure with its pronounced halocline, which is determined by a subtle balance between the surface buoyancy fluxes and vertical mixing and advection processes at the bottom of the surface mixed layer (Gordon and Huber, 1984; Gordon, 1991; Martinson, 1990, 1991, see also section 1.3.2). This important role that mixing plays for the vertical exchange in the Southern Ocean mostly stems from the combination of a low static stability with strong turbulent shear and wind-driven stirring.

3.2.1   Vertical interior ocean mixing

ROMS first calculates the vertical eddy viscosity and diffusivity for the entire water column in absence of the surface and bottom boundary layers. Following Large et al. (1994), these values are the sum of the corresponding contributions from turbulent shear, convection, double diffusion, and internal wave breaking. The latter dominates the kinetic energy spectrum at very small scales in the interior ocean (Wunsch and Ferrari, 2004; Ferrari and Wunsch, 2009; Nikurashin

et al., 2012) and is parameterized in ROMS as suggested by Large et al. (1994) with a constant background vertical viscosity of 10^{-4} m^2 s^{-1} and diffusivity of 10^{-5} m^2 s^{-1}. Turbulent mixing due to shear instabilities in the vertical velocity profile is much larger than the mixing by internal waves, but it is typically regionally and temporally confined to regions of strong currents and in close proximity to boundaries. In ROMS, the associated diffusivity is computed from the ratio of the local gradient Richardson number and a critical value Ri_0 of 0.7. The latter is an empirical value at which local destabilizing shear tends to dominate over stabilizing density stratification:

$$\hat{Ri}_g = \frac{1}{Ri_0} \cdot \frac{N^2}{(\partial u/\partial z)^2 + (\partial v/\partial z)^2} \; . \tag{3.1}$$

In this formulation, values of $\hat{Ri}_g$ larger than 1 are associated with a stable stratification that suppresses shear instabilities and ROMS sets $\hat{Ri}_g$ to an exact value of 1. If $\hat{Ri}_g$ drops below 0, N^2 must be negative and therefore the stratification must be unstable. In this case ROMS sets $\hat{Ri}_g$ to an exact value of 0. Using this ratio and a maximal diffusivity ν_0, the resulting diffusivity due to the turbulent shear ν is (see Large et al., 1994)

$$\nu = \nu_0 \cdot \left(1 - \hat{Ri}_g^2\right)^3 \; . \tag{3.2}$$

Therefore, ν is 0 if no shear instability occurs and increases towards ν_0 as either stratification weakens or the vertical velocity gradient strengthens. Large et al. (1994) suggest a value of 0.005 m^2 s^{-1} for ν_0, which is used in most standard applications of ROMS. I found that this value can change the representation of the water-mass structure in ROMS in the Southern Ocean and that a larger value of 0.01 m^2 s^{-1}, which I will use here, is more suitable. The main motivation for increasing the shear-induced diffusivity is an observed layer of increased diffusivity in the ACC region under the actual mixed layer (Forryan et al., 2015; Nicholson et al., 2016).

Due to the low static stability of the interior Southern Ocean, deep ocean convection is a process that can occur (Gordon, 1991). Therefore, and as a consequence of the hydrostatic approximation (section 3.1.2), convective processes due to local static instabilities should be parameterized in this model as well. The above equation 3.2 has the advantage that static instabilities are automatically accounted for because ν reaches its maximum value of ν_0. As long as ν_0 takes a sufficiently large finite value an additional parameterization of convective processes is not required. I therefore switched the C-preprocessing option (CPP-switch) *LMD_CONVEC* off. The value of ν_0 that is added to the overall diffusivity in case of static instabilities is somewhat smaller than the ROMS standard value of 0.1 m^2 s^{-1} in the *LMD_CONVEC* routine, but it corresponds to the value suggested by e.g. Timmermann and Beckmann (2004) for the Southern Ocean. Griffies et al. (2000a) argue that such an approach of enhancing the local diffusivity is physically more realistic and numerically more appropriate than classical convective adjustment approaches, which mix vertical grid boxes iteratively or add an infinitely large vertical diffusivity.

Molecular diffusion is typically several orders of magnitudes smaller than turbulent and con-

vective mixing processes and hence neglected in most ocean circulation models. Nevertheless, one exception to that is double diffusion, which results from the fact that heat diffuses more rapidly than salt leading to convective mixing (Turner, 1973). Regionally and locally, such processes can be important for the vertical exchange of nutrients to the surface (Oschlies et al., 2003). Zhang et al. (1998) even suggest that double diffusion could ultimately be important on a global scale through its effects on mixing of water masses and the overturning circulation. In the upper Southern Ocean, where cold and fresh water overlies warm and salty water, double diffusion can occur in the form of diffusive convection and numerous studies suggested that it contributes to the upper ocean water-mass structure (Middleton and Foster, 1980; Muench et al., 1990; Martinson, 1990). The opposite, i.e. salt-fingering, might occur at depth where warm and salty NADW overlies the colder and fresher AABW. In order to account for these processes, I will use a double diffusion parameterization implemented in the vertical mixing scheme of ROMS (Large et al., 1994; Marmorino and Caldwell, 1976). ROMS computes salt and temperature diffusivities that result from double diffusion as a function of the local density ratio. These diffusivities are added to the overall vertical diffusivity coefficients of each tracer at each grid point.

3.2.2   Boundary layer mixing

Models of the surface ocean boundary layer are typically formulated either in a bulk or continuous mixed layer scheme (Griffies et al., 2000a). The *K*-profile parameterization (KPP; Large et al., 1994; Shchepetkin, 2005; McWilliams et al., 2009) in ROMS is of the latter type. Consequently, it allows for a vertical structure of tracers and velocity over the mixed layer extent as compared to the uniform distribution in the bulk method (Griffies et al., 2000a). KPP first computes the local vertical acceleration a_c from shear, buoyancy, rotation, and turbulent entrainment according to (Shchepetkin, 2005; McWilliams et al., 2009):

$$a_c(z) = \int_z^0 \frac{|z|}{|z| + \epsilon h_{bl0}} \left[\left(\frac{\partial \vec{u}(z)}{\partial z} \right)^2 - \underbrace{\frac{N(z)^2}{Ri_c}}_{\text{buoyancy}} - \underbrace{C_{Ek} f^2}_{\text{rotation}} \right] dz + \underbrace{C_{ent} N(z) w_s}_{\text{entrainment}} . \tag{3.3}$$

Here, z is the height of the layer (negative downward), h_{bl0} is an initial guess of the depth of the mixed layer (usually the previous time step), $\vec{u}$ is the horizontal velocity vector, N is the buoyancy frequency, f is the Coriolis parameter, and w_s is the turbulent velocity scale that depends on the surface forcing. The depth of the mixed layer (h_{bl}) corresponds to the first level below the surface at which $a_c(z) = 0$. This is a modification (Shchepetkin, 2005; McWilliams et al., 2009) of the original bulk Richardson number formulation in KPP (Large et al., 1994) that essentially allows to diagnose separate contributions to vertical mixing. Subsequently, KPP fits a vertical profile of diffusivity through the boundary layer using a non-dimensional vertical shape function (Large et al., 1994) and therefore gives the boundary layer a vertical structure

that continuously transitions into the ocean interior with a value of 0 at the bottom of the surface boundary layer. The non-dimensional profile is then multiplied with the boundary layer depth and the turbulent velocity scale to get a value for the local diffusivity. This diffusivity is added to the background diffusivity (section 3.2.1). Additionally, KPP calculates a non-local transport term that accounts for the unresolved penetration into the layers below the mixed layer.

The separation of buoyancy and turbulent mixing effects, as well as the first-order turbulent closure technique in KPP, make it generally applicable to any region in the global ocean and under a variety of conditions. Therefore, KPP has become widely used in ocean models (Griffies et al., 2000a). Most models produce too shallow mixed layers in the Southern Ocean, especially in summer (Sallée et al., 2013a; Downes et al., 2015). Such a shallow bias, especially in the melting season of the sea ice, is a well-known bias in KPP (Dinniman et al., 2003, 2011; Timmermann and Beckmann, 2004; Li et al., 2016). This shallow bias during summer promotes in some extreme cases deep ocean convection in winter as the thin surface layer becomes statically unstable. In many respects this bias leads to large biases in the water-mass structure in both higher and lower latitudes as well as biases in the overturning circulation. Initial simulations with ROMS showed a very similar behavior with a strongly underestimated mixed layer depth (Eberenz, 2015), leading to a long-term degradation of AAIW and a too fresh surface layer. Sallée et al. (2013a) interpreted this too fresh surface ocean associated with the shallow mixed layer bias in the global models as a too strong surface freshwater forcing. Based on sensitivity tests with ROMS that I performed for this thesis, I argue that such an overly-fresh surface ocean in global models might also be related to a reduced mixing of freshwater into the deeper layers, leading to a generally salty bias in AAIW if mixed layers are too shallow. This is a critical process with respect to the amount of AAIW formed and the subduction of heat and carbon with these waters (Frölicher et al., 2015). Consequently, the shallow mixed layer bias in global models and the general tendency to take up less carbon than suggested by inverse models might be directly related (Khatiwala et al., 2013; Mikaloff Fletcher et al., 2006; Frölicher et al., 2015).

In ROMS, the overly-shallow summer-time mixed layer is associated with a very fast stabilization of the surface ocean as the sea ice melts and the surface ocean heats up. In extreme cases, the surface mixed layer continuously shoals until it only consists of half of the upper most grid cell and diffusivities drop to the background minimum. Therefore, the surface mixed layer was effectively absent in these cases. Such a run away process is critical because KPP is not able to properly fit a vertical profile if only one or two grid points are available. Increasing the vertical resolution, I found that the mixed layer deepens and that run away effects can be avoided because KPP has more grid points to fit a vertical profile. This effect is especially critical if KPP is used in combination with a terrain-following model in the deep ocean and vertical grid parameters have to be chosen carefully (see section 3.4.2). I further added a constraint to the model that the mixed layer diffusivity is always computed as described above for the interface between the first and the second layer, even if the mixing depth drops below the depth of the uppermost layer (CPP-switch *LMD_MIN_KPP*). A further deepening of the mixed layer occurs with an increase

in horizontal resolution (section 3.7). The computation of h_{bl} through equation 3.3 does not give many possibilities for further modifications, except for the entrainment term, which is not well constrained and could be used for further tuning (Danabasoglu et al., 2006). Additional improvements have been obtained in other studies by implementing mixing through surface waves (Huang et al., 2012; Qiao and Huang, 2012; Li et al., 2016), which is currently not included in ROMS and could significantly deepen the mixed layer in the Southern Ocean. Timmermann and Beckmann (2004) also suggest to parameterize keel stirring by sea ice as a function of ice drift velocity. The latter two processes would be highly desirable in future versions of ROMS.

While all the above suggestions lead to slight improvements, none of them seems to ultimately resolve the shallow bias and the insufficient subsurface mixing south of the frontal zone during summer. The key problem that I identified here as a cause of the shallow mixing during summer is not the mixing intensity, i.e. the diffusivity itself, or the critical depth that the mixing reaches, but rather a too quick shoaling of the mixed layer under stable conditions if the surface momentum stress decreases. Niiler and Kraus (1977), Lemke (1987), and Markus (1999) argue that the mixing depth h_{bl} for such a thinning mixed layer can be diagnosed through the ratio between the friction velocity u^{*3} and the surface buoyancy forcing B_0, which is the Monin-Obukhov length scale, and an exponential dissipation function. Both Timmermann and Beckmann (2004) and Dinniman et al. (2003, 2011) use this relation to adjust the vertical diffusivity in their respective continuous mixing schemes when the surface boundary layer shoals, following the suggestions by Lemke (1987) and Markus (1999). I here use a similar approach and recalculate the mixed layer depth when mixed layer thins through:

$$\hat{h}_{bl} = \frac{u^{*3}}{B_0 \, \kappa} \, e^{-h_{bl0}/h_0} \ . \tag{3.4}$$

Here, κ is the *von Karman* constant (0.41), h_{bl0} is an initial estimate of the mixed layer depth, which is here provided through the mixed layer depth of the previous time step, and h_0 is the dissipation length scale set to 20 m (Lemke, 1987; Markus, 1999). Hereafter, the calculation of the diffusivity throughout the adjusted mixed layer depth is performed in the normal way using the KPP shape function. This adjustment provides reasonable solutions of the mixed layer depth and is key to obtaining a better hydrography. The disadvantage of this formulation is that it overwrites the mixed layer depth calculated through equation 3.3 for thinning mixed layers. A potentially more ideal solution would be to dampen the decay of deep mixed layers under stabilizing conditions in time. Such a solution would be consistent with several observational and modeling studies that suggest that storms and eddies in the Southern Ocean induce strong inertial motions and shear induced mixing in the upper ocean that last for multiple days to weeks (Zhai et al., 2005; Brannigan et al., 2013; Meyer et al., 2015; Merrifield et al., 2016; Nicholson et al., 2016). Nicholson et al. (2016) recently suggested that this process might lead to the observed enhanced diffusivity in the subsurface layer in the Southern Ocean during summer. Given that this issue is the most critical to obtain a reasonable simulation and that many global models seem

to suffer from similar issues, it is an urgent matter to further investigate potential solutions in future.

Another surface mixing process is the development of convective salty plumes from the rejection of salty brine to the ocean when sea ice forms during winter. This process is spatially heterogeneous and typically happens on scales from centimeters to kilometers (Nguyen et al., 2009). Local static instabilities can occur in the water column below the sea ice leading to salt plume convection on horizontal scales that are much smaller than what is resolved by the model or the forcing. If shear induced turbulent mixing is small (Barthélemy et al., 2015), these plumes sink until they reach a neutrally buoyant depth, which is typically the halocline. If in the model the brine was added to the top layer, it would make the surface layers much saltier until a static instability and convective mixing occurs over the entire grid cell and for all tracers. In models such a process can lead to unrealistically deep winter-time mixed layers and an erosion of the halocline. In some cases, such elevated surface salinities can even lead to spurious deep convection in global climate models (Duffy and Caldeira, 1997; Duffy et al., 1999). Considering several studies that have investigated the effect of sub-grid scale brine rejection parameterizations (Duffy and Caldeira, 1997; Duffy et al., 1999; Nguyen et al., 2009; Barthélemy et al., 2015) and running some sensitivity experiments with ROMS, I conclude that the effect of a brine rejection parameterization is largely dependent on the model and the associated surface mixed layer parameters. I implemented a simplified version according to Duffy et al. (1999, CPP-switch *BRINE_PLUMES*) that distributes the salt flux from the sea-ice formation equally over the surface boundary layer calculated by KPP. I will here use this parameterization as it improves the representation of the surface mixed layer and surface heat fluxes in the sea-ice region. If this paramerization is not used, the winter-time heat loss from the surface ocean is unrealistically high and some local deep convection occurs.

The water-mass structure in the Southern Ocean is generally very sensitive to the surface mixed layer, especially in the sea-ice region (Goosse and Fichefet, 1999; Goosse et al., 1999; Stössel et al., 2002). A better representation of the mixed layer can usually be achieved by either adapting the surface forcing or tuning the mixed layer scheme (Kjellsson et al., 2015). Additional to the modifications of KPP and its parameters that I described in this section, an accurate treatment of the ice-ocean surface fluxes turned out to be critical for obtaining a realistic surface mixed layer (see section 3.5.2).

Additional to the surface boundary layer, I will also use the bottom boundary layer option of KPP in this thesis, which is computed in the same way as the surface boundary layer. I chose a bottom roughness length of 0.02 m, which is slightly higher than the value used originally (0.01 m). The reason for enhancing the bottom roughness length is to counteract the effects induced by smoothing the topography (see section 3.4.3). This modification helped to slow down an overly-fast coastal current around Antarctica.

3.2.3   Lateral mixing

A dominant fraction of the turbulent kinetic energy in the ocean is contained in the mesoscale, which spans from tens to a hundred kilometers (Ferrari and Wunsch, 2009; Nikurashin et al., 2012). A large portion of this energy is situated in the form of geostrophic eddies in regions of strong currents and high baroclinicity, such as the ACC, the Brazil-Malvinas confluence zone, or the Agulhas Current System (Wunsch and Stammer, 1998; Frenger et al., 2015). It is hence important to account for this mesoscale turbulence in model simulations especially in the Southern Ocean, where it contributes to both the lateral and overturning circulation (Hallberg and Gnanadesikan, 2001, 2006; Henning and Vallis, 2005; Sallée et al., 2011; Meredith et al., 2012; Morrison and Hogg, 2013).

In coarse resolution models, which do not resolve the mesoscale, lateral mixing is typically parameterized. However, simply mixing along horizontal surfaces would lead to spurious diapycnal mixing in regions of sloping isopycnals, such as the ACC region. Thus, an isopycnal mixing scheme has been implemented in most ocean circulation models to account for mesoscale eddy fluxes (Gent and McWilliams, 1990; Gent et al., 1995; Farneti and Gent, 2011). High-resolution simulations showed that a certain degree of horizontal adiabatic diffusion is still required, even if most of the mesoscale processes are resolved to ensure numerical stability (Roberts and Marshall, 1998). For this reason, resolution-dependent eddy parameterizations have been developed (Gent et al., 2002; Smith and Gent, 2004). However, no such parameterizations are implemented in ROMS. Instead the advection scheme in ROMS contains a resolution-dependent hyperdiffusion, as described in section 3.1.1, to ensure numerical stability (Shchepetkin and McWilliams, 1998). This diffusion operator vanishes as the resolution increases. Additionally, ROMS provides the possibility for harmonic (Laplacian) mixing through constant viscosity and diffusivity coefficients, which I will not use in this thesis. I here intend to resolve most of the mesoscale processes in the Southern Ocean (see section 3.4.1).

3.3   Biogeochemical-ecological component

In chapter 5, I will analyse the response of the Southern Ocean carbon fluxes to changes in surface freshwater fluxes and stratification. For this purpose, I will run simulations with a coupled biogeochemical and ecological component. ROMS has two optional biogeochemical-ecological submodels: A nitrogen based Nutrient-Phytoplankton-Zooplankton-Detritus (NPZD) model (Gruber et al., 2006) and the Biological Elemental Cycling (BEC) model (Moore et al., 2001b, 2004). Even though it is computationally more expensive due to a larger number of tracers, BEC is the obvious choice for simulations in the Southern Ocean because it includes iron limitation (Moore et al., 2001a).

BEC explicitly simulates the cycling of carbon, major nutrients (nitrate, ammonium, phosphate, dissolved iron, and silicate), dissolved oxygen, and alkalinity in the ocean (Moore et al., 2001b, 2004). The carbon cycle includes dissolved organic and inorganic carbon (DOC, DIC) pools, as well as the sinking of particulate organic matter (POM). The model has one prognostic zooplankton type and three prognostic phytoplankton groups, i.e. small phytoplankton, diatoms, and diazotrophs. Coccolithophores and the production of calcium carbonate ($CaCO_3$) are so far implicitly represented as a fraction of small phytoplankton. The development of an explicit coccolithophore group is currently underway at ETH Zürich (Ph.D. project by C. Nissen). All phytoplankton growth rates include limitations by several nutrients, temperature, and light. Zooplankton grazing on the phytoplankton is concentration-dependent. Next to the environmental forcing from the physical model, BEC is forced with atmospheric partial pressure of CO_2, and dust and iron deposition at the surface (see section 3.5).

BEC was originally developed as part of the Community Earth System Model (CESM) at the National Center for Atmospheric Research (Moore et al., 2001b, 2004). Jin et al. (2008) previously used BEC coupled to ROMS for simulations in the Pacific. The version that I will be using in this thesis includes all most recent developments such as a better representation of the sinks and sources of nutrients (Moore et al., 2013; Yang and Gruber, 2016). The computational expenses increase by roughly a factor three to four when running ROMS coupled with BEC. Next to the additional prognostic variables, the writing of numerous diagnostic variables required for example for the analysis of the carbon budget significantly increase the computational and post-processing efforts. Therefore, I will be running the coupled model only at a nominal resolution of 0.5° degrees, which should be improved in future efforts.

3.4   Model setup

For the purpose of this thesis, I developed a new ROMS setup that covers the entire Southern Ocean (Figure 3.3). Multiple aspects in this setup differ from applications of ROMS in other regions. In the meridional direction the setup extends from 24° S to about 78.8° S, with the latter exact value depending on the chosen horizontal resolution (see Table 3.1). This choice of the northern boundary has the advantage that most coastlines and ocean currents (center of the subtropical gyres) are oriented perpendicular to the boundary and therefore ensure a more stable model with less problematic boundary artifacts. The condition for the southern boundary was to include the entire Antarctic coastline and thereby creating a closed southern boundary for the model. In the zonal direction, the domain is east-west periodic (CPP-switch *EW_PERIODIC*) with an exchange between the eastern and western boundary at 24° E (λ_0). I chose this longitude over the center of the African continent in order not to interrupt the northern boundary in one of the ocean basins, which would be problematic for the northern boundary condition (section 3.5.5). The only open boundary is therefore the northern boundary (CPP-switch *OBC_NORTH*), which is divided into the three major ocean basins. I had to implement some adjustments to the open boundary condition in the north that are specific to this setup as I will describe in detail in section 3.5.5. In this section, I will continue to describe the different horizontal resolutions at which the setup is available, the vertical grid, the topography, and the land-sea-ice mask.

3.4.1   Horizontal grid & resolution

I here use a stretched longitude-latitude, staggered coordinate system in the horizontal. The model grid follows longitudes (λ) in the ξ-direction (x-direction) at a regular spacing. The grid cell center (ρ-points) in the ξ-direction is defined through:

$$\lambda_\rho(\xi) = \lambda_0 - \frac{\delta_\lambda}{2} + \xi \cdot \delta_\lambda \; . \tag{3.5}$$

Here, δ_λ denotes the spacing in degrees longitude in the ξ-direction. In the η-direction (y-direction), the model grid follows latitudes (ϕ) but the spacing is irregular. For each latitude band, I calculated the absolute distance between two λ_ρ points and applied this distance as spacing in η-direction. Therefore, each grid box has approximately the same size in ξ- and η-direction. The position of the grid point center is determined in two iterative steps from north to south:

$$\phi_\rho(\eta) = \phi_\rho(\eta + 1) - \delta_\lambda \cdot cos\left(\phi_\rho(\eta + 1) \cdot \frac{\pi}{180}\right) \; , \tag{3.6}$$

$$\phi_\rho(\eta) = \phi_\rho(\eta + 1) - 0.5 \cdot \delta_\lambda \cdot cos\left(\phi_\rho(\eta + 1) \cdot \frac{\pi}{180}\right) - 0.5 \cdot \delta_\lambda \cdot cos\left(\phi_\rho(\eta) \cdot \frac{\pi}{180}\right) \; . \tag{3.7}$$

After defining the horizontal grid, I used the standard *ROMSTOOLS* to create a grid-file that is used by the model and contains all necessary information.

Table 3.1   Model domain extent, resolution, and tiling of Southern Ocean ROMS setup.

δ_λ [° E]	δ_{south} [km]	δ_{north} [km]	$\phi_{south,\rho}$ [° N]	$\phi_{north,\rho}$ [° N]	$\lambda_{east,\rho}$ [° E]	$\lambda_{west,\rho}$ [° E]	n_η [-]	n_ξ [-]	p_η [-]	p_ξ [-]
1/2	10.7664	50.6087	-78.8826	-24.2280	23.7500	384.2500	218	722	36	8
1/4	5.4062	25.3501	-78.8102	-24.1141	23.8750	384.1250	434	1442	36	16
1/8	2.7089	12.6864	-78.7738	-24.0571	23.9375	384.0625	866	2882	24	32
1/10	2.168	10.1509	-78.7665	-24.0457	23.9500	384.0500	1082	3602	24	40

ϕ denotes the latitude, λ the longitude, δ_λ the resolution in the zonal direction, δ_{south} and δ_{north} the spatial resolution at the southern and northern boundaries, n the number of grid points, p the recommended number of partitions, η the meridional- or y-direction, ξ the zonal- or x-direction. Numbers include ghost-points on either side of the domain.
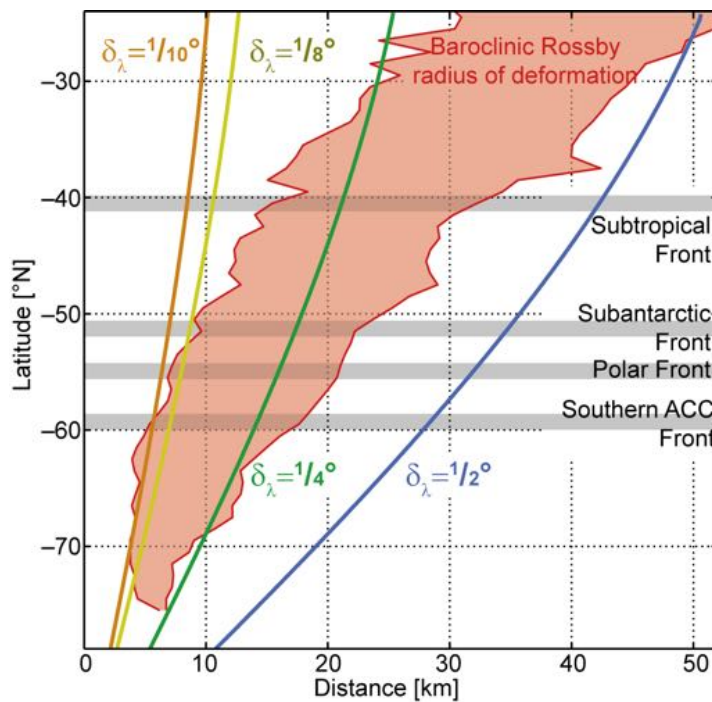
Figure 3.1   Variation of different model resolutions with latitude: Colored lines show the variation of the spatial resolution with the respective zonal resolution in degrees longitude as in Table 3.1. The red area spans the minimum and maximum baroclinic Rossby radius of deformation at each latitude from Chelton et al. (1998). The location of the fronts (gray) is the circumpolar mean of the fronts from Orsi et al. (1995).

ROMS requires so-called ghost points that are added on either boundary (one row or column each). In this setup, these ghost points exchange information from one side of the domain to the other in the east-west direction (CPP-switch *EW_PERIODIC*). The grid corner points and number of grid points in either direction including the ghost points are listed in Table 3.1 for four different possible resolutions. Note that this spatial resolution δ_λ only indicates the zonal resolution, since the actual resolution depends on the latitude. Such a grid has the advantage of naturally converging longitudes towards the pole and therefore a refinement of the spatial resolution towards the south. This stretching of the grid gives a considerable computational advantage. At the same time, it has a higher resolution where the eddy activity is high in the ACC region (Frenger et al., 2015) and follows the natural decrease of the baroclinic Rossby radius of deformation towards

the pole (Figure 3.1), which sets the length scale for baroclinic instabilities in the ocean (Chelton et al., 1998; Hallberg, 2013).

The coarsest resolution of 0.5° longitude ranges between about 50 km at the northern boundary and about 10 km at the Antarctic coast (Figure 3.1). In the ACC region, this grid has a resolution of about 30 km, which already allows to resolve some meso-scale eddies that have an average diameter of about 80 km (Frenger et al., 2013). The 0.25° longitude resolution closely follows the baroclinic Rossby radius of deformation (Chelton et al., 1998) and therefore permits for some meso-scale activity. The 0.125° and 0.1° longitude resolutions will be fully resolving the baroclinic variations in the Southern Ocean and therefore will provide the most accurate simulations. While both these high-resolution versions were tested, in this thesis, I will only run experiments with the 0.5° and 0.25° longitude resolutions due to temporal constraints. This too low resolution is one of the caveats of the findings in this thesis (see chapter 6) and some of the model biases (section 3.7) might result from it—an issue that will be addressed in future endeavors.

3.4.2   Vertical grid & resolution

I introduced and described the stretched, terrain-following vertical coordinate system in ROMS (Song and Haidvogel, 1994; Shchepetkin and McWilliams, 2003, 2005, 2009b) already in section 3.1.1. Here, I will discuss the parameters and the vertical resolution used for the Southern Ocean setup. This version of the coordinate system (version 3 of UCLA-ETH vertical coordinates) has the option to specify a critical depth h_c, the surface stretching parameter θ_s, the bottom stretching parameter θ_b, and the number of layers N. The lower most layers follow the terrain more closely than the upper layers (Figure 3.2c). The depth at which this transition occurs can generally be controlled by h_c. The deeper this level is, the flatter are the grid lines towards the surface. If θ_s increases the number of layers and therefore the resolution increases towards the surface. The same holds for the bottom layers when increasing θ_b.

I found that the results produced by KPP as well as the model drift in the water masses are inherently sensitive to the choice of parameters. The standard parameters used in most ROMS simulations are shown in gray in Figures 3.2a and b. Lowering h_c to 1000 m helped to preserve water masses due to a reduction in spurious mixing. However, this leads to a substantial reduction in resolution at the surface (inset of Figure 3.2a). Fewer layers at the surface led to larger biases in surface mixing processes, because KPP had less layers to fit the stability functions (section 3.2.2). In extreme cases this led to a complete disappearance of the surface mixed layer. Using a more reasonable value for h_c of 450 m and at the same time increasing θ_s to its maximum of 10, improved both the surface mixing and water masses (blue in Figure 3.2). This is owing to a higher resolution, reduced tilting, and more evenly spaced layers towards the surface. Using a maximum value of 4 for θ_b, allowed the resolution of the bottom boundary layer over more shallow regions. Note that the apparent low resolution of the bottom layers in Figure 3.2b is owing to the fact that
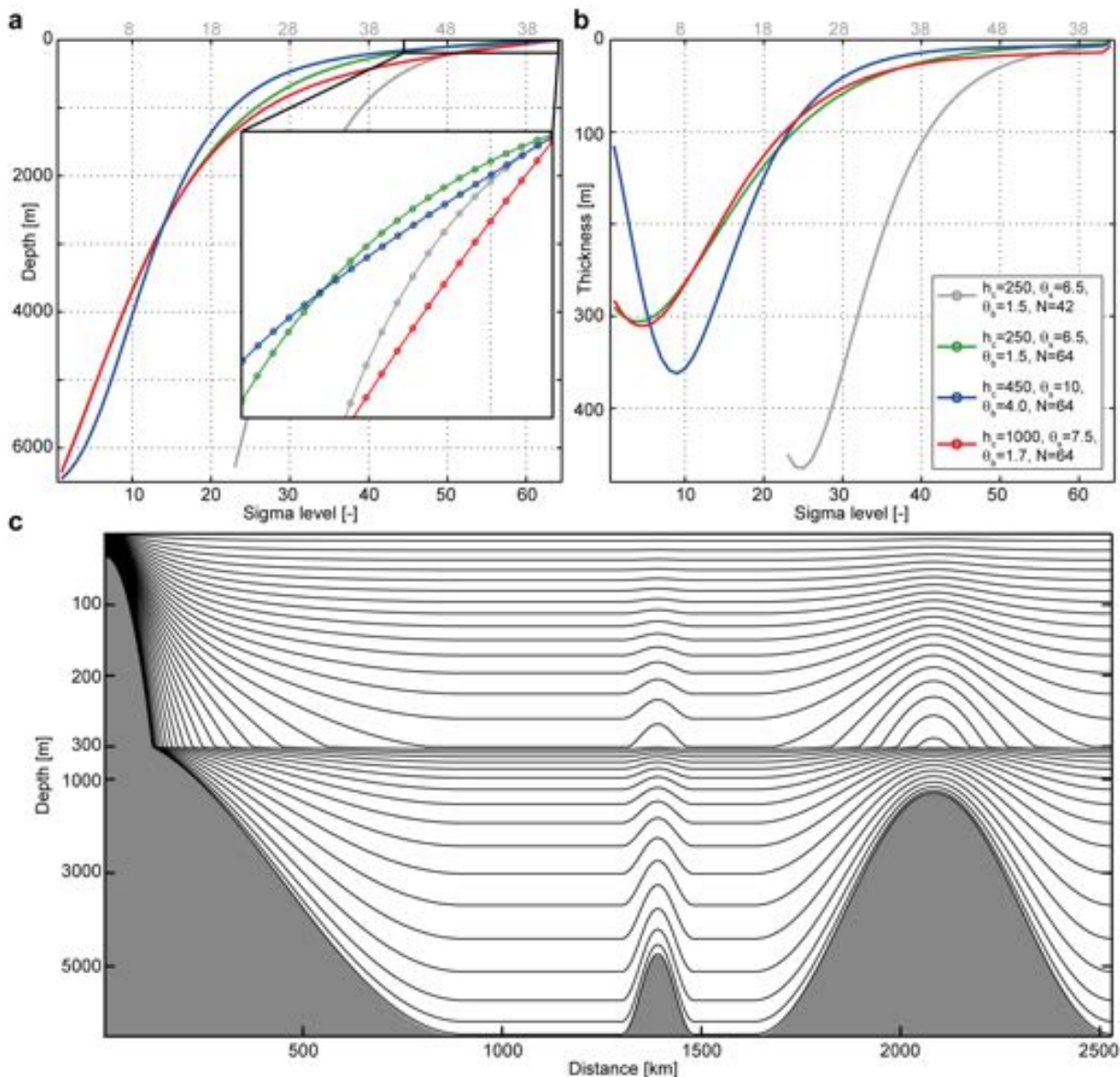
Figure 3.2   Vertical grid in the Southern Ocean ROMS: (**a**) Depth of vertical layers for different parameters of the vertical coordinate system at an ocean depth of 6500 m. The zoomed inset shows the top 200 m. (**b**) Vertical resolution of vertical layers for different parameters of the vertical coordinate system at an ocean depth of 6500 m. The final parameters used for the Southern Ocean model are shown in blue in **a** and **b**. (**c**) A vertical cross-section showing the final sets of parameters over an exemplary bathymetry (only every second layer is shown).

this figure is produced using the maximum ocean depth of 6500 m. In a more shallow region of about 500 m the bottom layers would have a vertical extent of about 8 m.

The performance of KPP improved considerably, especially in the deep ocean, when using more vertical layers (64 instead of 42). I chose 64 layers so that at least two layers were located in the upper most 10 m at the deepest location (6500 m). Such an increase of vertical resolution would theoretically lead to much higher computational expenses, not only due to the higher number of grid cells but also due to a much smaller time step, as the vertical motion became the limiting factor for not violating the *Courant-Friedrichs-Lewy* (CFL) criterion. This effect could be alleviated by using a new development that temporarily adjusts the time step on-line in the

model if the CLF criterion breaks in the vertical (Shchepetkin, 2015). In fact, the time step could be chosen much larger than previously when using this development allowing for a 50% higher vertical resolution at the same computational expense.

3.4.3   Topography & land-sea-ice mask

The bathymetry in the model (see Figure 3.3) is based on RTopo-1, which is a compilation of different data sets of the Antarctic continental shelf regions and ice shelf topographies merged into the global GEBCO bathymetry data set (Timmermann et al., 2010). The use of RTopo-1 is essential for an accurate ocean circulation in this setup. Previous attempts using ETOPO led to very large biases in the model that were largely induced by strong deviations in the bathymetry of up to several hundred meters over the Antarctic continental shelf between ETOPO or GEBCO compared to RTopo-1. Very recently, this data set was further improved to RTopo-2 (Schaffer et al., 2016). This update should be used in future applications.

I prepared the bathymetry for ROMS in multiple steps. I had to divide the grid into two parts as the *ROMSTOOLS* are not able to create a circumpolar bathymetry for the grid file. These two parts were overlapping and also extended on either side of the domain to ensure a smooth transition when merging them again and at the periodic boundary. Each of these two parts was processed in the same way. First, I used the Fortran-routine *etopo* of the *ROMSTOOLS* to average the 1-minute resolution topography from RTopo-1 onto the coarser ROMS grid without any smoothing. From the resulting bathymetry, I created a land-sea-mask by setting all grid points with a depth shallower than 5 m to land and enforcing connectivity between all ocean points to obtain a single ocean basin. Second, I re-applied the *etopo*-routine on RTopo-1 to average the bathymetry onto the ROMS grid, but this time applied a smoothing radius of 5 (ratio between characteristic smoothing width and local grid size). A value larger than one implies that the bathymetry is smoothed over multiple grid points. I found that using a value of 5 rather than a smaller value that I used originally helps to reduce spurious isopycnal mixing (section 3.1.1), because the vertical coordinates have a smaller local tilt, which can be better resolved by the model. In a final step, I applied the Fortran-routine *lsmooth* (conditional log-smoothing) of the *ROMSTOOLS* with an r-factor of 0.15, which ensures that the local slope can be resolved by the model. Through this routine, I also constrained the depth to a minimum value of 50 m and a maximum value of 6500 m. Especially, the former value helps to enhance the models stability.

Large parts of the Antarctic land-ice covered region are below sea level are covered by floating ice shelves or the grounded ice sheet. ROMS, in the version used here, does not include an ice-shelf cavity model but is forced with lateral fluxes from the ice shelves (see section 3.5.3). Therefore, the descent of the the ocean's surface under the ice shelves cannot be simulated. I here impose a vertical wall to the model at the ice-shelf edge by modifying the land mask. For this purpose, I interpolated the location of the land, ice shelves, and grounded ice sheet from RTopo-1

onto the ROMS grid using the CDO (2015) nearest neighbor interpolation. Any point covered by either one of these points in the interpolated mask was defined as land or ice in the final land-sea-ice mask of the grid file. The final bathymetry and land-sea-ice mask of the model are displayed in Figure 3.3. ROMS does not account for the so-called wetting and drying effects, which are a spill-over of land points as the sea level changes. Therefore, land points are never involved in any computation by the model and provide an effective lateral wall to the model.
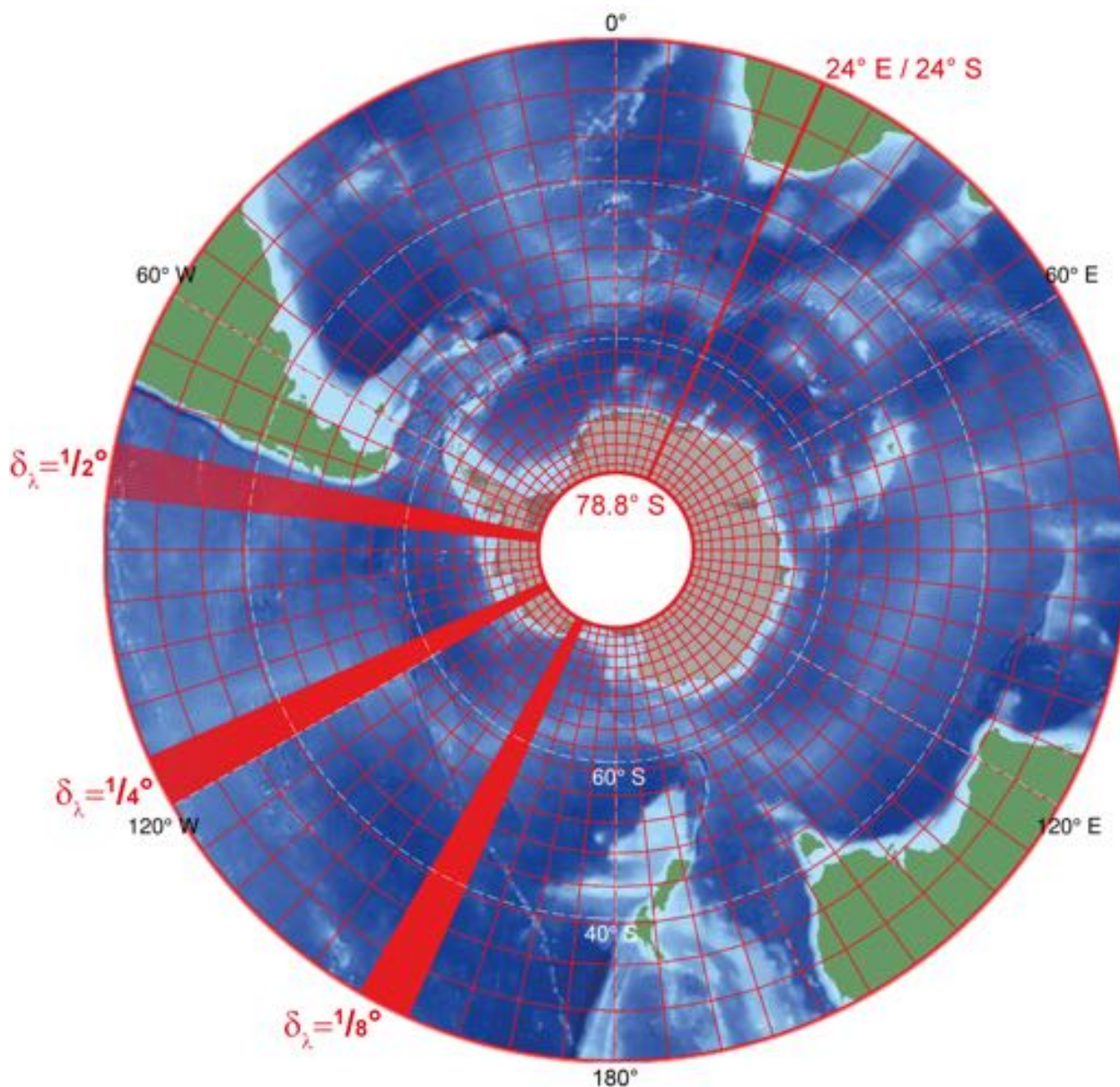
Figure 3.3   Model grid, bathymetry, and land-sea-ice mask of the Southern Ocean ROMS setup: The model grid is illustrated through the red lines that only show a few selected grid lines for illustration. The 0.5°, 0.25°, and 0.125° zonal resolutions are shown as examples in small sectors. The thick red lines indicate the model domain boundaries to the north and south and the periodic boundary in the east-west direction. The background shows the ocean bathymetry and land-sea-ice mask in the model (see text for details). The lighter gray shows the grounded ice sheet and the darker gray the ice shelves.

3.5   Forcing

The model is forced at the surface with freshwater, heat, and momentum fluxes from either the atmosphere (section 3.5.1), sea ice (section 3.5.2), or land ice (section 3.5.3). The latter partly enters the model as a surface forcing, i.e., melting icebergs, and a subsurface forcing, i.e., melting ice shelves. The model is directly forced with fluxes rather than using a bulk formula. Some of these fluxes are modified while the model is running as I will describe in more detail below. Additional surface fluxes are induced by a surface restoring to the observed salinity and temperature fields (section 3.5.4), which is here used as a flux correction. At the open northern boundary the model is forced with observation-based momentum and tracer fields (section 3.5.5). All model forcings are monthly mean climatologies. To account for high-frequency variability, which are critical for e.g. mixing processes, daily anomalies from the year 2003 were superimposed on the climatologies of the surface fluxes to form a so-called normal year forcing, which has the same monthly means as the climatology but accounts for daily weather effects. Perturbations of this mean forcing that I used for the sensitivity studies will be described in the chapters 4 and 5.

3.5.1   Atmosphere–ocean fluxes

At the atmosphere–ocean interface, the freshwater, heat, and momentum fluxes are mostly from the ERA-Interim global atmospheric reanalysis produced by the European Center for Medium-Range Weather Forecasts (ECMWF) (Dee et al., 2011; ECMWF, 2007). Some modifications to these fluxes are described below. Air–sea fluxes in the Southern Ocean are associated with very large uncertainties mostly owing to the lack of observational data (Bourassa et al., 2013). In many respects, ERA-Interim provides to date probably the most reliable estimate of these fluxes (Bromwich et al., 2011; Nicolas and Bromwich, 2011; Trenberth et al., 2011; Bracegirdle and Marshall, 2012; Bracegirdle, 2013). Nevertheless, I will apply multiple corrections to mitigate some of the known biases and large uncertainties will remain in the air–sea fluxes.

I here use 6 hourly ERA-Interim data from the native reduced N128 Gaussian grid, which has a spectral resolution of T255. The variables are the surface net solar and net thermal radiation, the surface sensible and latent heat flux, the instantaneous eastward and northward turbulent surface stress, the evaporation and the total precipitation. The data is masked with the ERA-Interim land-sea mask to only include ocean points, using a threshold of 0.5 from the land-sea mask (ECMWF, 2007). I used *ROMSTOOLS* to interpolate the data onto the Southern Ocean grid. However, the original *ROMSTOOLS* performed this interpolation based on the longitude-latitude coordinate system. This procedure provides good results for lower latitudes, but returned large interpolation errors in higher latitudes due to the converges of the longitudes towards the pole. Therefore, I implemented a method that projects the data first onto a polar stereographic grid and then uses the effective spatial distance for the interpolation. The interpolation is then performed using a natural

neighbor method. Additionally, the missing land points were filled by a linear extrapolation from the ocean points. The latter ensures that each ocean point on the ROMS grid has an associated surface flux. Using this method, I first created monthly mean fields over the period 1979 to 2014, and then averaged them to a monthly climatology. Additionally, I created daily forcing data for the year 2003 and calculated the anomalies of these daily fields to the monthly mean fields of the same year. At last, I added the daily anomalies of the year 2003 to the monthly mean climatology of the years 1979 through 2014 to obtain a normal year forcing with weather effects from the year 2003 and mean fluxes of the entire climatological mean period.

Large uncertainties and potential biases exist in the atmospheric surface freshwater flux, which is the evaporation minus the precipitation fields (E-P, Figure 3.4a–c). While the mean distribution shows a reasonable pattern of an exceeding evaporation in the lower latitudes and exceeding precipitation in the higher latitudes, the strength of the the net freshwater flux to the ocean in ERA-Interim is most likely overestimated in the polar frontal regions. This overestimation becomes apparent from a comparison to a satellite based estimate (HOAPS version 3.2; Andersson et al., 2010, see Figure 3.4b) and is also consistent with the findings by Cerovečki et al. (2011), who used a flux-correction method with the Southern Ocean State Estimate (SOSE). The integrated net atmospheric freshwater flux over the ocean south of 50° S amounts to about 0.65 Sv in ERA-Interim and about 0.35 Sv in HOAPS. The latter value is probably a slight underestimation, as the fluxes over sea ice are not included. The lower value from HOAPS is also consistent with the estimate by Abernathey et al. (2016), who calculated an amount of 0.28 Sv over the same region and an additional 0.14 Sv onto sea ice (total of 0.42 Sv) using the flux-corrected SOSE. I here correct for some the apparent overestimation in ERA-Interim by using a correction factor of 80% and, additionally, by applying a salinity restoring flux (section 3.5.4) in the northern part of the domain. I also applied a spatial correction to the atmospheric surface freshwater flux over sea ice by redistributing the snow layer according to the observed sea-ice advection (section 3.5.2). The total amount of snow or precipitation falling onto the Antarctic sea ice in ERA-Interim is about 0.11 Sv, which is in line with the estimate by Abernathey et al. (2016) above. A key problem of reanalysis products in general is that the global moisture budget does not close (Trenberth et al., 2011; Lorenz and Kunstmann, 2012). However, ERA-Interim shows a reasonable global closure (Lorenz and Kunstmann, 2012), making it a more reliable product in terms of temporal changes of the surface freshwater fluxes (Bromwich et al., 2011; Nicolas and Bromwich, 2011). Trends in the ERA-Interim E-P over the Southern Ocean are very small over recent decades, which agrees with observation based products (see table 4 by Bromwich et al., 2011).

The surface heat flux forcing equals the sum all heat fluxes described above. Additionally, the net surface solar radiation flux is provided as a separate forcing field to ROMS as it penetrates into the surface ocean. This shortwave radiation is prescribed to the model on a daily basis. Hence, diurnal variations have to be parameterized in order to account for night-time cooling and day-time warming of the mixed layer. In previous versions of ROMS, the diurnal cycle was simply modified by a cosine function leading to problematic situations in high latitudes. Therefore, a

more accurate formulation was implemented to account for variations of the diurnal cycle with latitude. Additionally, a dependence on longitude was implemented for a correct timing of the diurnal cycle. ERA-Interim overestimates the net shortwave and underestimates the net longwave radiation (Dussin et al., 2016). I corrected the monthly mean fields for these biases using the difference between the original ERA-Interim and the DFS5.2 (Dussin et al., 2016) fields in areas without sea ice. Moreover, ERA-Interim has a warm bias of in the near-surface temperature in the coastal region of Antarctica of up to $2°$ C (Bracegirdle and Marshall, 2012; Mathiot et al., 2012), which would lead an insufficient heat loss from the surface ocean. In most regions this bias is irrelevant in my simulations as the surface heat flux in the sea-ice covered area is over-written by an under-ice heat flux computation (section 3.5.2). Nevertheless, this bias could lead to an underestimation of the heat loss in some coastal polynya regions.

The large-scale circulation is generally well represented in ERA-Interim (Bracegirdle and Marshall, 2012; Bracegirdle, 2013; Sanz Rodrigo et al., 2013). Biases might exist in coastal regions, where the effect of local topographic wind systems is underrepresented. Such a bias is a common problem in coarse resolution atmospheric models. However, it mostly affects the ocean through the formation or absence of polynyas and sea-ice production (Mathiot et al., 2010, 2012; Stössel et al., 2011). As the sea-ice forcing of the ocean is prescribed in my simulations (section 3.5.2), this latter bias does not have an influence on the simulations. However, it might have an influence on wind-driven transport and mixing processes on the continental shelf.

BEC is forced with the climatological mean atmospheric partial pressure of CO_2 from the period 1998 to 2011 (Landschützer et al., 2014a). Additionally, surface deposition of iron and dust are used from the global model CCSM (Mahowald et al., 2009) and corrected for the deposition on sea ice (section 3.5.2).

3.5.2 Sea-ice–ocean fluxes

The UCLA-ETH version of ROMS—in contrast to the Rutgers version of ROMS and BRIOS mentioned earlier (see section 3.1)—is not coupled to a sea-ice model and I will not use one in this thesis. Nevertheless, as part of this project, I have partly implemented the sea-ice model by Budgell (2005) from the Rutgers version of ROMS (updated and maintained by K. Hedström). This sea-ice model has both a thermodynamic and dynamic component. The thermodynamics follow the formulation by Mellor and Kantha (1989) and Häkkinen and Mellor (1992). The model consists of two sea-ice layers, one snow layer, and one molecular sublayer beneath the sea ice. Frazil ice formation according to Steele et al. (1989) occurs when the ocean surface reaches the freezing point temperature. The sea-ice dynamics use the elastic-viscous-plastic (EVP) rheology by Hunke and Dukowicz (1997) and Hunke (2001). As the use of a thermodynamic-dynamic sea-ice model became obsolete throughout this thesis, I postponed the finalization of the implementation to future developments.
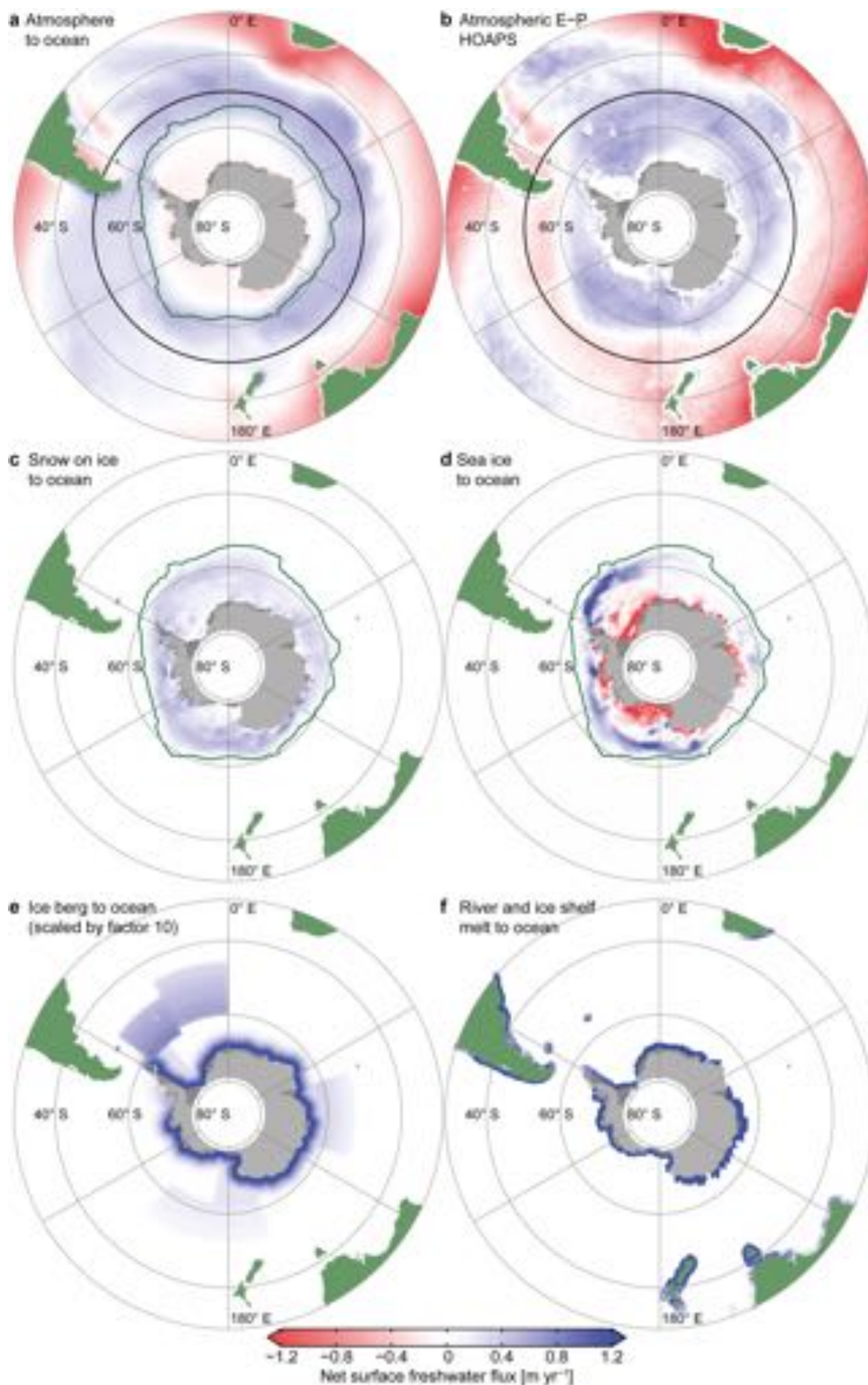
Figure 3.4   Surface freshwater flux forcing components: (**a**) Net annual atmosphere–ocean flux (E−P) modified from ERA-Interim. (**b**) Net annual atmospheric freshwater flux (E−P) HOAPS (compare to **a**+**c**). (**c**) Annual snow melting flux from sea ice. (**d**) Net annual freshwater flux from sea-ice formation and melting. (**e**) Net annual freshwater flux from iceberg melting (scaled by a factor 10). (**f**) Net annual land ice melting and river runoff (grid points are magnified). Green contour: climatological mean sea-ice edge; black line: 50° S. See text for details.

At the sea-ice–ocean interface, my approach differs from previous forced, regional modeling studies of the Southern Ocean. Instead of using a thermodynamic-dynamic sea-ice model, in this thesis, I will make use of the observation based ice-ocean surface fluxes derived in chapter 2. The main reason is that accurate simulations of sea ice in the Southern Ocean are very difficult and biases in the sea-ice fluxes can substantially influence the water-mass structure in the Southern Ocean. The difficulty of obtaining accurate sea-ice simulation is mostly owing to highly dynamic nature of the sea ice in this region (Emery et al., 1997; Haumann, 2011) and the Southern Ocean sea-ice dynamics are not well represented in models (Haumann et al., 2014; Uotila et al., 2014; Lecomte et al., 2016). This can lead to biases in the lateral transport of freshwater by sea ice, affecting both AABW and AAIW formation (see chapter 2). Moreover, there are strong atmosphere-ice-ocean feedbacks (Curry et al., 1995; Zhang, 2007; Liu and Curry, 2010; Stammerjohn et al., 2012) that can lead to large deviations in the sea-ice cover if there are only small inaccuracies in the atmosphere or ocean. As a consequence of these difficulties, coupled models notoriously suffer from very large biases in the sea-ice cover of the Southern Ocean (Mahlstein et al., 2013; Turner et al., 2013; Zunz et al., 2013). One particular issue that often leads to a very different water-mass structure in coupled models is the occurrence of spurious open-ocean polynyas and deep open-ocean convection (Stössel et al., 2015). Another common problem is the representation of coastal winds and the associated coastal polynya formation, which can alter the shelf water properties and therefore the AABW formation and ocean circulation (Petrelli et al., 2008; Mathiot et al., 2010; Stössel et al., 2011; Mathiot et al., 2012; Zhang et al., 2015).

In this study, I will prescribe the sea-ice concentration and the sea-ice–ocean freshwater fluxes (CPP-switch *ICEOBS*), because constraining the ocean circulation model with such a sea-ice forcing circumvents the problems described in the previous paragraph. Previous studies by Markus (1999) and Dinniman et al. (2003, 2007) have shown that prescribing the sea-ice cover can be great advantage when modeling the Southern Ocean surface and coastal waters. However, these studies calculated the sea-ice–ocean freshwater fluxes from the conductive and open-ocean heat fluxes and did not directly account for lateral advection of the sea ice, which redistributes the freshwater in the Southern Ocean (Haumann et al., 2016b). Therefore, additionally to the sea-ice cover, I here prescribe the climatological (1982–2008) daily mean sea-ice–ocean freshwater fluxes derived in chapter 2 (Figure 3.4d). The freezing fluxes were scaled so that the total annual freezing rate matches exactly the total annual melting rate in order not to induce any artificial model drift. The freezing and melting fluxes were both reduced by 10% to account for snow-ice formation (section 2.2.3), which would be part of the atmospheric forcing, even though the uncertainties in these fluxes are far larger than any of these effects (section 3.5.1).

The presence of a snow layer is calculated from the surface forcing prior to the model simulations (Figure 3.4c). For this purpose, $E - P$ is split in all grid boxes with ice into E and P. ERA-Interim evaporation already accounts for the sea ice fraction (ECMWF, 2007). Hence, there is no need to modify it. I scaled P with the ice concentration, which means that $P \cdot (1 - c_i)$ goes into the ocean and $P \cdot c_i$ is accumulated in an artificial snow layer over the year. The resulting

annual snow layer is then scaled with the ice export fraction obtained by Haumann et al. (2016b) to redistribute it. The freshwater is then added to the forcing as the snow melts. This melting is computed in a first step using the atmospheric surface heat flux, which is used when it is positive to melt the snow layer. The residual snow layer is then in a second step melted by scaling it with the sea-ice melt, assuming that the heat is provided from the ocean. The same procedure is applied to the surface iron and dust deposition on sea ice.

All surface freshwater fluxes are added to the surface layer of the model and converted to a salt flux depending on the surface ocean salinity. The melting and freezing fluxes from sea ice are treated separately from the other fluxes in order to allow for subsequent parameterizations such as the convection of brine plumes (section 3.2.2) or to optionally use the sea ice production for the computation of heat fluxes (see below). All freshwater fluxes, including the sea-ice freshwater fluxes, enter the dilution of other tracers in the model at the surface.

The sea-ice concentration forcing field is the satellite observed sea-ice concentration (c_i). Here, I will use the same CDR Bootstrap record that I also used to derive the freshwater fluxes (section 2.2.2). I replaced the sea-ice concentration field in the forcing files that was created from ERA-Interim data by the *ROMSTOOLS* with this data set, as the ERA-Interim provided sea-ice concentration suffers from multiple problems (Haumann, 2011) and to be consistent with the freshwater forcing.

The surface momentum forcing is modified under the sea ice to account for the atmosphere–ice–ocean momentum transfer. Due to the absence of lateral boundaries and the thin nature of Antarctic sea ice, it is in most regions at free drift. At free drift the momentum equation for sea ice can be simplified to (Omstedt et al., 1996; McPhee, 2008; Leppäranta, 2011):

$$\vec{u_i} = \vec{u_w} + N_a \vec{u_a} \ . \tag{3.8}$$

Here, $\vec{u}$ is the velocity vector for ice, water, and air respectively and N_a is the so-called Nansen number that is defined through the ratio between the atmospheric and oceanic drag. The latter number is generally small and about 3% for Antarctic sea ice. Given the uncertainty and potential underestimation of the surface momentum forcing (section 3.5.1) and as I am here only interested in the oceanic momentum, I will safely neglect the reduction of the momentum stress by sea ice if the sea-ice concentration is below 90%. However, as soon as the sea-ice gets more compact, i.e. if there is a high ice concentration, internal sea-ice stresses start to play a role in the momentum balance and the amount of momentum that is transferred from the atmosphere to the ocean decreases, which can also be interpreted as an increase of the Nansen number (Lu et al., 2016). I here use a simplified representation of this effect by linearly decreasing the stress for high sea-ice concentrations. Therefore, I apply a factor of 1 to the momentum stress for an ice concentration of 90% or smaller and decrease this factor to 0.1 for an ice concentration of 100%. This drastically simplified approach might be further improved in future simulations.

The surface heat flux is modified in two steps, whereas the first step is performed on the forcing field and the second step throughout the model simulation. I will build this modification on the premise that the sea ice forms from the atmospheric cooling (heat flux) and melts from the ocean heat flux, which is a good assumption for most of the Antarctic sea ice (Gordon and Huber, 1990; Gordon, 1991; Martinson, 1990, 1991). Therefore, in the first step, the total amount of latent heat of freezing H_{if} is subtracted from the surface heat flux and is defined through:

$$H_{if} = \rho_i \, L_i \, P_{if} \, , \tag{3.9}$$

where ρ_i is the density of sea ice (925 kg m^{-3}), L_i is the specific latent heat of melting and freezing ice ($334 \cdot 10^3$ J kg^{-1}), and P_{if} is the sea-ice formation rate. The result is then multiplied by the inverse sea-ice concentration. I also subtract the amount of shortwave radiation that is absorbed by sea ice and and only add the fraction that is absorbed by the ocean back to the net surface heat flux. For the latter calculation I used constant values for the sea-ice and ocean albedo of 0.85 and 0.06 respectively to be consistent with the original ERA-Interim formulation (ECMWF, 2007). At last, I subtract the latent heat flux that is used for melting snow and icebergs. The resulting product contains the sole net atmosphere–ocean heat flux in open water. The surface air temperature in ERA-Interim has a pronounced warm bias (see section 3.5.1), which most likely leads to an underestimation of the surface cooling in open water areas in high-latitudes. This bias might be corrected for in future simulations by using a bulk formula and correcting the surface temperature.

The second step of the heat flux modification is performed online during the simulation to account for the ice–ocean flux (H_i) in the ice covered ocean. For this calculation, I follow the approach by Markus (1999):

$$H_i = \rho_0 \, c_p \, c_h \, u^* \, (T_f - T_N) \tag{3.10}$$
$$= \frac{k_i \, k_s (T_a - T_f)}{k_i h_s + k_s h_i} + \rho_i \, L_i \, P_i \, . \tag{3.11}$$

In equation 3.10, ρ_0 is the reference density of the model (1027 kg m^{-3}), c_p the specific heat capacity of seawater (3985 J kg^{-1} K^{-1}), c_h is the heat transfer coefficient with a value of 0.0055 (Stanton number McPhee, 1992), u^* the friction velocity, T_N the temperature of the upper most model layer, and T_f the freezing point temperature, defined through (Steele et al., 1989):

$$T_f = -0.0543 \, S_N \, , \tag{3.12}$$

where S_N is the salinity of the model's surface layer. In equation 3.11, the first term denotes the conductive heat flux through the ice and the second term the latent heat of sea-ice formation and melting (see equation 3.9). Here, k_i (2.04 W m^{-1} K^{-1}) and k_s (0.31 W m^{-1} K^{-1}) are the heat conductivities of sea ice and snow, and T_a is the atmospheric surface temperature (Markus, 1999).

Markus (1999) calculates H_i according to equation 3.10 and uses equation 3.11 to calculate the sea-ice production and the associated freshwater flux. In this case, the ice–ocean freshwater fluxes depend on the ocean vertical heat exchange. However, here I am interested in the response of the ocean to the observation based surface freshwater fluxes that are used to force the model. Consequently, I could constrain H_i either through equation 3.10 or 3.11, both having their advantages and disadvantages. The use of 3.11 is influenced by biases in the atmospheric temperature, ice and snow thickness, and uncertainties in the ice production. In a first attempt, I used such a formulation of the surface heat flux. However, this led to large warm biases in the high-latitude surface ocean, mainly due to the warm bias in ERA-Interim data. Therefore, I here decided to use 3.10. The use of equation 3.10 is associated with different challenges. These are the influence of biases in the vertical mixing of heat and uncertainties in u^*. A more ideal implementation in future would be to accurately compute the H_i from equation 3.11 using a bias corrected surface air temperature and reasonable estimates for the sea-ice and snow thickness. This flux could be computed offline since the sea-ice melting and freezing fluxes observation based.

In the model the surface heat flux is additionally constrained, so that the model's surface temperature does not drop below the freezing point, which is computed through equation 3.12.

3.5.3   Land-ice–ocean fluxes

As for the sea ice, there is no explicit land ice component in ROMS that would simulate the interaction between the ocean and the ice shelves of the Antarctic continent. Yet, the melting of land ice is an important contributor to the water-mass transformation on the continental shelf that also contributes to the formation of AABW (Gordon, 1991, 2012, 2014; Jacobs, 2004). Land ice melting changes the water properties through a removal of sensible and latent heat from the ocean (buoyancy loss) and a net addition of freshwater to the ocean (buoyancy gain).

Spatial variation of theses sources and sinks determine different varieties of shelf waters and AABW found around the Antarctic continent. Therefore, ideally, in a model, the sources should vary as well. Another important factor is the partitioning of the melting between basal melting at the ice shelf edge and melting of icebergs that can drift and spread the melt water over a large distance (Silva et al., 2006; Tournadre et al., 2016). The partitioning between these two sources is about equal in a circumpolar sum but varies regionally (Depoorter et al., 2013; Rignot et al., 2013). In order to represent these fluxes as realistically as possible, I here force the model with spatially varying, observation-based estimates of iceberg and ice shelf melting rates for each ice shelf of the Antarctic continent (Depoorter et al., 2013).

I add iceberg fluxes directly to the surface forcing of freshwater and heat (Figure 3.4e; note that the iceberg flux is scaled by a factor of 10 in the figure). At this point in time the iceberg melting is not yet affecting the biogeochemistry through the input of nutrients and other tracers,

which should be implemented in future developments. The melting is distributed over the Southern Ocean following approximately the satellite-observed trajectories by Silva et al. (2006) and decreasing with distance from the coast, so that about 60% melt south of 63° S (see Figure 3.4). I scaled this spatial melting pattern in time using the shortwave radiative flux. A more sophisticated method would be to couple the model to an ice-berg trajectory model as suggested by numerous studies (Gladstone et al., 2001; Martin and Adcroft, 2010; Marsh et al., 2015; Merino et al., 2016). As such data sets are now available and are probably more realistic than my reconstruction, they should be used in future improvements of the surface forcing for this model. Ultimately, the magnitude of the total ice-berg melting fluxes is with about 0.04 Sv (Depoorter et al., 2013) very small compared to the other surface fluxes (sections 3.5.1 and 3.5.2). Therefore, their exact spatial pattern is not that essential in my simulations. However, it is important to move the iceberg melt away from the coastal grid cells. If all the melting was imposed in the coastal region, this would lead to a reduction in bottom water formation on the shelf (Martin and Adcroft, 2010; Stössel et al., 2015) and might enhance spurious open-ocean convection (Stössel et al., 2015; Merino et al., 2016).

A wide range of ways to represent basal ice-shelf melting exists in models. In coupled global models, these processes are vastly underrepresented and it is common practice to simply add the precipitation over Antarctica as runoff to the surface waters along the coast or spread it over a certain area (Marsland and Wolff, 2001; Stössel et al., 2015). A better, yet very simple, parameterization for coarse resolution was suggested by Beckmann and Goosse (2003), which calculates fluxes along the ice-shelf edge without the need to resolve the actual ice-shelf cavity. In higher-resolution models, ice-shelf cavity models (Holland and Jenkins, 1999) have been implemented and produce realistic melting rates around Antarctica (Timmermann et al., 2012; Hellmer et al., 2012; Goldberg et al., 2012; Timmermann and Hellmer, 2013; Nakayama et al., 2014). Such an ice-shelf cavity model was implemented into the Rutgers version of ROMS (Dinniman et al., 2007, 2012) and might be adapted for this version of ROMS in future.

In order to make use of the observation-based estimates of basal melting rates (Depoorter et al., 2013), I here implement a new option to ROMS (CPP-switch *TSOURCE*) that allows the addition of sources of water and associated tracer fluxes in the model interior anywhere in space and time. This new option reads the forcing data of freshwater volume, heat and tracer fluxes as four dimensional fields from a separate forcing file. In the model, the freshwater volume that is added dilutes all tracers and adds the additional tracer fluxes if they are provided as if they were advected into the grid cell. The implementation of these sources allows the addition of the freshwater and heat from ice-shelf melting to be spread over a certain depth range in the subsurface ocean and for each ice shelf separately. I created the forcing files by first spreading the estimated melt water of each ice shelf (Depoorter et al., 2013) in the horizontal direction along the first ocean grid cell off the ice-shelf edge that is given by the ice-shelf mask from RTopo-1 (see section 3.4.3). As these fluxes are representative of the year 2009, I lowered the meltwater input in the Amundsen and Bellingshausen Seas according to the suggested trends in the 1990s

and 2000s by Sutterley et al. (2014) and Paolo et al. (2015), which amounts to an integrated flux that is about 40% lower. So far, to my knowledge, there is no evidence for a significant trend in these fluxes prior to 1992, which I will use here as a climatological mean state (Figure 3.4f). In a second step, I scaled the total flux of each grid cell with the size of the grid boxes in the vertical and equally distributed the flux from 50 m depth to the bottom of the ocean to mimic the ice-shelf cavity. Adding the fluxes to the surface would lead to a too strong salinity stratification and inhibit the melt water from being mixed down, leading to too salty bottom waters. In the same way, I added the corresponding latent and sensible heat fluxes. For the sensible heat flux, I assumed that the ice that is melted had to be warmed from $-20°$ C to the melting point temperature. As the seasonal cycle of these fluxes is unknown, I used a constant annual mean flux throughout the year. The way that I implemented the basal melting does not allow the study of feedbacks between changes in the ocean and changes in the melting rate. However, it allows the study of the ocean response to an increases in basal ice-shelf melting observed over recent decades (Sutterley et al., 2014; Paolo et al., 2015).

Similar to the ice-shelf flux, I spread the estimated climatological annual river runoff from the GRDC (2014) data base to the first ocean grid box along the coast line (Figure 3.4f). However, in contrast to the ice-shelf flux, I added the river runoff to the surface forcing rather than distributing it vertically over the water column.

3.5.4   Restoring

During the simulations, I used a restoring of the surface salinity and temperature fields. This procedure helps to reduce biases in the surface forcing (Figure 3.4) and keeps the model from drifting strongly (section 3.6). Note that during the perturbation experiments the surface restoring is treated separately in order not to affect the model's response, which is discussed in chapters 4 and 5.

Surface salinity is restored to the monthly mean satellite observed surface salinity from Aquarius (version 4) over the period 2011 through 2015 (NASA Aquarius Project, 2015). As the salinity in higher latitudes is not available or not reliable, I only use a restoring north of 48° S and linearly decrease it towards 53° S (Figure 3.5c). The restoring time scale for the surface salinity is set to 0.022 d^{-1}. In future efforts, a restoring towards the surface salinity from e.g. ARGO data might further improve the high-latitude surface freshwater fluxes. Yet, such products exist mostly on an annual rather than monthly basis (CARS ARGO only; Ridgway et al., 2002). Potential products that might be tested are either the MIMOC climatology (Schmidtko et al., 2013) or the climatological monthly mean salinity (Zweng et al., 2013) fields from the 0.25° version of World Ocean Atlas 2013 (WOA13 Boyer et al., 2013).

The surface heat flux in ROMS is adjusted by restoring the surface temperature in the model to

an observed sea-surface temperature (SST) through a restoring term that varies in space and time and is referred to as the kinematic surface net heat flux sensitivity to the SST. This restoring term is calculated in the *ROMSTOOLS* from the SST and the atmospheric surface temperature, density, wind speed, and specific humidity. Originally, this routine used monthly mean COADS data. However, the resulting restoring field in ROMS was of very poor quality in the high latitudes of the Southern Ocean. Therefore, I updated this routine to use the monthly mean NOAA Optimum Interpolation SST from AVHRR (Reynolds et al., 2007) over the period 1982 to 2014 and monthly mean ERA-Interim data for the atmospheric variables (Dee et al., 2011; ECMWF, 2007) over the same time period. No SST restoring is applied in areas covered by sea ice as data is less reliable.

3.5.5 Lateral boundary conditions

At the open northern boundary the model is forced with the climatological monthly mean temperature (Locarnini et al., 2013) and salinity (Zweng et al., 2013) fields from the 0.25° version of World Ocean Atlas 2013 (WOA13 Boyer et al., 2013) and ocean currents and sea-surface height data from the Simple Ocean Data Assimilation (SODA; verion 1.4.2; Carton and Giese, 2008). The latter might be updated to SODA version 3 in future, which has the advantage of being consistent with the ERA-Interim surface forcing. BEC is forced with nutrient (Garcia et al., 2014b) and oxygen (Garcia et al., 2014a) fields from WOA13; dissolved inorganic carbon and alkalinity from the Global Data Analysis Project (Key et al., 2004; Lee et al., 2006); iron, ammonium, and dissolved nutrients from a global model simulation with CESM1.2 (Yang et al., 2017); and chlorophyll-a from the SeaWiFS climatology (SeaWiFS Project, 2003), which is extrapolated to depth according to Morel and Berthon (1989) and used for all phytoplankton functional types. I interpolated these fields onto the ROMS grid using a bi-cubic interpolation method from CDO (2015, version 1.6.8). ROMS has the possibility to either nudge the solution towards a given field over several grid boxes at the boundary or to use a prescribed boundary condition at the edge of the domain. Here, I use the latter and all tracers and the velocity are prescribed only at the northern most grid cells in the model. Therefore, the interior of the domain consists of a completely free running model.

I here use a radiation boundary condition for all tracers and the baroclinic mode that follows Orlanski (1976) and Raymond and Kuo (1984) and was implemented into ROMS by Marchesiello et al. (2001). This boundary condition radiates waves generated in the model domain out of the domain. It generally works well when the motion or wave propagation is exerted perpendicular to the boundary, which is the reason why the location of the northern boundary in the center of the subtropical gyres is of advantage (section 3.4). The barotropic mode and sea-surface height are imposed using the radiation boundary condition based on Flather (1976). However, the application of such a radiation boundary condition for the barotropic mode turned out to cause large model biases and model drift. These problems were visible in a drifting sea-surface height and
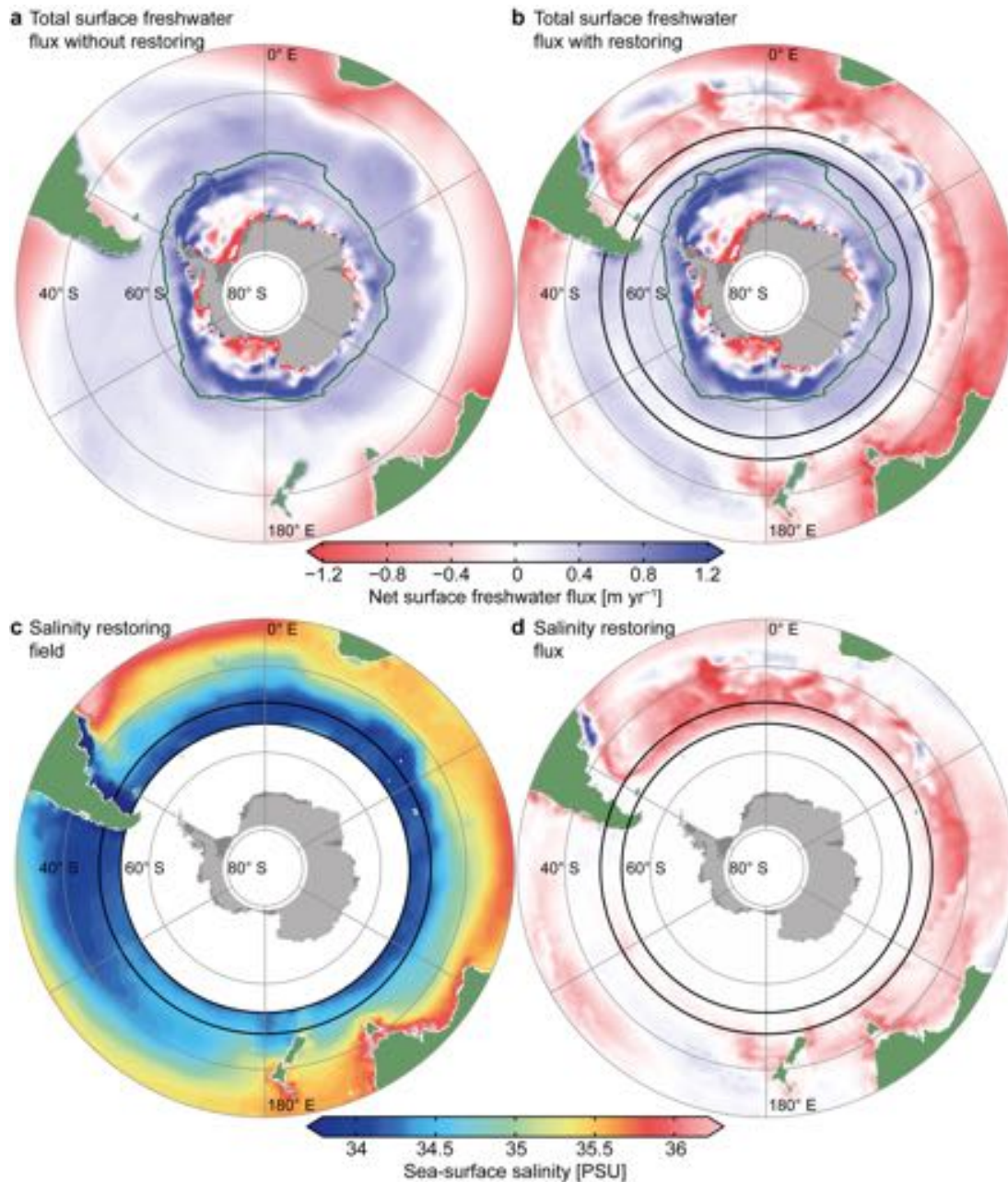
Figure 3.5   Total surface freshwater flux forcing with and without restoring: (**a**) Net annual total surface freshwater forcing without restoring flux. (**b**) Net annual total surface freshwater forcing with restoring flux. (**c**) Modified Aquarius sea-surface salinity field used for freshwater flux restoring. (**d**) Net annual surface restoring flux from the simulation years 21 to 40. Green contour: climatological mean sea-ice edge; black lines: 48° S and 53° S. See text for details.

a continuous northward displacement of the ACC. The key problem that I identified was that the model was open to all three ocean basins in the north, but had no knowledge on the mass exchange between these basins north of the model boundary. Therefore, it was free to change the mass balance between the ocean basins without knowing that the net exchange at the northern boundaries had to equal the trough-flow in the Bering Strait (1 Sv; Ganachaud and Wunsch, 2000) in the Atlantic, and the Indonesian Throughflow in the Indian Ocean (11 Sv; Stammer et al., 2003; Naveira Garabato et al., 2014). In order to solve this problem, I only apply the radiation condition in the Atlantic and specify the barotropic transport at the northern boundaries in the Pacific and Indian

Ocean to the fixed value provided by the boundary condition. While this solution works well, it has the disadvantage of trapping barotropic waves in the model domain. Such effects would mostly occur in the more narrow Atlantic basin, which is the reason for applying the radiation boundary condition in this basin. Additionally, I dampened trapped barotropic waves by applying a sponge layer with a viscosity of 400 m^2 s^{-1} over the northern most $10°$ of latitude (10 and 20 grid cells in the $0.5°$ and $0.25°$ configurations, respectively). In sum, these modifications allowed for an accurate simulation of the ocean circulation in the interior of the domain. In practice, the ROMS setup that I use here has compared to other regional domains a very good boundary with very little boundary artifacts such as strong along-boundary currents.

At the continental boundaries within the domain, ROMS imposes a free slip condition. While there is a setting in ROMS to use a no-slip condition, this condition only applies to closed domain boundaries but not the boundaries along the land-sea mask. However, implementing a partial slip condition along the continents might be useful in future to reduce e.g. overestimated coastal currents. The latter effect can be partially mitigated by using a bottom boundary layer and tuning the roughness length—a method that I applied here (section 3.2.2).

3.6   Computation, initialization, spin-up & model drift

The model runs with a calendar of 360 days and all month have an equal length of 30 days. Averages are written to the output for each month throughout the simulation. For the 0.5° model version, I found an ideal stable time step of 2700 s and for the 0.25° model a time step of 1200 s. I performed all simulations in parallel computing mode using the Message Passing Interface library Open MPI (version 1.6.5) on the ETH cluster *EULER* at the Swiss National Supercomputing Center (CSCS). The model's FORTRAN-77 code is compiled on *EULER* using the Intel© Ifort™ compiler (version 14.0.1). *EULER* uses the Linux CentOS 6.5 operating system and computes on multiple Hewlett-Packard BL460c Gen8 nodes with two 12-core Intel© Xeon© E5-2697v2 processors (Extended Memory 64 Technology) each. The model reads and writes data from and to Network Common Data Form files (NetCDF-4, version 4.3.1; using HDF5 library, version 1.8.12). Input and output fields are partitioned into horizontal tiles and each core computes one tile. The model performs most efficiently if the number of grid cells per tile in the ξ-direction is about 10 times larger than the number of grid cells per tile in the η-direction. Test experiments showed that an optimal performance is achieved for about 100 grid cells per tile in ξ-direction, which approximately corresponds to the recommended tiling provided in Table 3.1. However, the model scales reasonably well for multiples of the suggested tiling if a faster computation is required. Using the suggested settings the physical 0.5° model can be integrated at a speed of 5 model years per hour. If the model is coupled to BEC the computation time increases by a factor of 3. However, it should be noted that these computation times strongly depend on the number of variables and the averaging period of the data written to the output files. Therefore, a large number of variables, e.g. written by BEC, can considerably slow down the simulation.

ROMS is initialized from rest, i.e., all velocities at the beginning of the simulations are set to 0. Similarly, the sea-surface height is also initialized at 0. All tracers are initialized with the climatological mean fields described in section 3.5.5. The temperature and salinity tracers are initialized with the January climatological mean fields. Starting the model with austral summer-time conditions has the advantage that more observational data enter the initial fields.

Throughout this project, I ran more than 200 simulations (mostly 10 years) with the low-resolution (0.5°) version of the physical model to test certain paramertizations, forcings, and model developments. Very often biases in the model only occur after several years of integration. However, these test simulations were feasible as the model is running very fast and computationally efficient, i.e., 10 model years in two hours on 288 cores.

For this thesis, I performed a 40-year spin-up simulation with both the physical 0.25° version and the coupled physical-biogeochemical 0.5° version of the model as a starting point for the experiments presented in chapters 4 and 5, respectively. Due to biases in the forcing data and inaccuracies in the model's representation of physical processes through parameterizations, the model drifts away from the observation-based initial conditions in the first years of the simulation
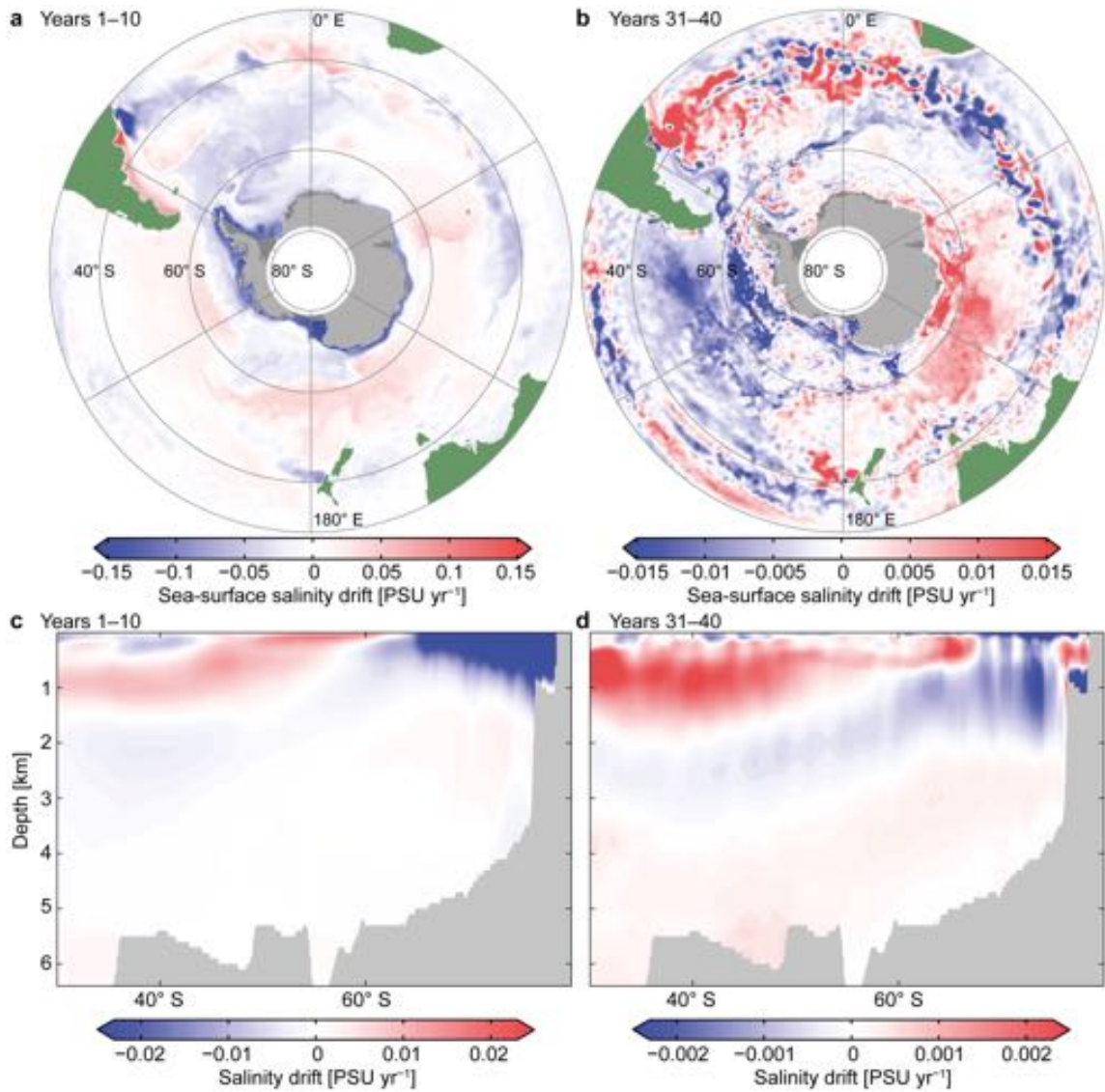
Figure 3.6 Salinity drift during spin-up simulation: Sea-surface salinity during simulation years 1 to 10 (**a**) and 31 to 40 (**b**). Cross-sections showing the zonal mean subsurface salinity drift during simulation years 1 to 10 (**c**) and 31 to 40 (**d**). Note the different scales.

towards a new equilibrium that is consistent with the forcing and model code (Figures 3.6, 3.7, and 3.8). Typically, a larger drift occurs in the first 10 years of the simulation and is about one order of magnitude smaller after the 40 spin-up years (note the different scales in Figures 3.6 and 3.7).

Strong drift occurs in the salinity fields over the continental shelf around Antarctica at the beginning of the simulation (Figure 3.6a,c). There are three potential reasons for this drift. Firstly, the WOA13 field that is used to initialize the model is a climatological mean over many decades, but the land ice melting (section 3.5.3) is estimated for the year 1992, which is a potentially higher melt rate than what would be consistent with WOA13. The second reason is the underestimated surface cooling over the continental shelf that leads to a reduced AABW formation in the model and therefore to a reduced subduction of the surface freshwater (section 3.7). Thirdly, an overly-stable surface layer or too little surface mixing also contributes to a lack of subduction of

freshwater in this region, making the surface ocean fresher and the deep ocean saltier. At the end of the spin-up the surface salinity drift is small (note the different scales) and depends on the region, indicating that the model's surface is largely equilibrated and most of the trends result from internal variability. In the subsurface ocean a prevailing salinification of the AAIW and SAMW is the most prominent feature (see section 3.7 for more details).
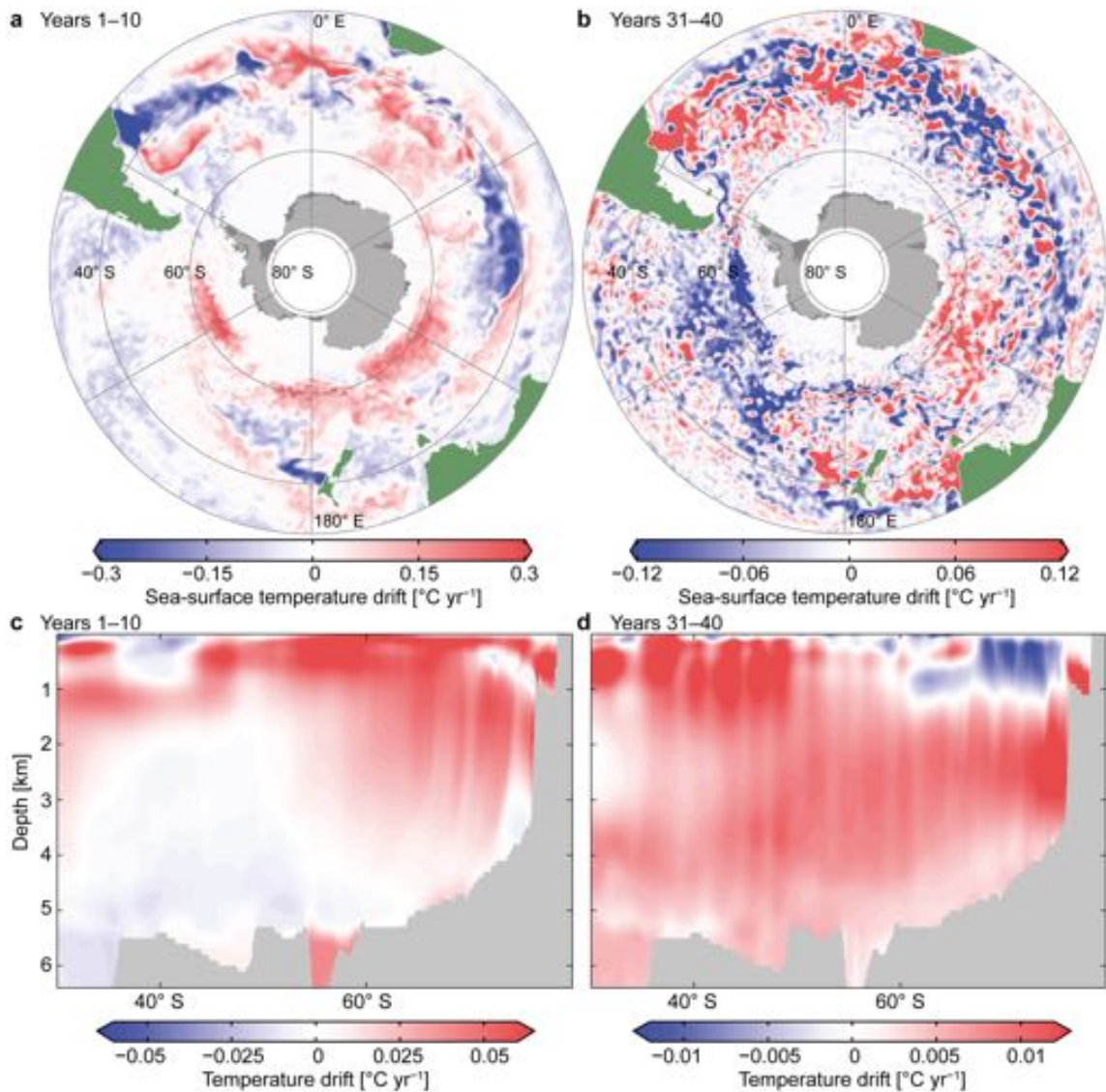
Figure 3.7 Temperature drift during spin-up simulation: Sea-surface temperature during simulation years 1 to 10 (**a**) and 31 to 40 (**b**). Cross-sections showing the zonal mean subsurface temperature drift during simulation years 1 to 10 (**c**) and 31 to 40 (**d**). Note the different scales.

The surface temperature drift shows a warming of high latitudes and a weak cooling of lower latitudes in the beginning of the simulation (Figures 3.7 a–b). At the end of the spin-up simulation, most of this surface temperature drift disappeared. A more critical feature is a broad-scale subsurface warming (Figures 3.7 c–d), which, even though at a much smaller rate, still persists at the end of the spin-up. This subsurface temperature drift can probably be attributed to a too stable surface layer and too little surface heat loss. As the Southern Ocean gains heat through the inflow of relatively warm NADW through the northern boundary, it needs to lose this heat to the

atmosphere at the high-latitude surface ocean or the outflow of surface waters, SAMW, or AAIW. If this heat loss does not equal the inflow at the northern boundary the model temperature will continue to drift in the subsurface. Future efforts should be devoted to resolving this issue.
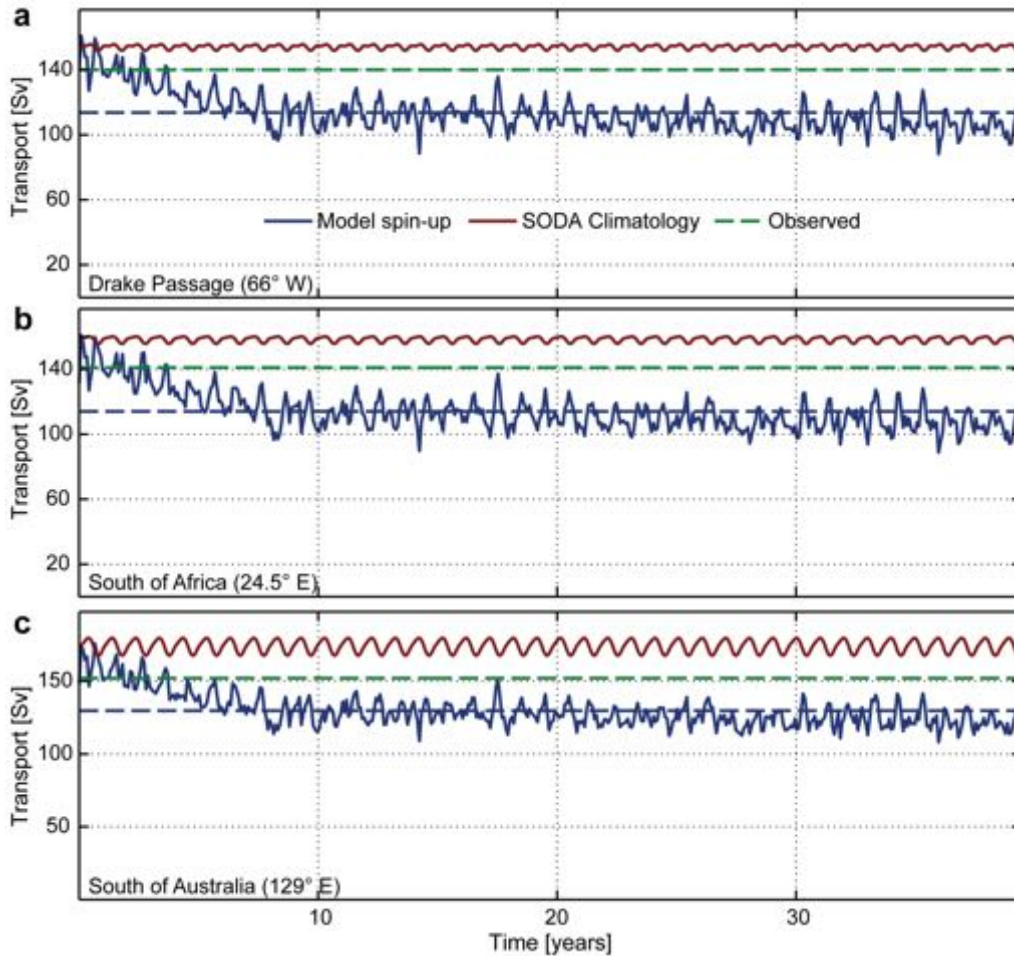
Figure 3.8   Transport drift during spin-up simulation: Time series of vertically integrated zonal volume transport (Sv) through (**a**) Drake Passage, (**b**) south of Africa, and (**c**) south of Australia. The blue curve shows the model spin-up simulation and the blue dashed line the respective mean, the red curve the SODA climatology that was used to force the model at the northern boundary (section 3.5.5, and the green dashed line shows the approximate mean values from observations (Ganachaud and Wunsch, 2000; Naveira Garabato et al., 2014; Koenig et al., 2014).

Figure 3.8 shows the temporal evolution of the vertically integrated zonal volume transport in the model with the ACC through Drake Passage, south of Africa, and south of Australia. Due to the fixation of the northern boundary (section 3.5.5), the relative transport ratio between these gateways does not change but its absolute magnitude changes over time depending on the surface forcing and the meridional density gradient. The transport decreases by about 30 Sv over the first 10 years and only slightly thereafter. A more detailed evaluation of the transport is provided is section 3.7. To account for any remaining model drift in each of the experiments, I ran an additional control simulation that is used to subtract the model drift from the experiments presented in chapters 4 and 5.

3.7   Model evaluation

In this section, I only evaluate the model physics of the 0.25° resolution model, because the ocean circulation model was the key focus of this chapter. A brief evaluation of the biogeochemical model is provided in chapter 5. The evaluation is based on the last 10 years of the climatological mean spin-up simulation (section 3.6), i.e., simulation years 31 to 40, when the model drift is comparably small.

3.7.1   Circulation

In section 3.5.5, I introduced a new concept for the northern boundary in ROMS, where the vertically integrated transport is fixed to the boundary condition in the Pacific and Indian Ocean sectors and is free to adjust in the Atlantic sector. Figure 3.9 shows this vertically integrated transport at the northern boundary compared to the SODA boundary forcing. The overall net transport through the boundary is zero, because the northern boundary is the only open boundary in the domain. Starting at the African continent and going eastward, the cumulative transport in the Indian Ocean amounts to -16 Sv, which agrees with the estimate by Ganachaud and Wunsch (2000) and is a slightly higher southward transport than the estimated -11 Sv by Sloyan and Rintoul (2001a), Stammer et al. (2003), or Talley (2003) for the Indian Ocean. In the model and in SODA, -20 Sv are transported through the Mozambique Channel and $+4$ are transported northward east of Madagascar. The former is a slightly higher southward transport than the estimated -17 Sv by Ridderinkhof et al. (2010). In the Pacific, $+16$ Sv are transported to the north by the model and SODA, which is again in good agreement with the estimate by Ganachaud and Wunsch (2000) and slightly higher than the one by Stammer et al. (2003) and Naveira Garabato
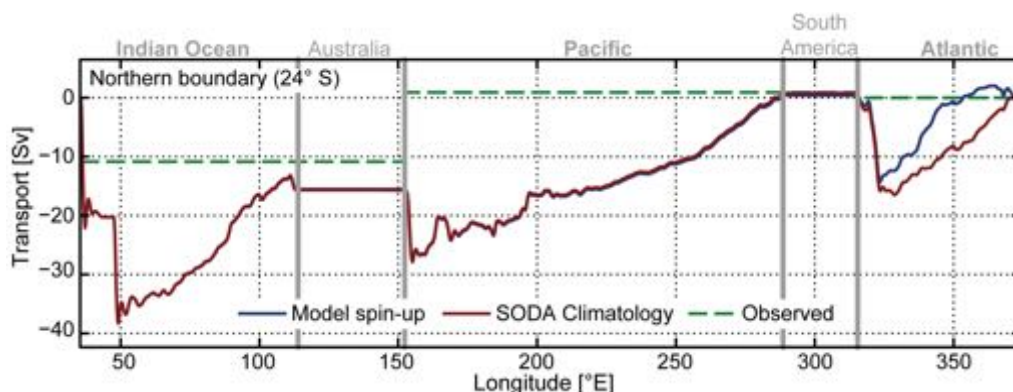
Figure 3.9   Meridional transport at the northern boundary: Cumulative, vertically integrated meridional volume transport (Sv) through the northern boundary. The blue curve shows the model simulation, the red curve the SODA climatology that was used to force the model at the northern boundary (section 3.5.5), and the green dashed line shows the approximate mean from observations for each basin, which has to sum up to zero over the entire northern boundary (Ganachaud and Wunsch, 2000; Stammer et al., 2003; Naveira Garabato et al., 2014). Gray bars denote continental margins.

et al. (2014). In the Atlantic, where the model can adjust the boundary transport, a slightly too weak southward transport occurs with the western boundary current. This lack of transport into the domain is compensated by a slightly too weak northward Sverdrup transport in the central and eastern Atlantic subtropical gyre. The overall transport in the Atlantic in the model amounts to -0.4 Sv, similar the observed values between 0 and -1 Sv (Ganachaud and Wunsch, 2000; Naveira Garabato et al., 2014), which should roughly equal the flow through Bering Strait.
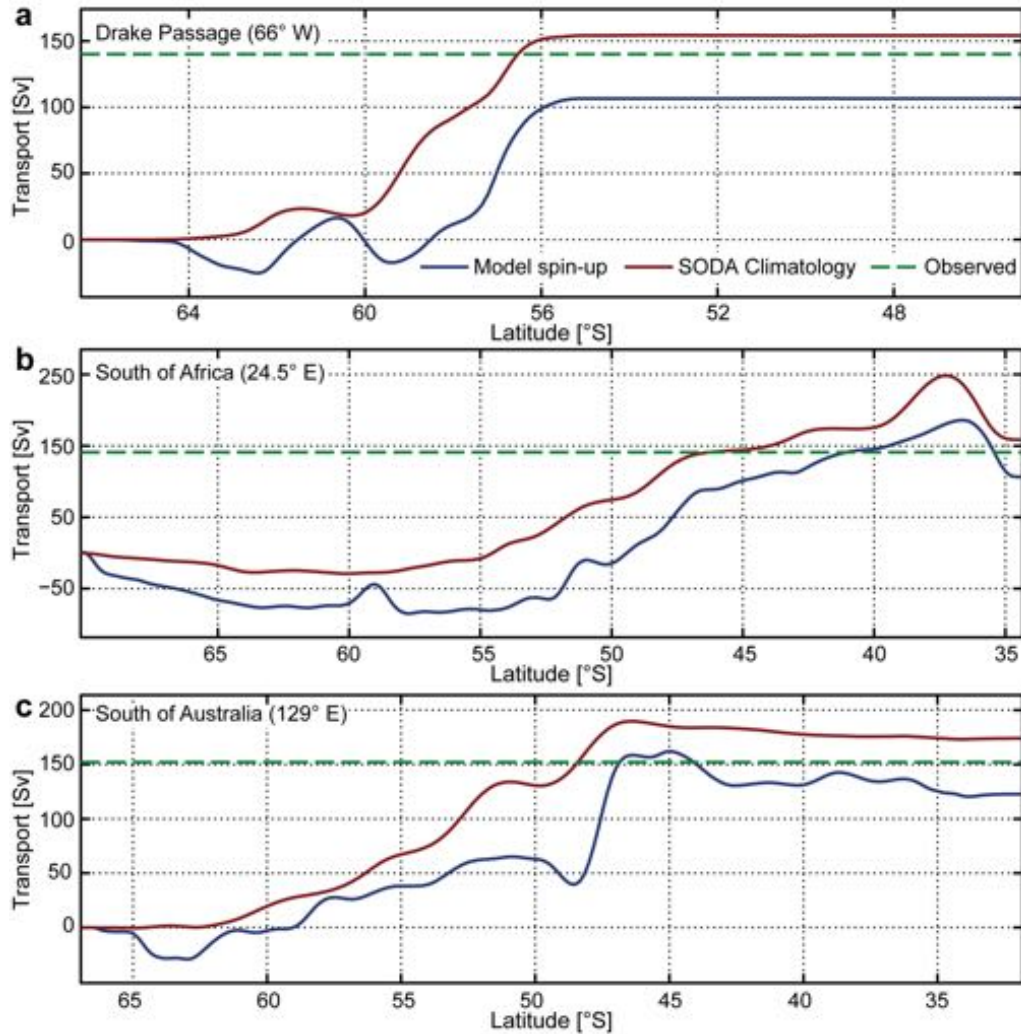
Figure 3.10   Zonal transport between ocean basins: Cumulative, vertically integrated zonal volume transport (Sv) through (**a**) Drake Passage, (**b**) south of Africa, and (**c**) south of Australia. The blue curve shows the model simulation, the red curve the SODA climatology that was used to force the model at the northern boundary (section 3.5.5), and the green dashed line shows the approximate overall mean from observations (Ganachaud and Wunsch, 2000; Naveira Garabato et al., 2014; Koenig et al., 2014).

Between the ocean basins there is a westward transport close the Antarctic continent with the coastal current and a much stronger eastward transport with the ACC further north as illustrated by the cumulative transport shown in Figure 3.10 for each of the three major gateways. In the model, these transports amount to $+103$ Sv through Drake Passage, $+104$ Sv south of Africa, and $+119$ Sv south of Australia. While the relative ratio between these transports is set through the northern boundary forcing and therefore agrees well with observations, their absolute eastward

transport is about 37 Sv lower than the observation based estimates (Ganachaud and Wunsch, 2000; Naveira Garabato et al., 2014; Koenig et al., 2014). This bias is related to a too small north—south density gradient in the model, which is typical for an overly-stable high-latitude surface ocean. In contrast, test experiments showed that the occurrence of high-latitude open-ocean deep convection would lead to an overestimation of the ACC transport, in agreement with the findings by Stössel et al. (2015). The transport shows a realistic meridional structure with two to three jets in the ACC region that are associated with the main fronts (Cunningham et al.,
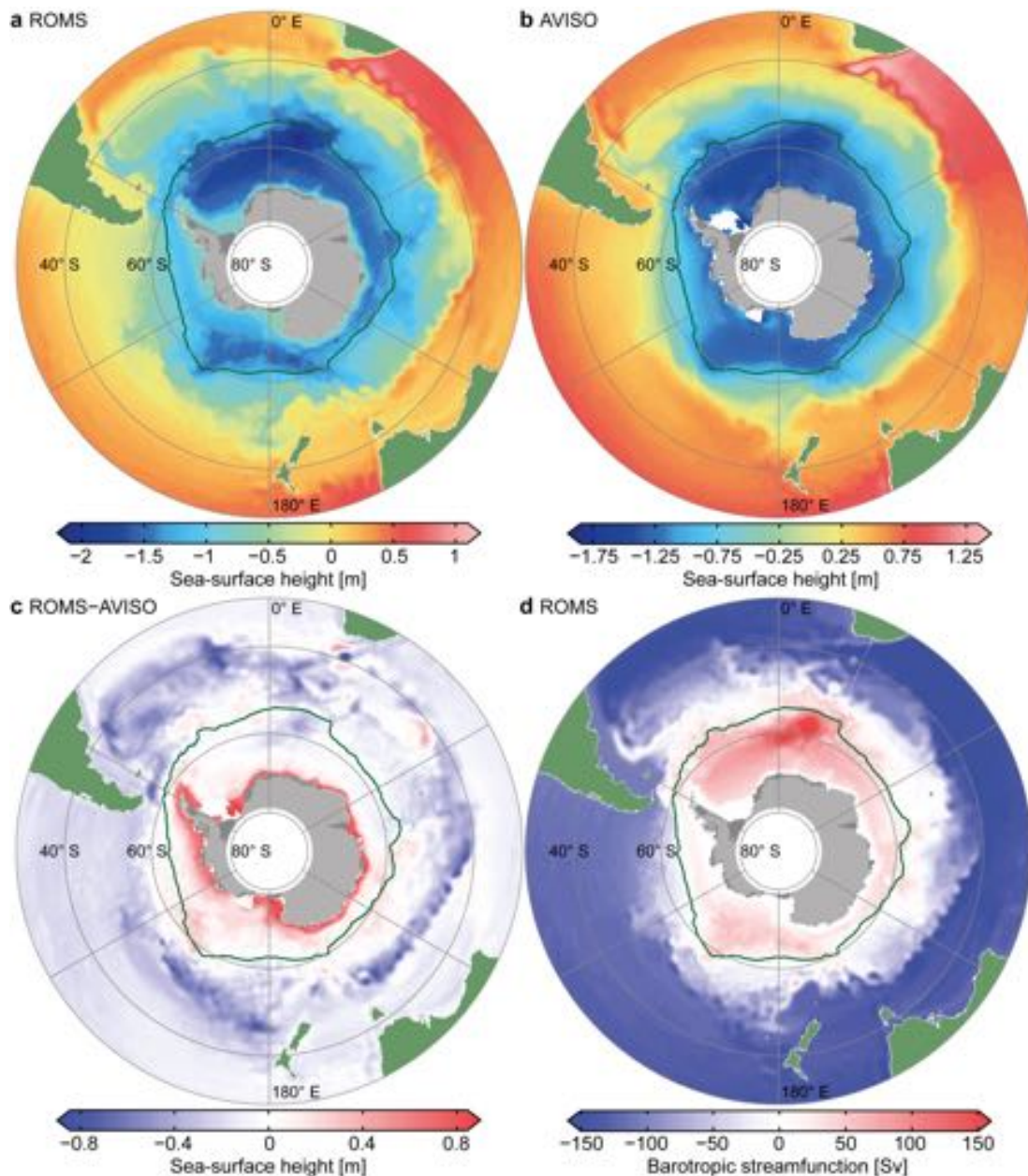
Figure 3.11   Sea-surface height and barotropic streamfunction showing the horizontal circulation: Sea-surface height from the model (**a**) and AVISO satellite product (**b**). The satellite product is produced by Ssalto/Duacs and distributed by AVISO with support from Cnes, http://www.aviso.altimetry.fr/duacs. Note the different color scale to adjust for the difference in mean sea level between the two estimates. (**c**) The sea-surface height difference between the model and the satellite data adjusted whereas the mean difference has been removed. (**d**) Barotropic stream-function from the model. Green contour line: climatological mean sea-ice edge.

2003). These jets are somewhat stronger than those by the coarser resolution SODA simulations. The westward coastal transport amounts to about −30 in most of the Indian Ocean and Pacific sectors, in agreement with the estimates by Peña-Molino et al. (2016). In the Atlantic sector, the transport is about −25 Sv in the vicinity of the Antarctic Slope Front, which is considerably higher than the estimate of about −10 Sv by Dong et al. (2016). The overall westward transport associated with the southern part of the Weddell Gyre (Figure 3.10b) amounts to about −70 Sv, which is comparable to the estimate by Schröder and Fahrbach (1999). In summary, the westward coastal transport is slightly overestimated due to a too strong meridional density gradient and the eastward ACC transport slightly underestimated due to a too weak meridional density gradient.

The simulated horizontal circulation pattern agrees generally well with the observed structure (Figure 3.11), which can be depicted from the comparison of the sea-surface height patterns in the model with the observed pattern from satellite data (AVISO; produced by Ssalto/Duacs and distributed by AVISO with support from Cnes, http://www.aviso.altimetry.fr/duacs). It shows strong gradients in the ACC region with several typical meridional excursions associated with topographic features. Overall, the meridional gradient is slightly too weak, confirming the previously stated underestimation of the ACC strength. On the Antarctic continental shelf, the sea-surface height is significantly overestimated in the model due to a too low density of the continental shelf waters. The stronger Weddell Gyre and the weaker Ross Gyre are clearly visible in the sea-surface height field and the barotropic stream-function of the model, which is the total transport integrated from the Antarctic continent towards the north (see e.g. Zika et al., 2012).
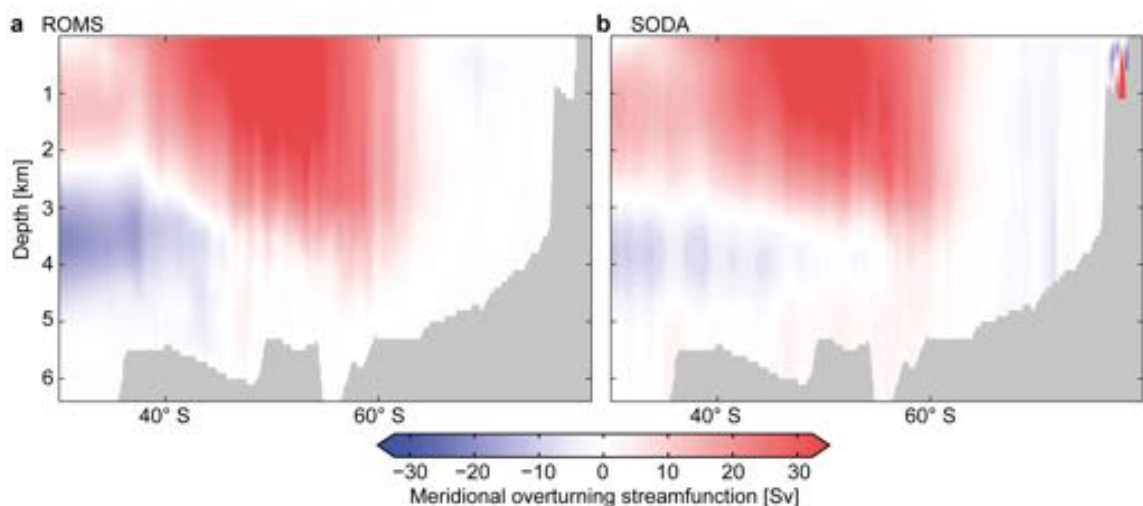
Figure 3.12 Meridional overturning circulation: Zonally averaged meridional overturning stream-function calculated from ROMS (**a**) and SODA (**b**).

In the vertical, the meridional overturning circulation (Figure 3.12) shows a clear upper and lower circulation cell in the model. This circulation looks very similar to the one in SODA, which is used to force the model at the northern boundary. However, it should be noted that the model's ocean interior runs freely, i.e., it is not adjusted to the SODA circulation. Nevertheless, it remains unclear how much of the overturning circulation in the model is governed by the northern

boundary forcing. Compared to the estimates by e.g. Lumpkin and Speer (2007) or Marshall and Speer (2012), the upper circulation cell seems too strong and the lower circulation cell too weak. Certainly, some of the biases in the model's water-mass structure (see below) might result from a dependence of the overturning circulation on the northern boundary and a replacement of the northern boundary transport by alternative products might improve the circulation.

3.7.2   Surface processes

In this section, I will evaluate the ocean's surface processes based on a comparison of sea-surface salinity (Figure 3.13), sea-surface temperature (Figure 3.14), and surface mixed layer depth (Figure 3.15) to observational data products. The latter products comprise the annual mean Argo-only climatology of CARS2009 (developed by CSIRO; Dunn and Ridgway, 2002; Ridgway et al., 2002), and the EN4 Objective analyses derived from quality controlled ocean profile data (version 4.2.0; 1979–2014; Ingleby and Huddleston, 2007; Good et al., 2013), and a combined Argo and CTD profile derived mixed layer depth product (de Boyer Montégut et al., 2004). For this comparison, the mixed layer depth from ROMS has been re-computed using the same density criterion as the observational product, because the mixing depth computed by ROMS itself uses a different criterion (for details see Eberenz, 2015).

The model suffers from a too fresh surface ocean in the sea-ice region, most of the South Atlantic, and, more extremely, over the Antarctic continental shelf (Figure 3.13). This signal becomes even more apparent during austral summer. A potential explanation for this fresh bias at the surface is provided by the too shallow mixed layer in the sea-ice region mostly during summer but also during winter (Figure 3.15). North of the sea-ice edge, a positive salinity bias exists in the Pacific and Indian Ocean sectors. A potential explanation for this bias is a reduced horizontal mixing of the water masses in the not fully eddy-resolving 0.25° model.

The sea-surface temperature shows a slight warm bias in the high-latitude surface ocean—mostly around the sea-ice edge (Figure 3.14). This warm bias originates from the austral summer period and is most likely related to an overly-weak summer-time mixing. Even though the modification of the mixing processes in KPP (section 3.2.2) that I introduced to ROMS greatly helped to reduce some of these biases, the model still has problems to accurately simulate mixing processes during the strongly stabilizing melting conditions during summer. Besides the shallow bias of the surface mixed layer in high latitudes during summer, a too deep mixed layer occurs north of the frontal region and downstream of Drake Passage during austral winter (Figure 3.15). Nevertheless, the model is generally able to simulate the spatial and temporal evolution and characteristic patterns of the surface mixed layer depth in the Southern Ocean (de Boyer Montégut et al., 2004) with deep winter-time mixed layers north of the frontal region during winter and a more annular and somewhat shallower mixed layer in the ACC region during summer.
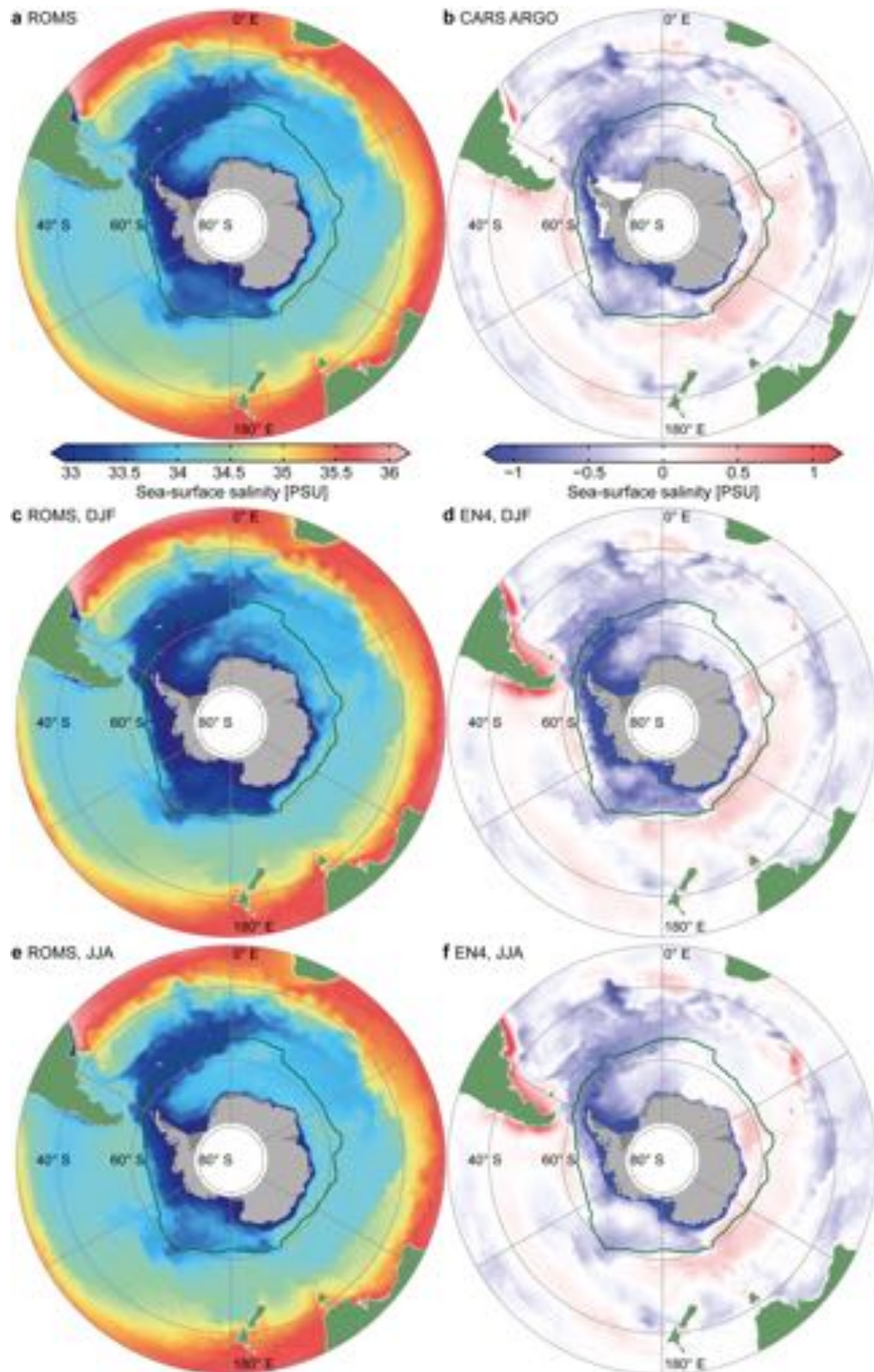
Figure 3.13 **Sea-surface salinity:** Annual mean sea-surface salinity in ROMS (**a**) and its difference to the Argo-only climatology of CARS2009 (**b**). Austral summer (DJF) mean sea-surface salinity in ROMS (**c**) and its respective difference to the EN4 climatology (**d**). (**e**) and (**f**) as (**c**) and (**d**) but for austral winter (JJA). The green contour line denotes the climatological mean sea-ice edge.
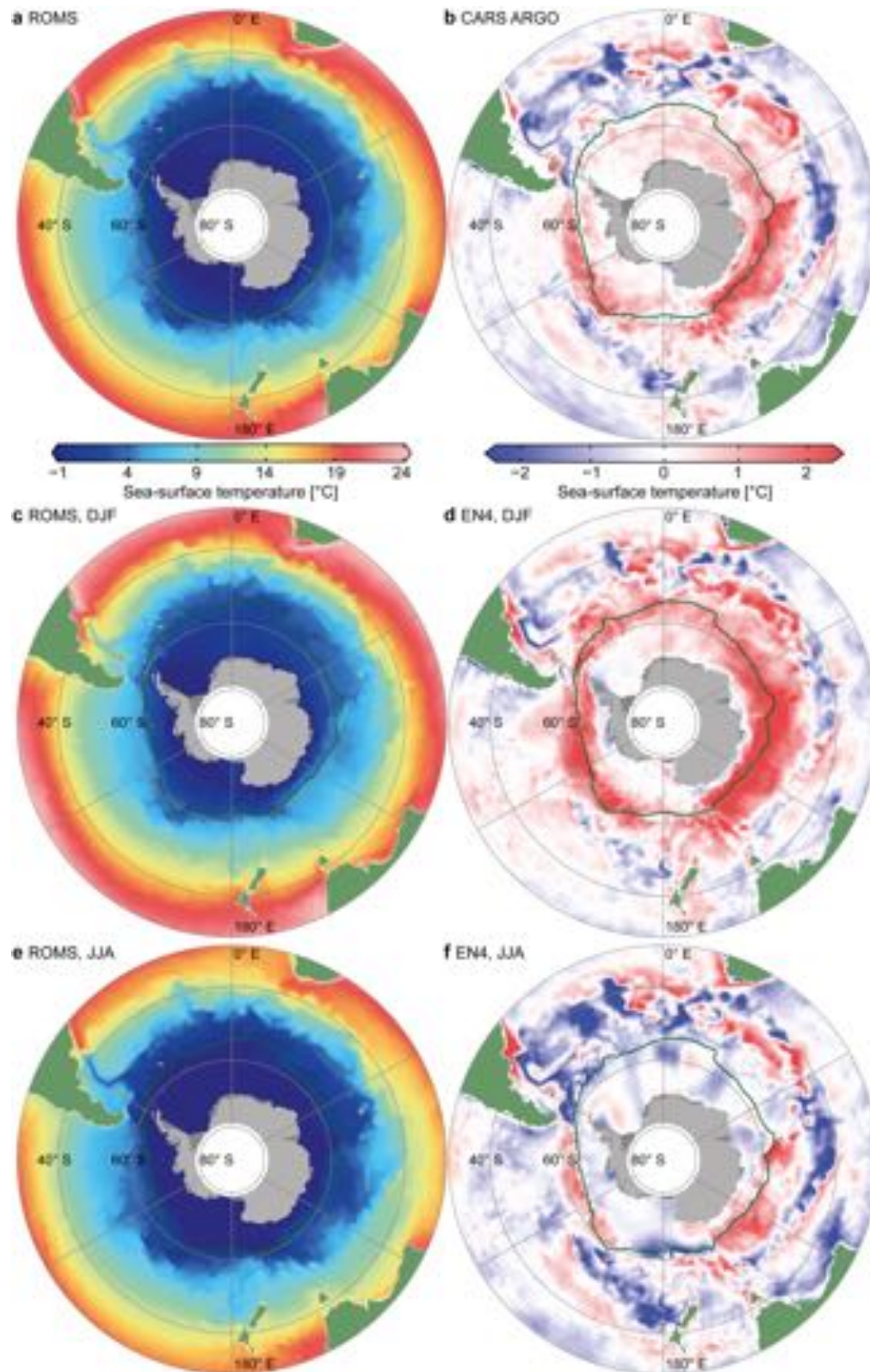
Figure 3.14   Sea-surface temperature: Annual mean sea-surface temperature in ROMS (**a**) and its difference to the Argo-only climatology of CARS2009 (**b**). Austral summer (DJF) mean sea-surface temperature in ROMS (**c**) and its respective difference to the EN4 climatology (**d**). (**e**) and (**f**) as (**c**) and (**d**) but for austral winter (JJA). The green contour line denotes the climatological mean sea-ice edge.
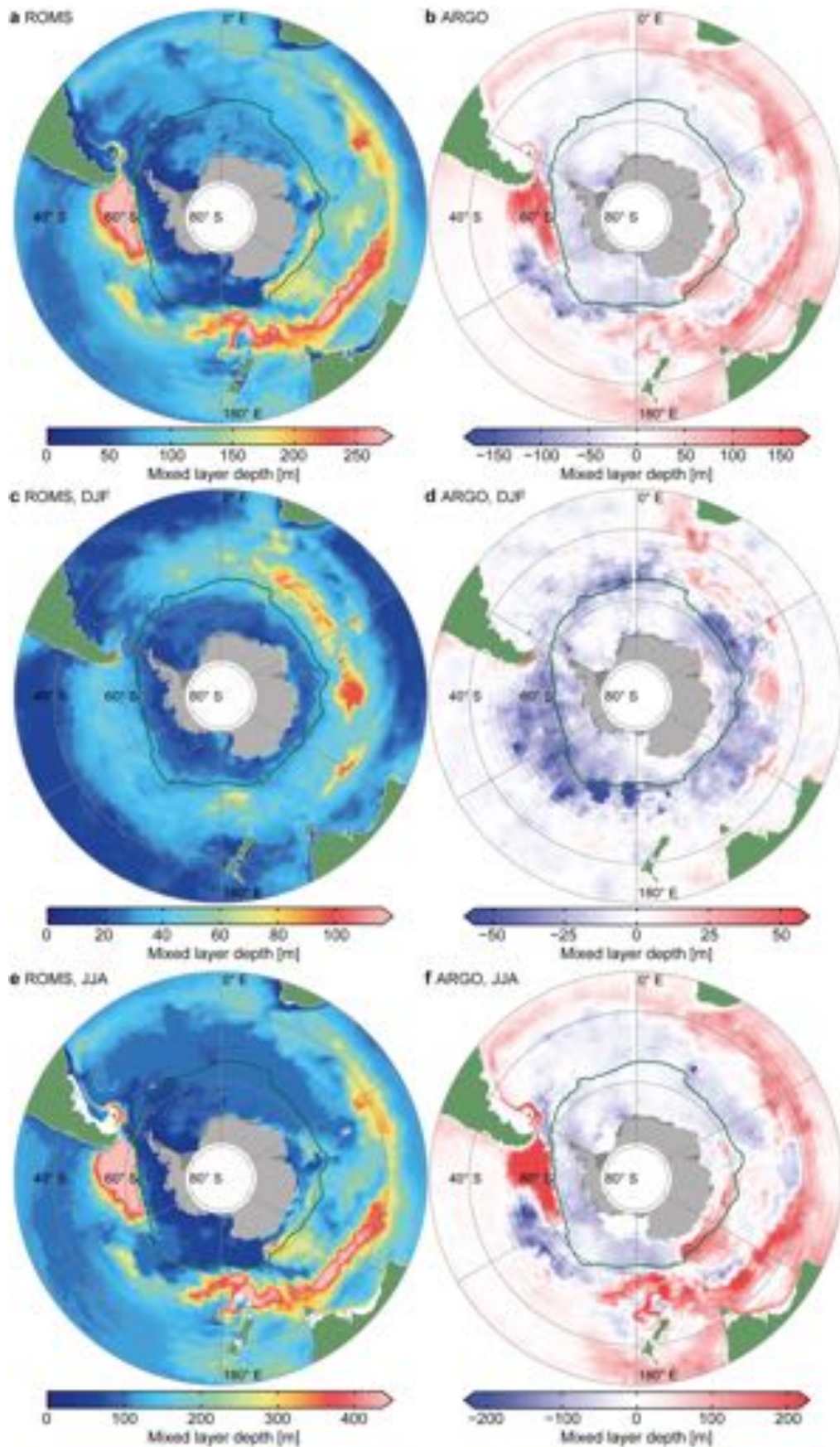
Figure 3.15 Surface mixed layer depth: Annual mean surface mixed layer depth computed from ROMS (**a**) and its difference to an Argo-derived product (**b**). (**c**) and (**d**), and (**e**) and (**f**) as (**a**) and (**b**) but for austral summer (DJF) and austral winter (JJA), respectively. The green contour line denotes the climatological mean sea-ice edge. Note the different scales. See text for details.

3.7.3 Hydrography & water masses

The most challenging comparison for an ocean circulation model of the Southern Ocean is the difference between the model's temperature and salinity and observational data in the vertical. Figure 3.16 shows these zonal mean fields compared to the WOA13 database (Boyer et al., 2013; Locarnini et al., 2013; Zweng et al., 2013). Overall, ROMS is able to represent the Southern Ocean water mass structure with a fresh and cold surface layer, a warm and salty deep water layer, and a cold bottom water layer. However, the latter layer is most likely not yet fully equilibrated by the end of the spin-up simulation. Close to the surface, the model is also able to represent the cold and relatively fresh subsurface winter-water layer with an even fresher and warmer summer-water layer on top (not shown). In lower latitudes the characteristic fresh AAIW and SAMW layer is visible in the model.

Despite this general ability of the model to represent the ocean water masses, major biases exist. Among these biases is a pronounced positive salinity bias in the region of the AAIW and SAMW, which are too shallow, too warm, and too salty in the model. These issues are
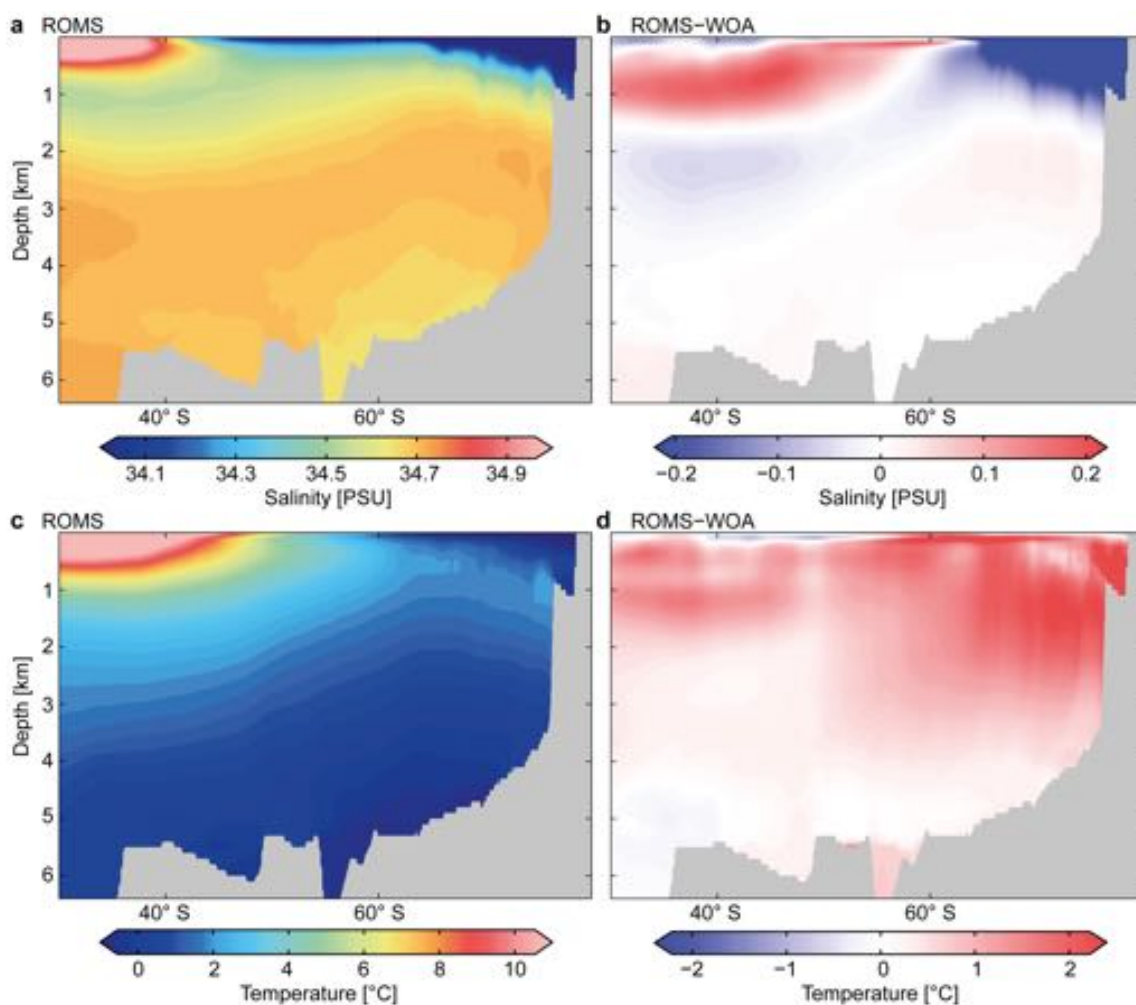
Figure 3.16 Zonal mean temperature and salinity: Annual, zonal mean temperature and salinity fields from ROMS (**a**) (**b**) (**c**) (**d**).

mostly related to the fresh biases at the high-latitude ocean surface, because too little freshwater is transported northward and mixed into the subsurface layers where it would be transported with AAIW and SAMW. An additional degradation of AAIW and SAMW might occur due to spurious diapycnal mixing in the ocean interior (section 3.1.1). A second major bias is the too fresh Antarctic continental shelf that I already noted when describing the surface salinity biases. This problem is directly related to a considerable subsurface warm bias in the high-latitude Southern Ocean. On the one hand, the too fresh surface ocean reduces the subduction of cold AABW, which leads to a subsurface warming. On the other hand, the too fresh surface ocean might also be related to a too weak surface heat loss in the coastal ocean that prevents the subduction of these water to the subsurface. This latter process becomes apparent as a slightly too salty deep ocean. Even though there is a large uncertainty in the total amount of AABW production and the strength of the lower circulation cell (about 30 Sv, see section 1.3.1), with only about 10 Sv of northward transport in the AABW layer, the model seems to have a too weak AABW production. In summary, most of the problems in the model's hydrography seem to result from an unrealistically weak vertical exchange.

3.8   Summary of model developments & future directions

In this chapter, I presented a new regional model for the Southern Ocean. The underlying physical ocean circulation model is a regional configuration of ROMS (Shchepetkin and McWilliams, 2003, 2005, 2009a), which has a stretched, terrain-following vertical coordinate system. A key challenge with models that have such a coordinate system is the occurrence of spurious diapycnal mixing in the deep ocean where isopyncals cross the vertical coordinates. This process leads to a long-term degradation of interior ocean water masses in basin-scale applications if the model is running freely, i.e., without restoring. I mitigated the problem in several ways: (1) Spurious diapycnal mixing is reduced through increasing the vertical and horizontal resolution; (2) a careful choice of the vertical stretching parameters leads to a damping of terrain-effects in the upper ocean and reduces the degradation of AAIW and SAMW; (3) an enhanced smoothing of the topography reduces terrain-effects throughout the water column and improves the representation of all water masses. I counteracted the reduction in bottom roughness induced by (3) by increasing the bottom roughness length scale in the mixing scheme to slow down unrealistically strong coastal currents. An important future development to further reduce these effects would be the implementation of an isoneutral advection scheme (Lemarié et al., 2012b).

To obtain a realistic mean ocean circulation, I modified the implementation of the northern boundary condition. Using a specified boundary condition for the barotropic mode that directly sets the outermost grid cell to the vertically integrated transport of the lateral forcing in the Pacific and Indian Ocean sectors, constrains the relative exchange of water masses between the basins. Without this constraint the model would drift due to an unknown water mass exchange north of the northern boundary. In order to reduce the effect of barotropic waves that might get trapped in the domain due to this fix, I added a sponge layer with enhanced viscosity along the northern boundary and used a radiation boundary condition in the Atlantic basin only. The latter enables the model to still adjust its mean circulation to the forcing. Moreover, the location of the northern boundary at a latitude where the transport is mostly perpendicular to the boundary helped to reduce boundary artifacts and increased the stability of the model. Another important change to obtain a realistic circulation around the southern boundary—the Antarctic continent—is the use of RTopo-1 (Timmermann et al., 2010) for the bathymetry, and land and ice-shelf masks. Finally, the refinement of the horizontal resolution towards the south, enables the model to better represent the ACC and coastal circulation around Antarctica at low computational cost. Moreover, this horizontal grid naturally follows the decreasing baroclinic Rossby deformation radius towards the south and therefore helps the model to resolve baroclinic instabilities. While I only use the $0.5°$ and $0.25°$ configurations of the model in this thesis, a fully eddy-resolving resolution of $0.1°$ will further improve the circulation and lateral mixing processes in future.

Vertical mixing processes in ROMS are parameterized through a first-order closure scheme (KPP; Large et al., 1994; McWilliams et al., 2009). This common mixing scheme tends to produce

a too shallow mixed layer in the Southern Ocean surface waters in summer, which led to too salty AAIW and SAMW and, in extreme cases, spurious deep ocean convection in the high-latitudes in winter. I found that this bias is induced by two problems. Firstly, the shallow mixed layer was not represented well when the vertical resolution was insufficient and the diffusivity dropped to a background value. The use of 64 vertical layers can mostly avoid such an effect. Additionally, I implemented an option that calculates the vertical diffusivity for the first layer interface based on the surface forcing if the mixed layer shoals below this level. The second issue is a very fast stabilization and a related decrease of the mixed layer depth during summer after strong mixing events, which occurs due to the strongly stabilizing buoyancy forcing. Consistent with Timmermann and Beckmann (2004) and Dinniman et al. (2003), I found that a formulation of the mixed layer depth as suggested by Lemke (1987) and Markus (1999) that solely depends on the surface forcing and an exponential dissipation function provides much more realistic results for the mixed layer depth decay under such strongly stabilizing conditions. This implementation resulted in the largest improvement. In future, the implementation of a damping function that accounts for the dissipation of inertial shear after the passage of a storm or eddy under strongly stabilizing conditions would be desirable. Additionally, the use of a higher maximum diffusivity for the calculation of the mixing induced by shear and stability improved the mixing processes just below the mixed layer and spared the need for an additional convective adjustment formulation.

The model is forced with momentum, heat, and freshwater fluxes from the atmosphere, sea ice, and land ice. I made multiple modifications to the surface forcing creation tools in ROMS. Among theses changes are an improved interpolation scheme, more suitable and consistent fields for the surface temperature and salinity restoring, a correction of the fluxes in the presence of sea ice, an addition of sea-ice melting and freezing fluxes, an addition of river input, and an addition of iceberg melting fluxes. Moreover, I implemented the possibility to add interior ocean sources of freshwater, heat, and tracers to add subsurface fluxes of ice-shelf melting. I added multiple options to treat the presence of sea ice in the model. Among these are a calculation of heat fluxes under ice, and a parameterization of convective brine plumes. I also added an option to perform only a partial surface restoring to temperature and salinity whenever reliable data is available. All these changes related to the surface forcing led to major improvements and a reduction of biases. One of the key remaining biases in the forcing data is a warm bias in the ERA-Interim surface heat flux, and a bias correction might result in further improvements.

While the above described changes to the model result in a general ability to represent the water-mass structure, circulation, and mixing processes in the Southern Ocean, several pronounced model biases and challenges remain for the future. The most problematic biases are a too fresh coastal ocean, too little AABW formation, a warm bias at the subsurface, a surface fresh bias in the sea-ice region and the South Atlantic, and a too shallow, warm, and salty AAIW and SAMW. Many of these biases are probably directly related. The circulation of the model is generally very well represented and biases are most likely related to either the surface heat flux or mixing processes. Especially, forcing the model with a mostly fixed surface heat flux seems prob-

lematic as the model builds up heat in the ocean interior that cannot be lost to the high-latitude atmosphere as long as the heat flux is prescribed. The implementation of a bulk formulation for the surface heat flux might help to mitigate this problem. In addition to the suggested future improvements above, an update of the equation of state to its newest version (TEOS-10), an implementation of surface mixing by waves, and a tidal model might help to reduce the remaining biases. Moreover, a completion of the partly implemented sea-ice model and and ice-shelf cavity model might be useful to study feedbacks between the ocean and the ice in future. Together with the sea-ice model a representation of sea-ice biogeochemistry and the input of nutrients associated with glacial discharge might also be desirable to better understand the biological production, the ecosystem, and the carbon fluxes in the high latitudes.

Chapter 4

Recent changes of Southern Ocean waters induced by sea-ice freshwater fluxes[*]

F. Alexander Haumann[1,2], Matthias Münnich[1], Samuel Eberenz[1], Nicolas Gruber[1,2]

[1]Environmental Physics, Institute of Biogeochemistry and Pollutant Dynamics, ETH Zürich, Zürich, Switzerland

[2]Center for Climate Systems Modeling, ETH Zürich, Zürich, Switzerland

Abstract

This study investigates the sources of recent changes in the Southern Ocean hydrography and circulation by forcing a regional ocean circulation model with recent observational constraints on changes in surface fluxes from sea ice and land ice and with atmospheric reanalysis data. Sensitivity experiments support the hypothesis that the freshening of open-ocean surface and intermediate waters is caused by an increased northward freshwater transport by sea ice. In the model, this freshening signal increases the surface density stratification of the open-ocean waters between the sea-ice edge and the Subantarctic Front, which results in a significant surface cooling and subsurface warming due to a reduced mixing of warmer deep waters into the surface layer and smaller heat capacity of the mixed layer. A remarkable agreement between the satellite-observed and simulated surface cooling suggests that this surface cooling occurs primarily due to an increased sea-ice freshwater flux. In contrast, the surface salinity and temperature weakly increase in response to the momentum flux changes. Overall, we find opposing tendencies induced by the surface wind stress changes and freshwater flux changes in the ocean hydrography and transport with the circumpolar current. One exception is the meridional overturning circulation that strengthens in both cases, but additionally shoals in the freshwater flux perturbation experiment. We conclude that the upwelling of deep waters in the Southern Ocean is greatly sensitive to the freshwater transport to the sea-ice edge and that this process is a major driver of changes observed over recent decades in the Southern Ocean surface waters south of the frontal region and water masses formed in this region.

4.1 Introduction

Observations of the Southern Ocean waters reveal pronounced changes in temperature and salinity over recent decades (e.g. Böning et al., 2008; Jones et al., 2016). Understanding these changes and their driving forces is of major concern because they may reflect or lead to changes in the vertical exchange of water masses between the surface and the deep ocean, which in turn influences the Southern Ocean's ability to take up carbon and heat from the atmosphere (Frölicher et al., 2015; Landschützer et al., 2015b). Therefore, such changes in the Southern Ocean could feedback on global climatic changes in the long-term (Knox and McElroy, 1984; Sarmiento and Toggweiler, 1984; Siegenthaler and Wenk, 1984; Sigman et al., 2010) and amplify or diminish global warming (Manabe and Stouffer, 1993; Sarmiento et al., 1998; Caldeira and Duffy, 2000). A detailed process understanding and an attribution of recent hydrographic changes to either surface freshwater, heat, or momentum flux changes has yet been limited by the availability of reliable surface flux data. In this study, we make use of most recent observation-based estimates in surface freshwater fluxes from sea ice (Haumann et al., 2016b) and land ice (Depoorter et al., 2013; Sutterley et al., 2014; Paolo et al., 2015) to investigate the response of the Southern Ocean salinity, temperature, density stratification, and circulation to the suggested changes in these fluxes and contrast this response with wind-induced ocean circulation and mixing changes, and observed changes.

The observed recent changes in the Southern Ocean have not been spatially uniform but instead exhibit vertical and horizontal patterns that relate to the characteristic water masses. Large areas of the high-latitude surface ocean (south of the Subantarctic Front) experienced a substantial surface freshening (Jacobs et al., 2002; Jacobs and Giulivi, 2010; Durack et al., 2012), and—despite global warming—a significant and persistent surface cooling (Fan et al., 2014; Armour et al., 2016) and sea-ice expansion (Comiso and Nishio, 2008; Stammerjohn et al., 2008) over recent decades. These signals at surface largely originate from the Pacific sector. In other sectors, the surface ocean has freshened less and experienced a slight warming. A stronger warming occurred in lower latitudes. At the subsurface, a pronounced freshening (Wong et al., 1999; Böning et al., 2008; Helm et al., 2010; Schmidtko and Johnson, 2012) and warming (Gille, 2002; Böning et al., 2008; Schmidtko and Johnson, 2012) of Antarctic Intermediate Water (AAIW) and Subantarctic Mode Water (SAMW) occurred in the open ocean. Along the Antarctic continental shelf, warming (Schmidtko et al., 2014; Cook et al., 2016) and freshening (Jacobs and Giulivi, 2010; Hellmer et al., 2011; Schmidtko et al., 2014) occurred in many regions. This signal potentially also propagated into the Antarctic Bottom Water (AABW) that is subducted from the continental shelf region (Jullion et al., 2013; Purkey and Johnson, 2013). All these changes in the water mass properties suggest either substantial changes ocean circulation, ocean mixing, surface freshwater or heat fluxes, or a combination of these factors.

The observed strengthening (Marshall, 2003; Thompson et al., 2011; Lee and Feldstein, 2013) and possible shift (Fyfe et al., 2007; Cai et al., 2010) of the westerly surface winds over

the Southern Ocean might have led to changes in wind-driven ocean circulation and mixing. In the subsurface, the observed warming of AAIW and SAMW in the Atlantic and Indian Ocean sectors has been related to a poleward shift of the ACC (Gille, 2008; Sokolov and Rintoul, 2009b; Meijers et al., 2011). Yet, large zonal (Freeman et al., 2016) and potentially temporal variations (Landschützer et al., 2015b) in these meridional shifts have occurred over recent decades that are related to zonal asymmetries in the atmospheric circulation changes (Turner et al., 2009; Hosking et al., 2013; Haumann et al., 2014). Together with an increased heat uptake from the atmosphere due to global warming (Cai et al., 2010; Armour et al., 2016), these processes could explain large portions of the observed warming of AAIW and SAMW, but not the observed freshening (Meijers et al., 2011). An increase in the meridional overturning circulation, as suggested by coarse resolution global climate models (Oke and England, 2004; Saenko et al., 2005; Fyfe and Saenko, 2006), would only initially cool and presumably freshen the surface waters (Sen Gupta et al., 2009; Thompson et al., 2011; Ferreira et al., 2015; Kostov et al., 2016; Seviour et al., 2016). On time-scales longer a few month to several years, the surface waters warm and become more salty due to increased upwelling deep waters, which would be inconsistent with the observed changes. High-resolution modeling experiments (Hallberg and Gnanadesikan, 2006; Farneti et al., 2010; Meredith et al., 2012; Patara et al., 2016) and observational studies (Böning et al., 2008; Hogg et al., 2015) suggest that the overturning circulation is much less sensitive to changes in the surface winds than initially thought. In the absence of changes in the overturning circulation, a delayed and reduced warming would still be expected because the upwelling deep waters did not yet experience global warming Armour et al. (2016). However, the observed surface cooling, sea-ice expansion, and broad-scale freshening over recent decades cannot be explained by the historical anthropogenic forcing in current global climate models (Wong et al., 1999; Helm et al., 2010; Bitz and Polvani, 2012; Haumann et al., 2014). Consequently, the origin of these changes proposes a major conundrum.

Changes in Southern Ocean salinity and temperature fields could result from changes in vertical density stratification that either enhance or reduce the vertical exchange of heat and salt (Gordon and Huber, 1984; Martinson, 1990; Hasselmann, 1991; Manabe and Stouffer, 1993; Bitz et al., 2006). Such changes in stratification would result from changes in the surface buoyancy forcing. While the surface ocean stratification north of the frontal region is mostly sensitive to surface heat flux changes (Manabe and Stouffer, 1993; Sarmiento et al., 1998), south of the frontal region it is predominantly controlled by surface freshwater fluxes (Sigman et al., 2004; Stewart et al., 2016). Therefore, a more stable halocline in the in the high-latitude Southern Ocean could induce a surface cooling and freshening of the surface waters and warmer and saltier deep waters (Gordon and Huber, 1984; Martinson, 1990; Bitz et al., 2006; Zhang, 2007; Bintanja et al., 2013; Goosse and Zunz, 2014)—a figure that is consistent with recently observed changes in the Southern Ocean. Observations in the Southern Ocean high latitudes indeed show such an increased surface density stratification due to a strengthening of the halocline (de Lavergne et al., 2014), which would imply an increased surface freshwater forcing in the upwelling region.

While observational evidence has been small, numerous modeling studies have suggested a surface freshening and cooling in the Southern Ocean could be induced by an increased surface freshwater flux from either the atmosphere (Zhang, 2007; Liu and Curry, 2010), glacial melt (Hellmer, 2004; Bintanja et al., 2013; Pauling et al., 2016), or northward transport of sea ice (Pollard and Thompson, 1994; Kirkman and Bitz, 2011; Goosse and Zunz, 2014). Global models suggest that atmospheric surface freshwater fluxes increase over the Southern Ocean with global warming (Liu and Curry, 2010; Knutti and Sedláček, 2013). However, over recent decades, very little change is observed in most reliable estimates of reanalysis and satellite-derived products (Bromwich et al., 2011; Nicolas and Bromwich, 2011), leaving a large uncertainty on atmospheric changes. Glacial meltwater discharge has considerably increased in the South Pacific sector due to increased grounding line fluxes (Sutterley et al., 2014) and increased ice shelf-thinning (Paolo et al., 2015) presumably due to warming of coastal waters (Spence et al., 2014; Cook et al., 2016). However, this meltwater largely acts to freshen the coastal ocean and presumably AABW (Hellmer, 2004; Jacobs and Giulivi, 2010; Purkey and Johnson, 2013; Kusahara and Hasumi, 2014; Nakayama et al., 2014; Pauling et al., 2016). Most recent observation-based estimates of northward transport of freshwater by sea ice suggest that these changes would be largely sufficient to explain most of the open ocean freshening of the surface waters and AAIW (Haumann et al., 2016b), with possible contributions to the increased surface stratification, surface cooling, and subsurface warming.

In this study, we explore the hypothesis that sea-ice changes drive a large-scale freshening of the open-ocean surface and intermediate waters and land-ice changes mostly the coastal and bottom waters as was previously implied from changes in the surface freshwater fluxes. We will then analyze if such a freshening induces an increased density stratification that could contribute to the observed surface cooling and subsurface warming in the Southern Ocean. For the purpose of this investigation, we will perturb a regional ocean circulation model with the observation-based magnitude and spatial pattern of changes in sea-ice and glacial freshwater fluxes. In order to place our results in context, we will run an additional experiment with an observation-based momentum flux perturbation and compare our results to observed changes in ocean temperature and salinity.

4.2   Model, experimental design & data

We here use the eddy permitting version (5 to 25 km horizontal resolution) of the Regional Ocean Modeling System (ROMS) that has been adapted for the Southern Ocean region south of 24° S as described in detail in section 3. The model is forced at the surface with climatological mean observation-based fluxes from the atmosphere, sea ice, and land ice. Therefore, it is suitable for studying the response of the ocean to perturbations in these fluxes, which is the aim of this study, but not to study feedback mechanisms. As discussed in detail in section 3.7, this mostly free running model in the interior ocean basin is generally able to reproduce the Southern Ocean circulation and water mass structure, but also suffers from some considerable biases. These biases involve a too weak surface mixing in summer, a too salty, warm, and shallow AAIW, a too fresh coastal ocean, and a too warm and salty deep ocean. Potential effects of these biases on our results are discussed in section 4.4.

After a spin-up simulation of 40 years, the model shows only very little drift in the ocean circulation and surface properties. Some model drift remains at the subsurface (see section 3.6). We account for this drift by running a control experiment that continues after the spin-up simulation for another 40 years using the climatological mean forcing. In addition to this control simulation, we run three perturbation experiments for 40 years. Each of these perturbation experiments uses the climatological mean forcing except for one respective variable that is perturbed according to observation-based estimates of changes over recent decades. Throughout the control and the perturbation experiments we add the restoring fluxes of heat and freshwater from the last ten years of the spin-up simulation to the surface forcing and restrict restoring to both surface temperature and salinity fields to the boundary region between 24° S and 40° S to prevent the model from drifting at the boundary. Therefore, the perturbations in the regions of interest (south of 40° S) are not influenced by the restoring of the model.

In one experiment, we only perturb the sea-ice melting and freezing fluxes (Haumann et al., 2016b,a). We estimate daily trends by calculating the trend in the net sea-ice production from a 11-day running mean window for each grid point over the period 1982 to 2008. Calculating the trend from the melting and freezing fluxes separately rather than using the net flux would have led to very large over- or underestimations and a very noisy product as these flux components have a much higher uncertainty (Haumann et al., 2016b). Even though the actual observational period is shorter, we multiplied the resulting trend by 35 years to obtain a magnitude that is comparable in terms of its time period to the wind perturbation (see below). The resulting annual perturbation (Figure 4.1a) agrees well with the original net sea-ice freshwater flux changes.

In a second experiment, we also perturb the sea-ice freshwater fluxes but additionally increase the glacial meltwater discharge from the Antarctic continent. The mean ice-shelf melting fluxes originate from Depoorter et al. (2013), who estimated a total discharge due to basal melting of 1454 Gt yr^{-1} for the year 2009. For the spin-up simulation and the control experiment we re-
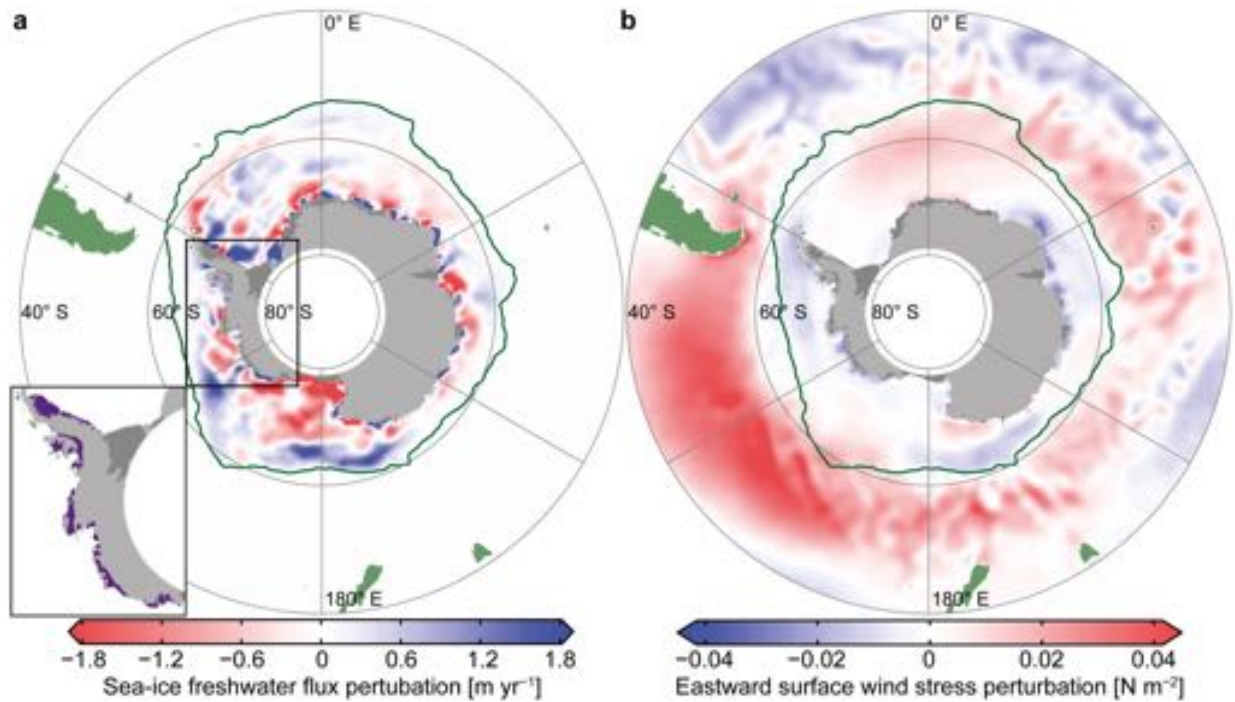
Figure 4.1   Observation-based surface freshwater flux and wind perturbations: (**a**) Surface freshwater flux perturbation from sea ice and land ice (purple in inset). (**b**) Eastward surface wind stress perturbation from ERA-Interim. Green contour line: climatological mean sea-ice edge. Black contour line: Antarctic continental shelf (shallower than 1000 m).

calculate these fluxes by reducing the discharge in the sector between 165° W and 60° W (inset in Figure 4.1a), i.e. the West Antarctic Ice Sheet, where most of the change over the recent decades occurred. Removing the contributions of changes in the grounding line flux (Sutterley et al., 2014) and the ice-shelf thinning (Paolo et al., 2015) since 1992, we approximate the discharge to about 860 Gt yr^{-1} for the spin-up and control simulations. For the perturbation experiment, we increase this flux to 1755 Gt yr^{-1}, to approximately mimic the year 2014. The decrease and increase has been scaled with the mean discharge of each ice shelf, so that ice shelves with a high discharge in 2009 experience the largest changes. We do not run experiments where we perturb the freshwater fluxes from ice berg melting or the atmosphere, as there is, to the authors knowledge, no observation-based evidence for considerable changes in these fluxes. The most reliable reanalysis product and observational estimates suggest that the atmospheric flux over the Southern Ocean did not change much over the recent decades (Bromwich et al., 2011; Nicolas and Bromwich, 2011).

We run a third experiment, in which we perturb both the eastward and northward surface wind stress in the forcing. Therefore, we calculate the monthly trends from the ERA-Interim atmospheric forcing data (see section 3.5.1; Dee et al., 2011) for each grid point over the period 1979 to 2014 and multiply the trends by the 35-year period (Figure 4.1b, note that only the eastward momentum stress is shown for illustration). These perturbations are than added to the climatological mean fluxes.

For the analysis, we calculate temporal averages from the last 20 years of each experiment and compare these to the last 20 years of the control experiment. Therefore, these differences correspond to an ocean response after 20 to 40 years after the perturbation has been applied. However, we expect that the response to the perturbation will be considerably larger than a response that could be expected in the real world over such a time period, since the forcing was perturbed instantaneously rather than gradually over time. Nevertheless, the relative change between the different perturbation experiments and the spatial pattern of these changes reveal valuable insights into drivers of the observed changes.

We will compare our model results to observation based changes from multiple data sets. These comprise an estimate of sea-surface salinity trends over the period 1950 to 2000 from ocean data (Durack and Wijffels, 2010; Durack et al., 2012), sea-surface temperature trends over the period 1982 to 2014 from the NOAA Optimum Interpolation SST from AVHRR satellite data (Reynolds et al., 2007), and sea-surface height trends over the period 1992 to 2011 from AVISO satellite data (produced by Ssalto/Duacs and distributed by AVISO with support from Cnes, http://www.aviso.altimetry.fr/duacs). We compare the sea-surface temperature and salinity trend estimates to those from the upper five layers (about 50 m) in the EN4 Objective analyses, which is derived from quality controlled ocean profile data (version 4.2.0; 1979–2014; Ingleby and Huddleston, 2007; Good et al., 2013). The same data set is also used to derive subsurface trends in ocean salinity and temperature. Trends are estimated based on a least-squares linear regression analysis. For a better comparison between all data sets and the model results, we scale all trends to a 30 year period, irrespective of their observational period. It should be noted that in the sea-ice covered region all observational products suffer from a summer-time bias and only very little data is available. Therefore, these trend estimates have very large uncertainties and are largely unreliable along the Antarctic coast. Nevertheless, they provide a good overview of observed changes in the Southern Ocean that have been evaluated more carefully by numerous previous studies (see section 4.1).

4.3 Results

We will first discuss the simulated Southern Ocean salinity response to the changes in surface freshwater fluxes from sea and land ice. This discussion serves the purpose of validating the findings by Haumann et al. (2016b), who used a simple box-model approach to infer salinity changes induced by the surface flux changes rather than an ocean circulation model used here. Subsequently, we will investigate their effect on the vertical density stratification and temperature. Throughout this discussion, we will contrast the response to freshwater flux changes with the response to surface wind stress changes. Moreover, we will compare our simulations to observation-based estimates of temperature and salinity changes to identify the potential sources of the observed changes. At last, we will analyze the response of the vertically integrated transport and zonal mean meridional overturning circulation to these changes in the surface fluxes to further understand how these changes relate to changes in water mass properties.

4.3.1 Salinity response

The simulated surface salinity responds with a broad-scale open-ocean freshening (Figure 4.2a) to the observation-based changes in northward sea-ice freshwater transport (Figure 4.1a). The largest response occurs in the South Pacific sector, directly downstream of the increased northward sea-ice transport in the Ross Sea. This anomaly partly propagates through Drake Passage into the South Atlantic and is partly subducted into the AAIW and SAMW layers (Figure 4.3a). The spatial patterns of these surface and subsurface salinity changes in the open ocean broadly agree with the observed spatial patterns (Figures 4.2d–e and 4.3d). However, the response of the simulated salinity is considerably larger at the surface and weaker at the subsurface compared to the observed estimates. These differences could partly be related to a too weak subduction of freshwater into AAIW and SAMW in the model and partly due to compensations by other changes. Surprisingly, the coastal ocean also freshens substantially at the surface despite an increased northward export of freshwater by sea ice (Figure 4.1). The main reason of this surface freshening is an increased freezing and melting cycle in the forcing data and the mixing parameterization in the model that mixes the brine from the sea-ice formation deeper in the water column. Sensitivity experiments with this mixing parameterization showed that this result is not very robust and therefore, at the current stage of model development, we cannot reliably interpret changes in the coastal ocean.

Adding the glacial meltwater perturbation to the model did not considerably change the results (Figure 4.2b), since the freshwater flux perturbation is considerably smaller than the vertical freshwater redistribution flux by the changing sea-ice melting and freezing cycle in the model. Nevertheless, we conclude that the additional glacial meltwater cannot be the driving force of the open-ocean salinity trends because its magnitude is too small for such a broad scale freshening,

consistent with another recent study (Pauling et al., 2016). As the coastal ocean response seems to be a model dependent result, we will focus in this study rather on the open-ocean response from the sea-ice forcing which is induced by the increased northward transport. In summary, the model's response to recent changes in surface freshwater fluxes from sea ice supports the conclusion by Haumann et al. (2016b) that sea-ice changes could explain the observed freshening of the open ocean surface and intermediate waters and the coastal freshening seems to be more complex than previously thought.

In contrast to the surface freshwater flux perturbations, the surface wind stress perturbation leads to a broad-scale sea-surface salinity increase in most of the low- and high-latitude surface ocean (Figure 4.2c). Largest changes occur in the south-eastern Pacific, where an increased upwelling of salty deep waters through transport and mixing enhances the surface salinity and
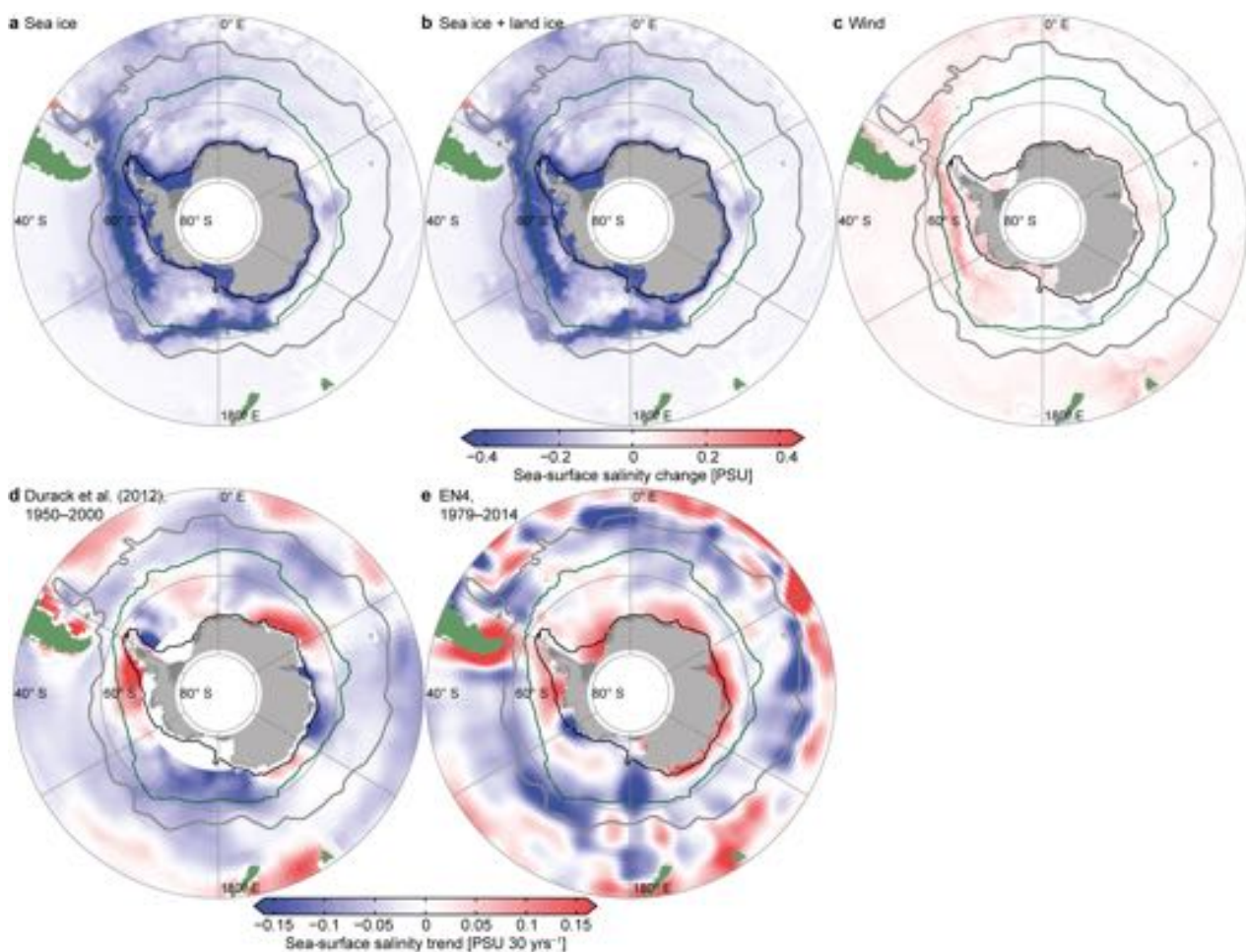
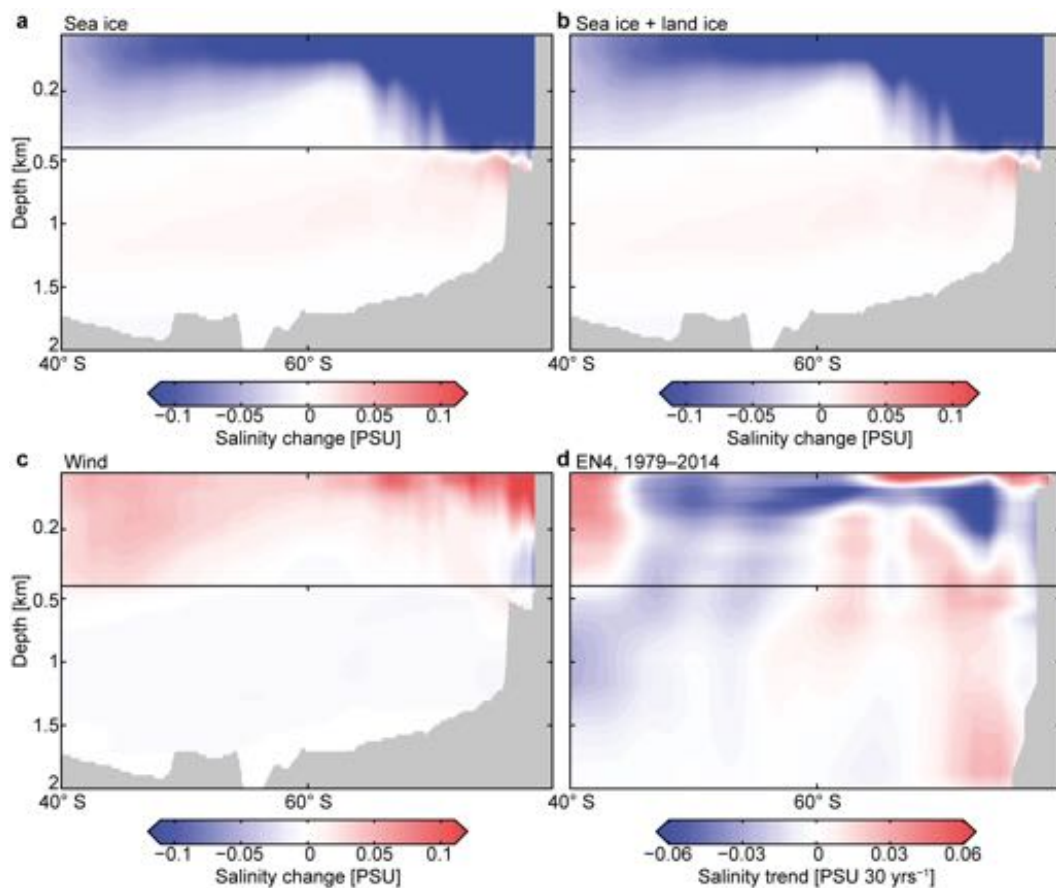**Figure 4.2   Sea-surface salinity response:** Response to the sea-ice freshwater flux perturbation (**a**), to the combined sea-ice and land-ice freshwater flux perturbations (**b**), and to the surface wind stress perturbation (**c**). Shown are the differences of the last 20 years of a 40-year perturbation experiment to a control simulation with constant forcing. (**d**) Observed sea-surface salinity trends from Durack et al. (2012, 1950–2000), scaled to a 30 year period. (**e**) Observed salinity trends derived from the upper 50 m of the EN4 Objective analyses (1979–2014; Ingleby and Huddleston, 2007; Good et al., 2013), scaled to a 30 year period. Green contour line: climatological mean sea-ice edge; gray contour line: Subantarctic Front (Orsi et al., 1995); black contour line: Antarctic continental shelf (shallower than 1000 m).

slightly reduces the subsurface salinity of Circumpolar Deep Water (CDW; Figure 4.3c). The salty surface anomaly is also subducted into AAIW and SAMW, slightly counteracting the freshening of these waters from the surface freshwater fluxes. An increased salinity occurs over large areas of the continental shelf and is most pronounced in the South Pacific sector in response to enhanced easterly winds (Figure 4.1b) that increase the advection and mixing of salty CDW onto the continental shelf, consistent with the results by Spence et al. (2014). This process further counteracts the freshening of the continental shelf waters from the freshwater perturbation. In conclusion, the wind-driven response of the salinity due changes in ocean transport and mixing processes opposes the salinity changes induced by the surface freshwater fluxes. However, the magnitude of the salinity response to the surface wind stress perturbation is much weaker than the response to the surface freshwater fluxes. Therefore, our simulations suggest that the overall observed salinity changes in the higher latitude Southern Ocean are largely due to the changes in the surface freshwater fluxes from sea ice, with regional exceptions depending on the strength of each forcing.

Figure 4.3   Zonal mean subsurface salinity response: Response to the sea-ice freshwater flux perturbation (**a**), ot the combined sea-ice and land-ice freshwater flux perturbations (**b**), and to the surface wind stress perturbation (**c**). Shown are the differences of the last 20 years of a 40-year perturbation experiment to a control simulation with constant forcing. (**d**) Observed salinity trends derived from the EN4 Objective analyses (1979–2014; Ingleby and Huddleston, 2007; Good et al., 2013), scaled to a 30 year period.

4.3.2   Stratification response

South of the ACC frontal region the stable surface density stratification is mostly established by the vertical salinity profile (Stewart et al., 2016) since the vertical temperature stratification becomes seasonally unstable. At such low temperatures the vertical density stratification is much more sensitive to changes in salinity due to the non-linearities in the equation of state (Turner, 1973; Sigman et al., 2004). Therefore, the strong changes in surface salinity induced by the sea-ice and land-ice freshwater fluxes imply considerable changes in the surface density stratification south of the ACC frontal region with a decreasing effect further to the north where temperature starts to dominate the density stratification. Indeed, the surface ocean freshening induced by the sea-ice freshwater fluxes induces a sharp increase in surface density stratification adjacent to the sea-ice edge, where the coldest waters, a very marginal stability, and deep mixing occur during
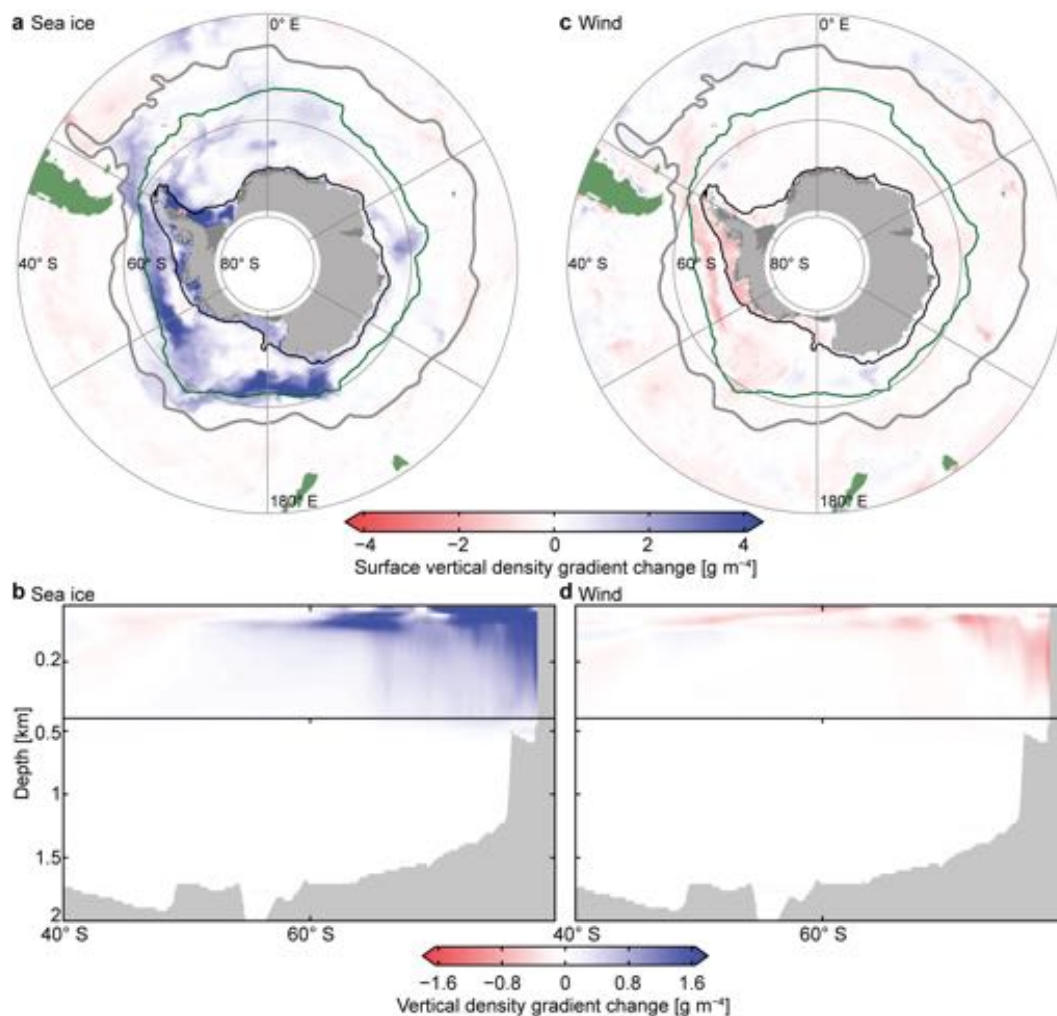
Figure 4.4   Density stratification response: Response to the sea-ice freshwater flux perturbation (**a–b**), and to the surface wind stress perturbation (**c–d**). Positive values denote a stabilizing ocean and negative values a destabilizing ocean. Upper two panels: averaged over the top 100 m. Lower two panels: zonal mean. Shown are the differences of the last 20 years of a 40-year perturbation experiment to a control simulation with constant forcing. Green contour line: climatological mean sea-ice edge; gray contour line: Subantarctic Front (Orsi et al., 1995); black contour line: Antarctic continental shelf (shallower than 1000 m).

winter-time (Figure 4.4a–b). Further to the north, this effect vanishes. In the coastal ocean, a very strong stabilization occurs due to the increased melting and freezing cycle, explaining the strong freshening at the surface. As discussed above, whether or not this coastal stabilization is realistically represented in the model is debatable, as it depends on the mixing parameterization of brine to the subsurface in the model. Nevertheless, the increased northward transport of freshwater stabilizes the ocean in the upwelling region around the sea-ice edge. The surface wind stress perturbation shows a much weaker response due to the surface salinity increase that slightly oppose the freshwater response (Figure 4.4).

4.3.3   Temperature response

As a response to the considerable increase in surface density stratification induced by the sea-ice freshwater perturbation in the upwelling region, we expect an influence on vertical temperature profile due a reduction in the upwelling of CDW that is several degrees warmer than the surface waters south of the ACC frontal region. The sea-surface temperature response to this perturbation reveals a strong cooling between the sea-ice edge and the Subantarctic Front (SAF) in the entire Pacific sector and parts of the Atlantic sector (Figure 4.5a). This surface cooling is, in terms of its spatial pattern, strikingly consistent with the satellite derived cooling trends in this region (Figure 4.5d). However, the simulated magnitude from this perturbation alone is considerably larger than the observed trend. If the warming from the surface wind stress perturbation in this region is considered as well (Figure 4.5c), both effects together seem to agree very well with the observed magnitude of the cooling. Moreover, the surface wind stress response reveals that a large fraction of the surface warming observed in the lower latitudes can be attributed to wind-driven changes in ocean circulation and mixing. In the high-latitude Atlantic sector and parts of the Indian Ocean sector the wind stress perturbation results in a weak cooling south of the SAF. This cooling can be attributed to a reduction of the meridional gradient in the wind stress along the sea-ice edge in this region, as it can be depicted from Figure 4.1b. Very little cooling is found south of the sea-ice edge, because these waters are very close to their natural limit of the freezing point temperature and actual temperature trends could only occur during summer. But at that time of the year the surface layer is strongly stratified and very little subsurface heat enters the surface layer. In summary, our simulations suggest that most of the observed cooling in the Pacific and western Atlantic sectors of the Southern Ocean surface waters results from increased northward freshwater transport by sea ice, which reduces the upwelling of warm CDW due to an increased density stratification. Surface wind stress changes partly counteract this signal and are probably responsible for sea-surface temperature changes in the other regions of the Southern Ocean.

The strong cooling signal in the Pacific sector occurs right at the sea-ice edge and provides probably a positive feedback on the sea-ice cover changes. Such a feedback mechanism cannot be studied directly with our model simulations. However, they might have contributed considerably

to the observed persistent expansion of the sea ice as suggested by Goosse and Zunz (2014). Our simulations suggest that an increased sea-ice advection to the sea-ice edge in the Ross Sea could effectively prolong the period of seasonal sea-ice cover since the sea-surface temperature and therefore the melting is reduced or delayed and freezing might occur earlier. To obtain a surface cooling, the location of the freshwater input is critical because it can only be initiated if a surface freshening occurs in the upwelling region between the sea-ice edge and the SAF, where the surface temperatures are critically influenced by the subsurface heat flux. If the surface freshening
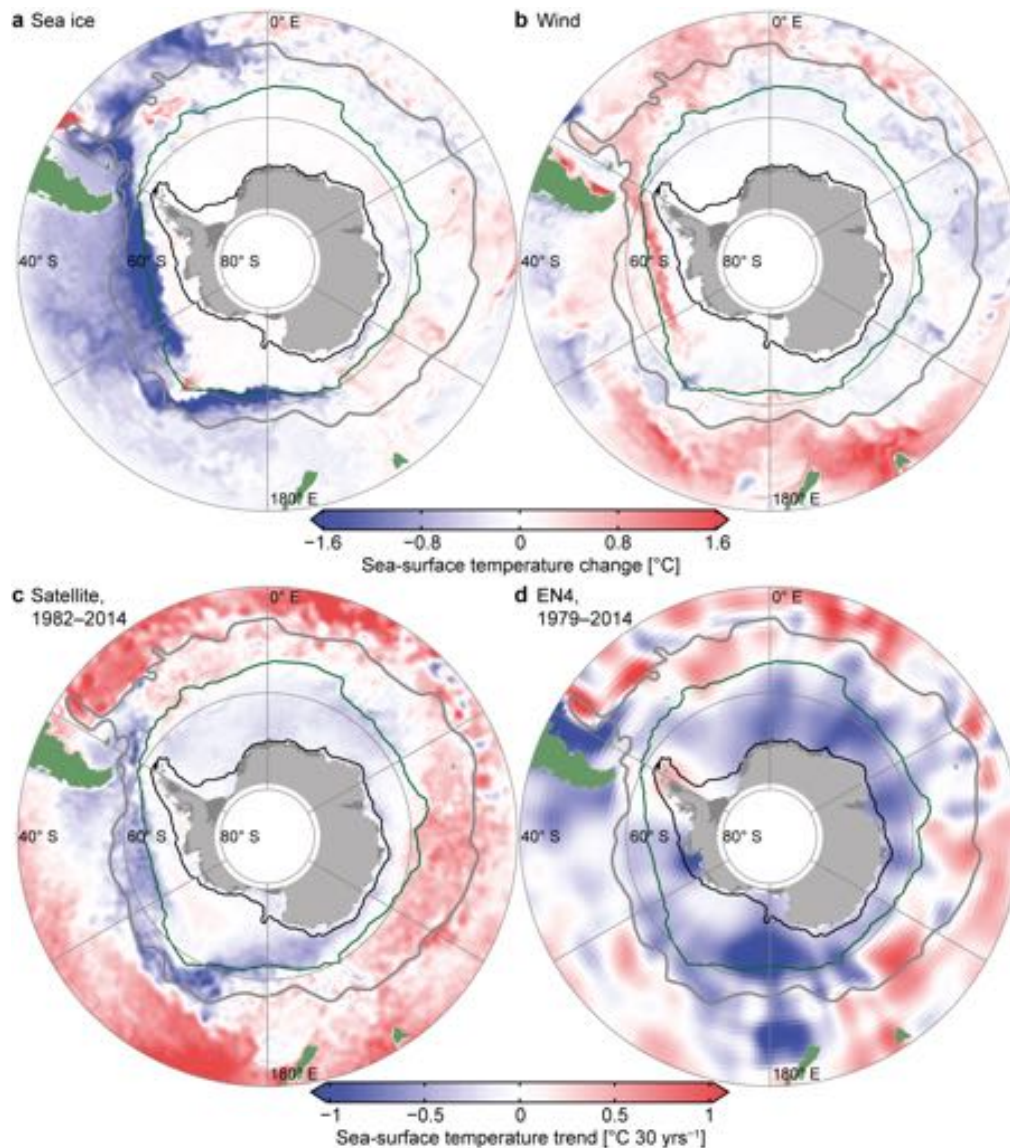
Figure 4.5   Sea-surface temperature response: Response to the sea-ice freshwater flux perturbation (**a**), and to the surface wind stress perturbation (**b**). Shown are the differences of the last 20 years of a 40-year perturbation experiment to a control simulation with constant forcing. (**c**) Observed sea-surface temperature trends derived from the AVHRR satellite data (1982–2014; Reynolds et al., 2007), scaled to a 30 year period. (**d**) Observed temperature trends derived from the upper 50 m of the EN4 Objective analyses (1979–2014; Ingleby and Huddleston, 2007; Good et al., 2013), scaled to a 30 year period. Green contour line: climatological mean sea-ice edge; gray contour line: Subantarctic Front (Orsi et al., 1995); black contour line: Antarctic continental shelf (shallower than 1000 m).
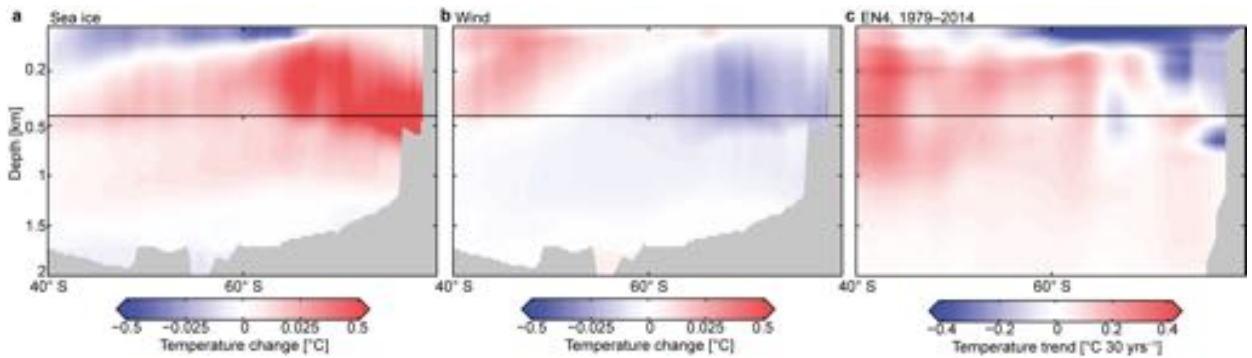
Figure 4.6 Zonal mean subsurface temperature response: Response to the sea-ice freshwater flux perturbation (**a**), and to the surface wind stress perturbation (**b**). Shown are the differences of the last 20 years of a 40-year perturbation experiment to a control simulation with constant forcing. (**c**) Observed temperature trends derived from the EN4 Objective analyses (1979–2014; Ingleby and Huddleston, 2007; Good et al., 2013), scaled to a 30 year period.

occurred further to the north, it would not considerably change the surface temperature because it had not much influence on the density stratification in these warmer regions and because the upwelling of deep waters is drastically reduced further to the north. Nevertheless, a surface cooling occurs north of the SAF in the freshwater perturbation experiment (Figure 4.5a). This cooling can be explained by a northward transport of the anomaly that originates from south of the SAF, which is an essential process in terms of the heat uptake from the atmosphere by these waters and subsequent subduction into AAIW and SAMW (Armour et al., 2016).

The observation-based estimates of zonal mean temperature changes in the Southern Ocean (Figure 4.6d) suggest that the surface cooling only occurs in the upper 100 m of the water column and are therefore, in contrast to the subsurface warming, probably not related to meridional shifts of the ACC. The distinct cooling of this surface layer around the sea-ice edge in the zonal mean profile also occurs in the sea-ice freshwater perturbation experiment (Figure 4.6a). In the surface layer south of the sea-ice edge, cooling is mostly absent in any of the model experiments. However, the observational data from EN4 suggests that also a strong cooling occurred south of the sea-ice edge. Comparing the EN4 surface layer trends with the satellite derived trends (Figures 4.5d–e) and other observational studies (de Lavergne et al., 2014; Schmidtko et al., 2014), suggests that this trend in EN4 might also be unrealistically large. This discrepancy in the observational data south of the sea-ice edge is certainly related to the sparse coverage of this region with oceanographic data. At the subsurface, the observational profiles suggest a warming of CDW, AAIW, and SAMW. The CDW warming is consistent with a reduced upwelling of heat into the surface layer as a result of the increased surface stabilization in the upwelling region from the sea-ice freshwater fluxes (Figure 4.6a). The model probably overestimates this CDW warming due to the overly strong stabilization of the coastal ocean from both the sea-ice and land-ice perturbations and an insufficient heat loss in the coastal ocean. The surface wind stress counteracts this warming of CDW and dominates the warming of AAIW and SAMW further to the north (Figure 4.6b). In conclusion, the response of the subsurface ocean temperature also shows opposing effects induced by the freshwater perturbation and the surface wind stress pertur-

bation, and the former dominates changes in the high latitudes, whereas the latter changes become comparably larger in the low latitudes.

4.3.4   Circulation response

Since the changes in the density structure associated with the freshwater perturbation as well as the wind stress changes presumably influence the ocean circulation, we proceed to analyze the circulation response to these forcing changes. Similar to the changes in temperature and salinity, we find opposing tendencies imposed on the circulation by the freshwater and wind perturbation experiments. Figures 4.7b–c show that the freshwater perturbation tends to increase the sea-surface height south of the frontal region and therefore reduces the meridional sea-surface height gradient in the Southern Ocean, which is a consequence of a decrease in density in the surface
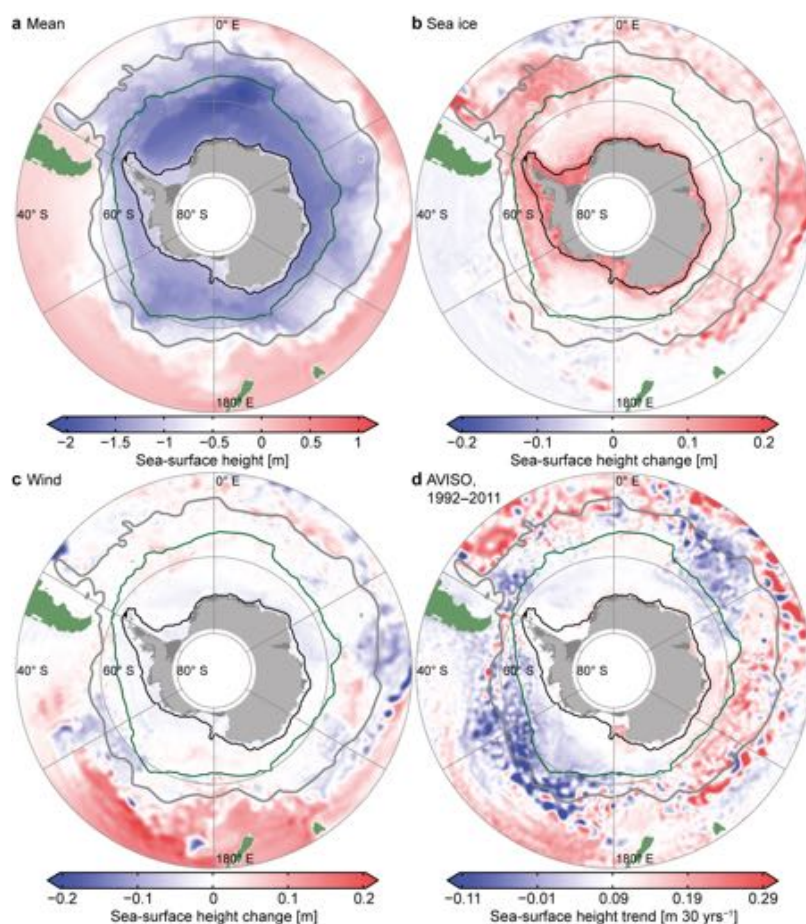
Figure 4.7   Sea-surface height response: Mean simulated sea-surface height (**a**), response to the sea-ice freshwater flux perturbation (**b**), and the response to the surface wind stress perturbation (**c**). The responses show the differences of the last 20 years of a 40-year perturbation experiment to a control simulation with constant forcing. (**d**) Observation-based sea-surface height trend from AVISO satellite data (produced by Ssalto/Duacs and distributed by AVISO with support from Cnes, http://www.aviso.altimetry.fr/duacs) over the period 1992 to 2011, scaled to a 30 year period. Green contour line: climatological mean sea-ice edge; gray contour line: Subantarctic Front (Orsi et al., 1995); black contour line: Antarctic continental shelf (shallower than 1000 m).

waters due to the surface freshening. In contrast, the wind stress perturbation experiment shows little response in the high latitudes but a strong sea-surface height increase in the low latitudes, especially in the Pacific sector. This response results in an increase in the meridional sea-surface height gradient, which incorporates an increasing ACC transport of 1.9 Sv. The freshwater perturbation decreases the ACC transport by about 3.3 Sv. Therefore, almost no change or a slight decrease would occur in the net transport consistent with observational data that show very little long-term changes in the ACC transport (Meredith et al., 2011b; Koenig et al., 2014). The reduction in density on the Antarctic continental shelf and therefore an increase in the sea-surface height (Figure 4.7b) appears from the freshwater flux perturbation experiment. This finding is consistent with the results by Rye et al. (2014), who find an increasing sea-surface height around most of the Antarctic continental margin in response to increased glacial meltwater. However, due to the difficulties of ROMS to accurately simulate the continental shelf process at its current state, this response might not be reliable in our simulations.
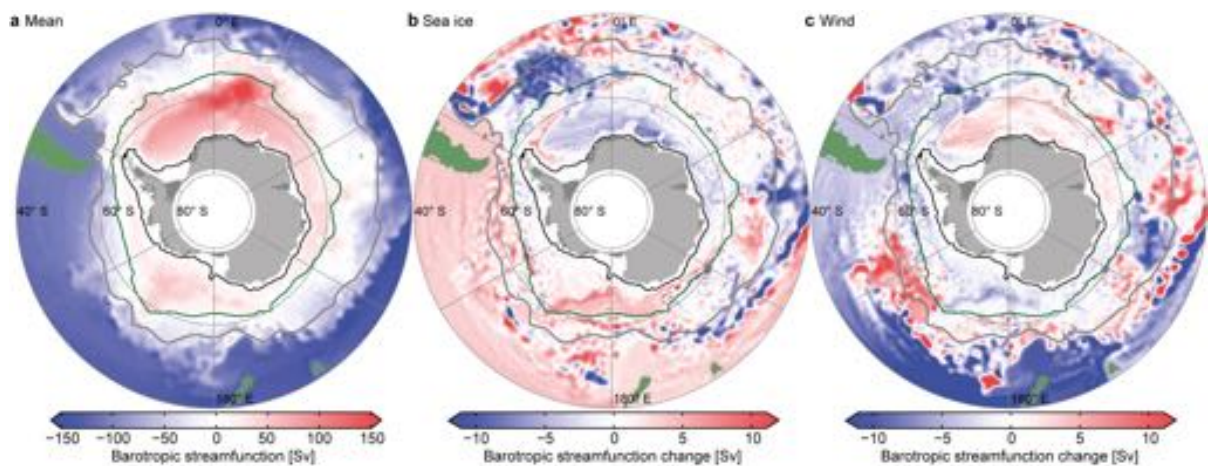
Figure 4.8   Barotropic streamfunction response: Mean simulated barotropic streamfunction (**a**), the response to the sea-ice freshwater flux perturbation (**b**), and the response to the surface wind stress perturbation (**c**). The responses show the differences of the last 20 years of a 40-year perturbation experiment to a control simulation with constant forcing. Green contour line: climatological mean sea-ice edge; gray contour line: Subantarctic Front (Orsi et al., 1995); black contour line: Antarctic continental shelf (shallower than 1000 m).

The model simulations suggest changes in the gyre circulation. One of the most prominent features in the wind stress perturbation experiment is a spin-up of the subtropical gyre in the South Pacific that can be depicted from both changes in sea-surface height and the barotropic streamfunction (Figures 4.7 and 4.8). This finding is consistent with the observed changes in sea-surface height (Figures 4.7d). However, observational estimates of changes in the sea-surface height from the AVISO satellite data only exist since 1992. Therefore, the observation based changes reflect a much shorter period and might deviate considerably from the simulated response. In the higher latitudes, the changes in the barotropic streamfunction reveal changes in the subpolar gyre circulation (Figure 4.8). The wind stress perturbation spins up the Ross Sea gyre and expands it north-eastward. This change is consistent with the observed deepening and expansion of the Amundsen Sea Low (Haumann et al., 2014). In the Weddell Sea, the wind stress

perturbation leads to a slight spin-up and contraction of the Weddell Sea gyre, which seems to be partly counteracted by the freshwater flux perturbation.

The meridional overturning circulation in the model strengthens in response to the surface wind stress perturbation, especially the upper circulation cell (Figure 4.9c). It is likely that the model overestimates this response, as it is not fully eddy-resolving. Consistent with results by Morrison et al. (2011), the meridional overturning circulation also weakly strengthens with an increased surface freshwater forcing in high-latitudes (Figure 4.9b). The explanation for a strengthening of the upper circulation cell is probably provided by the finding that these freshwater fluxes are an important contributor to the AAIW formation process. The slight increase in the overturning in our model would actually bring more deep water to the surface and counteract the changes induced by the increased stratification. Therefore, the cooling of the surface waters can only result from an increased stratification and reduced mixing, rather than through changes in vertical advection. Furthermore, a weak shoaling of the upper circulation cell and an expansion of the lower circulation cell in our simulation (Figure 4.9b) suggest that the upwelled waters are advected from a shallower depth. A shoaling of the upper circulation cell and AAIW over recent decades is also consistent with the findings by Schmidtko and Johnson (2012). While most of the simulated response shows opposing effects induced by the freshwater and wind perturbations, the meridional overturning circulation strengthens in both cases. This finding is in line with a few observation-based estimates that suggest an increased subduction of AAIW and SAMW over recent decades (Waugh et al., 2013; Waugh, 2014), which would be supported by both an increased northward sea-ice freshwater transport and increased meridional surface wind stress gradient in our simulations.
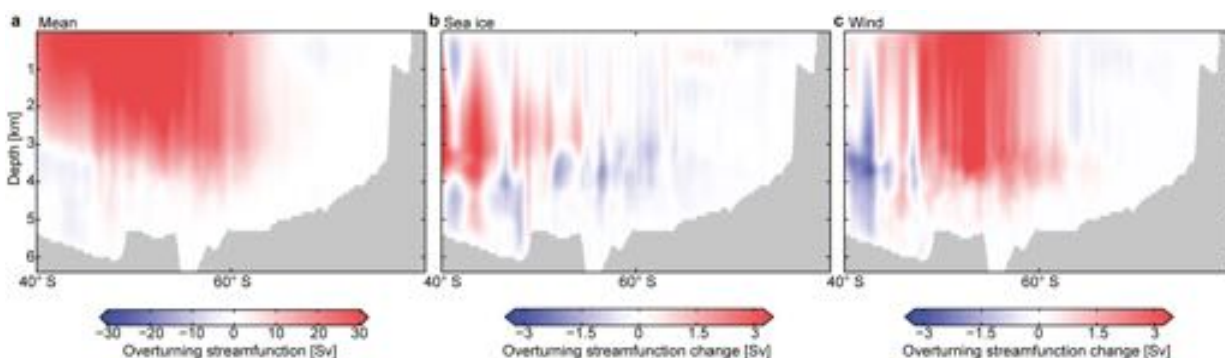
Figure 4.9   Zonal mean meridional overturning response: Mean of the simulated meridional overturning circulation (**a**), response to the combined sea-ice and land-ice freshwater flux perturbations (**b**), and response to the surface wind stress perturbation (**c**). The responses show the differences of the last 20 years of a 40-year perturbation experiment to a control simulation with constant forcing. Note that apparent vertical lines are artifacts from interpolating the transport from the model's σ-coordinates to depth-levels.

4.4 Discussion

While our simulations show a strong agreement with observed changes in temperature and salinity of the Southern Ocean, several limitations arise from model biases, the experimental design, and uncertainties in the forcing data. One limitation is that we performed these simulations at an eddy-permitting but not fully eddy-resolving resolution of 5 to 25 km and about 18 km in the ACC region. Since ROMS does not include a parameterization of mesoscale instabilities, the response of the overturning circulation and therefore the wind stress response is most likely too sensitive and the horizontal mixing of tracers and their anomalies is too small in the model. Another limitation is the large model bias in the coastal ocean around Antarctica. This bias prevent us at the current state of the model development to reliably analyze the effect of the perturbations on the observed changes over the continental shelf and the AABW. The model has a far too stable density stratification over the continental shelf region, which reduces the advection of the anomalies to the subsurface and leaves a too strong response at the surface. Similar problems, but not as severe, occur in the subduction of AAIW and SAMW. Therefore, the freshening and cooling response at the surface in the open ocean might be exaggerated and the freshening response of AAIW and SAMW underestimated. A further exaggeration of the response might result from the experimental design, because we instantaneously increase the forcing rather than applying a gradual increase. Moreover, at the current stage, we did not run a combined wind stress and freshwater perturbation experiment that might reveal some non-linear effects between the changes. Such a simulation should be additionally performed in future efforts. Finally, we did not run perturbation experiments where we change the surface heat flux. However, our simulations reveal that most of the changes in the Southern Ocean south of the ACC frontal region can be explained without changes in the surface heat flux. Additional cooling in might be induced along the expanding sea-ice edge by the ice–albedo feedback. North of the frontal regions, our simulations show a much weaker warming of AAIW and SAMW than suggested by observations. This discrepancy can most likely be explained by the increased heat uptake through AAIW and SAMW over recent decades (Frölicher et al., 2015), which is not included in our simulations as the surface heat flux is fixed.

Our simulations suggest that the upwelling of CDW into the surface waters south of the SAF, as well as the properties of the surface waters and the water masses formed in this region strongly depend on the northward transport of freshwater by sea-ice into this region. Such a high sensitivity of the upwelling to buoyancy-driven stratification changes, and freshwater flux changes in particular, is consistent with earlier idealized model experiments (Watson and Naveira Garabato, 2006; Morrison et al., 2011; Watson et al., 2015), theoretical considerations (Ferrari et al., 2014), and ocean proxy data of glacial–interglacial changes (Francois et al., 1997; Adkins et al., 2002; Sigman et al., 2004). Our results suggest that the sea-ice freshwater transport into this upwelling region is the dominant surface buoyancy flux that controls stratification changes in this region, which could provide an explanation for a more stratified ocean in the upwelling

region during cold climates and a less stratified ocean during warm climates. The sea-ice transport effectively removes freshwater from the lower circulation cell and adds it to the upper circulation cell, making the deep ocean saltier and the upper ocean fresher during increased sea-ice formation and transport (Haumann et al., 2016b). Our results support the theory that such changes occurred over recent decades. However, this effect might be reversed in the coming decades if the sea-ice region warms and sea ice retreats.

We here argue that the recent changes in Southern Ocean temperature and salinity are to a large extent driven by the sea-ice changes. These sea-ice changes have been previously attributed to changes in southerly winds, which increased the northward transport of sea-ice and led to a sea-ice expansion (Haumann, 2011; Holland and Kwok, 2012; Haumann et al., 2014). Therefore, the freshwater flux changes are indirectly induced by the changes in the surface winds and the atmospheric circulation changes are the overall driver of all these changes. Our simulations, in which we do not run a coupled sea-ice or atmosphere model, enabled us to disentangle the wind-induced freshwater flux changes from the wind-induced ocean circulation and mixing changes. A critical factor for the observed increase in the northward sea-ice transport in the Ross Sea is the zonal asymmetry in the atmospheric circulation changes (Haumann et al., 2014, 2016b). To date, it is still strongly debated whether these zonally asymmetric changes result from natural variability or anthropogenic sources (Ding et al., 2012; Fan et al., 2014; Haumann et al., 2014; Li et al., 2014; Meehl et al., 2016; Hobbs et al., 2016), which is the result of a rather short observational record in combination with difficulties of global models to reproduce these changes and a potentially large multi-decadal variability. Yet, proxy data (Thomas and Abram, 2016) and a recent ocean reanalysis product (Giese et al., 2016) suggest that the changes in sea-ice and surface temperature in the Ross Sea might have persisted over a much longer time-period. Therefore, the Southern Ocean surface freshening, cooling, and sea-ice expansion might also be an initial response to the anthropogenic forcing that lasts for several decades as the differential warming of high and low latitudes and ozone depletion could induce zonally asymmetric circulation changes that are not captured by climate models (Haumann et al., 2014). A further reason for the under-representation or absence of the surface cooling and freshening in climate models might be their poor representation of the sea-ice transport (Uotila et al., 2014; Lecomte et al., 2016). We argue that models that do not accurately capture this process would not be able to reproduce the recent cooling of the high-latitude Southern Ocean, independent of a natural or anthropogenic cause.

4.5   Summary & conclusions

In this study, we investigated the sensitivity of the Southern Ocean salinity, temperature, density stratification, and circulation to recently observed changes in surface freshwater fluxes from sea ice and land ice, as well as changes in the surface wind stress. We find a freshening of the open-ocean surface and intermediate waters in the Pacific and Atlantic sectors that is consistent with observed changes. This freshening considerably increases the surface density stratification between the sea-ice edge and the Subantarctic Front in the Pacific sector, which reduces the upwelling of warm and salty deep waters into the surface layer. As a consequence, the simulations show a strong surface cooling and a subsurface warming. The spatial pattern of the surface cooling agrees remarkably well with the satellite-observed cooling of this region in recent decades that occurred despite a globally warming surface ocean. Therefore, our analysis suggests that this cooling signal is driven by an increased northward transport of freshwater by sea ice into the upwelling region.

The response of temperature and salinity to surface wind stress changes slightly opposes the sea-ice freshwater flux induced changes in most regions. While they are much weaker south of the Subantarctic Front, in lower latitudes these changes and potentially surface heat flux changes dominate the observed warming of surface waters, AAIW, and SAMW. This warming increases the meridional density gradient and enhance the ACC transport in our simulations. However, the freshwater fluxes reduce both the meridional density gradient and ACC transport due to the high-latitude surface freshening. Therefore, the net effect of these two processes would lead to a weaker sensitivity of ACC transport changes to the hydrographic changes.

The response to changes in land-ice freshwater fluxes is much weaker in our simulations than an apparent vertical redistribution of freshwater from freezing and melting of sea ice along the Antarctic coast. However, this latter response might be a model specific result that depends on the surface mixing parameterization, leaving no conclusive answer on the source of changes observed over the continental shelf from our simulations. Therefore, at the current state of the model development, we cannot robustly estimate changes over the continental shelf and in AABW.

We conclude that the observed changes between the Subantarctic Front and the sea-ice edge, as well as in the water masses formed in this region, are largely induced by changes in surface freshwater fluxes from sea ice. This conclusion is consistent with the earlier findings by Pollard and Thompson (1994) and Kirkman and Bitz (2011) that sea-ice transport could delay global warming in the high-latitude Southern Ocean. We argue that this process led to the observed surface cooling of the Southern Ocean over recent decades. Since this cooling occurs mostly around the sea-ice edge, it could provide an important positive feedback that probably contributed to recently observed expansion of Antarctic sea ice, in line with the arguments by Goosse and Zunz (2014). While the freshwater anomalies propagate from the sea-ice edge region across the frontal region into the AAIW and SAMW, the cooling signal most likely vanishes more quickly in re-

ality due to an anomalous uptake of heat towards the north (Armour et al., 2016). Therefore, our results promote an at first sight counter-intuitive, more effective ocean heat uptake due the increased surface stratification from the surface freshwater fluxes. This effect can mostly be explained by our finding that the increased freshwater fluxes lead to a shallower upwelling and therefore to a reduced upwelling of CDW but not to a reduced subduction of AAIW and SAMW. In fact, the overturning circulation weakly increases in our simulations in response to the freshwater forcing consistent with the model experiments by Morrison et al. (2011). Therefore, both buoyancy- and wind-driven changes in the upper overturning circulation cell are consistent with observed strengthening of this cell (Waugh et al., 2013; Waugh, 2014). Our results imply that the upwelling of warm, salty, and carbon- and nutrient-rich deep waters in the Southern Ocean is highly sensitive to stratification changes induced by freshwater fluxes from sea ice—a finding that could provide a possible explanation for an increasing vertical density stratification during glacial climates (Sigman et al., 2010).

Chapter 5

Strengthening of Southern Ocean carbon uptake through increasing stratification[*]

F. Alexander Haumann[1,2], Nicolas Gruber[1,2], Matthias Münnich[1], Samuel Eberenz[1]

[1]Environmental Physics, Institute of Biogeochemistry and Pollutant Dynamics, ETH Zürich, Zürich, Switzerland
[2]Center for Climate Systems Modeling, ETH Zürich, Zürich, Switzerland

---

Abstract

To date, the Southern Ocean constitutes the strongest sink for anthropogenic carbon-dioxide in the global ocean. Concerns have been raised that increased surface ocean density stratification and increased westerly winds due to the anthropogenic perturbation of the climate system could weaken this sink and potentially amplify global warming. Here, we study the sensitivity of the Southern Ocean carbon-dioxide uptake to stratification changes induced by recent changes surface freshwater fluxes from sea ice using a regional ocean circulation model. Contrary to expectations, our simulations reveal a strengthening of the net carbon-dioxide uptake in response to an increasing stratification. This strengthened uptake is mostly a response to an increased surface freshwater input from sea ice into the upwelling region, which inhibits the upwelling of deep, warm, and carbon-rich waters into the surface layer, and outweighs a reduction of the uptake that is associated with the subduction of carbon-dioxide by intermediate and mode waters. Additionally, our simulations reveal no substantial reduction in response to changes in the surface winds that occurred over recent decades. Consequently, our results provide a potential explanation for the recent finding that the Southern Ocean carbon-dioxide sink has not weakened but rather strengthened over recent decades. While the sea-ice freshwater input to the upwelling region increased during this period, global climate models project a future decline of the sea-ice cover, which would imply a reversal of the effect. In contrast, in a cold glacial climate, stronger sea-ice fluxes could considerably enhance the stratification in the upwelling region, resulting in a reduced outgassing of carbon-dioxide, which provides a potential explanation for lower atmospheric carbon-dioxide concentrations during past cold climates.

5.1   Introduction

The increase in the atmospheric carbon-dioxide (CO_2) concentrations through human activity since the pre-industrial era has turned the Southern Ocean from a region of net CO_2 release to a CO_2 sink (Hoppema, 2004; Gruber et al., 2009). Thereby, it has taken up a proportionally much larger amount of anthropogenic CO_2 than any other region of the global ocean (Mikaloff Fletcher et al., 2006; Khatiwala et al., 2009; Frölicher et al., 2015). Simulations with global climate models suggest that an increasing surface density stratification due to future warming and enhanced surface freshwater fluxes could weaken this uptake of anthropogenic CO_2 and therefore amplify global warming (Manabe and Stouffer, 1993; Sarmiento et al., 1998). In contrast, paleoceanographic data indicate that an increasing stratification reduces the outgassing of natural CO_2 by inhibiting the upwelling of deep and carbon-rich waters—a process that was suggested to control atmospheric CO_2 variations over past glacial–interglacial climate states (Francois et al., 1997; Toggweiler, 1999; Sigman et al., 2004; Watson and Naveira Garabato, 2006; Skinner et al., 2010). Combining these two lines of argument, an increasing stratification in the Southern Ocean could either decrease or increase the atmospheric CO_2 concentration, depending on the net effect of changes in upwelling and subduction of CO_2. Model experiments show that this net effect is very sensitive to the background atmospheric CO_2 concentration as well as the type, pattern, magnitude of the surface fluxes (Matear and Lenton, 2008; Lovenduski and Ito, 2009; Bernardello et al., 2014a,b). As a consequence of large uncertainties in the observed surface fluxes (Speer et al., 2012; Bourassa et al., 2013) and global models (Downes et al., 2010; Sallée et al., 2013a; Stössel et al., 2015), the response of the Southern Ocean carbon fluxes to changes in the surface stratification remains largely unconstrained for past, present, and future climates. In this study, we address this issue by using new observation-based constraints on the surface fluxes from the sea ice and their changes over recent decades (Haumann et al., 2016b) to analyze the sensitivity of the carbon fluxes to stratification changes in a present-day climate.

The majority of the global ocean's deep waters surface through upwelling in the Southern Ocean (Talley, 2013). This upwelling occurs due to wind- and buoyancy-driven vertical transport (Speer et al., 2000; Morrison et al., 2011; Marshall and Speer, 2012) and mixing (Watson et al., 2013), which return large amounts of dissolved inorganic carbon (DIC) and nutrients from the deep ocean to the surface (Marinov et al., 2006). While vertical transport is mostly responsible for elevating the DIC-rich waters from the deep ocean to waters below the mixed layer, mixing at the base of the mixed layer is the predominant reason for the penetration of these waters to the surface (Dufour et al., 2013). The resulting over-saturation of the partial pressure of CO_2 (pCO_2) in the surface waters with respect to the atmosphere leads to a natural CO_2 release from the Southern Ocean (Gruber et al., 2009). This release occurs during austral winter in a region between the sea-ice edge and the Subantarctic Front (SAF) where deep mixed layers and a weak density stratification ease the surfacing of the deep waters (Takahashi et al., 2002; Landschützer et al., 2014b). The situation is reversed during austral summer, when wind-driven mixing decreases and surface

waters stratify due to warming and sea-ice melting (Haumann et al., 2016b). As these waters are transported northward by surface Ekman transport, intense biological production removes carbon from the surface ocean (Hauck et al., 2013). As a result, the pCO_2 at the surface drops below the atmospheric level leading to a natural uptake of CO_2 by the ocean during summer. However, this uptake is considerably smaller than the outgassing during winter, leading to a net annual loss of natural CO_2 from these waters to the atmosphere before they are subducted as Antarctic Intermediate Water (AAIW; Mikaloff Fletcher et al., 2007; Gruber et al., 2009). Another portion of these southern sourced waters mixes with southward flowing subtropical waters, that were enriched in CO_2, between the SAF and the Subtropical Front (STF). Therefore, the subduction of these waters as Subantarctic Mode Water (SAMW) leads to a natural uptake of CO_2 from the atmosphere (Mikaloff Fletcher et al., 2007).

The uptake of anthropogenic CO_2 is the sum of a reduced outgassing from the upwelling waters and an enhanced uptake, which result from the elevated pCO_2 in the atmosphere relative to the pre-industrial ocean's pCO_2. The net uptake would saturate very rapidly if the CO_2 was not removed from the surface ocean through mixing and transport (Sarmiento et al., 1992). Since most of the global subsurface waters form in the Southern Ocean (DeVries and Primeau, 2011), it is one of the most effective regions to take up anthropogenic CO_2. AAIW and SAMW draw down anthropogenic CO_2 from the surface ocean and store it in deeper layers (Caldeira and Duffy, 2000). However, while AAIW mainly subducts anthropogenic CO_2 through a reduced outgassing, SAMW subducts it through an enhanced uptake (Mikaloff Fletcher et al., 2006; Gruber et al., 2009; Iudicone et al., 2011). Besides this transport mechanism, mixing at the base of the mixed layer is a critical factor for the invasion of anthropogenic CO_2 to the subsurface layers (Dufour et al., 2013; Bopp et al., 2015).

Changes in surface winds and buoyancy forcing could alter both the natural CO_2 release and the uptake of anthropogenic CO_2 by changing the vertical transport and mixing. The increase in westerly winds in response to the anthropogenic forcing (Thompson et al., 2011; Abram et al., 2014) potentially enhances the net overturning circulation and changes its vertical structure despite a compensation by meso-scale eddies (Meredith et al., 2012). At the same time, the increasing winds deepen the surface mixed layer (Sallée et al., 2010b). Both these processes would enhance the natural CO_2 release from the Southern Ocean (Le Quéré et al., 2007; Lovenduski et al., 2007, 2008; Lenton et al., 2009; Dufour et al., 2013). Yet, very recent observational studies show that contrary to expectations, the Southern Ocean carbon sink actually strengthened again over the last decade despite a continued strengthening of the westerly winds (Fay et al., 2014; Landschützer et al., 2015b; Munro et al., 2015). Observation-based estimates of surface CO_2 fluxes over the past 30 years suggest that Southern Ocean CO_2 sink did not saturate but actually strengthened according to what is expected from the increase of atmospheric pCO_2 alone (Landschützer et al., 2015b). This finding raises the questions if other mechanisms are at work in the long-term that counter-act a potential decreasing CO_2 sink due to increasing winds. Matear and Lenton (2008) suggest that a more stable surface ocean due to increasing surface heat and fresh-

water fluxes could have balanced the effect induced by the increasing winds over recent decades. Salinity observations reveal a wide-spread surface freshening in this region (Durack et al., 2012), which led to an overall increased surface stabilization (chapter 4; Haumann et al., 2017). A major portion of this freshening and stabilization can be attributed to an increased transport of freshwater by sea ice into this region (chapter 2; Haumann et al., 2016b).

Here, we study the sensitivity of the present-day Southern Ocean carbon fluxes to stratification changes by perturbing a regional ocean model that realistically simulates the Southern Ocean surface stratification in the upwelling region. We specifically address the question whether observed changes in surface freshwater fluxes from sea ice could have counter-acted the wind-driven increased upwelling of carbon-rich deep waters over recent decades and thereby maintained an efficient Southern Ocean carbon sink. The recent constraints on the surface freshwater flux balance and its changes enable us to better understand this response of the Southern Ocean CO_2 uptake. Moreover, our findings have direct implications for the understanding on changes in the Southern Ocean CO_2 uptake in response to stratification changes in colder past and warmer future climates as outlined in section 5.4.

5.2   Methods

We used the Regional Ocean Modeling System (ROMS; UCLA-ETH version; Shchepetkin and McWilliams, 2005; Gruber et al., 2011), which was adapted for the use in the Southern Ocean as described in detail by Haumann et al. (2017, chapters 3 and 4). In this study, we run ROMS at a horizontal resolution of 0.5°, which corresponds to a resolution of about 50 km at the northern boundary (24° S) and about 25 km at the Antarctic coast. ROMS does not have any eddy-parameterizations, instead the advection scheme contains a resolution dependent hyperdiffusion to ensure numerical stability (Shchepetkin and McWilliams, 1998). Vertical mixing processes are parameterized using the *K*-profile parameterization (KPP; Large et al., 1994; Shchepetkin, 2005; McWilliams et al., 2009) with some modifications described in detail in chapter 3. In the vertical, the stretched, terrain-following coordinate system (Song and Haidvogel, 1994; Shchepetkin and McWilliams, 2003, 2005) is divided into 64 layers. ROMS generally reproduces a realistic water mass structure and circulation in the Southern Ocean as described in the evaluation of the physical model by Haumann et al. (chapter 3; 2017).

For this study, we additionally use the coupled Biological Elemental Cycling (BEC) model (Moore et al., 2004; Jin et al., 2008; Yang and Gruber, 2016, see section 3.3 for details). BEC is forced at the surface with the climatological mean atmospheric CO_2 concentration of 370 ppm and surface deposition of iron and dust from Mahowald et al. (2009). At the northern boundary and as initial conditions we use World Ocean Atlas 2013 (Boyer et al., 2013) for nutrients (Garcia et al., 2014b) and oxygen (Garcia et al., 2014a), the Global Data Analysis Project for dissolved inorganic carbon and alkalinity (Key et al., 2004; Lee et al., 2006), the SeaWiFS climatology of chlorophyll-a (SeaWiFS Project, 2003), which is extrapolated to depth according to Morel and Berthon (1989) and used for all phytoplankton functional types, and the fields of a global model simulation with CESM1.2 for iron, ammonium, and dissolved nutrients (Yang et al., 2017).

The experimental design is the same as the one presented in chapter 4 (Haumann et al., 2017). The model is spun up with the climatological mean forcing for 40 years until the ocean circulation and the surface ocean are stable in time. Hereafter, we perform a set of three simulations of 40 years that are each restarted from the model spin-up simulation. One simulation is a simple control simulation using the same climatological forcing as the model spin up. In a second simulation, the freshwater flux forcing from sea ice is perturbed using the data set by Haumann et al. (2016b,a, Figure 5.1a) and in a third simulation only the surface momentum forcing (ERA-Interim, 1979–2014; Dee et al., 2011) is perturbed (Figure 5.1b). All perturbations vary throughout the year. Therefore, the sea-ice melting flux perturbation is mostly added in summer and the freezing flux perturbation in winter. The surface wind stress perturbation is more zonally symmetric during austral summer and zonally asymmetric during winter (Figure 5.1c–f). We averaged the last 20 years in all three simulations and subtracted the control simulation from the two perturbation experiments. We note that the atmospheric pCO_2 is kept constant throughout the
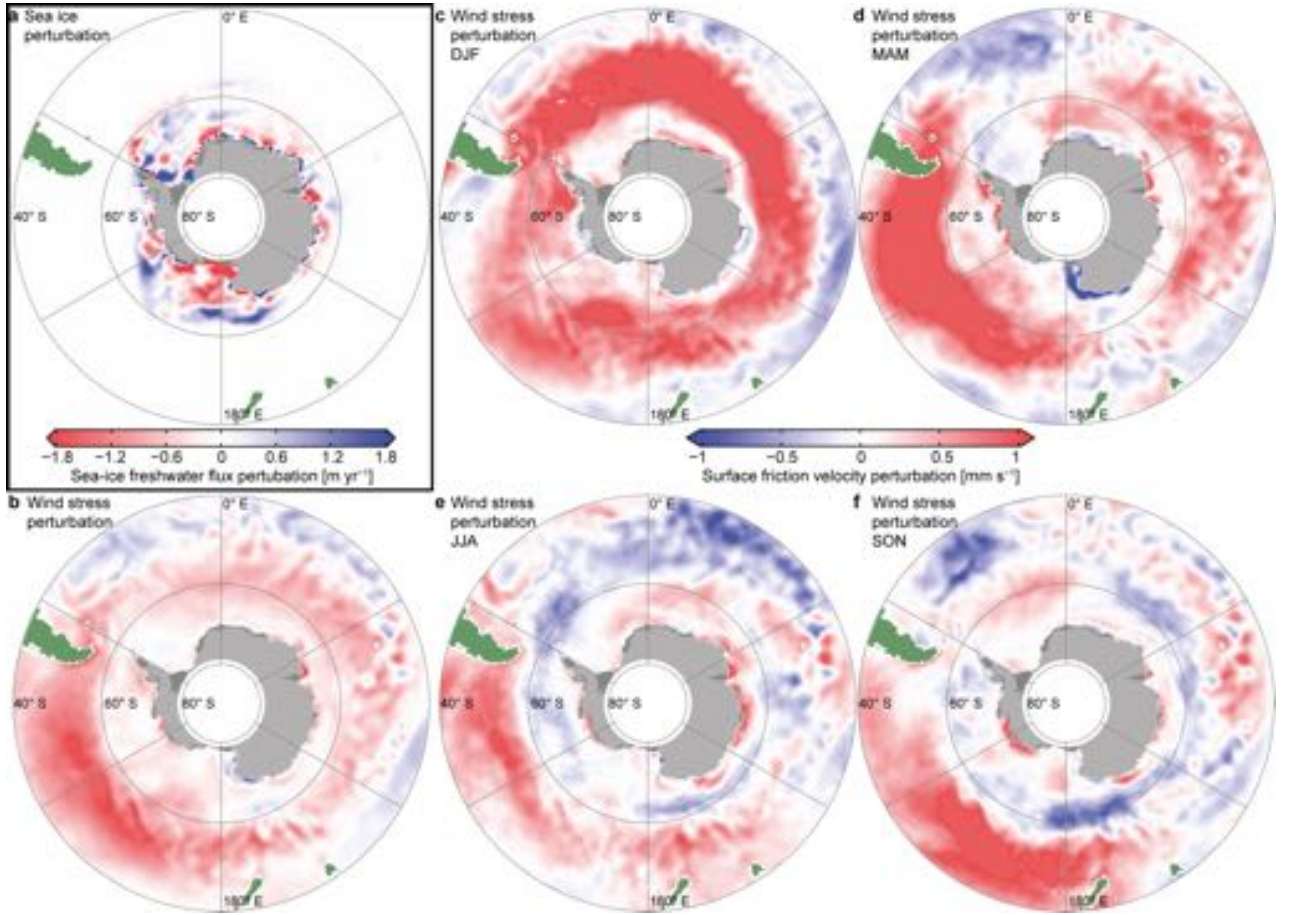
Figure 5.1   Perturbation of sea-ice freshwater flux and wind stress surface forcing: (**a**) Sea-ice freshwater flux change. (**b–f**) Surface friction velocity change: annual mean (**b**), austral summer (DJF, **c**), autumn (MAM, **d**), winter (JJA, **e**), spring (SON, **f**).

simulations. Therefore, our simulations do not reflect any changes associated with the increase in atmospheric pCO_2 over recent decades, but include the mean uptake of anthropogenic CO_2 by the ocean.

   We here analyze the spatially integrated surface CO_2 flux and its spatial and temporal changes. Additionally, we decompose the signal by estimating the contribution from changes in surface temperature to the air-sea pCO_2 gradient, and residual changes that result mostly from changes in dissolved inorganic carbon (DIC) and alkalinity (Alk) as well as biological production. The thermal contribution is approximated according to Takahashi et al. (2002):

$$\Delta pCO_2^T = pCO_2^O(\exp^{0.0423 \cdot \Delta SST} - 1). \tag{5.1}$$

Here, pCO_2^O denotes the mean surface ocean pCO_2 and ΔSST the change in sea-surface temperature. We will compare our results to observation-based estimates from Landschützer et al. (1982–2014; 2015b, expanded as in Le Quéré et al. (2016)). Moreover, we will use the location of the SAF as estimated by Orsi et al. (1995) and an Argo and CTD profile derived mixed layer depth product (de Boyer Montégut et al., 2004).

5.3 Results

The Southern Ocean south of 30° S takes up 1.5 PgC yr^{-1} in our simulations. This value is higher than the observation-based estimate of 1.0 PgC yr^{-1}. Figures 5.2a–b illustrate that the spatial pattern of the surface CO_2 flux in the model agrees well with the observed spatial pattern, with high CO_2 uptake north of the SAF (around 50° S; Orsi et al., 1995) and CO_2 release between the SAF and the annual mean sea-ice edge (around 65° S) where carbon-rich waters upwell to the surface. South of the SAF, the model overestimates the carbon uptake compared to the observational product by 0.55 PgC yr^{-1}, which is the main reason for the overall discrepancy. This overestimation is caused by a too strong summer-time uptake in the model that is mostly driven by biological production (Figure 5.2c). The band between the SAF and the sea-ice edge experiences a very large seasonal cycle with strong CO_2 release during austral winter and spring and uptake during austral summer (Figure 5.2c–f). In some regions of this band, the uptake in the model outweighs the winter-time outgassing. The outgassing is associated with dynamical upwelling of CDW into
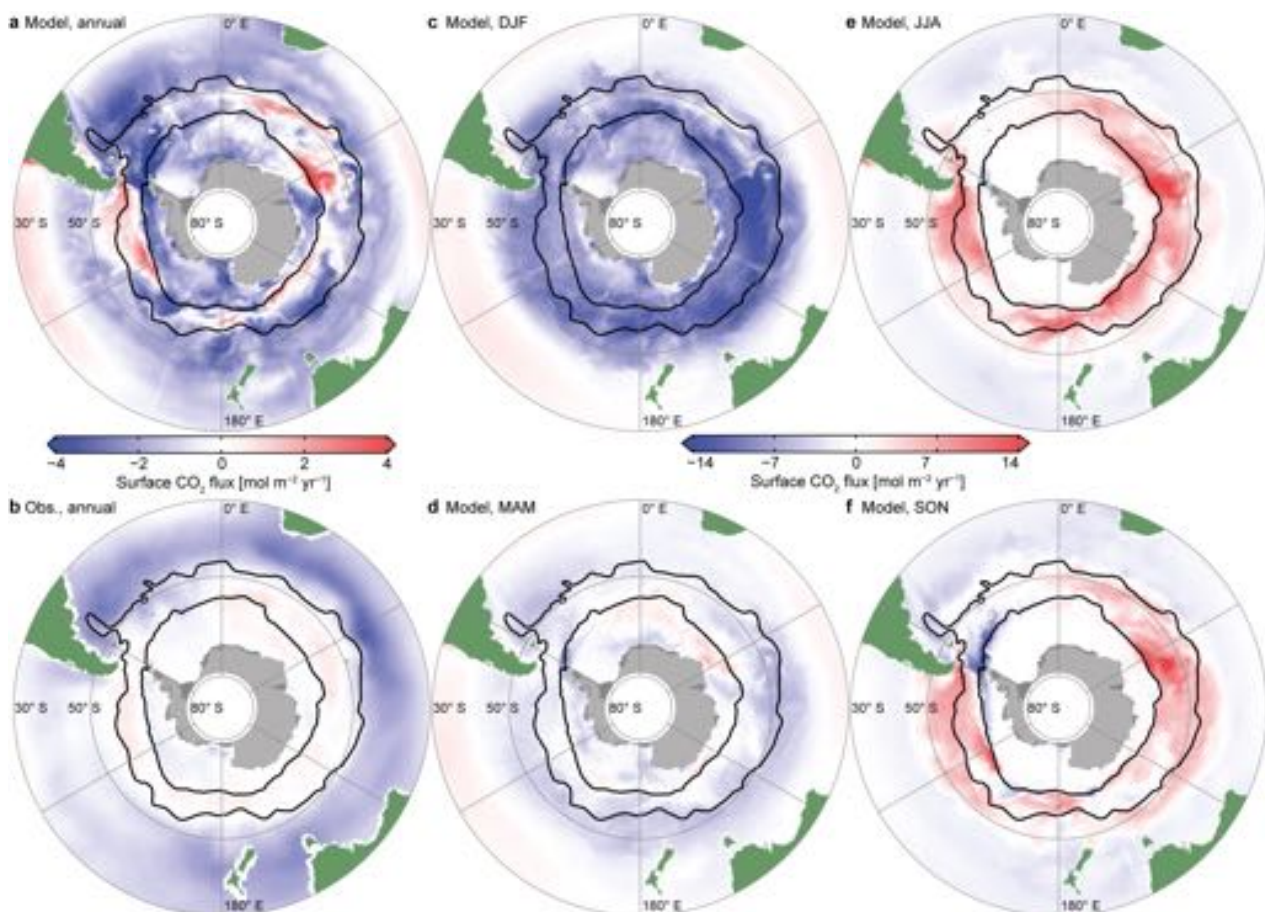
Figure 5.2   Simulated and observed surface CO_2 flux: (**a**) Simulated annual mean surface CO_2 flux. (**b**) Observation-based annual mean surface CO_2 flux (1982–2014; Landschützer et al., 2015b, expanded as in Le Quéré et al. (2016)). Seasonal means of the simulated surface CO_2 flux for austral summer (DJF, **c**), autumn (MAM, **d**), winter (JJA, **e**), and spring (SON, **f**). Positive values (red) show outgassing and negative values (blue) uptake by the ocean. The thick black lines denote the SAF and annual mean sea-ice edge (10% sea-ice concentration).

the surface waters, which are subsequently subducted in the same band as AAIW (Sallée et al., 2010a). The spatial gradients and the seasonal cycle are generally much stronger in the model than in the observation based product. This difference can partly be attributed to the strong spatial and temporal smoothing induced by the method to derive the observational data (personal communication P. Landschützer and N. Gruber). Overall, the model produces the characteristic spatial and temporal evolution of surface CO_2 fluxes very well, but probably overestimates the magnitude of the fluxes.

In the sea-ice freshwater flux perturbation experiment, the surface freshwater flux around the sea-ice edge in the Pacific sector increases substantially due to the increased northward transport of freshwater by sea ice in this region (Figure 5.1a; Haumann et al., 2016b). In response, the model simulates a strong anomalous net annual CO_2 uptake in the Pacific sector that is confined
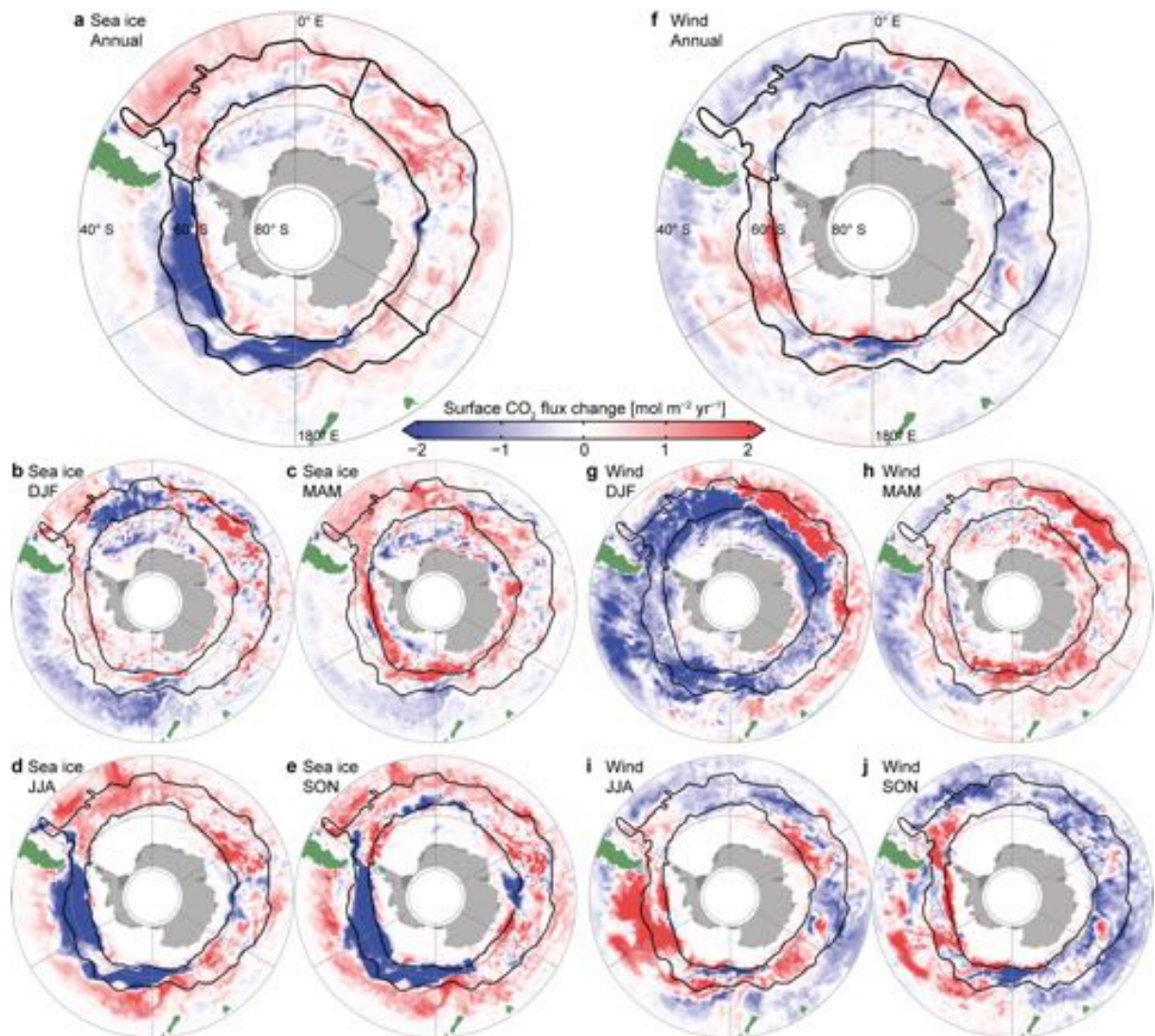
Figure 5.3   Surface CO_2 flux response to freshwater flux and wind perturbation: Annual mean (**a,f**), austral summer (DJF, **b,g**), autumn (MAM, **c,h**), winter (JJA, **d,i**), and spring (SON, **e,j**) response of the surface CO_2 flux to the sea-ice freshwater flux perturbation (**a–e**) and surface wind stress perturbation (**f–j**). The thick black lines denote the SAF and annual mean sea-ice edge (10% sea-ice concentration). This band is divided into the Pacific, Atlantic, and Indian Ocean sectors.

to the region between the sea-ice edge and the SAF, where the net annual uptake increases by 0.13 PgC yr^{-1} (Figure 5.3a). This anomalous uptake is counteracted by anomalous net annual CO_2 release of 0.02 PgC yr^{-1} in the Atlantic and 0.04 PgC yr^{-1} in the Indian Ocean sectors. As a result, the net annual uptake of CO_2 in this band increases by about 25%. An additional anomalous carbon release occurs north and south of this band in all three sectors. Splitting the results into the seasonal responses (Figure 5.3b–e), reveals that the signal originates from austral winter and spring and therefore results from a reduction in outgassing.

The response to the surface wind stress perturbation shows less extreme changes in the net annual CO_2 flux, which are zonally asymmetric (Figure 5.3f), consistent with the zonally asymmetric changes in the surface wind forcing (Figure 5.1b). In many regions, they oppose the changes induced by the surface freshwater flux perturbation. An anomalous net annual CO_2 release of 0.01 PgC yr^{-1} occurs in the Pacific sector between the sea-ice edge and the SAF, which is outbalanced by an anomalous net annual CO_2 uptake of 0.03 PgC yr^{-1} in this same band in the other two sectors together. The seasonal changes reveal that this weak net annual response is the result of strong opposing seasonal changes (Figures 5.3g–j). During austral summer, strong enhanced uptake occurs in most of the Southern Ocean except for the lower latitudes in the Atlantic and Indian Ocean sectors, where the CO_2 uptake is reduced. Especially in the Pacific sector, this picture is reversed during austral winter and to some extent also during austral spring, when the wind perturbation experiment reveals a strongly enhanced CO_2 release in this sector. This signal is opposed by a reduced CO_2 release in the Atlantic and Indian Ocean sectors during austral winter and spring. In summary, both the sea-ice freshwater flux and surface wind stress perturbation experiments lead to a spatially and temporally very complex response of the surface CO_2 flux, whereas the response to the sea-ice freshwater flux changes is stronger than the one to the wind stress forcing. Summing both effects together, the Southern Ocean CO_2 uptake strengthens by 0.09 PgC yr^{-1} south of 50° S, which is opposed by a reduction in the uptake by 0.05 PgC yr^{-1} north of 50° S.

To better understand the drivers of these changes, we decompose the surface pCO_2 gradient between the atmosphere (pCO_2^A) and the ocean ($\Delta pCO_2 = pCO_2^O - pCO_2^A$) into the thermal and non-thermal components (see section 5.2). The air–sea gradient (Figure 5.4a,d) shows very similar changes as the surface CO_2 flux (Figure 5.3a,f), except for the sea-ice region where the gas-exchange is reduced by the sea-ice cover. The observed ΔpCO_2 trend differs regionally from the simulated changes. However, the general picture of an enhanced uptake around the sea-ice edge and a reduced uptake north of the SAF seems to be a consistent feature in both the observed and simulated changes. The enhanced uptake of between the sea-ice edge and the SAF in our simulations mostly results from the surface cooling induced by the sea-ice freshwater fluxes (Figure 5.4b), which is consistent with the observed trend, even though the observed trend is much weaker (Figure 5.4h). The non-thermal component suggests a reduced outgassing directly at the sea-ice edge in some regions and an enhanced outgassing or reduced uptake north and south of this region due to the sea-ice freshwater flux changes (Figure 5.4c). North of the sea-ice edge

the thermal and the non-thermal contributions oppose each other, which can also be seen in the observed trends. Overall the sea-ice freshwater flux changes have a much larger effect on the air–sea CO_2 gradient in our simulations than the surface wind stress changes.
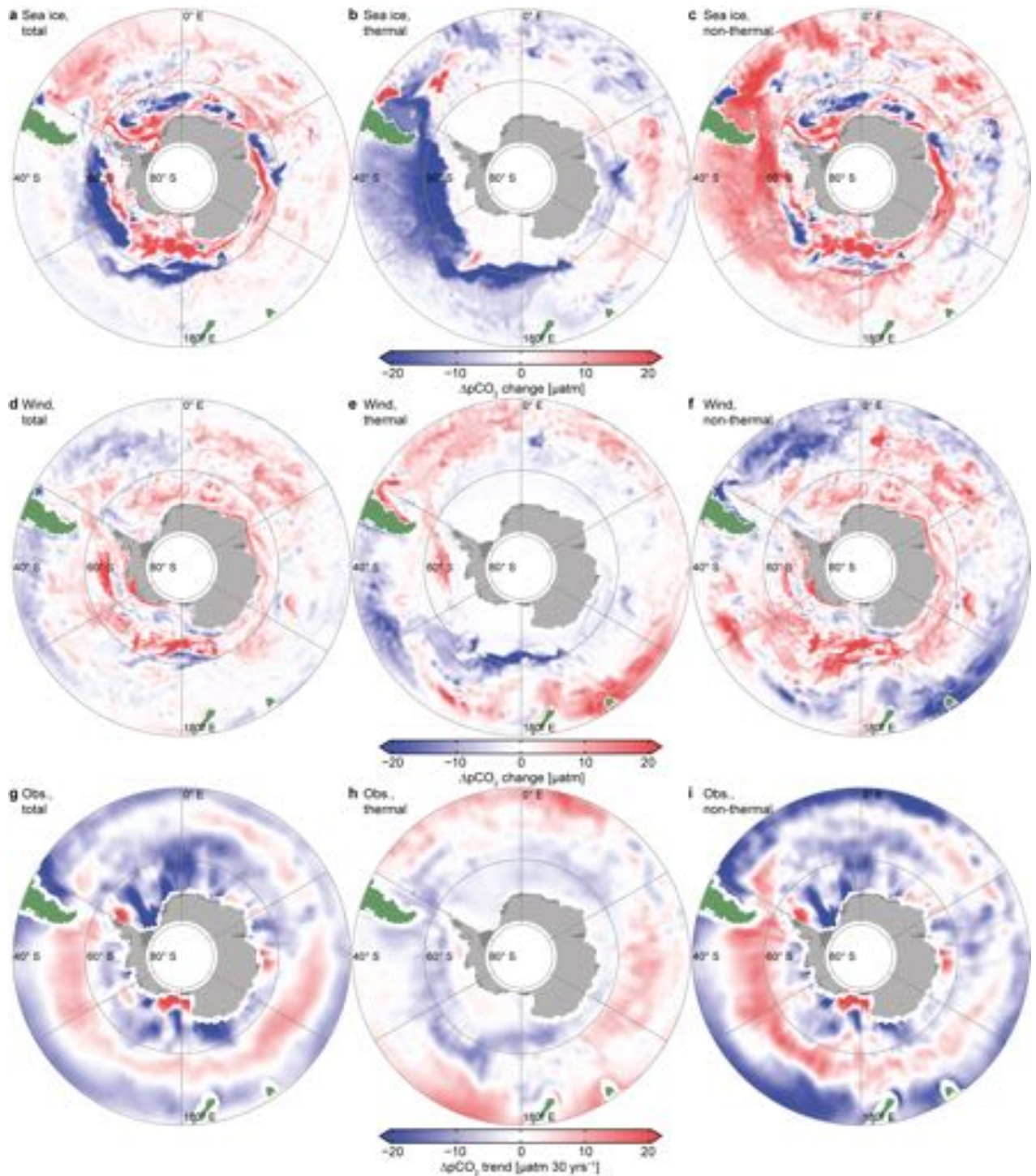

Figure 5.4 Observed and simulated ΔpCO_2 changes and its thermal and non-thermal contributions: (**a–c**) Simulated ΔpCO_2 change due to the sea-ice freshwater flux perturbation. (**d–f**) Simulated ΔpCO_2 change due to the surface wind stress perturbation. (**g–i**) Observed trends derived from the period 1982–2014 Landschützer et al. (2015b, expanded as in Le Quéré et al. (2016)), scaled to a 30-year period. The middle column (**b,e,h**) shows the respective thermal contribution and the right column (**c,f,i**) the respective non-thermal contribution.

The surface cooling that is responsible for a most of the enhanced CO_2 uptake in the sea-ice freshwater flux experiment is driven by an increased stratification and a reduced mixed-layer depth in the Pacific sector. This enhanced stratification and shoaling of the mixing is illustrated in Figure 5.5. While most of the freshwater flux perturbation is added to the surface ocean during the melting period in summer, the response of the reduced surface mixing occurs in winter. We argue that the main reason is that the surface freshwater in summer pre-conditions the surface ocean. Therefore, the erosion of the stable summer-time halocline by the surface cooling and increasing winds between May and September is much slower and the mixing is more shallow (Figure 5.5c). As a consequence, the upwelling of warmer CDW into the surface layer is reduced during winter-time. In comparison, the surface wind stress perturbation only leads to a small increase in winter-time mixing.
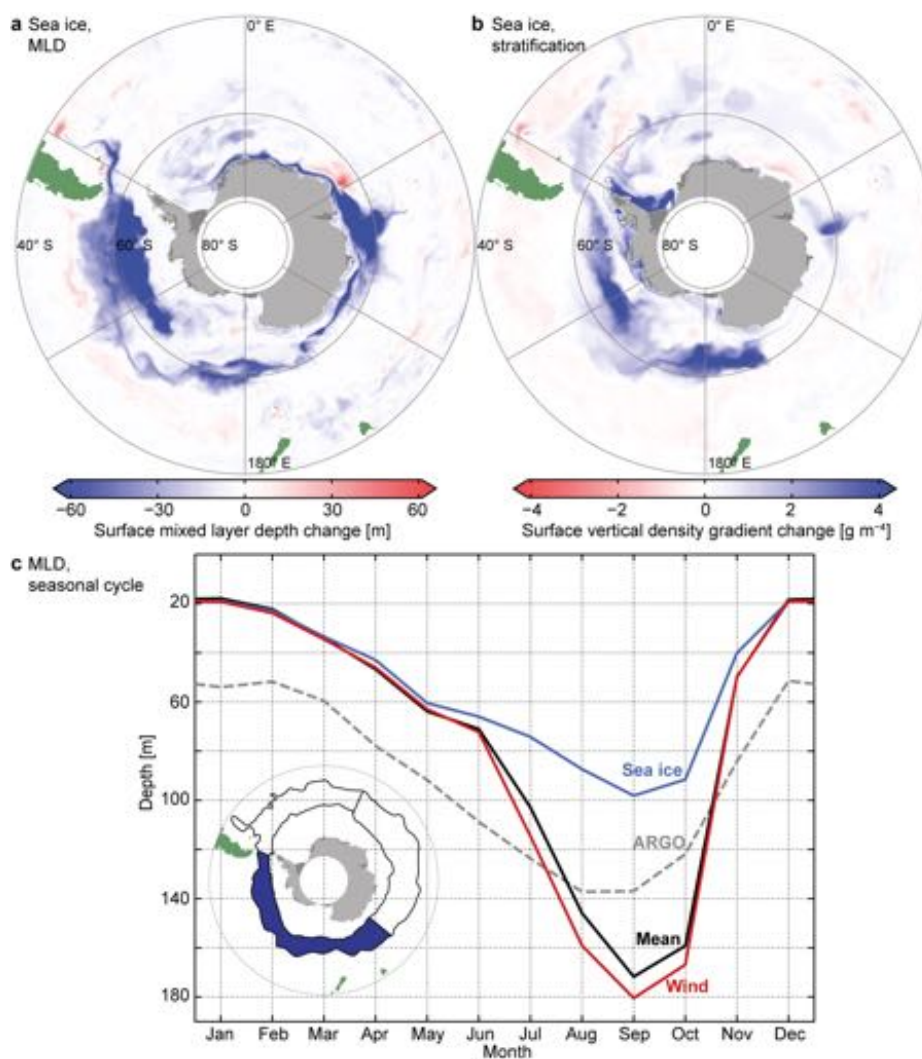
Figure 5.5   Surface stratification and mixed-layer depth response: (a) Change of the surface density gradient (averaged over the top 100 m) and (b) surface mixed-layer depth to the sea-ice freshwater flux perturbation. (c) Seasonal cycle of the spatially averaged mixed-layer depth between the sea-ice edge and the SAF in the Pacific sector. The averaging region is displayed in blue in the inset. Black line: mean of the control simulation, blue line: sea-ice freshwater flux experiment, red: surface wind stress experiment, gray dashed line: mean of the observed mixed-layer depth from ARGO data (de Boyer Montégut et al., 2004).

The causes for the response in the non-thermal component of the ΔpCO_2 to the sea-ice freshwater flux perturbation can be further investigated by considering the opposing seasonal changes in this component (Figure 5.6). During summer and autumn, when the high-latitude Southern Ocean takes up CO_2, the surface stabilization in the Pacific sector reduces the subduction of CO_2 into the subsurface, which increases the surface ocean pCO_2. This process would lead to a reduction in the CO_2 uptake during summer and autumn if it were not for the surface cooling that partly compensates for this effect. During winter and spring this situation is reversed in the region between the sea-ice edge and the SAF in the Pacific sector, when a reduction of upwelling of CDW that is rich in dissolved inorganic carbon (DIC) lowers the surface pCO_2 in this region. North of the SAF, where waters are subducted with SAMW during winter the subduction of CO_2 decreases. Consequently, the increased stability from the sea-ice freshwater flux omits upwelling of DIC-rich CDW during winter and, at the same time, hinders the subduction of CO_2 with AAIW and SAMW during all seasons.
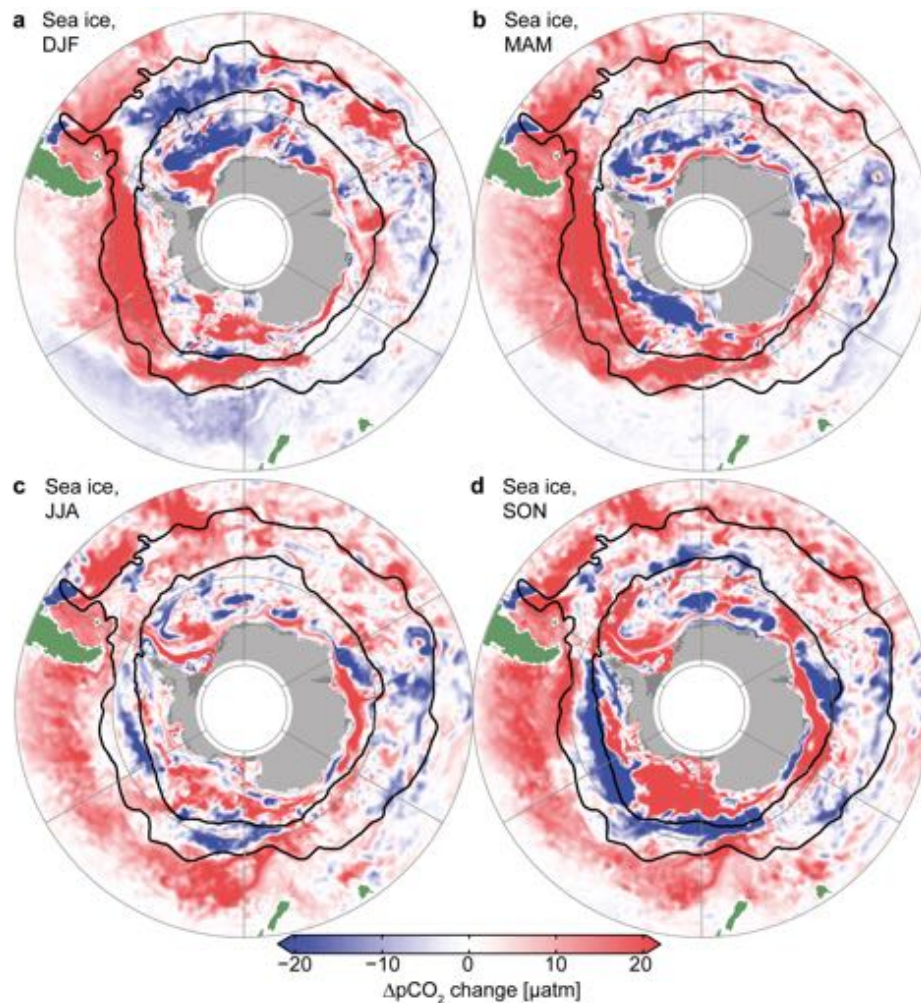
Figure 5.6 Seasonal response of non-thermal ΔpCO_2 changes to sea-ice freshwater fluxes:
For the austral summer (DJF, **a**), autumn (MAM, **b**), winter (JJA, **c**), and spring (SON, **d**). The thick black lines denote the SAF and annual mean sea-ice edge (10% sea-ice concentration).

5.4   Discussion and conclusions

In this study, we analyzed the sensitivity of the Southern Ocean surface CO_2 fluxes to an increased surface stratification from recent changes in sea-ice–ocean surface freshwater fluxes. We find that the increased stratification in the region between the sea-ice edge and the SAF drives a substantial reduction in the release of natural CO_2. There are two major reasons for the reduced CO_2 release. Firstly, the increased stratification cools the surface ocean throughout the year, which increases the solubility of CO_2 in the seawater and reduces the outgassing. Secondly, a reduced and shallower mixing during austral winter reduces the upwelling of DIC-rich waters into the surface layer. These two effects are opposed by a reduction in subduction of CO_2 from the surface layer into AAIW during summer and a reduced subduction into SAMW north of the SAF during winter. Consistent with the study by Matear and Lenton (2008), we find a net strengthening of the CO_2 uptake in response to the surface freshwater fluxes. They also argue that the net effect of reduced outgassing and reduced uptake will depend on the background atmospheric CO_2 concentration. Therefore, a much higher atmospheric CO_2 concentration in a future climate could reverse the net effect (Manabe and Stouffer, 1993; Sarmiento et al., 1998; Lovenduski and Ito, 2009; Bernardello et al., 2014b) and a much lower atmospheric CO_2 concentration in a past climate could have led to a much stronger reduction in CO_2 release in response to an increasing stratification than today.

Our findings are limited to the response to changes in sea-ice–ocean freshwater fluxes that dominated the recent observed freshening in the upwelling region of the open Southern Ocean (Haumann et al., 2016b). However, we did not consider potential changes in the atmospheric freshwater flux or additional glacial meltwater from Antarctica. Both these fluxes are expected to increase substantially in a warming climate (Knutti and Sedláček, 2013; Golledge et al., 2015). Our study highlights that the location of the additional freshwater is a critical aspect for the CO_2 flux response. Sea-ice freshwater fluxes at the sea-ice edge due to increased northward transport are very effective in changing the CO_2 flux as they stabilize a region of major vertical water-mass exchange, i.e., the region between the sea-ice edge and the SAF. South of the sea-ice edge the vertical exchange is strongly reduced due to the isolating sea-ice layer that prevents strong surface cooling in winter and deep mixed layers (Gordon and Huber, 1984; Martinson, 1990). North of the SAF, the surface ocean stratification is very stable due to warmer surface waters preventing the upwelling of deep waters. The increased sea-ice freshwater transport into this region over recent decades is mainly driven by changes in the atmospheric circulation (Haumann et al., 2014). Whether or not such an increase will continue in future, is uncertain as global climate models simulate sea-ice decline over recent decades and in future. A decreasing future sea-ice cover could reverse the effects and lead to an enhanced outgassing of natural CO_2 due to a decrease in the vertical stability of the water column around the sea-ice edge. In contrast, during cold glacial climates an expanded sea-ice cover and an associated increased sea-ice freshwater flux could enhance the stratification in the upwelling region and reduce the outgassing of natural CO_2 (Fischer et al., 2010; Sigman et al., 2010). Consequently, this mechanism could provide

an explanation for co-varying glacial–interglacial changes in the atmospheric CO_2 concentration and Antarctic surface temperature (Petit et al., 1999; Parrenin et al., 2013).

We contrasted our results with effects induced by surface wind stress changes from the period 1979 to 2014. While multiple studies have previously investigated the effects of increasing winds over the Southern Ocean (e.g. Le Quéré et al., 2007; Lovenduski et al., 2007, 2008; Lenton et al., 2009; Dufour et al., 2013; Hauck et al., 2013), they mostly studied the response to changes in the Southern Annular Mode. Here, we use a perturbation that accounts for spatial and seasonal variations in the wind changes as reconstructed by ERA-Interim reanalysis data. We find strongly opposing tendencies in the surface CO_2 flux changes with an increased summer-time uptake and an increased winter-time release. The increased winter-time release is a consequence of increasing upwelling of DIC-rich waters in the Pacific sector and the other sectors rather show a reduction in CO_2 release, which is associated with zonally asymmetric circulation changes during winter (Figure 5.1). The summer-time increased uptake in our simulations is probably associated with a higher subduction of CO_2 from increased biological productivity (Hauck et al., 2013) and stronger subduction into SAMW (Iudicone et al., 2011). This interpretation of contrasting seasonal responses to changes in surface winds is consistent with the findings by Hauck et al. (2013). However, in our simulations the increased summer-time uptake is larger than increased winter-time release, which might be a model dependent result, since our model overestimates the summer-time CO_2 uptake. In conclusions, these results illustrate that the paradigm of a saturating Southern Ocean carbon sink with increasing winds is more complex than previously thought and might not hold for the changes over recent decades due to opposing seasonal and spatial variations in the wind-response.

We conclude that the recent finding that the Southern Ocean carbon sink did not saturate despite increasing winds (Landschützer et al., 2015b) could be explained by an increasing stratification from sea-ice freshwater fluxes on the one hand, and a more complex response to surface wind stress changes than previously thought on the other hand. The net response of these two changes together in our simulations would result in a reduced outgassing or enhanced uptake in higher latitudes, i.e., south of the SAF, and a reduced uptake in lower latitudes, i.e. north of the SAF. However, these changes have to be understood on top of the background increase in atmospheric CO_2 concentrations that we did not account for in our simulations. Therefore, the reduced uptake north of the SAF would result in a reduction in the uptake of anthropogenic CO_2, which is compensated by a reduction in release of natural CO_2 south of the SAF. This figure is consistent with the long-term trends in Southern Ocean CO_2 uptake over the period 1982 to 2014 derived from sparse observational data.

Chapter 6

Synthesis

Most of the interior ocean waters upwell to the surface through the Southern Ocean. Through this process these waters return carbon and nutrients to the surface and have therefore been identified as a critical component in controlling long-term changes in the global climate system (Knox and McElroy, 1984; Sarmiento and Toggweiler, 1984; Siegenthaler and Wenk, 1984; Marinov et al., 2006; Sigman et al., 2010). Yet, the processes that drive changes in this upwelling of deep waters have been less well understood and have been highly debated in scientific literature. We could make a first step towards a better comprehension of these processes by analyzing their observed changes over recent decades. Numerous studies have investigated the response of the Southern Ocean to changes in the wind-driven ocean circulation (e.g. Oke and England, 2004; Saenko et al., 2005; Fyfe and Saenko, 2006; Toggweiler and Russell, 2008; Sigmond et al., 2011; Thompson et al., 2011). However, many of the observed changes in temperature and salinity seem inconsistent with the response induced by the wind-driven ocean circulation. Alternatively, changes in the vertical exchange of water masses could be caused by changes in the marginally stable density stratification of the Southern Ocean (Watson and Naveira Garabato, 2006; Matear and Lenton, 2008; Morrison et al., 2011; Watson et al., 2015), which is controlled by the surface salinity (Sigman et al., 2004). In this dissertation, I investigated the recent changes in the surface freshwater fluxes over the Southern Ocean and the response of the Southern Ocean hydrography, circulation, and vertical exchange of heat and carbon to changes in these fluxes. With this synthesis, I intend to first summarize my main findings and conclusions (section 6.1), and then discuss the limitations of my results (section 6.2) as well as their implications in the context of long-term changes in the global climate system (section 6.3) that I introduced in chapter 1. This discussion will elucidate that sea-ice freshwater fluxes could play a crucial role in driving glacial–interglacial changes in the global carbon cycle and could entail a substantial risk in under- or overestimating feedbacks in projected future changes in the carbon cycle. At last, I will provide an outlook and suggestions for future research activities on this topic (section 6.4).

6.1   Findings & conclusions

I will here summarize the main findings and conclusions from my investigation of the research
objectives that I posed in section 1.5:

**(1) How large are sea-ice–ocean freshwater fluxes associated with sea-ice formation, trans-
port, and melting in the Southern Ocean, and how do they compare to freshwater fluxes
from the atmosphere and from land ice?**

In chapter 2, we presented the first observation-based estimate of sea-ice–ocean freshwater fluxes
associated with sea-ice formation, transport, and melting over the period 1982 to 2008. An anal-
ysis of this data set revealed that overall 410 ± 110 mSv of freshwater are removed and added to
the Southern Ocean surface waters due to the formation and melting of sea ice. About $80 \pm 20\%$
(320 ± 70 mSv) of the freezing flux arises from the coastal ocean, where cold temperatures and
a divergent sea-ice field fuel the ice production. About $40 \pm 10\%$ (130 ± 30 mSv) of this ice that
is produced in the coastal ocean is transported to the north, towards the sea-ice edge, and melts
there in the warmer surface waters. An additional 50 ± 50 mSv of sea ice probably form through
snow-ice formation from the atmospheric flux and contribute to the total melting flux. Estimates
of the net atmospheric freshwater flux vary substantially between 650 mSv in ERA-Interim (Dee
et al., 2011) over the ocean south of $50°$ S and 350 mSv in satellite-derived HOAPS estimate (ver-
sion 3.2; Andersson et al., 2010). South of the climatological mean sea-ice edge (1% mean annual
ice concentration), the atmospheric freshwater flux from ERA-Interim amounts to about 200 mSv
of which about 80 mSv fall in the coastal region and slightly oppose the sea-ice formation flux.
The freshwater fluxes from land ice through basal and iceberg melting amount to about 46 ± 6
mSv and 42 ± 5 mSv, respectively (Depoorter et al., 2013). In summary, the seasonal melting and
freezing fluxes from sea ice exceed both the land ice and the atmospheric flux substantially. In
the coastal ocean, the northward export of freshwater by sea ice is balanced by the other two
freshwater fluxes and in the open ocean the sea-ice freshwater flux exceeds the atmospheric flux
substantially in certain regions. Therefore, sea ice provides the dominant freshwater flux in the
seasonally ice covered region of the Southern Ocean.

**(2) What is the contribution of sea-ice–ocean freshwater fluxes and their recent changes to
the Southern Ocean's salinity distribution?**

A simple box model approach taken in chapter 2 revealed that the northward transport of fresh-
water by sea ice increases the coastal-ocean salinity by about $+0.15\pm0.06$ g kg^{-1} and lowers the
open-ocean salinity by about -0.33 ± 0.09 g kg^{-1}. The former can be regarded as the effect on
AABW, i.e., the lower overturning cell, and the latter as the effect on AAIW and SAMW, i.e.,
the upper circulation cell. Therefore, the sea ice effectively re-allocates freshwater and buoy-
ancy from the lower ocean circulation cell to the upper ocean circulation cell and increases the
meridional and vertical salinity and density gradients. This northward transport of freshwater
has substantially increased by about $20 \pm 10\%$ over the period 1982 to 2008 (or by $+9\pm5$ mSv

per decade), which corresponds to a salinity decrease of about -0.02 ± 0.01 g kg^{-1} per decade in open-ocean surface waters and AAIW when using our box model estimate. The magnitude of this change agrees very well with the observed magnitude of change over recent decades (Wong et al., 1999; Helm et al., 2010; Durack et al., 2012). Largest freshening signals have been observed in the open-ocean Ross Sea surface waters and in the Pacific AAIW, coinciding with the largest changes in northward sea-ice freshwater transport. Our findings are further supported by the sensitivity experiments with the regional ocean model performed in chapter 4 that show a large-scale freshening of the open-ocean surface and intermediate waters in response to the observed sea-ice fluxes in the Pacific sector and also in parts of the Atlantic sector. While one would expect that the increased northward sea-ice transport counteracts the freshening induced by glacial meltwater in the coastal region, the model simulations suggest that also the vertical distribution of brine might play a role and actually freshen the surface waters as well. Yet, this coastal response in the model might be unrealistic and increasing melting from Antarctica remains the most likely reason for the coastal and AABW freshening.

(3) Is it possible to study the Southern Ocean response to observation-based changes in the surface freshwater fluxes in an ocean circulation model?

In chapter 3, I presented a regional ocean model for the Southern Ocean that is forced with observation-based surface freshwater, heat, and momentum fluxes. For this purpose, I implemented a number of modifications to the model's lateral boundary conditions in the north and south, its mixing scheme, and surface forcing in the sea-ice region. The model realistically simulates the general water-mass structure of the Southern Ocean, the ocean circulation, and the surface processes in the open ocean. Despite the major advances that I made throughout this thesis, large model biases remain in the coastal ocean and in the subsurface waters. Nevertheless, a good representation of the region of interest, i.e., the upwelling region, allows to study changes in the surface stratification induced by surface freshwater fluxes. While this flux-forced model cannot be used to study feedbacks between the ocean and the sea ice, land ice, or atmosphere, I can analyze the ocean's response to changes in the surface fluxes. I conclude that my approach of constraining an ocean model with observation based sea-ice–ocean freshwater fluxes provides a novel tool to study the effect of changes in the surface condition on the Southern Ocean. This approach circumvents many of the common problems in coupled ocean–ice models that are often overly sensitive to subtle inaccuracies in the atmospheric or sea-ice conditions, which can lead to an unrealistic water-mass structure in these models.

(4) How do Southern Ocean stratification, temperature, and circulation respond to recent changes in surface freshwater fluxes; and could increased northward freshwater transport provide an explanation for the observed surface stabilization and cooling?

The perturbation experiments that we presented in chapter 4 illustrate that the freshening associated with the recent increase in northward freshwater transport by sea ice considerably increased the surface density stratification of the open-ocean waters around the sea-ice edge in most of the

Pacific sector, and, to a lesser degree, also in the high-latitudes of the other ocean basins. This increased stratification reduces the upwelling of warm deep water into the surface layer in our simulations, resulting in a substantial cooling of the surface waters between the sea-ice edge and the Subantarctic Front in the Pacific sector and parts of the Atlantic sector. The cooling response of the model in this region shows a spatial pattern that is remarkably similar to the cooling derived from the to-date probably most complete observational ocean data set—the satellite observed sea-surface temperature record. At the subsurface, the model responds with a warming of CDW due to the reduced mixing of CDW into the surface layer. This response seems consistent with the trends derived from the few available observational subsurface data.

In contrast to the freshwater flux perturbation experiment, the simulated response to the observation-based changes in the surface wind stress exhibits a weak surface salinity and temperature increase in the high-latitude Pacific sector, a cooling of CDW, and a warming of AAIW and SAMW due to an increased overturning circulation and mixing. While the simulated response to surface wind stress changes south of the ACC frontal region is broadly inconsistent with observed changes, our simulations suggest that these changes might have contributed to the observed warming of the surface waters, AAIW, and SAMW north of the ACC frontal region. Therefore, we suggest that the observed surface cooling of large regions of the Southern Ocean high latitudes, which occurred despite global warming, is primarily caused by an increased sea-ice freshwater flux and an associated increased surface density stratification. Generally, we find opposing tendencies induced by the surface wind stress changes and freshwater flux changes in the simulated ocean hydrography and horizontal transport, with a relatively larger response induced by the freshwater flux perturbations. One exception is the meridional overturning circulation that strengthens in both perturbation experiments, consistent with the results by Morrison et al. (2011), and more strongly in the wind stress perturbation experiment. In summary, our simulations revealed that the upwelling of deep waters to the surface in the Southern Ocean is very sensitive to the freshwater fluxes from sea ice.

(5) What is the effect of changing surface freshwater fluxes on the release and uptake of CO_2 by the Southern Ocean and could this process provide an explanation why the Southern Ocean carbon sink did not saturate over recent decades despite an increase in westerly winds?

We analyzed the response of the surface CO_2 flux to the perturbations in sea-ice freshwater fluxes and surface wind stress in chapter 5. This analysis showed an increase of the net annual carbon uptake in the region between the sea-ice edge and the Subantarctic Front of 25% (0.06 PgC per year) in the sea-ice freshwater flux perturbation experiment and, surprisingly, an additional increase of 7% (0.02 PgC per year) in the wind stress perturbation experiment. We identified two major contributors to the increased carbon uptake in the freshwater flux perturbation experiment: One effect is that the surface cooling induced by the increased stratification increases the solubility of CO_2 in the seawater, which reduces the outgassing during all seasons. The other effect is a

reduction in the upwelling of carbon-rich deep waters into the surface layer, which also reduces the natural release of CO_2 but only occurs during austral winter and spring. Both effects can be attributed to a decrease in upwelling in this simulation due to a reduced and shallower winter-time mixing. These two effects are countered by a reduced subduction of CO_2 into AAIW south of the SAF during summer and a reduced subduction into SAMW north of the SAF during winter, which originate from reduced mixing due to the increasing stratification. The surface wind stress response is more complex and has strong opposing seasonal and spatial tendencies. We find a strong increase in summer-time CO_2 uptake, which might however be a model-dependent result. This effect is mostly compensated by an increased winter-time outgassing in the Pacific sector that also compensates part of the reduction in outgassing from the freshwater flux perturbation in this region. Our study highlights that the freshening of the surface ocean induced by the sea ice could have strengthened the Southern Ocean carbon sink over recent decades, providing a potential explanation why observations show an observed strengthening of the Southern Ocean carbon sink over recent decades (Landschützer et al., 2015b) rather than a long-term saturation that was suggested by earlier studies (e.g. Le Quéré et al., 2007). These findings are in line with the results by Matear and Lenton (2008), who argue that increase surface buoyancy forcing might compensate for the wind-driven reduction in carbon uptake.

The overarching picture that arises from all three studies (chapters 2, 4, and 5) of my thesis suggests that the increased northward sea-ice transport in the Pacific sector of the Southern Ocean is a predominant driver of the observed changes in the region south of the Subantarctic Front over recent decades. This conclusion is supported by a consistent emerging signal from many different data sets that I have analyzed throughout this thesis, i.e., satellite-based sea-ice data, atmospheric reanalysis data, in-situ ocean salinity and temperature data, satellite-based sea-surface temperature data, and simulations with a regional ocean model. I argue that the importance of processes related to changes in sea-ice–ocean fluxes have not sufficiently been accounted for so far in the context of changes in the Southern Ocean system. My thesis revealed that sea ice is an active element in this system and probably in the climate system as a whole rather than simply an indicator of changes in the surface climate (Maksym, 2016). Through its dominant role in the surface freshwater balance, its changes can effectively alter the surface stratification and therefore the deep-to-surface exchange of heat and carbon—a process that was so far underestimated and has important implications for long-term changes in the global climate system (see section 6.3).

6.2   Limitations

While the research that I presented in this thesis provides substantial progress in quantifying the surface freshwater fluxes in the Southern Ocean and in understanding the ocean's response to changes in these fluxes, a number of limitations arise from data uncertainties, the methodological approach, and model shortcomings. I will here outline these limitations that should provide a basis for further investigations.

In this thesis, I focused on the response of the Southern Ocean to changes in surface freshwater fluxes from sea ice and, to some extent, to changes from land ice. However, there are reasonable grounds to believe that also the net atmospheric freshwater flux increased over the Southern Ocean in recent decades, because theoretical arguments and global model simulations support an increasing precipitation in this region with global warming (Knutti and Sedláček, 2013). While my findings suggest that a large portion of the observed freshening can be attributed to sea-ice freshwater fluxes, the changes in the atmospheric flux and their contribution to the freshening remain largely unconstrained. Most of the freshening from the sea ice occurs in the Pacific sector just north of the sea-ice edge and partly in the Atlantic, as well as in the intermediate waters that are predominantly formed in this region. Yet, observations also suggest freshening in other regions of the Southern Ocean and in lower latitudes, which could be induced by a changing atmospheric freshwater flux. A detailed assessment of the potential freshening induced by the atmospheric freshwater flux is to-date still hindered by the unavailability of reliable data. The uncertainty in such data is almost 50% for the spatially integrated mean flux (see section 3.5), and different data products disagree on the sign and magnitude of trends over the Southern Ocean (Bromwich et al., 2011). Due to these uncertainties and because the most reliable products do currently not show very large changes over recent decades (Bromwich et al., 2011; Nicolas and Bromwich, 2011), I did not further investigate this contribution in my dissertation.

A major caveat of this thesis arises from the large uncertainties in the observation-based sea-ice freshwater fluxes. While the sea-ice concentration from which I derived these fluxes is well constrained, the sea-ice thickness and the sea-ice drift products induce large spatial and temporal uncertainties. Currently, sea-ice thickness observations are still very sparse in time and space, which is mostly related to the challenges in retrieving satellite-based thickness. We combined the few observational products with a reanalysis product to assess the uncertainties in the mean sea-ice thickness distribution, which turned out to be a major source of uncertainty in the freshwater flux estimates. A largely unknown source of uncertainty remains the trend in sea-ice thickness, which purely originates from the reanalysis product in our estimates. Due to the non-linearity between the different variables in our calculations, it is difficult to attribute a specific fraction of the freshwater flux trend to the sea-ice thickness trend. However, a sensitivity test with a mean sea-ice thickness distribution revealed that the freshwater flux trends mostly arise from the trends in sea-ice drift. The sea-ice drift is a variable that could be estimated robustly in principle,

given that these data can be derived from the long-term passive microwave satellite data. The major challenge for sea-ice drift data that we identified in our study presented in chapter 2 are the algorithms used to derive the sea-ice drift and the consistency between data from different satellite platforms. Therefore, such data sets must be handled with great care and the temporal inhomogeneities incorporate another major source of uncertainty when deriving long-term trends in sea-ice freshwater fluxes. At the same time, there is a large potential to substantially reduce uncertainties from sea-ice drift data by developing new algorithms, by adapting the algorithm parameters, time-steps, and resolution to the underlying data, and by treating consistent sensors and frequencies separately. The overall uncertainties in the sea-ice freshwater flux trends are as large as 40% to 50% in the spatially integrated fluxes and substantially larger on a grid box scale. In combination with an even larger uncertainty in the ocean salinity trends (P. Durack, personal communication), it is impossible to directly attribute a specific fraction of the freshening trend to the sea-ice freshwater fluxes. However, their spatial pattern and the order of magnitude of the trends agrees well.

Multiple limitations are associated with the simulated ocean response presented in chapters 4 and 5. Among these limitations are large persisting biases in the simulated temperature and salinity fields in the subsurface and in the coastal ocean around the Antarctic continent, which reside in the model despite major advances in the model developments. In the coastal ocean, the model has a too stable surface density stratification, which limits the mixing of waters on the continental shelf and reduces the subduction of AABW. This problem is most likely related to the brine plume parameterization, since it is less severe if the paramerization is switched off. However, if this parameterization was switched off, the representation of the open-ocean surface waters would be unrealistic because spurious, deep open-ocean convection destroys the water-mass structure. Therefore, we decided to use such a parameterization in these simulations with the downside of not being able to reliably assess the coastal ocean and AABW response. The brine plume parameterization would become obsolete if sufficient surface mixing occurred in the model, which is the main source of this issue. A second reason for the too stable surface ocean in the coastal region and the subsurface warm bias in the model is the prescribed surface heat flux from ERA-Interim, which underestimates the heat loss to the atmosphere in the high latitudes and therefore leads to a build up of the heat in the deep ocean. A third issue is the too salty and too shallow AAIW core and a too fresh surface ocean in the mean state. This issue might also be directly related to the insufficient surface mixing by the model. All three issues in the model might lead to a too high sensitivity to stratification changes and therefore an overestimation of the inferred surface temperature and carbon flux response. Hence, we have less confidence in the absolute magnitude of the response. Despite the biases, the model is able to generally reproduce the characteristic water-mass structure in the surface ocean of the upwelling region and spatial and temporal evolution of surface mixing processes, which indicates that it is able to reproduce the underlying upwelling mechanisms. The agreement of spatial patterns of the model response with the observed spatial pattern of trends provides further confidence that the simulated response

provides valuable insights.

Another limitation in our simulations results from a too coarse resolution of the experiments to fully resolve meso-scale instabilities, which was applied due to constraints in the computation time. A consequence of this too coarse resolution is a too strong meridional overturning circulation in the mean state and a probably too sensitive response to changes in the surface wind stress. Moreover, it is very likely that the model underestimates the lateral dissipation of signals in temperature and salinity or other tracers due to the underrepresented lateral mixing by eddies. This issue is counteracted by the models resolution-dependent hyper-diffusion in the advection scheme. However, at the current state, it is not clear how large and how realistic the compensation from this lateral mixing process is. A fully eddy-resolving simulation will elucidate in the future how large the effects of resolution on the simulated responses are.

Finally, several limitations result from the experimental design of the model experiments. We perturbed the model with an instantaneous change in the forcing rather than imposing the real trend that gradually changes over time. This procedure is certainly a strong simplification and potentially leads to an overestimation of the magnitude of the response. However, it clearly illustrates the sensitivity of the model to changes in freshwater flux forcing relative to changes in the surface wind stress. Additionally, non-linearities between the variables could arise that might influence the response to a certain degree. Moreover, we did not perform any experiments related to changes in the surface heat flux or changes in the atmospheric pCO_2. Accounting for changes in the surface heat flux would potentially amplify the cooling around the sea-ice edge due to the ice-albedo feedback related with the expanding sea ice and amplify the warming of the lower latitude surface ocean, AAIW, and SAMW due to an increased uptake of anthropogenic heat. Similarly, the carbon sink would strengthen simply due to the increase in anthropogenic CO_2 in the atmosphere. A number of additional simulations could further clarify the relative magnitude of these changes compared to the changes in surface freshwater fluxes.

6.3 Implications

Throughout this thesis, I analyzed recent changes that are constraint by observational data and therefore provide a better ground to comprehend the important processes in the Southern Ocean, rather than past and potential future changes that can only be inferred from model and proxy data. However, my findings summarized in section 6.1 have direct implications for past and future changes that I will outline in this section.

My results suggest that an increased northward transport of sea ice makes the lower ocean circulation cell more salty and the upper circulation cell fresher. Thereby it strengthens the Southern Ocean halocline and the deep to surface ocean density gradient. In the long-term, this process decouples the deep ocean from the surface ocean and limits the exchange of waters between the two circulation cells. The upper circulation cell shoals and draws water from shallower depths. Therefore, less of the warm and carbon-rich deep waters enter the surface layer in the region between the sea-ice edge and the Subantarctic Front, which reduces the CO_2 and heat release to the atmosphere from these surface waters in the upwelling region and increases the net annual uptake of carbon. The deep waters that no longer upwell into the upper circulation cell probably enter the lower circulation instead through mixing between the dense shelf waters and CDW, essentially enhancing the volume and age of bottom water and the storage of carbon in the deep ocean. Ultimately, such a process could alter the long-term balance between the amount of carbon stored in the upper circulation cell and therefore the atmosphere, and the amount of carbon stored in the deep ocean.

The above interpretations are based on the most recent observed changes in the sea-ice freshwater fluxes that show an expansion of the sea ice and an increased northward transport. However, it is not yet clear whether these changes are a response to anthropogenic changes in the climate system or whether they are due to multi-decadal natural variability. If they were due to the anthropogenic forcing, one would expect that the current changes are a transient response due to an adjustment of the atmospheric circulation to changes in meridional temperature gradients (Haumann et al., 2014), and that the changes would reverse in future once the sea-ice region starts to warm and the sea ice starts to retreat as suggested by global climate model simulations. In any case, the current trends most likely reflect a cold phase of the high-latitude Southern Ocean with expanding sea ice. Therefore, this situation, rather reflects a cold glacial climate during which the sea ice extended to lower latitudes and sea-surface temperatures were colder (Gersonde et al., 2005; Wolff et al., 2006; Roche et al., 2012; Benz et al., 2016; Xiao et al., 2016), even though the current changes are probably less extreme. A critical difference between the present situation and the situation in a glacial climate might be the process that expands the sea-ice cover. The current increase is driven by increasing southerly winds that transport more freshwater towards the sea-ice edge and probably increase the coastal divergence, which leads to a stronger sea-ice formation. In a glacial climate, sea-ice formation is potentially enhanced by colder surface tem-

peratures. Nevertheless, one would still expect an increasing northward freshwater transport since thicker ice would be transported northward. At the same time, an increasing sea-ice formation could strengthen the halocline even without an increasing northward transport, because the seasonal freezing and melting redistributes the salt vertically in the water column by mixing the salty winter-time waters deeper down than the fresher summer-time waters.

In contrast to many other mechanisms that have been suggested to cause the glacial–interglacial variations in the atmospheric CO_2 concentration, physical changes in the vertical exchange of water in the Southern Ocean have been identified to be consistent with proxy data (Toggweiler, 1999; Fischer et al., 2010; Sigman et al., 2010). Proxy data reveals a reduced export production (Jaccard et al., 2013) and a more complete nutrient utilization (Francois et al., 1997; Anderson et al., 2009) in the upwelling region during glacial states and an increased age of the deep waters around Antarctica derived from radiocarbon data (Skinner et al., 2010). All these data suggest a reduction in upwelling of deep carbon- and nutrient-rich waters to the surface. At the same time, $\delta^{13}C$ data suggest an enhanced volume of the lower circulation cell and a shoaling of the upper cell (Curry and Oppo, 2005; Lynch-Stieglitz et al., 2007). This change in ocean circulation is accompanied by a much saltier AABW in a glacial climate as inferred from pore water in sediment cores (Adkins et al., 2002), suggesting a major change surface freshwater balance. Today, AABW formation is mostly driven by cooling on the continental shelf as the freshwater fluxes in the coastal ocean balance and is enhanced by mixing with CDW. An enhanced glacial sea-ice formation and a reduced freshwater input from the Antarctic continent and the atmosphere could considerably shift the freshwater balance in the coastal ocean towards a higher salinity and therefore a salinity- rather than a temperature-driven AABW formation. Such a shift of the AABW formation mechanism towards a sea-ice brine-driven formation is also supported by the $\delta^{18}O$ data analyzed by Adkins et al. (2002).

The results that I presented in this thesis imply that glacial salinity, stratification, and circulation changes could be induced by increased sea-ice freshwater fluxes, which redistribute salt between the lower circulation cell and the upper circulation cell. Such a process would be very appealing since Antarctic sea-ice formation and extent are directly related to the Antarctic surface temperature that shows a striking correlation to the atmospheric CO_2 concentration (Petit et al., 1999; EPICA community members et al., 2004; Jouzel et al., 2007; Parrenin et al., 2013, see section 1.1.2;). Several mechanisms that involve either sea-ice or other buoyancy fluxes have been suggested by a number of studies (Gildor and Tziperman, 2000; Watson and Naveira Garabato, 2006; Bouttes et al., 2010, 2012; Ferrari et al., 2014; Sun et al., 2016), but none of them considers the addition of freshwater to the upwelling region from melting sea-ice as the process that drives the increasing stratification, except for the review by Fischer et al. (2010), who argue that such a mechanism could play a critical role. While sea-ice-driven changes in ocean stratification provide a hypothetical explanation for glacial-interglacial changes in the carbon cycle that seems consistent with proxy data, it remains unclear how much such an effect would contribute to the overall change in the atmospheric CO_2 concentration of 80 to 100 ppm.

The opposite effect to this hypothetical glacial situation could be expected for a warming Southern Ocean, such as during the deglaciation or a potential future climate. A retreat of the sea-ice edge and the northward transport would potentially degrade the halocline in the upwelling region giving rise to either facilitated upwelling from deeper levels or even convective instabilities during winter-time when the temperature stratification becomes statically unstable and overwhelms the stable salinity stratification. Since the subsurface waters are typically warmer the sea ice would retreat even faster, inducing a positive feedback that effectively lifts the carbon stored in the deep ocean to the surface. While this process could have led to a rapid release of CO_2 during the deglaciation, possible future implications are more complex. One aspect is that as soon as the atmospheric pCO_2 reaches a level above the pCO_2 of the deep waters, any additional upwelling would not lead to an additional release of natural CO_2 (Matear and Lenton, 2008). However, the higher CO_2 concentration of the upwelling waters from deeper levels would saturate the uptake of anthropogenic CO_2, similar to the mechanism suggested by Le Quéré et al. (2007) but induced by a weaker halocline. Therefore, decreasing sea-ice freshwater fluxes could substantial amplify global warming due to a reduced uptake of anthropogenic CO_2 and heat. These possible effects only concern the changes sea ice, but other processes like an increasing atmospheric freshwater flux (Liu and Curry, 2010; Knutti and Sedláček, 2013) and an increasing warming would stabilize the Southern Ocean surface waters (Manabe and Stouffer, 1993; Sarmiento et al., 1998). However, most of this stabilization would occur in lower latitudes, which limits the CO_2 subduction (Caldeira and Duffy, 2000) rather than its upwelling. In higher latitudes, temperature stratification during winter would still remain unstable, despite global warming, and increasing atmospheric and land ice fluxes will be critical to compensate for a sea-ice retreat in the upwelling region. Several recent studies suggested massive changes in the future land-ice flux (Golledge et al., 2015; Ritz et al., 2015; DeConto and Pollard, 2016) and their effects on the future ocean stratification in the upwelling region are to-date very uncertain (Fogwill et al., 2015). In summary, future changes in Southern Ocean stratification remain highly uncertain and incorporate a substantial risk for positive feedbacks on global warming.

6.4   Outlook & suggestions for further research

Our findings and their limitations and implications raise numerous questions that should be addressed in future research. Among the obvious issues to address is to further reduce the model biases. This goal could be achieved by further improving the model's vertical mixing scheme. However, one should note that the mixing problems that identified in this thesis are not unique to our model but apply to most existing numerical ocean models. Therefore, a general advance in the numerical representation of the strongly stabilizing summer-time surface boundary layer in the Southern Ocean should have high priority and has a high potential to reduce uncertainties in global model simulations. One of the suggestions is to account for the temporal decay of deep mixing events under stabilizing conditions, which occurs in reality due to inertial shear. Specific to the Southern Ocean ROMS setup, an advance in the treatment of the surface heat flux and a bias correction of the ERA-Interim surface heat flux would be desirable. Further improvements in the model would result from repeating the simulations at an eddy-resolving resolution of $0.1°$. At last, running additional experiments in which also the heat flux and the atmospheric pCO_2 is perturbed and in which combined perturbations are applied might explain some of the discrepancies between the changes in our experiments and the observed changes. The latter suggestion might also be realized by running a hind-cast simulation with a temporally varying forcing field.

The substantial increase in data that is currently collected in the Southern Ocean will considerably reduce some of the large uncertainties in the surface freshwater fluxes and ocean salinity. Among these advances are new satellite platforms for continuous monitoring of sea-surface salinity (e.g. Gordon, 2016) and sea-ice thickness (e.g. Schwegmann et al., 2016) in time and space. At the same time, further improvements of existing algorithms that are used to derive sea-ice drift and sea-ice thickness from existing satellite data are urgently required to obtain more consistent and therefore more reliable time-series. The availability of subsurface physical and biogeochemical data will also considerably increase by the deployment of Argo floats in the Southern Ocean that are by now also able to collect data under sea ice (e.g. Riser et al., 2016). A further opportunity to better constrain the surface freshwater fluxes and their distribution in the ocean arises from the unique isotopic signature that can be derived from oxygen isotopes and ocean salinity (e.g. Jacobs et al., 2002; Meredith et al., 2013). A large number of seawater oxygen isotope data exist already in the Southern Ocean but not all are yet compiled in the global data base (Schmidt et al., 1999). Together with a large number of data collected during the Antarctic Circumnavigate Expedition, new constraints on the surface freshwater fluxes will emerge (Leonard et al., 2016). A more complete picture of the oxygen isotopic composition in the modern Southern Ocean could also help to gain insights into the shifts between the present day surface freshwater budget and the one of past glacial climates (e.g. Adkins et al., 2002). All these new data sets will provide fantastic opportunities to improve our understanding and monitoring of the Southern Ocean surface freshwater fluxes and the surface stratification.

In this thesis, I mostly focused on the physical response of temperature, salinity, stratification, and circulation, as well as the air–sea CO_2 flux. However, changing surface freshwater fluxes will also affect the heat uptake by the Southern Ocean or the upwelling of nutrients. The response of the ocean heat uptake is most likely rather complex. In our current model setup it is not possible to study changes in the heat uptake since the surface heat flux is prescribed and cannot adjust to changes in the surface ocean conditions. However, the cooling response suggest that both the sensible and the outgoing longwave radiative flux to the atmosphere would decrease in the high-latitudes. In lower latitudes, where the atmosphere becomes warmer than the surface ocean, the cooling of the surface ocean would result in an increased heat uptake. All these considerations would suggest an increased net heat uptake by the Southern Ocean in response to the increased stratification. Since most of the excess anthropogenic heat has been taken up by the Southern Ocean, this issue requires further investigation in future studies. Similar to the heat and the carbon, less nutrients would upwell to the surface ocean in response to an increasing stratification with potential consequences for the ecosystem. While less nutrients would be available for biological production, the increased stratification could still enhance biological production in the Southern Ocean because it reduces the light-limitation and the production is not nutrient limited (Eveleth et al., 2017). In the long-term, changes in Southern Ocean stratification could critically affect the global biological productivity because it depends on the return of nutrients to the surface ocean in the Southern Ocean (Marinov et al., 2006). Therefore, numerous open questions exist in terms of the ecosystem response, which might be sensitive to the processes reported in this thesis.

A pressing question that arises from the results presented in this thesis is why many of the observed changes are not reproduced in the historical simulations with global climate models. These model simulations suggest that a sea-ice retreat, a surface ocean warming, and a much weaker surface freshening occurred over recent decades. I propose that four potential explanations exist for this discrepancy that require further investigation. Firstly, the freshwater redistribution by sea ice in many global models is most likely poorly represented due to difficulties in the accurate representation of the sea-ice dynamics and atmospheric circulation over the sea-ice region (Haumann et al., 2014; Uotila et al., 2014; Lecomte et al., 2016). This issue could considerably affect the representation of the surface ocean density stratification in the models and could therefore explain some of the large biases in their water-mass structure. Secondly, global models might be too sensitive to changes in the surface wind stress that drives most of the response in these simulations, which might outweigh changes from surface freshwater fluxes. Thirdly, the issues in the mixing scheme that I identified in ROMS might also be present in several global models and could lead to model biases that affect their Southern Ocean response to climatic changes. Finally, it is still unclear whether the observed changes over recent decades are a response to the anthropogenic forcing or simply an expression of multi-decadal variability. While several of these issues might explain the discrepancies between some of the observed and simulated changes in the Southern Ocean, they might at the same time be a core reason for the large spread of the historical Southern

Ocean heat and CO_2 uptake in these simulations (Frölicher et al., 2015) and their inconsistency with proxy data of past changes (Sigman et al., 2004; Otto-Bliesner et al., 2007; Roche et al., 2012; Rojas, 2013).

If the current response of the models to changes in the sea-ice freshwater fluxes was underestimated, one would expect that also their response to future and past climatic changes in this process is not accurate. In order to test how reliable Southern Ocean stratification changes in global models are, I suggest to assess their surface freshwater budget in detail and use the currently available observational data to develop constraints that might reduce the uncertainties in their future projections. Additionally, one could replace sea-ice freshwater fluxes in a coupled global model with the observed fluxes to further investigate the current changes, but also the past and future changes by imposing idealized perturbations on the prescribed freshwater flux that resemble potential future or past climates as outlined in section 6.3. Further extending such experiments by additionally perturbing the glacial or atmospheric freshwater fluxes could provide valuable insights into the drivers of glacial–interglacial changes in the climate system and into the risks that are associated with future changes in the Southern Ocean density stratification.

Appendix A

Anthropogenic influence on recent circulation-driven Antarctic sea-ice changes[*]

F. Alexander Haumann[1,2,3], Dirk Notz[1], Hauke Schmidt[1]

[1]Max Planck Institute for Meteorology, Hamburg, Germany

[2]Environmental Physics, Institute of Biogeochemistry and Pollutant Dynamics, ETH Zürich, Zürich, Switzerland

[3]Center for Climate Systems Modeling, ETH Zürich, Zürich, Switzerland

Key points:

- Observed Antarctic sea ice trends could be caused by anthropogenic drivers

- A zonally asymmetric circulation change drives observed net sea-ice increase

- A zonally too symmetric circulation change in models causes sea-ice decrease

---

Abstract

Observations reveal an increase of Antarctic sea ice over the past three decades, yet global climate models tend to simulate a sea-ice decrease for that period. Here, we combine observations with model experiments (MPI-ESM) to investigate causes for this discrepancy and for the observed sea-ice increase. Based on observations and atmospheric reanalysis, we show that on multi-decadal time scales Antarctic sea-ice changes are linked to intensified meridional winds that are caused by a zonally asymmetric lowering of the high-latitude surface pressure. In our simulations, this surface-pressure lowering is a response to a combination of anthropogenic stratospheric ozone depletion and greenhouse gas increase. Combining these two lines of argument, we infer a possible anthropogenic influence on the observed sea-ice changes. However, similar to other models, MPI-ESM simulates a surface-pressure response that is rather zonally symmetric, which explains why the simulated sea-ice response differs from observations.

A.1   Introduction

Atmospheric circulation changes around Antarctica substantially influence Antarctic sea ice. This relation emerges as an imprint of the Southern Annual Mode (SAM), the dominant mode of circulation variability in the Southern Hemisphere, on interannual sea-ice variations (Stammerjohn et al., 2008; Simpkins et al., 2012). Over the past three decades, the near-surface circulation has significantly intensified, shifting the SAM to more positive phases (Abram et al., 2014). This is most likely due to anthropogenic stratospheric ozone depletion and greenhouse-gas (GHG) increase (Lee and Feldstein, 2013; Abram et al., 2014). However, the response of Antarctic sea ice to this circulation intensification, and thus to the underlying anthropogenic forcing, is not well understood (Bitz and Polvani, 2012; Polvani and Smith, 2013; Sigmond and Fyfe, 2014). This is owing to the puzzling disagreement between observed and modeled Antarctic sea-ice trends and to a lack of process understanding concerning the influence of recent multi-decadal atmospheric circulation changes on the sea ice. We here combine observations with model simulations to address both these issues.

Satellite observations show an Antarctic sea-ice increase since the late 1970s (Comiso and Nishio, 2008), which results from strong opposing regional changes (Stammerjohn et al., 2008). The sea-ice increase in the Ross Sea since the early 1990s is related to enhanced northward ice advection due to stronger southerly winds from Antarctica, whereas advection of warmer air masses from lower latitudes causes a sea-ice decrease in that period in the West Antarctic Peninsula (WAP) region (Haumann, 2011; Holland and Kwok, 2012). These opposing regional sea-ice changes can be explained by a cyclonic circulation anomaly in the region of the Amundsen Sea Low (ASL) (Turner et al., 2009).

These observed circulation and sea-ice changes could either be caused by a change in the external forcing or simply be a manifestation of internal variability, which is of comparable magnitude to the observed trend in model simulations (Polvani and Smith, 2013; Zunz et al., 2013). A recent study by Fan et al. (2014) supports the latter suggestion by relating multi-decadal variations in temperature records to sea-ice changes. Such changes in the Antarctic surface climate show connections to the tropical Atlantic (Li et al., 2014; Simpkins et al., 2014) and Pacific (Ding et al., 2011; Schneider et al., 2012a) that alter the surface pressure in the ASL region.

In current global models, however, the recent sea-ice response seems to be dominated by changes in the external forcing. Otherwise, there would be no reason for coupled global models to consistently simulate an Antarctic sea-ice decrease over the observational period (Mahlstein et al., 2013). This simulated ice loss must hence be a direct response to increasing GHGs, stratospheric ozone depletion, and other external forcings. Bitz and Polvani (2012) and Sigmond and Fyfe (2014) explain this response by the modeled strengthening and poleward shift of the near-surface westerly winds, which enhances upwelling of warmer water in the Southern Ocean that melts the ice. These findings contradict the suggestion by Turner et al. (2009) that stratospheric ozone depletion could be the cause for the observed sea-ice changes.

Here, we further explore the possibility of a dominating external driver: Could ozone depletion and/or GHG increase cause the observed sea-ice changes if natural variability was not a sufficient explanation? To answer this question, we examine if the observed and the modeled changes in atmospheric circulation and the related sea-ice response are consistent with a primarily anthropogenic forcing. Doing so, we also gain insights that explain the disagreement between the modeled and the observed evolution of Antarctic sea ice and tropospheric circulation.

A.2   Methods, model & data

We compare model simulations to the atmospheric circulation (sea-level pressure (SLP), 10-m winds, and geopotential height) from ERA-Interim reanalysis (Dee et al., 2011) and to the observed sea-ice concentration (Meier et al., 2013a) and drift (Fowler et al., 2013a). The ERA-Interim reanalysis provides the most reliable atmospheric circulation and its changes in the southern high-latitudes among the reanalysis data (Bracegirdle and Marshall, 2012). We use the fully coupled Max Planck Institute for Meteorology Earth System Model (MPI-ESM) in its low-resolution configuration (Giorgetta et al., 2013), which contributed to the fifth Climate Model Intercomparison Project (CMIP5). The atmospheric component (ECHAM6) (Stevens et al., 2013) is run at a T63 (1.875°) horizontal resolution with 47 vertical hybrid levels reaching up to 0.01 hPa, thus resolving stratospheric changes (Schmidt et al., 2013). The ocean component (MPIOM) (Jungclaus et al., 2013) has a horizontal resolution of about 1.5° on a bipolar grid with 40 unevenly spaced vertical levels. Sea ice is implemented as a thermodynamic-dynamic model (Notz et al.,

2013). In the Arctic, MPI-ESM realistically simulates the sea-ice cover and its response to an-thropogenic forcings (Notz et al., 2013). However, in the Antarctic, it underestimates the mean sea-ice extent in all seasons and considerably overestimates its natural variability over the past few decades, as do other CMIP5 models (Turner et al., 2013; Zunz et al., 2013).

We use two sets of simulations that differ in their prescribed stratospheric ozone concentra-tion. One set uses historical GHG emissions and stratospheric ozone depletion (Experiment 1). For this set, we use the three historical simulations carried out with MPI-ESM for CMIP5, cov-ering the period 1850–2005 (Giorgetta et al., 2012a). The evolution of GHGs and total column ozone (Cionni et al., 2011) in these simulations is shown in Figure A.1 (solid lines). A second set of three simulations (Experiment 2) is driven by the same forcings except for stratospheric ozone: We modified the forcing as such that the stratospheric ozone (mixing ratio above 150 ppb) only follows seasonal and interannual variations in the solar irradiance. Anthropogenic changes in stratospheric ozone concentration are hence excluded (Figure A.1; green dashed line). Changes in all other forcings such as solar irradiance, tropospheric ozone, and aerosols (Giorgetta et al., 2013) are identical in both experiments. These two experiments allow us to directly study MPI-ESM's response to (1) the combined effect of GHG increase and stratospheric ozone depletion, (2) the effect of GHG increase alone, and (3) the effect of stratospheric ozone depletion alone, where the latter is estimated by examining the difference between the two experiments. In addition, we assess the mean state and internal variability in the model using a 1000-year pre-industrial (prior to 1850) control simulation with constant external forcing (Giorgetta et al., 2012b).
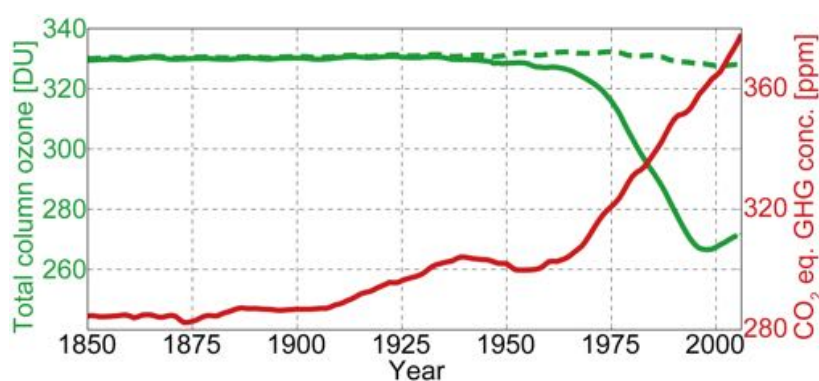
Figure A.1   External forcings of model experiments: Red: GHG forcing of Experiments 1 and 2. Green: total column ozone between $63°$ S and $90°$ S of Experiment 1 (solid) and Experiment 2 (dashed).

We analyze the ensemble mean of three realizations in each respective forcing experiment. Each of these realizations started from different initial conditions taken from the pre-industrial control simulation. We use annual means since we are interested in the net response to the forc-ing. Hence, we neglect possible differences in seasonal variations and trends (Simpkins et al., 2012; Holland, 2014). We calculate linear trends with a least squares regression analysis for the observational period 1979 to 2011 and, to minimize the impact of internal variability, a longer model period from 1960 to 2005 (see supplemental material for details).

A.3 Results

The annual mean near-surface wind field from the ERA-Interim reanalysis shows that the Antarctic sea ice experiences westerly winds near the ice edge (Figure A.2a), whereas most of the coastal and interior sea-ice regions experience easterly to southerly winds. The low-pressure belt around Antarctica consists of three distinct climatological SLP minima, with the ASL showing the lowest SLP (Figure A.2a). The zonal SLP gradients induced by the asymmetric distribution determine the advection of warmer air masses west of the WAP and the advection of cold continental air over the south-western Ross and Weddell Seas, influencing the sea-ice formation and export (Haumann, 2011). This zonal asymmetry intensifies between 1979 and 2011 (Figure A.2c). In particular, the low SLP in the ASL region expands and deepens significantly, leading to increased southerly winds in the western Ross Sea and increased northerly winds in the WAP region. In all other regions the westerlies strengthen. Similar asymmetric structures in the SLP trends have been reported for other reanalysis data sets, but the detailed spatial structure and the magnitude of the trends varies among them (Bromwich et al., 2011).

The meridional wind changes (Figure A.2c) go along with a sea-ice concentration increase in the Ross Sea and a decrease west of the WAP (Figure A.2e). The southerly wind anomaly in the Ross Sea, the expansion of the ASL, and the associated decrease in westerly winds in this region explain the dominating sea-ice increase in the western Ross Sea compared to the smaller increase in the eastern Ross Sea. Generally, sea ice drifts at a turning angle of roughly $20°$ to $40°$ to the wind direction (Kottmeier et al., 1992). Consequently, we show that the finding by Haumann (2011) and Holland and Kwok (2012), that ice-drift changes (Figure A.2e) are induced by wind changes (Figure A.2c), is also evident over the period 1979 to 2011. Potential inconsistencies in the drift trend (Fowler et al., 2013a; Olason and Notz, 2014) do not affect these results qualitatively (Figure A.4). The increased northward drift in the Ross Sea causes a higher sea-ice production at the coast, a higher northward advection, thus an expansion and concentration increase at the ice edge. The decrease in the WAP region is associated with the advection of warmer air masses from lower latitudes (Haumann, 2011; Holland and Kwok, 2012). The increase of the total Antarctic sea-ice area over the observational period (Comiso and Nishio, 2008) is mostly due to a large sea-ice area gain in the Ross Sea and a weaker increase in the Weddell Sea, which overcompensate the sea-ice decrease in the WAP region.

The pre-industrial control simulation also shows three climatological low-pressure areas (Figure A.2b) at approximately the same locations as in the reanalysis. However, throughout the entire control simulation neither the observed strength of the ASL nor the observed zonal SLP asymmetry is ever reached. In addition, the modeled ASL is the weakest of the three climatological low-pressure systems. The representation of the ASL is generally poor in current global models (Hosking et al., 2013), which limits the quality of their simulated sea ice. The model additionally overestimates the strength and extent of the coastal easterlies, confining the sea ice at the East
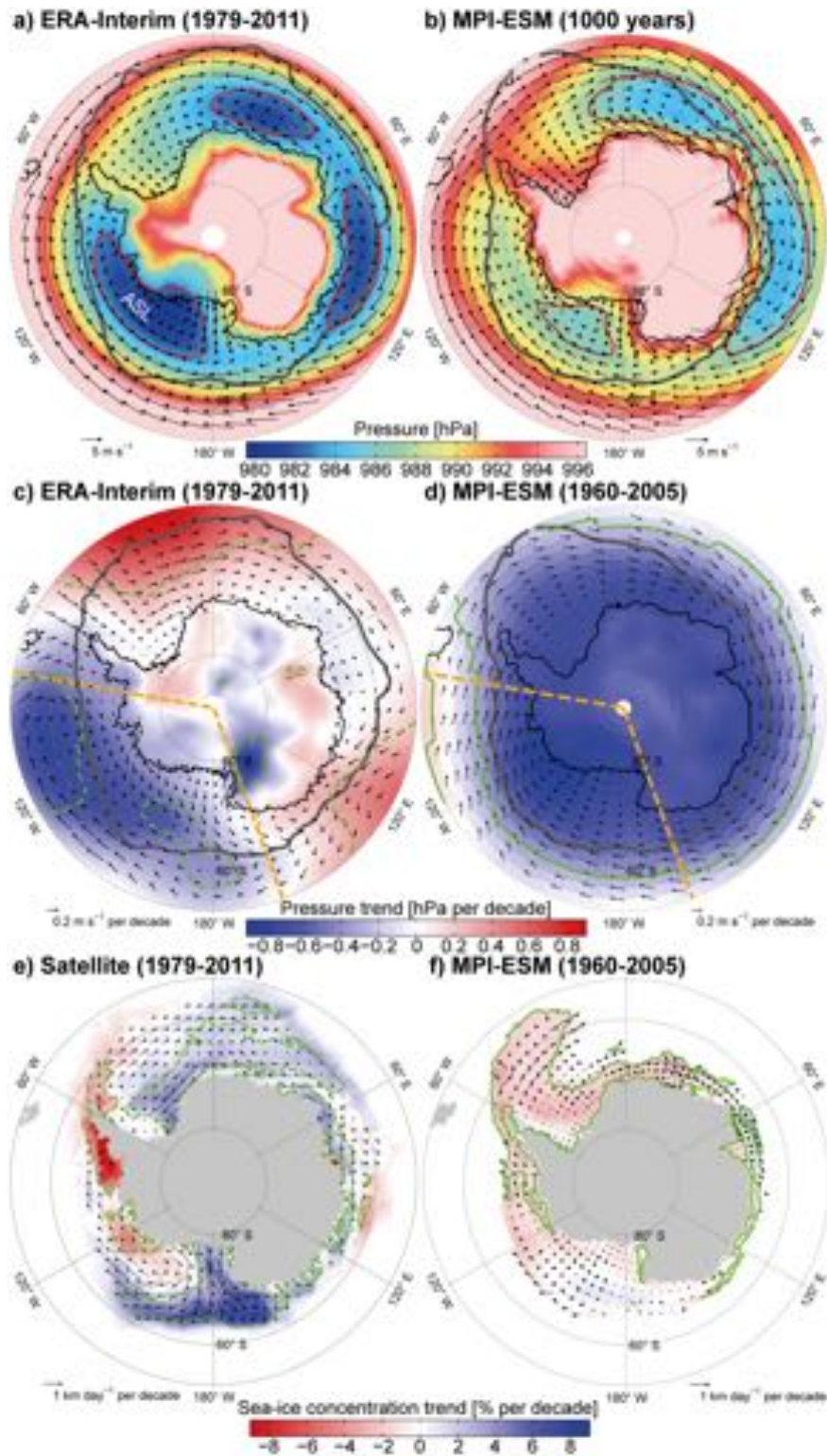
Figure A.2   Annual surface circulation driving Antarctic sea-ice changes: **(a)** ERA-Interim mean (1979–2011) SLP (shading; red: 983-hPa isobar) and 10-m wind field (vectors). ASL: Amundsen Sea Low. **(b)** Simulated (pre-industrial) mean SLP (red: 987-hPa isobar) and surface wind field. **(c)** ERA-Interim decadal SLP and 10-m wind field trends (1979–2011). **(d)** Simulated decadal SLP and wind field trends (1960–2005, Experiment 1). Black bold lines **(a-d)**: mean annual ice edge. Dashed orange lines **(c-d)**: sector for Figure A.3. **(e)** Observed (1979–2011) and **(f)** simulated (1960–2005, Experiment 1) decadal sea-ice concentration (shading) and drift trends (vectors). Dashed and solid green lines: significance of SLP and ice concentration trends (90% confidence level).

Antarctic coast. This rather zonally symmetric circulation is intensified in the historical simulations with all forcings (Experiment 1; 1960–2005; Figure A.2d) due to a statistically significant lowering of the SLP with a somewhat stronger response than the changes in the reanalysis. However, the simulated, zonally almost constant, and poleward shifted SLP lowering causes a westerly to north-westerly wind anomaly everywhere.

The model response (Figure A.2f) does not reproduce the observed sea-ice trends in terms of sign and spatial pattern, which is in line with other models (Turner et al., 2013). The simulated sea-ice changes (1960–2005) are much weaker than the observed ones and amount to an overall decrease. There is a statistically significant ice concentration decrease in the WAP region, in the Weddell Sea, and along the coast of East Antarctica. Also simulated changes in the ice drift are much weaker than observed and rather zonal. This response of the sea ice agrees with the findings by Bitz and Polvani (2012) and Sigmond and Fyfe (2014). They show that in global models increased zonal winds enhance upwelling of warmer water from below that melts the ice. Figure A.2d shows such a westward circulation intensification over most of the sea-ice region, whereas in the ERA-Interim reanalysis intensified westerlies are mostly restricted to the Weddell Sea (Figure A.2c). We conclude that the difference in the observed and simulated sea-ice changes is caused by rather zonal simulated circulation changes and comparably small changes in the meridional winds in the model simulations, which are caused by a weaker asymmetry in the SLP lowering. This also holds if the observational period 1979 to 2011 is analyzed in the model simulation (Figure A.5).

The lowering of the high-latitude SLP leading to the zonal wind intensification in the model most likely results from anthropogenic forcing (Thompson et al., 2011; Lee and Feldstein, 2013). Consequently, we proceed to analyze whether the lowering of the SLP in the ASL region in the reanalysis, thus the sea-ice changes, can also be attributed to these anthropogenic influences. We investigate annual mean geopotential-height changes in vertical cross-sections zonally averaged between 160° E and 80° W (dashed orange lines in Figure A.2c and d). In the reanalysis data (1979–2011), we find three areas of significant (90% confidence level) geopotential-height change (dashed green lines in Figure A.3a). First, the cooling in regions of seasonal ozone depletion in the stratosphere leads to a lowering of the geopotential height there (Thompson et al., 2011). Second, the warming of the troposphere in lower latitudes, most likely caused by the GHG increase, increases the geopotential height there (Santer et al., 2003). As a consequence, the significant lowering of the geopotential height in the high-latitude troposphere is induced by a downward propagation of the stratospheric anomaly from ozone depletion (arrow 1, Figure A.3a), by increasing GHGs and other changes in the external forcing (arrow 2), or by their combination (Lee and Feldstein, 2013).

Our simulations including both GHG increase and stratospheric ozone depletion (Experiment 1, Figure A.3b) show a similar structure and magnitude of the geopotential-height trends (1960–2005) as in ERA-Interim. However, discrepancies occur in the lower troposphere in high
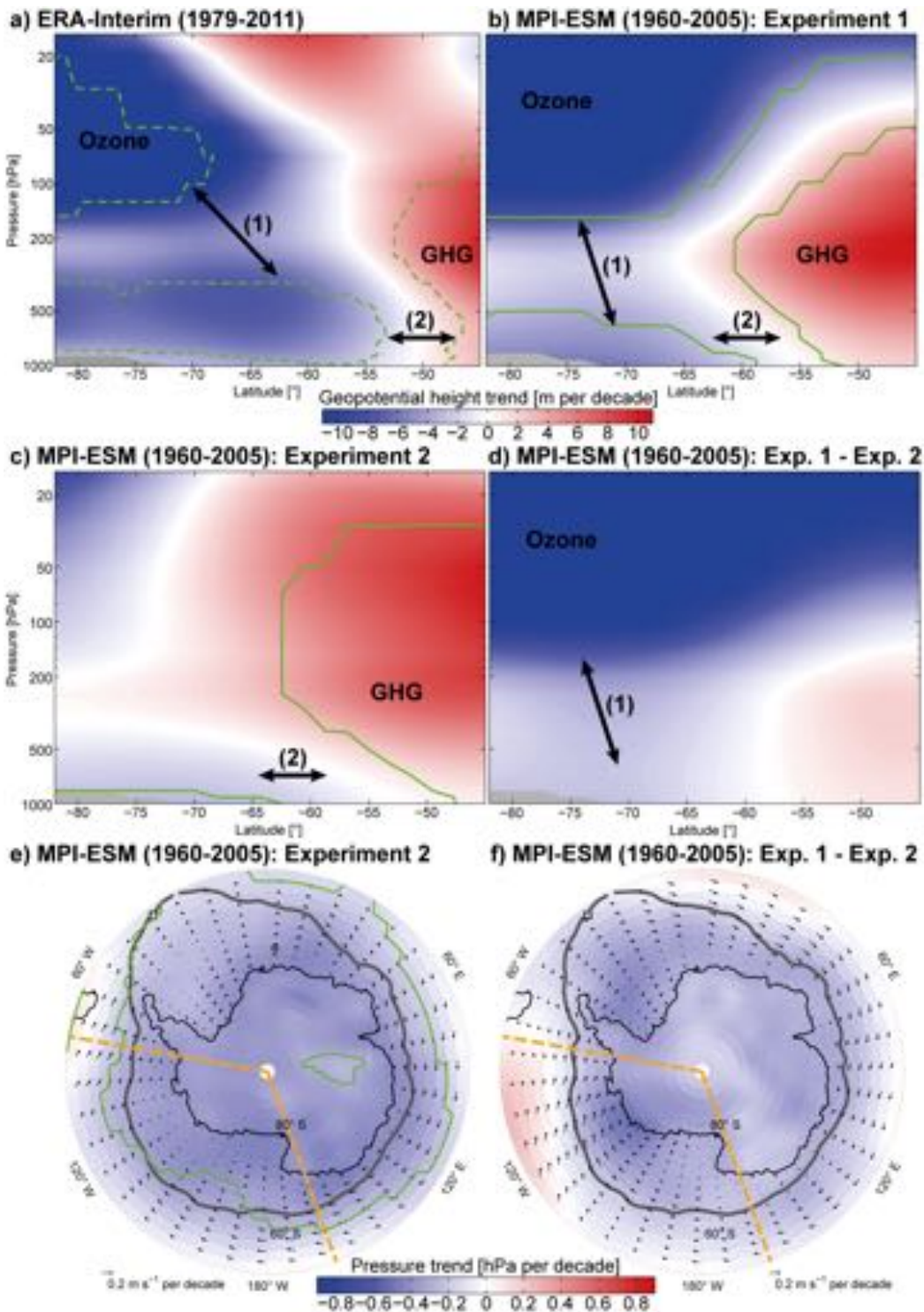
Figure A.3   Attribution of annual surface circulation changes to (1) stratospheric ozone depletion and (2) GHG increase: (a-d) Vertical cross-sections of decadal zonal mean geopotential-height changes between 160° E and 80° W (dashed orange lines in Figure A.2). Experiments as in Figure A.1. **(a)** ERA-Interim (1979–2011). **(b)** Simulations with all forcings (1960–2005). **(c)** Simulations without stratospheric ozone depletion illustrating mainly response to GHG increase (1960–2005). **(d)** Differences between simulations with **(b)** and without stratospheric ozone depletion **(c)** illustrating effect of ozone depletion. **(e and f)** as **(c and d)** but for SLP (shading) and surface wind changes (vectors). Dashed orange lines: sector analyzed in **(a-d)**. Black bold lines: mean annual ice edge. Dashed and solid green lines: significance of geopotential-height and SLP trends (90% confidence level).

latitudes (south of 55° S), where modeled trends are slightly weaker, more confined to the surface, and occur at higher latitudes. The simulation with largely constant stratospheric ozone forcing (Experiment 2) results in a significant tropospheric geopotential-height decrease in high latitudes (Figure A.3c), but the trend is much weaker than in the simulation with all forcings (Figure A.3b). The difference of the trends between the two experiments is primarily due to stratospheric ozone depletion (Figure A.3d). Consequently, the SLP trends in the ASL region can mostly be explained by the combined effect of stratospheric ozone depletion and GHG increase (Figure A.3e and f). If we analyze the model output only during the observational period (1979–2011; Figure A.6), the effect of ozone depletion dominates the near-surface changes compared to the GHG increase, which is consistent with previous studies (Thompson et al., 2011; Lee and Feldstein, 2013).

We conclude that the observed SLP lowering in the ASL region and the associated surface circulation changes (Figure A.2c), thus the observed sea-ice trends in this region, are influenced by the combination of anthropogenic ozone depletion and GHG increase, where the signal from ozone depletion presumably dominates. These conclusions are consistent with the suggestions by Turner et al. (2009). We show that the difference in the sea-ice response between global model simulations and observations occurs primarily due to the zonal distribution of the SLP response. A simulated rather zonal circulation intensification leads to a weak overall sea-ice decline, consistent with Bitz and Polvani (2012), while the observed intensified meridional circulation induces strong regional changes and acts to increase the overall sea-ice concentration in the period 1979 to 2011, consistent with Holland and Kwok (2012). In the following, we will discuss whether this difference in the spatial distribution of the changes can be attributed to general shortcomings in the model circulation or to multi-decadal natural variability.

A.4   Discussion

A rather zonally symmetric simulated SLP and circulation response to the anthropogenic forcing, as in our simulations, is a common feature among global models (Son et al., 2010). Yet, this response is not consistent with, for example, observed asymmetric tropospheric geopotential-height changes that have been related to stratospheric ozone depletion (Neff et al., 2008). The observed mean asymmetric circulation (Figure A.2a) is related to orographic blocking effects (Fogt et al., 2012), the asymmetric Antarctic land mass (Lachlan-Cope et al., 2001), and topography-driven boundary layer wind systems (Haumann, 2011). These arguments suggest that the too zonal near-surface circulation in the mean state and also the rather zonal response pattern over the sea ice in global models could be caused by a too smooth topography due to the models' coarse resolution and a not very realistic representation of the Antarctic surface climate. Our findings support this, since the response pattern differs mostly in the high-latitude troposphere in the ASL region (Figure A.2) and the other sectors (40° W to 150° E; Figure A.7).

The Antarctic sea-ice response in global models to zonal wind changes as described by Bitz and Polvani (2012) and Sigmond and Fyfe (2014) is presumably sensitive to the vertical stability of the underlying ocean. In MPI-ESM the high-latitude Southern Ocean vertical stability is underestimated (Stössel et al., 2015), which is a common feature among global models (Heuzé et al., 2013). We hypothesize that a comparably unstable ocean responds with a stronger subsurface heat flux to increasing zonal winds, because the observed changes in the westerly wind component at the ice edge in the Weddell Sea (Figure A.2c) lead to changes in the zonal advection of the ice (Figure A.2e), whereas the westerly anomaly in the model (Figure A.2d) leads to a decreasing ice cover (Figure A.2f). Thus, the underlying mechanism responsible for the simulated sea-ice changes seems to differ from the observed one. Even if the atmospheric circulation response was similar to the observed changes the sea-ice response could still differ from the observations, as it is the case in the Weddell Sea, for example.

Our result that the Antarctic sea-ice response to the anthropogenic influence depends on the asymmetry of the SLP response is in line with the observed response of sea ice to interannual (Fogt et al., 2012; Simpkins et al., 2012) and multi-decadal (Li et al., 2014) variability. These studies show that sea ice changes strongly with the non-annular component of the SAM rather than with the zonally symmetric patterns, where a more positive SAM index is often associated with a lower SLP in the ASL region. However, the spatial structure of the sea-ice changes associated with the positive SAM anomalies during the observational period differs from that of the observed trends (Simpkins et al., 2012). For example, while interannual variations mostly show a change of the strength of the ASL, in the observed trend the ASL additionally expands (see section 3). Abram et al. (2014) show that the SAM shifts to more positive values due to the anthropogenic forcing, which is consistent with both our model simulations and the pressure changes in the ERA-Interim reanalysis since the meridional pressure gradient increases (Figure A.2). However, the effect that this has on the sea ice depends on the zonal structure.

Patterns of sea-ice changes induced by multi-decadal variability in the ASL SLP through connections with the tropics are similar to the observed trends (Li et al., 2014). Consequently, recent changes in the Antarctic sea ice might be influenced by natural variability. A multi-decadal variability in the observed summer-time air temperature records supports such an influence (Fan et al., 2014). Within the 1000-year long control simulation with MPI-ESM about 9% of all possible 968 33-year long periods have an ASL SLP trend larger than the observed trend (averaged over the ocean surface south of 60° S and between 180° E and 80° W). This suggests that the current observed Antarctic sea-ice trends could also be fully explained by natural variability in the SLP and the related wind forcing. In turn, this would be inconsistent with a strong simulated circulation response to the anthropogenic influence. Thus, it is more likely that the observed changes are a mixture of an anthropogenic influence and multi-decadal variations. Yet, we cannot quantify their contributions since neither the pattern of the modeled sea-ice variability, nor that of the modeled response to the forcing currently reproduce the observed pattern of sea-ice trends in coupled models.

Several other mechanisms have been suggested to contribute to the observed Antarctic sea-ice changes. The recent freshening of the Southern Ocean could have increased the sea-ice cover by stabilizing the water column (Bintanja et al., 2013). Goosse and Zunz (2014) suggested that the sea-ice increase is largely driven by a positive ice-ocean feedback that decreases oceanic upwelling and might be initiated by changes in ice advection due to variations in the atmospheric circulation. However, as we show here, there is confidence that the dominant cause of observed sea-ice changes are persisting changes in the atmospheric circulation because the patterns of circulation changes almost perfectly match those of ice drift and concentration in independent data sets over multi-decadal time scales (cf. Figures A.2c and e), confirming the findings by Haumann (2011) and Holland and Kwok (2012). It is possible that these changes in atmospheric circulation cause additional feedbacks through changes in precipitation, oceanic upwelling, or gyre circulation. Atmospheric circulation changes, nevertheless, remain the most likely driver of the observed Antarctic sea-ice changes independent of the question whether multi-decadal variability or anthropogenic forcing is the underlying cause.

A.5   Summary & conclusions

Combining observations with model simulations, we find that the recently observed Antarctic sea-ice changes (1979–2011) are mostly driven by atmospheric circulation changes, which are in turn consistent with at least a partial anthropogenic influence. Satellite and reanalysis data show that intensified meridional winds increase the northward ice advection in the Ross Sea and meridional heat exchange in the Ross Sea and WAP regions, where the largest sea-ice changes are observed. This confirms the findings by Haumann (2011) and Holland and Kwok (2012) for the full observational period. These circulation changes are caused by a significant, zonally asymmetric lowering of the SLP, which is evident as an expansion and strengthening of the ASL.

Our model experiments (MPI-ESM) show that such SLP changes in this region can be explained by a combination of stratospheric ozone depletion and GHG increase (in line with Son et al. (2010)), where the former dominates during the observational period (1979–2011). We conclude that also the observed circulation-driven sea-ice changes are influenced by these anthropogenic forcings (consistent with Turner et al. (2009)). However, similar to other global models (Son et al., 2010), MPI-ESM's SLP response is rather zonally symmetric leading to a circumpolar westerly wind anomaly and little changes in meridional winds. A too zonally symmetric SLP compared to observations also occurs in the mean state and the natural variability. Thus, we argue that also the response to the anthropogenic influence might lack in zonal asymmetry, which might be caused by the coarse resolution of the Antarctic topography and inaccuracies of the representation of the Antarctic surface climate in the sea-ice area in global models. Consistent with findings by Bitz and Polvani (2012) and Sigmond and Fyfe (2014), this zonal circulation change leads to a weak modeled overall sea-ice decline, whereas regions that experience strengthened

westerlies in the observations (e.g. the Weddell Sea) mostly show a zonal redistribution of the sea ice. We argue that an underestimated vertical stability of the underlying ocean in our model (Stössel et al., 2015) and other global models (Heuzé et al., 2013) might cause this difference. We conclude that most of the discrepancy between the observed and modeled Antarctic sea-ice trends arises from the difference in the zonal distribution of SLP changes and the different sea-ice response to zonal and meridional wind changes.

The model simulates multi-decadal variations of SLP in the ASL region of comparable magnitude to the observed trends. This supports recent suggestions of an influence of multi-decadal variability on observed sea-ice trends (Fan et al., 2014; Li et al., 2014). However, we show that the recent argument that observed sea-ice changes could be purely driven by multi-decadal variability (Polvani and Smith, 2013) is inconsistent with the simulated SLP response to the anthropogenic influence. A clear distinction between effects imposed by natural variability and anthropogenic forcing will only become possible once models accurately represent asymmetries in the near-surface circulation and the associated sea-ice patterns.

A.6 Supplementary methods

Simulated trends are calculated from 1960 to 2005 and observed trends from 1979 to 2011. We choose a different period for the simulations to obtain a clear forcing response (cf. Figure A.1) and avoid influences of natural variability. However, for consistency, we extend the historical simulations (1850–2005) with the respective RCP4.5 scenario simulations (Giorgetta et al., 2012c) to obtain the model response for the full observation period (until 2011). Figures A.5 and A.6 show that our conclusions are not affected by the different analysis period. At each grid point, we test the trends against internal variability applying a t-test that accounts for a lag-1 temporal auto-correlation. As a measure of internal variability in the observations, the reanalysis data, and the model data, we use the slope's standard error from the residuals. For the simulated trends, we additionally calculate at each grid point the standard deviation from the total pre-industrial control simulation and the standard deviation from each 46-year interval in the pre-industrial control sim-

ulation. We conservatively take the maximum of these two measures and of the slope's standard error from the residuals as a measure of internal variability.

A.7   Supplementary figures
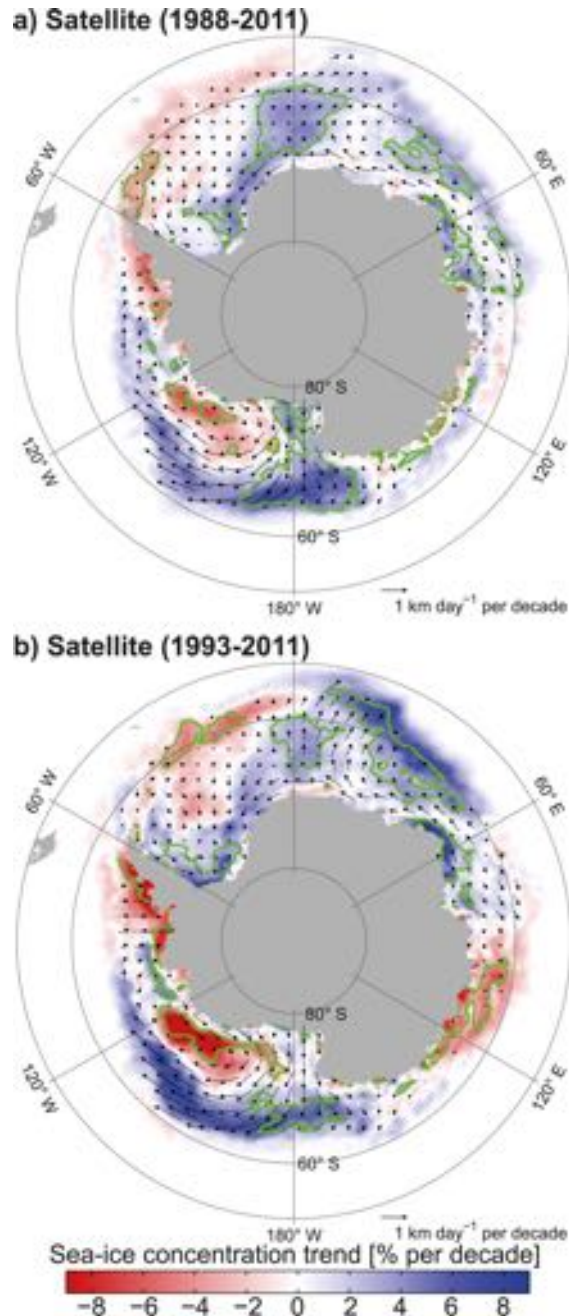
Figure A.4   Observed decadal sea-ice concentration and drift trends for different periods: As Figure A.2e but for the periods 1988 to 2011 and 1993 to 2011 to show that potential inconsistencies in the data set occurring in 1987 and 1992 do not influence the results qualitatively. Prior to 1987 the accuracy of the drift data derived from the SMMR instrument was lower and a potential error in the algorithm parameters in the version 2 of this product could affect the data consistency. After 1992 the availability of the 85 GHz channel improved the accuracy of the drift data (Fowler et al., 2013a).
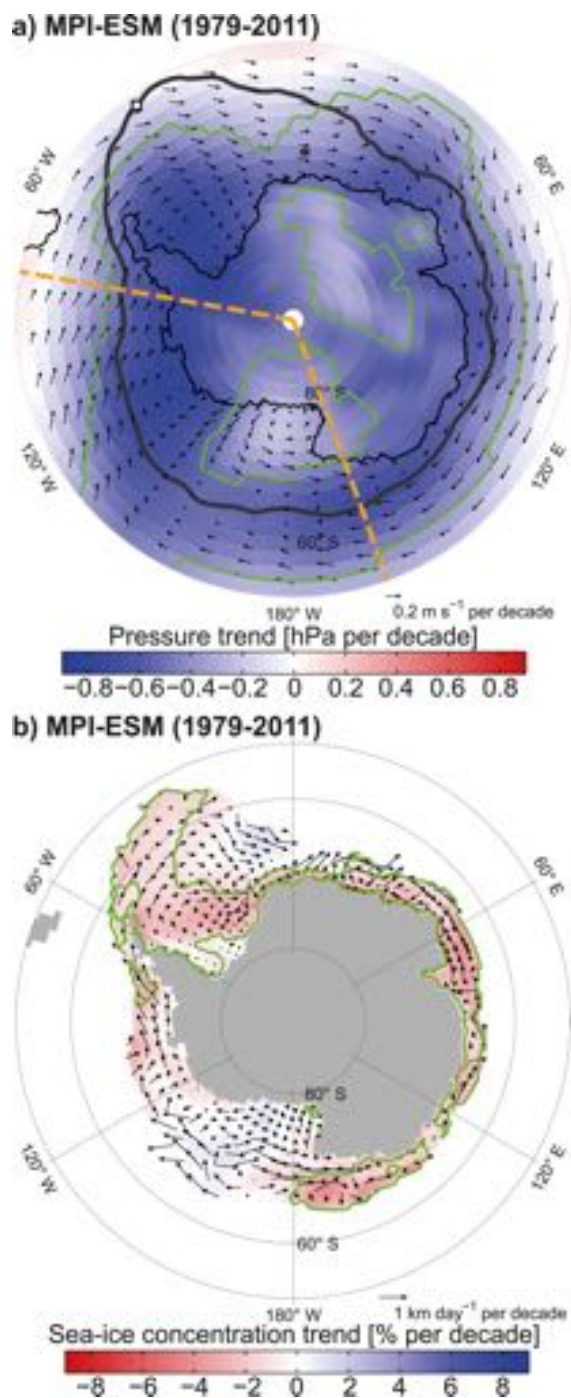
Figure A.5　Simulated decadal atmospheric circulation and sea-ice trends (1979–2011): As Figures A.2d and f but for the period 1979 to 2011 by extending the historical simulation (1979–2005) with the RCP4.5 scenario simulation (2006–2011).
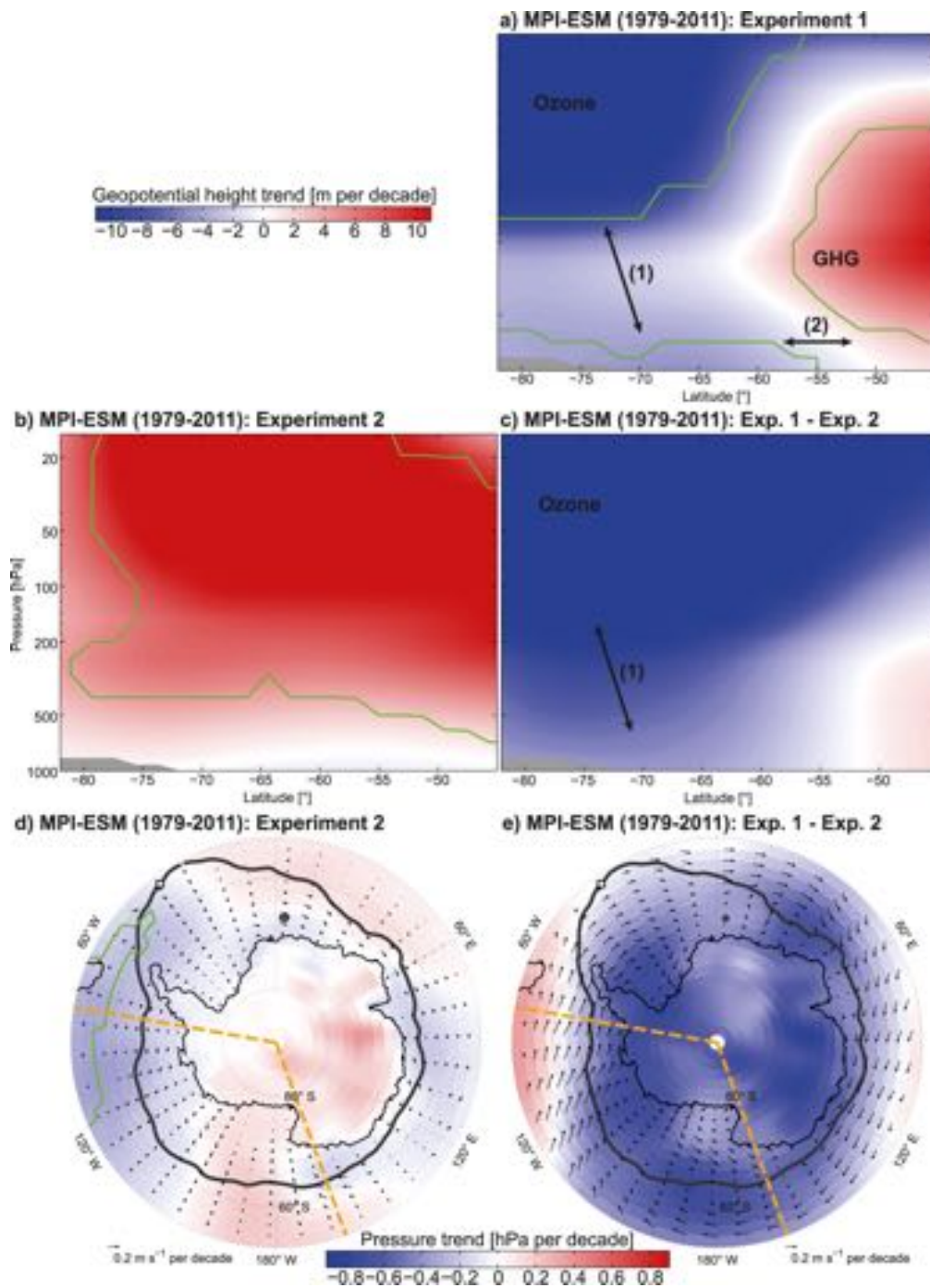
Figure A.6 Attribution of circulation changes to stratospheric ozone depletion and GHG increase (1979–2011): As Figures A.3b through f but for the period 1979 to 2011 by extending the historical simulation (1979–2005) with the RCP4.5 scenario simulation (2006–2011).
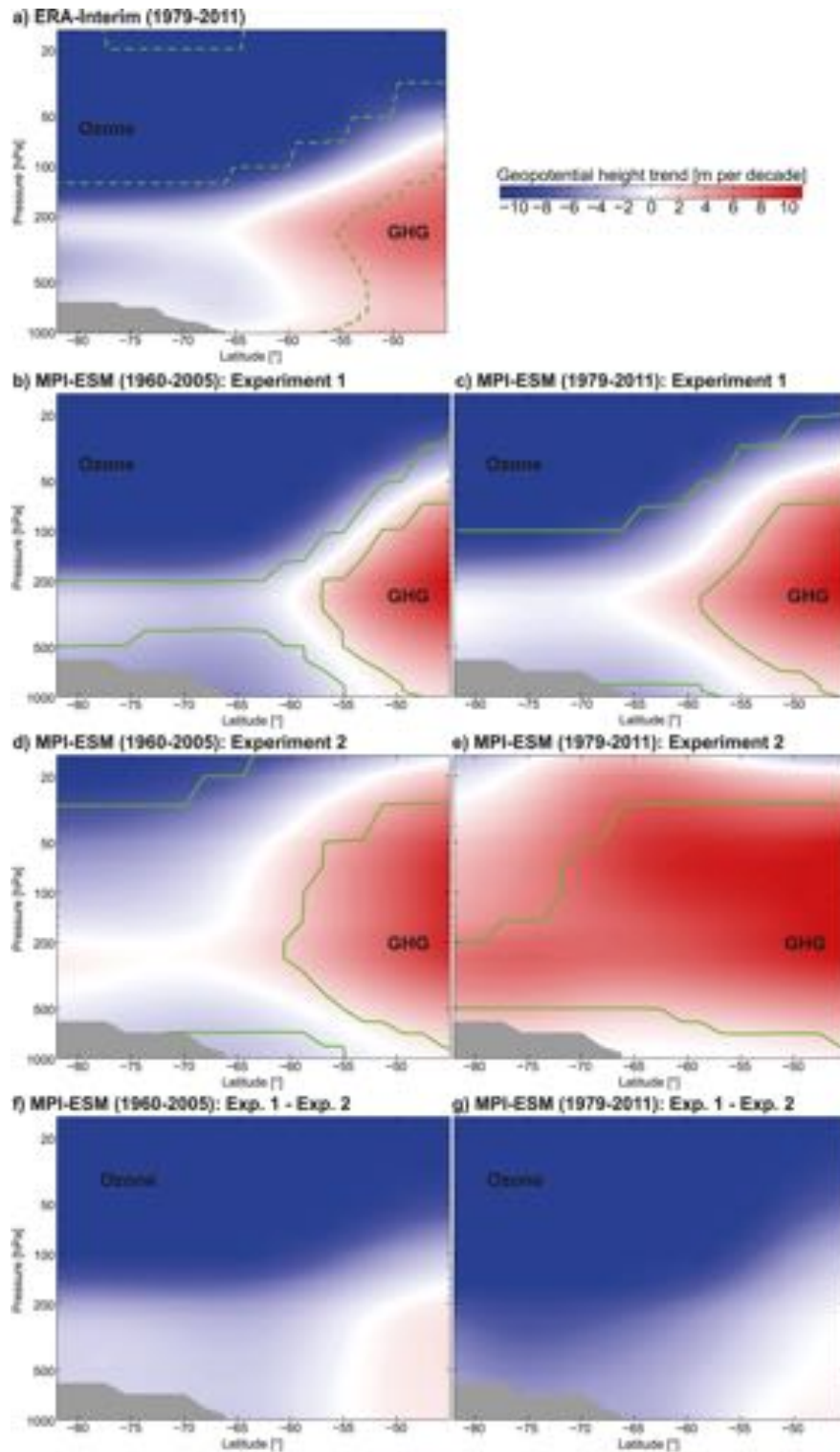
Figure A.7   Vertical cross-sections of decadal zonal mean geopotential-height changes over the sector 40° W to 150° E (based on annual means): Experiments as in Figure A.1. **(a)** ERA-Interim (1979–2011). **(b)** Historical simulations with all forcings (1960–2005). **(c)** Historical+RCP4.5 simulations with all forcings (1979–2011). **(d)** Historical simulations without stratospheric ozone depletion (1960–2005). **(e)** Historical+RCP4.5 simulations without stratospheric ozone depletion (1979–2011). **(f)** Differences between the historical simulations with **(b)** and without stratospheric ozone depletion **(d)** (1960–2005). **(g)** Differences between the historical+RCP4.5 simulations with **(c)** and without stratospheric ozone depletion **(e)** (1979–2011). Dashed and solid green lines: significance of geopotential-height and SLP trends (90% confidence level).

List of Figures

List of Tables

Bibliography

Aagaard, K. and Carmack, E. C. (1989). The role of sea ice and other fresh water in the Arctic circulation. *Journal of Geophysical Research*, 94(1):414–485. doi:10.1029/JC094iC10p14485.

Aagaard, K., Coachman, L., and Carmack, E. (1981). On the halocline of the Arctic Ocean. *Deep Sea Research Part A. Oceanographic Research Papers*, 28(6):529–545. doi:10.1016/0198-0149(81)90115-1.

Abe-Ouchi, A., Saito, F., Kawamura, K., Raymo, M. E., Okuno, J., Takahashi, K., and Blatter, H. (2013). Insolation-driven 100,000-year glacial cycles and hysteresis of ice-sheet volume. *Nature*, 500(7461):190–193. doi:10.1038/nature12374.

Abernathey, R. P., Cerovecki, I., Holland, P. R., Newsom, E., Mazloff, M., and Talley, L. D. (2016). Water-mass transformation by sea ice in the upper branch of the Southern Ocean overturning. *Nature Geoscience*, 9:596–601. doi:10.1038/ngeo2749.

Abram, N. J., McGregor, H. V., Tierney, J. E., Evans, M. N., McKay, N. P., Kaufman, D. S., Thirumalai, K., Martrat, B., Goosse, H., Phipps, S. J., Steig, E. J., Kilbourne, K. H., Saenger, C. P., Zinke, J., Leduc, G., Addison, J. A., Mortyn, P. G., Seidenkrantz, M.-S., Sicre, M.-A., Selvaraj, K., Filipsson, H. L., Neukom, R., Gergis, J., Curran, M. A. J., and von Gunten, L. (2016). Early onset of industrial-era warming across the oceans and continents. *Nature*, 536(7617):411–418. doi:10.1038/nature19082.

Abram, N. J., Mulvaney, R., Vimeux, F., Phipps, S. J., Turner, J., and England, M. H. (2014). Evolution of the Southern Annular Mode during the past millennium. *Nature Climate Change*, 4:564–569. doi:10.1038/nclimate2235.

Adkins, J. F., McIntyre, K., and Schrag, D. P. (2002). The Salinity, Temperature, and $\delta^{18}O$ of the Glacial Deep Ocean. *Science*, 298(5599):1769–1773. doi:10.1126/science.1076252.

Aguilar, E., Auer, I., Brunet, M., Peterson, T. C., and Wieringa, J. (2003). Guidelines on climate metadata and homogenization. Technical report, World Meteorological Organization.

Anderson, R. F., Ali, S., Bradtmiller, L. I., Nielsen, S. H. H., Fleisher, M. Q., Anderson, B. E., and Burckle, L. H. (2009). Wind-driven upwelling in the Southern Ocean and the deglacial rise in atmospheric CO_2. *Science*, 323(5920):1443–1448. doi:10.1126/science.1167441.

Andersson, A., Fennig, K., Klepp, C., Bakan, S., Graßl, H., and Schulz, J. (2010). The Hamburg Ocean Atmosphere Parameters and Fluxes from Satellite Data HOAPS-3. *Earth System Science Data*, 2(2):215–234. doi:10.5194/essd-2-215-2010.

Andrews, T., Gregory, J. M., Webb, M. J., Andrews, T., Gregory, J. M., and Webb, M. J. (2015). The Dependence of Radiative Forcing and Feedback on Evolving Patterns of Surface Temperature Change in Climate Models. *Journal of Climate*, 28(4):1630–1648. doi:10.1175/JCLI-D-14-00545.1.

Arakawa, A. and Lamb, V. R. (1977). *General Circulation Models of the Atmosphere*, volume 17 of *Methods in Computational Physics: Advances in Research and Applications*. Elsevier. doi:10.1016/B978-0-12-460817-7.50009-4.

Arblaster, J. M. and Meehl, G. A. (2006). Contributions of external forcings to Southern Annular Mode trends. *Journal of Climate*, 19(12):2896–2905. doi:10.1175/JCLI3774.1.

Archer, D., Winguth, A., Lea, D., and Mahowald, N. (2000). What caused the glacial/interglacial atmospheric pCO_2 cycles? *Reviews of Geophysics*, 38(2):159–189. doi:10.1029/1999RG000066.

Armour, K. C., Marshall, J., Scott, J. R., Donohoe, A., and Newsom, E. R. (2016). Southern Ocean warming delayed by circumpolar upwelling and equatorward transport. *Nature Geoscience*, 9(7):549–554. doi:10.1038/ngeo2731.

Assmann, K. M. and Timmermann, R. (2005). Variability of dense water formation in the Ross Sea. *Ocean Dynamics*, 55(2):68–87. doi:10.1007/s10236-004-0106-7.

Ballantyne, A. P., Alden, C. B., Miller, J. B., Tans, P. P., and White, J. W. C. (2012). Increase in observed net carbon dioxide uptake by land and oceans during the past 50 years. *Nature*, 488(7409):70–72. doi:10.1038/nature11299.

Barnier, B., Marchesiello, P., De Miranda, A. P., Molines, J. M., and Coulibaly, M. (1998). A sigma-coordinate primitive equation model for studying the circulation in the South Atlantic. Part I: Model configuration with error estimates. *Deep-Sea Research Part I: Oceanographic Research Papers*, 45(4-5):543–572. doi:10.1016/S0967-0637(97)00086-1.

Barth, A., Canter, M., van Schaeybroeck, B., Vannitsem, S., Massonnet, F., Zunz, V., Mathiot, P., Alvera-Azcárate, A., and Beckers, J. M. (2015). Assimilation of sea surface temperature, sea ice concentration and sea ice drift in a model of the Southern Ocean. *Ocean Modelling*, 93:22–39. doi:10.1016/j.ocemod.2015.07.011.

Barthélemy, A., Fichefet, T., Goosse, H., and Madec, G. (2015). Modeling the interplay between sea ice formation and the oceanic mixed layer: Limitations of simple brine rejection parameterizations. *Ocean Modelling*, 86:141–152. doi:10.1016/j.ocemod.2014.12.009.

Beckmann, A. and Goosse, H. (2003). A parameterization of ice shelf–ocean interaction for climate models. *Ocean Modelling*, 5(2):157–170. doi:10.1016/S1463-5003(02)00019-7.

Beckmann, A., Hellmer, H. H., and Timmermann, R. (1999). A numerical model of the Weddell Sea: Large-scale circulation and water mass distribution. *Journal of Geophysical Research*, 104(C10):23375–23391. doi:10.1029/1999JC900194.

Benz, V., Esper, O., Gersonde, R., Lamy, F., and Tiedemann, R. (2016). Last Glacial Maximum sea surface temperature and sea-ice extent in the Pacific sector of the Southern Ocean. *Quaternary Science Reviews*, 146:216–237. doi:10.1016/j.quascirev.2016.06.006.

Berger, A., Tricot, C., Gallee, H., and Loutre, M. F. (1993). Water Vapour, CO_2 and Insolation over the Last Glacial-Interglacial Cycles. *Philosophical Transactions of the Royal Society B: Biological Sciences*, 341(1297):253–261. doi:10.1098/rstb.1993.0110.

Bernardello, R., Marinov, I., Palter, J. B., Galbraith, E. D., and Sarmiento, J. L. (2014a). Impact of Weddell Sea deep convection on natural and anthropogenic carbon in a climate model. *Geophysical Research Letters*, 41(20):7262–7269. doi:10.1002/2014GL061313.

Bernardello, R., Marinov, I., Palter, J. B., Sarmiento, J. L., Galbraith, E. D., and Slater, R. D. (2014b). Response of the ocean natural carbon storage to projected twenty-first-century climate change. *Journal of Climate*, 27(5):2033–2053. doi:10.1175/JCLI-D-13-00343.1.

Bintanja, R., van Oldenborgh, G. J., Drijfhout, S. S., Wouters, B., and Katsman, C. A. (2013). Important role for ocean warming and increased ice-shelf melt in Antarctic sea-ice expansion. *Nature Geoscience*, 6(5):376–379. doi:10.1038/ngeo1767.

Bitz, C. M., Gent, P. R., Woodgate, R. A., Holland, M. M., and Lindsay, R. (2006). The influence of sea ice on ocean heat uptake in response to increasing CO_2. *Journal of Climate*, 19(11):2437–2450. doi:10.1175/JCLI3756.1.

Bitz, C. M. and Polvani, L. M. (2012). Antarctic climate response to stratospheric ozone depletion in a fine resolution ocean climate model. *Geophysical Research Letters*, 39(20):L20705. doi:10.1029/2012GL053393.

Blumberg, A. F. and Mellor, G. L. (1987). A description of a three-dimensional coastal ocean circulation model. In *Three-dimensional coastal ocean models (ed N.S. Heaps)*, volume 4, pages 1–16. American Geophysical Union. doi:10.1029/CO004p0001.

Boé, J., Hall, A., and Qu, X. (2009). Deep ocean heat uptake as a major source of spread in transient climate change simulations. *Geophysical Research Letters*, 36(22):L22701. doi:10.1029/2009GL040845.

Böning, C. W., Dispert, A., Visbeck, M., Rintoul, S. R., and Schwarzkopf, F. U. (2008). The response of the Antarctic Circumpolar Current to recent climate change. *Nature Geoscience*, 1(12):864–869. doi:10.1038/ngeo362.

Bopp, L., Lévy, M., Resplandy, L., and Sallée, J.-B. (2015). Pathways of anthropogenic carbon subduction in the global ocean. *Geophysical Research Letters*, 42(15):6416–6423. doi:10.1002/2015GL065073.

Bourassa, M. A., Gille, S. T., Bitz, C., Carlson, D., Cerovecki, I., Clayson, C. A., Cronin, M. F., Drennan, W. M., Fairall, C. W., Hoffman, R. N., Magnusdottir, G., Pinker, R. T., Renfrew, I. A., Serreze, M., Speer, K., Talley, L. D., and Wick, G. A. (2013). High-latitude ocean and sea ice surface fluxes: Challenges for climate research. *Bulletin of the American Meteorological Society*, 94(3):403–423. doi:10.1175/BAMS-D-11-00244.1.

Bouttes, N., Paillard, D., and Roche, D. M. (2010). Impact of brine-induced stratification on the glacial carbon cycle. *Climate of the Past*, 6(5):575–589. doi:10.5194/cp-6-575-2010.

Bouttes, N., Paillard, D., Roche, D. M., Waelbroeck, C., Kageyama, M., Lourantou, A., Michel, E., and Bopp, L. (2012). Impact of oceanic processes on the carbon cycle during the last termination. *Climate of the Past*, 8(1):149–170. doi:10.5194/cp-8-149-2012.

Boyer, T. P., Antonov, J. I., Baranova, O. K., Coleman, C., Garcia, H. E., Grodsky, A., Johnson, D. R., Locarnini, R. A., Mishonov, A. V., O'Brien, T. D., Paver, C. R., Reagan, J. R., Seidov, D., Smolyar, I. V., and Zweng, M. M. (2013). World Ocean Database 2013, p. 209, Silver Spring. NOAA Atlas NESDIS 72, S. Levitus, Ed., A. Mishonov, Technical Ed. doi:10.7289/V5NZ85MT.

Bracegirdle, T. J. (2013). Climatology and recent increase of westerly winds over the Amundsen Sea derived from six reanalyses. *International Journal of Climatology*, 33(4):843–851. doi:10.1002/joc.3473.

Bracegirdle, T. J. and Marshall, G. J. (2012). The reliability of Antarctic tropospheric pressure and temperature in the latest global reanalyses. *Journal of Climate*, 25(20):7138–7146. doi:10.1175/JCLI-D-11-00685.1.

Bracegirdle, T. J., Shuckburgh, E., Sallée, J.-B., Wang, Z., Meijers, A. J. S., Bruneau, N., Phillips, T., and Wilcox, L. J. (2013). Assessment of surface winds over the Atlantic, Indian, and Pacific Ocean sectors of the Southern Ocean in CMIP5 models: Historical bias, forcing response, and state dependence. *Journal of Geophysical Research Atmospheres*, 118(2):547–562. doi:10.1002/jgrd.50153.

Brannigan, L., Lenn, Y.-D., Rippeth, T. P., McDonagh, E., Chereskin, T. K., and Sprintall, J. (2013). Shear at the Base of the Oceanic Mixed Layer Generated by Wind Shear Alignment. *Journal of Physical Oceanography*, 43(8):1798–1810. doi:10.1175/JPO-D-12-0104.1.

Broecker, W. S. (1987). The biggest chill. *Natural History*, 96(10):74.

Broecker, W. S. (1991). The Great Ocean Conveyor. *Oceanography*, 4(2):79–89. doi:10.5670/oceanog.1991.07.

Broecker, W. S. (1997). Thermohaline Circulation, the Achilles Heel of Our Climate System: Will Man-Made CO_2 Upset the Current Balance? *Science*, 278(5343):1582–1588. doi:10.1126/science.278.5343.1582.

Broecker, W. S. and Peng, T.-H. (1982). *Tracers in the sea*. Lamont-Doherty Geological Observatory, Columbia University, New York.

Bromwich, D. H., Nicolas, J. P., and Monaghan, A. J. (2011). An Assessment of Precipitation Changes over Antarctica and the Southern Ocean since 1989 in Contemporary Global Reanalyses. *Journal of Climate*, 24(16):4189–4209. doi:10.1175/2011JCLI4074.1.

Budgell, W. P. (2005). Numerical simulation of ice-ocean variability in the Barents Sea region. *Ocean Dynamics*, 55(3-4):370–387. doi:10.1007/s10236-005-0008-3.

Butterworth, B. J. and Miller, S. D. (2016). Air-sea exchange of carbon dioxide in the Southern Ocean and Antarctic marginal ice zone. *Geophysical Research Letters*, 43(13):7223–7230. doi:10.1002/2016GL069581.

Byrne, D., Papritz, L., Frenger, I., Münnich, M., and Gruber, N. (2014). Atmospheric Response to Mesoscale Sea Surface Temperature Anomalies: Assessment of Mechanisms and Coupling Strength in a High-Resolution Coupled Model over the South Atlantic. *Journal of the Atmospheric Sciences*, 72(5):1872–1890. doi:10.1175/JAS-D-14-0195.1.

Cai, W., Cowan, T., Godfrey, S., Wijffels, S., Cai, W., Cowan, T., Godfrey, S., and Wijffels, S. (2010). Simulations of Processes Associated with the Fast Warming Rate of the Southern Midlatitude Ocean. *Journal of Climate*, 23(1):197–206. doi:10.1175/2009JCLI3081.1.

Caldeira, K. and Duffy, P. B. (2000). The role of the southern ocean in uptake and storage of anthropogenic carbon dioxide. *Science*, 287(5453):620–622. doi:10.1126/science.287.5453.620.

Cao, M. and Woodward, F. I. (1998). Dynamic responses of terrestrial ecosystem carbon cycling to global climate change. *Nature*, 393(6682):249–252. doi:10.1038/30460.

Carril, A. F. and Navarra, A. (2001). Low-frequency variability of the Antarctic Circumpolar Wave. *Geophysical Research Letters*, 28(24):4623–4626. doi:10.1029/2001GL013804.

Carton, J. A. and Giese, B. S. (2008). A Reanalysis of Ocean Climate Using Simple Ocean Data Assimilation (SODA). *Monthly Weather Review*, 136(8):2999–3017. doi:10.1175/2007MWR1978.1.

Cavalieri, D. J. and Parkinson, C. L. (2008). Antarctic sea ice variability and trends, 19792006. *Journal of Geophysical Research*, 113(C7):C07004. doi:10.1029/2007JC004564.

CDO (2015). Climate Data Operators (version 1.6.8). Available at: http://www.mpimet.mpg.de/cdo.

Cerovečki, I. and Mazloff, M. R. (2016). The Spatiotemporal Structure of Diabatic Processes Governing the Evolution of Subantarctic Mode Water in the Southern Ocean. *Journal of Physical Oceanography*, 46(2):683–710. doi:10.1175/JPO-D-14-0243.1.

Cerovečki, I., Talley, L. D., and Mazloff, M. R. (2011). A Comparison of Southern Ocean Air-Sea Buoyancy Flux from an Ocean State Estimate with Five Other Products. *Journal of Climate*, 24(24):6283–6306. doi:10.1175/2011JCLI3858.1.

Chassignet, E. P., Arango, H., Dietrich, D., Ezer, T., Ghil, M., Haidvogel, D. B., Ma, C. C., Mehra, A., Paiva, A. M., and Sirkes, Z. (2000). DAMEE-NAB: The base experiments. *Dynamics of Atmospheres and Oceans*, 32(3-4):155–183. doi:10.1016/S0377-0265(00)00046-4.

Chassignet, E. P., Smith, L. T., Halliwell, G. R., and Bleck, R. (2003). North Atlantic Simulations with the Hybrid Coordinate Ocean Model (HYCOM): Impact of the Vertical Coordinate Choice, Reference Pressure, and Thermobaricity. *Journal of Physical Oceanography*, 33(1981):2504–2526. doi:10.1175/1520-0485(2003)033<2504:NASWTH>2.0.CO;2.

Chassignet, E. P., Xu, X., and Danabasoglu, G. (2014). Overflow parameterisations in climate models. *CLIVAR Exchanges*, 65(19/2):34–37.

Chelton, D. B., DeSzoeke, R. A., Schlax, M. G., El Naggar, K., Siwertz, N., Chelton, D. B., DeSzoeke, R. A., Schlax, M. G., Naggar, K. E., and Siwertz, N. (1998). Geographical Variability of the First Baroclinic Rossby Radius of Deformation. *Journal of Physical Oceanography*, 28(3):433–460. doi:10.1175/1520-0485(1998)028<0433:GVOTFB>2.0.CO;2.

Cheng, L., Trenberth, K. E., Palmer, M. D., Zhu, J., and Abraham, J. P. (2016). Observed and simulated full-depth ocean heat-content changes for 1970–2005. *Ocean Science*, 12(4):925–935. doi:10.5194/os-12-925-2016.

Cionni, I., Eyring, V., Lamarque, J. F., Randel, W. J., Stevenson, D. S., Wu, F., Bodeker, G. E., Shepherd, T. G., Shindell, D. T., and Waugh, D. W. (2011). Ozone database in support of CMIP5 simulations: Results and corresponding radiative forcing. *Atmospheric Chemistry and Physics*, 11(21):11267–11292. doi:10.5194/acp-11-11267-2011.

Clark, P. U., Pisias, N. G., Stocker, T. F., and Weaver, A. J. (2002). The role of the thermohaline circulation in abrupt climate change. *Nature*, 415(6874):863–869. doi:10.1038/415863a.

Comiso, J. C. (1986). Characteristics of Arctic winter sea ice from satellite multispectral microwave observations. *Journal of Geophysical Research*, 91(C1):975–994. doi:10.1029/JC091iC01p00975.

Comiso, J. C., Cavalieri, D. J., Parkinson, C. L., and Gloersen, P. (1997). Passive microwave algorithms for sea ice concentration: A comparison of two techniques. *Remote Sensing of Environment*, 60(3):357–384. doi:10.1016/S0034-4257(96)00220-9.

Comiso, J. C., Kwok, R., Martin, S., and Gordon, A. L. (2011). Variability and trends in sea ice extent and ice production in the Ross Sea. *Journal of Geophysical Research*, 116(4):C04021. doi:10.1029/2010JC006391.

Comiso, J. C. and Nishio, F. (2008). Trends in the sea ice cover using enhanced and compatible AMSR-E, SSM/I, and SMMR data. *Journal of Geophysical Research*, 113(C2):C02S07. doi:10.1029/2007JC004257.

Cook, A. J., Holland, P. R., Meredith, M. P., Murray, T., Luckman, A., and Vaughan, D. G. (2016). Ocean forcing of glacier retreat in the western Antarctic Peninsula. *Science*, 353(6296):1261–1273. doi:10.1126/science.aae0017.

Cox, P. M., Betts, R. A., Jones, C. D., Spall, S. A., and Totterdell, I. J. (2000). Acceleration of global warming due to carbon-cycle feedbacks in a coupled climate model. *Nature*, 408(6809):184–187. doi:10.1038/35041539.

Cummins, P. F., Masson, D., and Saenko, O. A. (2016). Vertical heat flux in the ocean: Estimates from observations and from a coupled general circulation model. *Journal of Geophysical Research: Oceans*, 121(6):3790–3802. doi:10.1002/2016JC011647.

Cunningham, S. A., Alderson, S. G., King, B. A., and Brandon, M. A. (2003). Transport and variability of the Antarctic Circumpolar Current in Drake Passage. *Journal of Geophysical Research*, 108(C5):8084. doi:10.1029/2001JC001147.

Cunningham, S. A., Kanzow, T., Rayner, D., Baringer, M. O., Johns, W. E., Marotzke, J., Longworth, H. R., Grant, E. M., Hirschi, J. J.-M., Beal, L. M., Meinen, C. S., and Bryden, H. L. (2007). Temporal variability of the Atlantic meridional overturning circulation at 26.5 degrees N. *Science*, 317(5840):935–938. doi:10.1126/science.1141304.

Curry, J. A., Schramm, J. L., and Ebert, E. E. (1995). Sea ice-albedo climate feedback mechanism. *Journal of Climate*, 8(2):240–247. doi:10.1175/1520-0442(1995)008<0240:SIACFM>2.0.CO;2.

Curry, W. B. and Oppo, D. W. (2005). Glacial water mass geometry and the distribution of $\delta^1 3C$ of $\sum CO_2$ in the western Atlantic Ocean. *Paleoceanography*, 20(1):1–12. doi:10.1029/2004PA001021.

Cushman-Roisin, B. and Beckers, J.-M. (2011). *Introduction to Geophysical Fluid Dynamics - Physical and Numerical Aspects*, volume 101 of *International Geophysics Series*. Elsevier Academic Press, Burlington, San Diego, London, 2 edition.

Danabasoglu, G., Large, W. G., Tribbia, J. J., Gent, P. R., Briegleb, B. P., and McWilliams, J. C. (2006). Diurnal coupling in the tropical oceans of CCSM3. *Journal of Climate*, 19(11):2347–2365. doi:10.1175/JCLI3739.1.

de Boer, A., Sigman, D. M., Toggweiler, J. R., and Russell, J. L. (2007). Effect of global ocean temperature change on deep ocean ventilation. *Paleoceanography*, 22(PA2210):15. doi:10.1029/2005PA001242.

de Boyer Montégut, C., Madec, G., Fischer, A. S., Lazar, A., and Iudicone, D. (2004). Mixed layer depth over the global ocean: An examination of profile data and a profile-based climatology. *Journal of Geophysical Research*, 109(12):1–20. doi:10.1029/2004JC002378.

de Lavergne, C., Palter, J. B., Galbraith, E. D., Bernardello, R., and Marinov, I. (2014). Cessation of deep convection in the open Southern Ocean under anthropogenic climate change. *Nature Climate Change*, 4(4):278–282. doi:10.1038/nclimate2132.

Deacon, G. E. R. (1937). The hydrology of the Southern Ocean, In *Discovery reports*, pages 1–124. Cambridge University Press.

DeConto, R. M. and Pollard, D. (2016). Contribution of Antarctica to past and future sea-level rise. *Nature*, 531(7596):591–597. doi:10.1038/nature17145.

Dee, D. P., Uppala, S. M., Simmons, A. J., Berrisford, P., Poli, P., Kobayashi, S., Andrae, U., Balmaseda, M. A., Balsamo, G., Bauer, P., Bechtold, P., Beljaars, A. C. M., van de Berg, L., Bidlot, J., Bormann, N., Delsol, C., Dragani, R., Fuentes, M., Geer, A. J., Haimberger, L., Healy, S. B., Hersbach, H., Hólm, E. V., Isaksen, L., Kållberg, P., Köhler, M., Matricardi, M., Mcnally, A. P., Monge-Sanz, B. M., Morcrette, J. J., Park, B. K., Peubey, C., de Rosnay, P., Tavolato, C., Thépaut, J. N., and Vitart, F. (2011). The ERA-Interim reanalysis: configuration and performance of the data assimilation system. *Quarterly Journal of the Royal Meteorological Society*, 137(656):553–597. doi:10.1002/qj.828.

Delworth, T., Manabe, S., and Stouffer, R. J. (1993). Interdecadal Variations of the Thermohaline Circulation in a Coupled Ocean-Atmosphere Model. *Journal of Climate*, 6(11):1993–2011. doi:10.1175/1520-0442(1993)006<1993:IVOTTC>2.0.CO;2.

Depoorter, M. A., Bamber, J. L., Griggs, J. A., Lenaerts, J. T. M., Ligtenberg, S. R. M., van den Broeke, M. R., and Moholdt, G. (2013). Calving fluxes and basal melt rates of Antarctic ice shelves. *Nature*, 502(7469):89–92. doi:10.1038/nature12567.

DeVries, T. and Primeau, F. (2011). Dynamically and observationally constrained estimates of water-mass distributions and ages in the global ocean. *Journal of Physical Oceanography*, 41(12):2381–2401. doi:10.1175/JPO-D-10-05011.1.

Ding, Q., Steig, E. J., Battisti, D. S., and Kuttel, M. (2011). Winter warming in West Antarctica caused by central tropical Pacific warming. *Nature Geoscience*, 4(6):398–403. doi:10.1038/ngeo1129.

Ding, Q., Steig, E. J., Battisti, D. S., and Wallace, J. M. (2012). Influence of the Tropics on the Southern Annular Mode. *Journal of Climate*, 25(18):6330–6348. doi:10.1175/JCLI-D-11-00523.1.

Dinniman, M. S., Klinck, J. M., and Hofmann, E. E. (2012). Sensitivity of Circumpolar Deep Water Transport and Ice Shelf Basal Melt along the West Antarctic Peninsula to Changes in the Winds. *Journal of Climate*, 25(14):4799–4816. doi:10.1175/JCLI-D-11-00307.1.

Dinniman, M. S., Klinck, J. M., and Smith, W. O. (2003). Cross-shelf exchange in a model of the Ross Sea circulation and biogeochemistry. *Deep Sea Research Part II: Topical Studies in Oceanography*, 50(22-26):3103–3120. doi:10.1016/j.dsr2.2003.07.011.

Dinniman, M. S., Klinck, J. M., and Smith, W. O. (2011). A model study of Circumpolar Deep Water on the West Antarctic Peninsula and Ross Sea continental shelves. *Deep Sea Research Part II: Topical Studies in Oceanography*, 58(13-16):1508–1523. doi:10.1016/j.dsr2.2010.11.013.

Dinniman, M. S., Klinck, J. M., and Smith, W. O. J. (2007). Influence of sea ice cover and icebergs on circulation and water mass formation in a numerical circulation model of the Ross Sea, Antarctica. *Journal of Geophysical Research*, 112(C11):C11013. doi:10.1029/2006JC004036.

Doney, S. C. and Hecht, M. W. (2002). Antarctic Bottom Water formation and deep-water Chlorofluorocarbon distributions in a global ocean climate model. *Journal of Physical Oceanography*, 32(6):1642–1666. doi:10.1175/1520-0485(2002)032<1642:ABWFAD>2.0.CO;2.

Doney, S. C., Lindsay, K., Caldeira, K., Campin, J.-M., Drange, H., Dutay, J.-C., Follows, M., Gao, Y., Gnanadesikan, A., Gruber, N., Ishida, A., Joos, F., Madec, G., Maier-Reimer, E., Marshall, J. C., Matear, R. J., Monfray, P., Mouchet, A., Najjar, R., Orr, J. C., Plattner, G.-K., Sarmiento, J., Schlitzer, R., Slater, R., Totterdell, I. J., Weirig, M.-F., Yamanaka, Y., and Yool, A. (2004). Evaluating global ocean carbon models: The importance of realistic physics. *Global Biogeochemical Cycles*, 18(3):GB3017. doi:10.1029/2003GB002150.

Dong, J., Speer, K., and Jullion, L. (2016). The Antarctic Slope Current near 30°E. *Journal of Geophysical Research: Oceans*, 121(2):1051–1062. doi:10.1002/2015JC011099.

Döös, K. and Webb, D. J. (1994). The Deacon Cell and the Other Meridional Cells of the Southern Ocean. *Journal of Physical Oceanography*, 24(2):429–442. doi:10.1175/1520-0485(1994)024<0429:TDCATO>2.0.CO;2.

Downes, S. M., Bindoff, N. L., and Rintoul, S. R. (2010). Changes in the subduction of Southern Ocean water masses at the end of the twenty-first century in eight IPCC models. *Journal of Climate*, 23(24):6526–6541. doi:10.1175/2010JCLI3620.1.

Downes, S. M., Farneti, R., Uotila, P., Griffies, S. M., Marsland, S. J., Bailey, D., Behrens, E., Bentsen, M., Bi, D., Biastoch, A., Böning, C., Bozec, A., Canuto, V. M., Chassignet, E., Danabasoglu, G., Danilov, S., Diansky, N., Drange, H., Fogli, P. G., Gusev, A., Howard, A., Ilicak, M., Jung, T., Kelley, M., Large, W. G., Leboissetier, A., Long, M., Lu, J., Masina, S., Mishra, A., Navarra, A., George Nurser, A. J., Patara, L., Samuels, B. L., Sidorenko, D., Spence, P., Tsujino, H., Wang, Q., and Yeager, S. G. (2015). An assessment of Southern Ocean water masses and sea ice during 1988-2007 in a suite of interannual CORE-II simulations. *Ocean Modelling*, 94:67–94. doi:10.1016/j.ocemod.2015.07.022.

Downes, S. M., Gnanadesikan, A., Griffies, S. M., and Sarmiento, J. L. (2011). Water Mass Exchange in the Southern Ocean in Coupled Climate Models. *Journal of Physical Oceanography*, 41(2001):1756–1771. doi:10.1175/2011JPO4586.1.

Downes, S. M. and Hogg, A. M. C. C. (2013). Southern Ocean circulation and eddy compensation in CMIP5 models. *Journal of Climate*, 26(18):7198–7220. doi:10.1175/JCLI-D-12-00504.1.

Drucker, R., Martin, S., and Kwok, R. (2011). Sea ice production and export from coastal polynyas in the Weddell and Ross Seas. *Geophysical Research Letters*, 38(17):L17502. doi:10.1029/2011GL048668.

Duffy, P. B. and Caldeira, K. (1997). Sensitivity of simulated salinity in a three-dimensional ocean model to upper ocean transport of salt from sea-ice formation. *Geophysical Research Letters*, 24(11):1323–1326. doi:10.1029/97GL01294.

Duffy, P. B., Eby, M., and Weaver, A. J. (1999). Effects of sinking of salt rejected during formation of sea ice on results of an ocean-atmosphere-sea ice climate model. *Geophysical Research Letters*, 26(12):1739–1742. doi:10.1029/1999GL900286.

Dufour, C. O., Griffies, S. M., de Souza, G. F., Frenger, I., Morrison, A. K., Palter, J. B., Sarmiento, J. L., Galbraith, E. D., Dunne, J. P., Anderson, W. G., and Slater, R. D. (2015). Role of Mesoscale Eddies in Cross-Frontal Transport of Heat and Biogeochemical Tracers in the Southern Ocean. *Journal of Physical Oceanography*, 45(12):3057–3081. doi:10.1175/JPO-D-14-0240.1.

Dufour, C. O., Sommer, J. L., Gehlen, M., Orr, J. C., Molines, J.-M., Simeon, J., and Barnier, B. (2013). Eddy compensation and controls of the enhanced sea-to-air CO_2 flux during positive phases of the Southern Annular Mode. *Global Biogeochemical Cycles*, 27(3):950–961. doi:10.1002/gbc.20090.

Dukowicz, J. K. (2001). Reduction of Density and Pressure Gradient Errors in Ocean Simulations. *Journal of Physical Oceanography*, 31(7):1915–1921. doi:10.1175/1520-0485(2001)031<1915:RODAPG>2.0.CO;2.

Dunn, J. and Ridgway, K. (2002). Mapping ocean properties in regions of complex topography. *Deep Sea Research Part I: Oceanographic Research Papers*, 49(3):591–604. doi:10.1016/S0967-0637(01)00069-3.

Durack, P. J., Gleckler, P. J., Landerer, F. W., and Taylor, K. E. (2014). Quantifying underestimates of long-term upper-ocean warming. *Nature Climate Change*, 4(11):999–1005. doi:10.1038/nclimate2389.

Durack, P. J. and Wijffels, S. E. (2010). Fifty-year trends in global ocean salinities and their relationship to broad-scale warming. *Journal of Climate*, 23(16):4342–4362. doi:10.1175/2010JCLI3377.1.

Durack, P. J., Wijffels, S. E., and Matear, R. J. (2012). Ocean salinities reveal strong global water cycle intensification during 1950 to 2000. *Science*, 336(6080):455–458. doi:10.1126/science.1212222.

Dussin, R., Barnier, B., Brodeau, L., and Molines, J. M. (2016). The making of the DRAKKAR FORCING SET DFS5. Technical report, LGGE, Grenoble, France.

Eberenz, S. (2015). Effect of sea ice freshwater flux on Southern Ocean mixed layer processes. *Master's Thesis: ETH Zürich*, p. 64.

ECMWF (2007). Part IV: Physical Processes. In *IFS Documentation CY31R1*, p. 155. ECMWF.

Eisenman, I., Meier, W. N., and Norris, J. R. (2014). A spurious jump in the satellite record: has Antarctic sea ice expansion been overestimated? *The Cryosphere*, 8(4):1289–1296. doi:10.5194/tc-8-1289-2014.

Emery, W. J., Fowler, C. W., and Maslanik, J. A. (1995). Satellite remote sensing of ice motion. In Ikeda, M. and Dobson, F. W., editors, *Oceanographic applications of remote sensing*, Oceanographic Applications of Remote Sensing, chapter 23, pages 367–379. CRC Press.

Emery, W. J., Fowler, C. W., and Maslanik, J. A. (1997). Satellite-derived maps of Arctic and Antarctic sea ice motion: 1988 to 1994. *Geophysical Research Letters*, 24(8):897–900. doi:10.1029/97GL00755.

England, M. H. (1992). On the Formation of Antarctic Intermediate and Bottom Water in Ocean General Circulation Models. *Journal of Physical Oceanography*, 22(8):918–926. doi:10.1175/1520-0485(1992)022<0918:OTFOAI>2.0.CO;2.

England, M. H., Godfrey, J. S., Hirst, A. C., and Tomczak, M. (1993). The mechanism for Antarctic Intermediate Water renewal in a world ocean model. *Journal of Physical Oceanography*, 23(7):1553–1560. doi:10.1175/1520-0485(1993)023<1553:TMFAIW>2.0.CO;2.

EPICA community members, Augustin, L., Barbante, C., Barnes, P. R. F., Marc Barnola, J., Bigler, M., Castellano, E., Cattani, O., Chappellaz, J., Dahl-Jensen, D., Delmonte, B., Dreyfus, G., Durand, G., Falourd, S., Fischer, H., Flückiger, J., Hansson, M. E., Huybrechts, P., Jugie, G., Johnsen, S. J., Jouzel, J., Kaufmann, P., Kipfstuhl, J., Lambert, F., Lipenkov, V. Y., Littot, G. C., Longinelli, A., Lorrain, R., Maggi, V., Masson-Delmotte, V., Miller, H., Mulvaney, R., Oerlemans, J., Oerter, H., Orombelli, G., Parrenin, F., Peel, D. A., Petit, J.-R., Raynaud, D., Ritz, C., Ruth, U., Schwander, J., Siegenthaler, U., Souchez, R., Stauffer, B., Peder Steffensen, J., Stenni, B., Stocker, T. F., Tabacco, I. E., Udisti, R., van de Wal, R. S. W., van den Broeke, M., Weiss, J., Wilhelms, F., Winther, J.-G., Wolff, E. W., and Zucchelli, M. (2004). Eight glacial cycles from an Antarctic ice core. *Nature*, 429(6992):623–628. doi:10.1038/nature02599.

Eveleth, R., Cassar, N., Sherrell, R., Ducklow, H., Meredith, M., Venables, H., Lin, Y., and Li, Z. (2017). Ice melt influence on summertime net community production along the Western Antarctic Peninsula. *Deep Sea Research Part II: Topical Studies in Oceanography*, 139:89–102. doi:10.1016/j.dsr2.2016.07.016.

Fahrbach, E., Augstein, E., and Olbers, D. (1994). Impact of shelf and sea ice on water mass modifications and large-scale oceanic circulation in the Weddell Sea. In *Antarctic Science*, pages 167–187. Springer Berlin Heidelberg, Berlin, Heidelberg. doi:10.1007/978-3-642-78711-9_12.

Fahrbach, E., Rohardt, G., and Krause, G. (1992). The Antarctic coastal current in the southeastern Weddell Sea. *Polar Biology*, 12(2):171–182. doi:10.1007/BF00238257.

Fan, T., Deser, C., and Schneider, D. P. (2014). Recent Antarctic sea ice trends in the context of Southern Ocean surface climate variations since 1950. *Geophysical Research Letters*, 41(7):2419–2426. doi:10.1002/2014GL059239.

Farneti, R., Delworth, T. L., Rosati, A. J., Griffies, S. M., and Zeng, F. (2010). The Role of Mesoscale Eddies in the Rectification of the Southern Ocean Response to Climate Change. *Journal of Physical Oceanography*, 40(7):1539–1557. doi:10.1175/2010JPO4353.1.

Farneti, R., Downes, S. M., Griffies, S. M., Marsland, S. J., Behrens, E., Bentsen, M., Bi, D., Biastoch, A., Böning, C., Bozec, A., Canuto, V. M., Chassignet, E., Danabasoglu, G., Danilov, S., Diansky, N., Drange, H., Fogli, P. G., Gusev, A., Hallberg, R. W., Howard, A., Ilicak, M., Jung, T., Kelley, M., Large, W. G., Leboissetier, A., Long, M., Lu, J., Masina, S., Mishra, A., Navarra, A., George Nurser, A. J., Patara, L., Samuels, B. L., Sidorenko, D., Tsujino, H., Uotila, P., Wang, Q., and Yeager, S. G. (2015). An assessment of Antarctic Circumpolar Current and Southern Ocean meridional overturning circulation during 1958-2007 in a suite of interannual CORE-II simulations. *Ocean Modelling*, 93:84–120. doi:10.1016/j.ocemod.2015.07.009.

Farneti, R. and Gent, P. R. (2011). The effects of the eddy-induced advection coefficient in a coarse-resolution coupled climate model. *Ocean Modelling*, 39(1-2):135–145. doi:10.1016/j.ocemod.2011.02.005.

Fay, A. R., McKinley, G. A., and Lovenduski, N. S. (2014). Southern Ocean carbon trends: Sensitivity to methods. *Geophysical Research Letters*, 41(19):6833–6840. doi:10.1002/2014GL061324.

Ferrari, R., Jansen, M. F., Adkins, J. F., Burke, A., Stewart, A. L., and Thompson, A. F. (2014). Antarctic sea ice control on ocean circulation in present and glacial climates. *Proceedings of the National Academy of Sciences*, 111(24):8753–8758. doi:10.1073/pnas.1323922111.

Ferrari, R. and Wunsch, C. (2009). Ocean Circulation Kinetic Energy: Reservoirs, Sources, and Sinks. *Annual Review of Fluid Mechanics*, 41(1):253–282. doi:10.1146/annurev.fluid.40.111406.102139.

Ferreira, D., Marshall, J., Bitz, C. M., Solomon, S., and Plumb, A. (2015). Antarctic ocean and sea ice response to ozone depletion: A two-time-scale problem. *Journal of Climate*, 28(3):1206–1226. doi:10.1175/JCLI-D-14-00313.1.

Fischer, H., Schmitt, J., Lüthi, D., Stocker, T. F., Tschumi, T., Parekh, P., Joos, F., Köhler, P., Völker, C., Gersonde, R., Barbante, C., Le Floch, M., Raynaud, D., and Wolff, E. (2010). The role of Southern Ocean processes in orbital and millennial CO_2 variations - A synthesis. *Quaternary Science Reviews*, 29(1-2):193–205. doi:10.1016/j.quascirev.2009.06.007.

Flather, R. A. (1976). A tidal model of the northwest European continental shelf. *Memoires de la Societe Royale des Sciences de Liege*, 6(10):141–164.

Fogt, R. L., Jones, J. M., and Renwick, J. (2012). Seasonal zonal asymmetries in the Southern Annular Mode and their impact on regional temperature anomalies. *Journal of Climate*, 25(18):6253–6270. doi:10.1175/JCLI-D-11-00474.1.

Fogwill, C. J., Phipps, S. J., Turney, C. S. M., and Golledge, N. R. (2015). Sensitivity of the Southern Ocean to enhanced regional Antarctic ice sheet meltwater input. *Earth's Future*, 3(10):317–329. doi:10.1002/2015EF000306.

Forryan, A., Naveira Garabato, A. C., Polzin, K. L., and Waterman, S. (2015). Rapid injection of near-inertial shear into the stratified upper ocean at an Antarctic Circumpolar Current front. *Geophysical Research Letters*, 42(9):3431–3441. doi:10.1002/2015GL063494.

Fowler, C., Emery, W. J., and Tschudi, M. A. (2013a). Polar Pathfinder daily 25 km EASE-Grid sea ice motion vectors, version 2, 1979–2011, Boulder, Colorado USA. National Snow and Ice Data Center, distributed in netCDF format by the Integrated Climate Data Center University of Hamburg. Digital media.

Fowler, C., Emery, W. J., and Tschudi, M. A. (2013b). Polar Pathfinder daily 25 km EASE-Grid sea ice motion vectors, version 2, 1980–2009, Boulder, Colorado USA. National Snow and Ice Data Center, distributed in netCDF format by the Integrated Climate Data Center University of Hamburg. Digital media.

Francois, R., Altabet, M. A., Yu, E.-F., Sigman, D. M., Bacon, M. P., Frank, M., Bohrmann, G., Bareille, G., and Labeyrie, L. D. (1997). Contribution of Southern Ocean surface-water stratification to low atmospheric CO_2 concentrations during the last glacial period. *Nature*, 389(6654):929–935. doi:10.1038/40073.

Freeman, N. M., Lovenduski, N. S., and Gent, P. R. (2016). Temporal variability in the Antarctic Polar Front (2002-2014). *Journal of Geophysical Research: Oceans*, 121. doi:10.1002/2016JC012145.

Frenger, I., Gruber, N., Knutti, R., and Münnich, M. (2013). Imprint of Southern Ocean eddies on winds, clouds and rainfall. *Nature Geoscience*, 6(8):608–612. doi:10.1038/ngeo1863.

Frenger, I., Münnich, M., Gruber, N., and Knutti, R. (2015). Southern Ocean eddy phenomenology. *Journal of Geophysical Research*, 120(11):7413–7449. doi:10.1002/2015JC011047.

Friedlingstein, P., Bopp, L., Ciais, P., Dufresne, J.-L., Fairhead, L., LeTreut, H., Monfray, P., and Orr, J. (2001). Positive feedback between future climate change and the carbon cycle. *Geophysical Research Letters*, 28(8):1543–1546. doi:10.1029/2000GL012015.

Friedlingstein, P., Cox, P., Betts, R., Bopp, L., von Bloh, W., Brovkin, V., Cadule, P., Doney, S., Eby, M., Fung, I., Bala, G., John, J., Jones, C., Joos, F., Kato, T., Kawamiya, M., Knorr, W., Lindsay, K., Matthews, H. D., Raddatz, T., Rayner, P., Reick, C., Roeckner, E., Schnitzler, K.-G., Schnur, R., Strassmann, K., Weaver, A. J., Yoshikawa, C., and Zeng, N. (2006). Climate–carbon cycle feedback analysis: Results from the C4MIP model intercomparison. *Journal of Climate*, 19(14):3337–3353. doi:10.1175/JCLI3800.1.

Frischknecht, M., Münnich, M., and Gruber, N. (2015). Remote versus local influence of ENSO on the California Current System. *Journal of Geophysical Research*, 120(2):1353–1374. doi:10.1002/2014JC010531.

Frölicher, T. L., Sarmiento, J. L., Paynter, D. J., Dunne, J. P., Krasting, J. P., and Winton, M. (2015). Dominance of the Southern Ocean in anthropogenic carbon and heat uptake in CMIP5 models. *Journal of Climate*, 28(2):862–886. doi:10.1175/JCLI-D-14-00117.1.

Frölicher, T. L., Winton, M., and Sarmiento, J. L. (2014). Continued global warming after CO_2 emissions stoppage. *Nature Climate Change*, 4(1):40–44. doi:10.1038/nclimate2060.

Fyfe, J. C. and Saenko, O. A. (2006). Simulated changes in the extratropical Southern Hemisphere winds and currents. *Geophys. Res. Lett.*, 33(6):L06701.

Fyfe, J. C., Saenko, O. A., Zickfeld, K., Eby, M., and Weaver, A. J. (2007). The role of poleward-intensifying winds on Southern Ocean warming. *Journal of Climate*, 20(21):5391–5400. doi:10.1175/2007JCLI1764.1.

Ganachaud, A. and Wunsch, C. (2000). Improved estimates of global ocean circulation, heat transport and mixing from hydrographic data. *Nature*, 408(6811):453–457. doi:10.1038/35044048.

Ganopolski, A. and Rahmstorf, S. (2001). Rapid changes of glacial climate simulated in a coupled climate model. *Nature*, 409(6817):153–158.

Garcia, H. E., Locarnini, R. A., Boyer, T. P., Antonov, J. I., Baranova, O. K., Zweng, M. M., Reagan, J. R., and Johnson, D. R. (2014a). World Ocean Atlas 2013, Volume 3: Dissolved Oxygen, Apparent Oxygen Utilization, and Oxygen Saturation, p. 27. NOAA Atlas NESDIS 75.

Garcia, H. E., Locarnini, R. A., Boyer, T. P., Antonov, J. I., Baranova, O. K., Zweng, M. M., Reagan, J. R., and Johnson, D. R. (2014b). World Ocean Atlas 2013, Volume 4: Dissolved Inorganic Nutrients (phosphate, nitrate, silicate), p. 25. NOAA Atlas NESDIS 76.

Gargett, A. E. (1991). Physical processes and the maintenance of nutrient-rich euphotic zones. *Limnology and Oceanography*, 36(8):1527–1545. doi:10.4319/lo.1991.36.8.1527.

Gent, P. R., Craig, A. P., Bitz, C. M., and Weatherly, J. W. (2002). Parameterization improvements in an eddy-permitting ocean model for climate. *Journal of Climate*, 15(12):1447–1459. doi:10.1175/1520-0442(2002)015<1447:PIIAEP>2.0.CO;2.

Gent, P. R. and McWilliams, J. C. (1990). Isopycnal Mixing in Ocean Circulation Models. *Journal of Physical Oceanography*, 20(1):150–155. doi:10.1175/1520-0485(1990)020<0150:IMIOCM>2.0.CO;2.

Gent, P. R., Willebrand, J., McDougall, T. J., and McWilliams, J. C. (1995). Parameterizing Eddy-Induced Tracer Transports in Ocean Circulation Models. *Journal of Physical Oceanography*, 25(4):463–474. doi:10.1175/1520-0485(1995)025<0463:PEITTI>2.0.CO;2.

Gersonde, R., Crosta, X., Abelmann, A., and Armand, L. (2005). Sea-surface temperature and sea ice distribution of the Southern Ocean at the EPILOG Last Glacial Maximum - A circum-Antarctic view based on siliceous microfossil records. *Quaternary Science Reviews*, 24(7-9):869–896. doi:10.1016/j.quascirev.2004.07.015.

Giese, B. S., Seidel, H. F., Compo, G. P., and Sardeshmukh, P. D. (2016). An ensemble of ocean reanalyses for 1815-2013 with sparse observational input. *Journal of Geophysical Research: Oceans*, 121(9):6891–6910. doi:10.1002/2016JC012079.

Gildor, H. and Tziperman, E. (2000). Sea ice as the glacial cycles' climate switch: role of seasonal and orbital forcing. *Paleoceanography*, 15(6):605–615. doi:10.1029/1999PA000461.

Gille, S. T. (2002). Warming of the Southern Ocean since the 1950s. *Science*, 295(5558):1275–1277. doi:10.1126/science.1065863.

Gille, S. T. (2008). Decadal-scale temperature trends in the Southern Hemisphere ocean. *Journal of Climate*, 21(18):4749–4765. doi:10.1175/2008JCLI2131.1.

Giorgetta, M. A., Jungclaus, J. H., Reick, C. H., Legutke, S., Bader, J., Böttinger, M., Brovkin, V., Crueger, T., Esch, M., Fieg, K., Glushak, K., Gayler, V., Haak, H., Hollweg, H.-D., Ilyina, T., Kinne, S., Kornblueh, L., Matei, D., Mauritsen, T., Mikolajewicz, U., Mueller, W., Notz, D., Pithan, F., Raddatz, T., Rast, S., Redler, R., Roeckner, E., Schmidt, H., Schnur, R., Segschneider, J., Six, K. D., Stockhause, M., Timmreck, C., Wegner, J., Widmann, H., Wieners, K.-H., Claussen, M., Marotzke, J., and Stevens, B. (2013). Climate and carbon cycle changes from 1850 to 2100 in MPI-ESM simulations for the Coupled Model Intercomparison Project phase 5. *Journal of Advances in Modeling Earth Systems*, 5(3):572–597. doi:10.1002/jame.20038.

Giorgetta et al. (2012a). CMIP5 Simulations of the Max Planck Institute for Meteorology (MPI-M) Based on the MPI-ESM-LR Model: The Historical Experiment, Served by ESGF, World Data Cent. for Clim. doi:10.1594/WDCC/CMIP5.MXELhi.

Giorgetta et al. (2012b). CMIP5 Simulations of the Max Planck Institute for Meteorology (MPI-M) Based on the MPI-ESM-LR Model: The piControl Experiment, Served by ESGF, World Data Cent. for Clim. doi:10.1594/WDCC/CMIP5.MXELpc.

Giorgetta et al. (2012c). CMIP5 Simulations of the Max Planck Institute for Meteorology (MPI-M) Based on the MPI-ESM-LR Model: The RCP45 Experiment, Served by ESGF, World Data Cent. for Clim. doi:10.1594/WDCC/CMIP5.MXELr4.

Gladstone, R. M., Bigg, G. R., and Nicholls, K. W. (2001). Iceberg trajectory modeling and meltwater injection in the Southern Ocean. *Journal of Geophysical Research: Oceans*, 106(C9):19903–19915. doi:10.1029/2000JC000347.

Gleckler, P. J., Durack, P. J., Stouffer, R. J., Johnson, G. C., and Forest, C. E. (2016). Industrial-era global ocean heat uptake doubles in recent decades. *Nature Climate Change*, 6(4):394–398. doi:10.1038/nclimate2915.

Gnanadesikan, A. (1999). A Simple Predictive Model for the Structure of the Oceanic Pycnocline. *Science*, 283(5410):2077–2079. doi:10.1126/science.283.5410.2077.

Goldberg, D. N., Little, C. M., Sergienko, O. V., Gnanadesikan, A., Hallberg, R., and Oppenheimer, M. (2012). Investigation of land ice-ocean interaction with a fully coupled ice-ocean model: 1. Model description and behavior. *Journal of Geophysical Research: Earth Surface*, 117(F2):F02037. doi:10.1029/2011JF002246.

Golledge, N. R., Kowalewski, D. E., Naish, T. R., Levy, R. H., Fogwill, C. J., and Gasson, E. G. W. (2015). The multi-millennial Antarctic commitment to future sea-level rise. *Nature*, 526(7573):421–425. doi:10.1038/nature15706.

Good, S. A., Martin, M. J., and Rayner, N. A. (2013). EN4: Quality controlled ocean temperature and salinity profiles and monthly objective analyses with uncertainty estimates. *Journal of Geophysical Research: Oceans*, 118(12):6704–6716. doi:10.1002/2013JC009067.

Goosse, H., Deleersnijder, E., Fichefet, T., and England, M. H. (1999). Sensitivity of a global coupled ocean-sea ice model to the parameterization of vertical mixing. *J. Geophys. Res.*, 104(C6):13681–13695. doi:10.1029/1999JC900099.

Goosse, H. and Fichefet, T. (1999). Importance of ice-ocean interactions for the global ocean circulation: A model study. *J. Geophys. Res.*, 104(C10):23337–23355.

Goosse, H. and Zunz, V. (2014). Decadal trends in the Antarctic sea ice extent ultimately controlled by ice-ocean feedback. *The Cryosphere*, 8(2):453–470. doi:10.5194/tc-8-453-2014.

Gordon, A. L. (1986a). Interocean exchange of thermocline water. *J. Geophys. Res.*, 91(C4):5037–5046. doi:10.1029/JC091iC04p05037.

Gordon, A. L. (1986b). Is there a global scale ocean circulation? *Eos, Transactions American Geophysical Union*, 67(9):109. doi:10.1029/EO067i009p00109.

Gordon, A. L. (1991). Two Stable Modes of Southern Ocean Winter Stratification. In Chu, P. C. and Gascard, J. C., editors, *Elsevier Oceanography Series*, volume 57 of *Elsevier Oceanography Series*, pages 17–35. Elsevier. doi:10.1016/S0422-9894(08)70058-8.

Gordon, A. L. (2012). Circumpolar View of the Southern Ocean from 1962 to 1992. *Oceanography*, 25(3):18–23. doi:10.5670/oceanog.2012.69.

Gordon, A. L. (2014). Southern Ocean polynya. *Nature Climate Change*, 4(April):249–250. doi:10.1038/nclimate2179.

Gordon, A. L. (2016). The marine hydrological cycle: the ocean's floods and droughts. *Geophysical Research Letters*, 43:7649–7652. doi:10.1002/2016GL070279.

Gordon, A. L. and Huber, B. A. (1984). Thermohaline stratification below the Southern Ocean sea ice. *Journal of Geophysical Research*, 89(C1):641–648. doi:10.1029/JC089iC01p00641.

Gordon, A. L. and Huber, B. A. (1990). Southern ocean winter mixed layer. *Journal of Geophysical Research*, 95(C7):11655. doi:10.1029/JC095iC07p11655.

Gordon, A. L., Huber, B. A., and Busecke, J. (2015). Bottom water export from the western Ross Sea, 2007 through 2010. *Geophysical Research Letters*, 42(13):5387–5394. doi:10.1002/2015GL064457.

Gordon, A. L. and Taylor, H. W. (1975). Seasonal Change of Antarctic Sea Ice Cover. *Science*, 187(4174):346–347.

GRDC (2014). Annual freshwater inputs to the oceans—5 latitudinal bands (1971-2000). Global Freshwater Fluxes into the World Oceans., Koblenz, Germany. Global Runoff Data Centre, Federal Institute of Hydrology (BfG).

Griffies, S. M., Böning, C., Bryan, F. O., Chassignet, E. P., Gerdes, R., Hasumi, H., Hirst, A., Treguier, A.-M., and Webb, D. (2000a). Developments in ocean climate modelling. *Journal of Computational Physics*, 2(3-4):123–192. doi:10.1016/S1463-5003(00)00014-7.

Griffies, S. M., Pacanowski, R. C., and Hallberg, R. W. (2000b). Spurious Diapycnal Mixing Associated with Advection in a z-Coordinate Ocean Model. *Monthly Weather Review*, 128(3):538–564. doi:10.1175/1520-0493(2000)128<0538:SDMAWA>2.0.CO;2.

Gruber, N. (2011). Warming up, turning sour, losing breath: ocean biogeochemistry under global change. *Philosophical Transactions of the Royal Society A*, 369(1943):1980–1996. doi:10.1098/rsta.2011.0003.

Gruber, N., Frenzel, H., Doney, S. C., Marchesiello, P., McWilliams, J. C., Moisan, J. R., Oram, J. J., Plattner, G. K., and Stolzenbach, K. D. (2006). Eddy-resolving simulation of plankton ecosystem dynamics in the California Current System. *Deep-Sea Research Part I: Oceanographic Research Papers*, 53(9):1483–1516. doi:10.1016/j.dsr.2006.06.005.

Gruber, N., Friedlingstein, P., Field, C. B., Valentini, R., Heimann, M., Richey, J. E., Lankao, P. R., Schulze, E.-D., and Chen, C.-T. A. (2004). The vulnerability of the carbon cycle in the 21st century: An assessment of carbon-climate-human interactions. In Field, C. B. and Raupach, M. R., editors, *The Global Carbon Cycle: Integrating Humans, Climate, and the Natural World*, volume 62, chapter 3, pages 45–76. Island Press, Washington, D. C.

Gruber, N., Gloor, M., Mikaloff Fletcher, S. E., Doney, S. C., Dutkiewicz, S., Follows, M. J., Gerber, M., Jacobson, A. R., Joos, F., Lindsay, K., Menemenlis, D., Mouchet, A., Müller, S. A., Sarmiento, J. L., and Takahashi, T. (2009). Oceanic sources, sinks, and transport of atmospheric CO_2. *Global Biogeochemical Cycles*, 23(1):GB1005. doi:10.1029/2008GB003349.

Gruber, N., Lachkar, Z., Frenzel, H., Marchesiello, P., Münnich, M., McWilliams, J. C., Nagai, T., and Plattner, G.-K. (2011). Eddy-induced reduction of biological production in eastern bounday upwelling systems. *Nature Geoscience*, 4(October):1–6. doi:doi:10.1038/ngeo1273.

Gruber, N. and Sarmiento, J. L. (2002). Large-scale biogeochemical/physical interactions in elemental cycles. In Robinson, A. R., McCarthy, J. J., and Rothschild, B. J., editors, *The Sea: Biological-Physical Interactions in the Oceans*, pages 337–399. John Wiley and Sons, Ltd., New York.

Haidvogel, D. B., Arango, H., Budgell, W. P., Cornuelle, B. D., Curchitser, E., Di Lorenzo, E., Fennel, K., Geyer, W. R., Hermann, A. J., Lanerolle, L., Levin, J., McWilliams, J. C., Miller, A. J., Moore, A. M., Powell, T. M., Shchepetkin, A. F., Sherwood, C. R., Signell, R. P., Warner, J. C., and Wilkin, J. (2008). Ocean forecasting in terrain-following coordinates: Formulation and skill assessment of the Regional Ocean Modeling System. *Journal of Computational Physics*, 227(7):3595–3624. doi:10.1016/j.jcp.2007.06.016.

Haidvogel, D. B., Arango, H. G., Hedstrom, K., Beckmann, A., Malanotte-Rizzoli, P., and Shchepetkin, A. F. (2000). Model evaluation experiments in the North Atlantic Basin: Simulations in nonlinear terrain-following coordinates. *Dynamics of Atmospheres and Oceans*, 32(3-4):239–281. doi:10.1016/S0377-0265(00)00049-X.

Haidvogel, D. B. and Beckmann, a. (1999). *Numerical Ocean Circulation Modeling*, volume 2 of *Environmental Science and Management*. Imperial College Press. doi:10.2277/0521781825.

Haidvogel, D. B., Wilkin, J. L., and Young, R. (1991). A semi-spectral primitive equation ocean circulation model using vertical sigma and orthogonal curvilinear horizontal coordinates. *Journal of Computational Physics*, 94(1):151–185. doi:10.1016/0021-9991(91)90141-7.

Häkkinen, S. and Mellor, G. L. (1992). Modeling the seasonal variability of a coupled Arctic ice-ocean system. *Journal of Geophysical Research*, 97(C12):20285. doi:10.1029/92JC02037.

Hallberg, R. (2013). Using a resolution function to regulate parameterizations of oceanic mesoscale eddy effects. *Ocean Modelling*, 72:92–103. doi:10.1016/j.ocemod.2013.08.007.

Hallberg, R. and Gnanadesikan, A. (2001). An Exploration of the Role of Transient Eddies in Determining the Transport of a Zonally Reentrant Current. *Journal of Physical Oceanography*, 31(2000):3312–3330. doi:10.1175/1520-0485(2001)031<3312:AEOTRO>2.0.CO;2.

Hallberg, R. and Gnanadesikan, A. (2006). The Role of Eddies in Determining the Structure and Response of the Wind-Driven Southern Hemisphere Overturning: Results from the Modeling Eddies in the Southern Ocean (MESO) Project. *Journal of Physical Oceanography*, 36(12):2232–2252. doi:10.1175/JPO2980.1.

Hansen, J., Ruedy, R., Sato, M., and Lo, K. (2010). Global surface temperature change. *Reviews of Geophysics*, 48(4):RG4004. doi:10.1029/2010RG000345.

Harms, S., Fahrbach, E., and Strass, V. H. (2001). Sea ice transports in the Weddell Sea. *Journal of Geophysical Research*, 106(C5):9057–9073. doi:10.1029/1999JC000027.

Hartin, C. A., Fine, R. A., Sloyan, B. M., Talley, L. D., Chereskin, T. K., and Happell, J. (2011). Formation rates of Subantarctic mode water and Antarctic intermediate water within the South Pacific. *Deep-Sea Research Part I*, 58(5):524–534. doi:10.1016/j.dsr.2011.02.010.

Hasselmann, K. (1991). Ocean circulation and climate change. *Tellus B*, 43(4):82–103. doi:10.1034/j.1600-0889.1991.t01-2-00008.x.

Hauck, J., Völker, C., Wang, T., Hoppema, M., Losch, M., and Wolf-Gladrow, D. A. (2013). Seasonally different carbon flux changes in the Southern Ocean in response to the Southern Annular Mode. *Global Biogeochemical Cycles*, 27(4):1236–1245. doi:10.1002/2013GB004600.

Haug, G. H., Sigman, D. M., Tiedemann, R., Pedersen, T. F., and Sarntheink, M. (1999). Onset of permanent stratification in the subarctic Pacific Ocean. *Nature*, 401(6755):21–24. doi:10.1038/44550.

Haumann, F. A. (2011). Dynamical interaction between atmosphere and sea ice in Antarctica. *Master's Thesis: Utrecht University*, p. 131.

Haumann, F. A., Gruber, N., Münnich, M., Frenger, I., and Kern, S. (2016a). Antarctic sea-ice freshwater fluxes associated with freezing, transport, and melting, Zurich, Switzerland. ETH Zurich. doi:10.16904/8.

Haumann, F. A., Gruber, N., Münnich, M., Frenger, I., and Kern, S. (2016b). Sea-ice transport driving Southern Ocean salinity and its recent trends. *Nature*, 537(7618):89–92. doi:10.1038/nature19101.

Haumann, F. A., Münnich, M., Gruber, N., and Eberenz, S. (2017). Recent changes of Southern Ocean waters induced by sea-ice freshwater fluxes. *Journal of Climate*, In prep.

Haumann, F. A., Notz, D., and Schmidt, H. (2014). Anthropogenic influence on recent circulation-driven Antarctic sea ice changes. *Geophysical Research Letters*, 41(23):8429–8437. doi:10.1002/2014GL061659.

Hays, J. D., Imbrie, J., and Shackleton, N. J. (1976). Variations in the Earth's Orbit: Pacemaker of the Ice Ages. *Science*, 194(4270):1121–1132. doi:10.1126/science.194.4270.1121.

Heil, P., Fowler, C. W., Maslanik, J. A., Emery, W. J., and Allison, I. (2001). A comparison of East Antarctic sea-ice motion derived using drifting buoys and remote sensing. *Annals of Glaciology*, 33(1):139–144. doi:10.3189/172756401781818374.

Heinze, C., Maier-Reimer, E., and Winn, K. (1991). Glacial pCO_2 Reduction by the World Ocean: Experiments With the Hamburg Carbon Cycle Model. *Paleoceanography*, 6(4):395–430. doi:10.1029/91PA00489.

Hellmer, H. H. (2004). Impact of Antarctic ice shelf basal melting on sea ice and deep ocean properties. *Geophysical Research Letters*, 31(10):L10307. doi:10.1029/2004GL019506.

Hellmer, H. H., Huhn, O., Gomis, D., and Timmermann, R. (2011). On the freshening of the northwestern Weddell Sea continental shelf. *Ocean Science*, 7(3):305–316. doi:10.5194/os-7-305-2011.

Hellmer, H. H., Kauker, F., Timmermann, R., Determann, J., and Rae, J. (2012). Twenty-first-century warming of a large Antarctic ice-shelf cavity by a redirected coastal current. *Nature*, 485(7397):225–228. doi:10.1038/nature11064.

Helm, K. P., Bindoff, N. L., and Church, J. A. (2010). Changes in the global hydrological-cycle inferred from ocean salinity. *Geophysical Research Letters*, 37(18):L18701. doi:10.1029/2010GL044222.

Helm, K. P., Bindoff, N. L., and Church, J. A. (2011). Observed decreases in oxygen content of the global ocean. *Geophysical Research Letters*, 38(23):L23602. doi:10.1029/2011GL049513.

Henning, C. C. and Vallis, G. K. (2005). The Effects of Mesoscale Eddies on the Stratification and Transport of an Ocean with a Circumpolar Channel. *Journal of Physical Oceanography*, 35(5):880–896. doi:10.1175/JPO2727.1.

Heuzé, C., Heywood, K. J., Stevens, D. P., and Ridley, J. K. (2013). Southern Ocean bottom water characteristics in CMIP5 models. *Geophysical Research Letters*, 40(7):1409–1414. doi:10.1002/grl.50287.

Heuzé, C., Heywood, K. J., Stevens, D. P., and Ridley, J. K. (2015). Changes in global ocean bottom properties and volume transports in CMIP5 models under climate change scenarios. *Journal of Climate*, 28(8):2917–2944. doi:10.1175/JCLI-D-14-00381.1.

Hewitt, A. J., Booth, B. B. B., Jones, C. D., Robertson, E. S., Wiltshire, A. J., Sansom, P. G., Stephenson, D. B., and Yip, S. (2016). Sources of uncertainty in future projections of the carbon cycle. *Journal of Climate*, 29:7203–7213. doi:10.1175/JCLI-D-16-0161.1.

Hobbs, W. R., Massom, R., Stammerjohn, S., Reid, P., Williams, G., and Meier, W. (2016). A review of recent changes in Southern Ocean sea ice, their drivers and forcings. *Global and Planetary Change*, 143:228–250. doi:10.1016/j.gloplacha.2016.06.008.

Hogg, A. M. (2010). An Antarctic Circumpolar Current driven by surface buoyancy forcing. *Geophysical Research Letters*, 37(23):L23601. doi:10.1029/2010GL044777.

Hogg, A. M., Meredith, M. P., Chambers, D. P., Abrahamsen, E. P., Hughes, C. W., and Morrison, A. K. (2015). Recent trends in the Southern Ocean eddy field. *Journal of Geophysical Research C: Oceans*, 120(1):257–267. doi:10.1002/2014JC010470.

Holland, D. M. and Jenkins, A. (1999). Modeling Thermodynamic Ice-Ocean Interactions at the Base of an Ice Shelf. *Journal of Physical Oceanography*, 29(8):1787–1800. doi:10.1175/1520-0485(1999)029<1787:MTIOIA>2.0.CO;2.

Holland, P. R. (2014). The seasonality of Antarctic sea ice trends. *Geophysical Research Letters*, 41(12):4230–4237. doi:10.1002/2014GL060172.

Holland, P. R. and Kwok, R. (2012). Wind-driven trends in Antarctic sea-ice drift. *Nature Geoscience*, 5(12):872–875. doi:10.1038/ngeo1627.

Hoppema, M. (2004). Weddell Sea turned from source to sink for atmospheric CO_2 between pre-industrial time and present. *Global and Planetary Change*, 40(3):219–231. doi:10.1016/j.gloplacha.2003.08.001.

Hosking, J. S., Orr, A., Marshall, G. J., Turner, J., and Phillips, T. (2013). The Influence of the Amundsen-Bellingshausen Seas Low on the Climate of West Antarctica and Its Representation in Coupled Climate Model Simulations. *Journal of Climate*, 26(17):6633–6648. doi:10.1175/JCLI-D-12-00813.1.

Huang, C. J., Qiao, F., Shu, Q., and Song, Z. (2012). Evaluating austral summer mixed-layer response to surface wave-induced mixing in the Southern Ocean. *Journal of Geophysical Research: Oceans*, 117(C11):C00J18. doi:10.1029/2012JC007892.

Hunke, E. C. (2001). Viscous–Plastic Sea Ice Dynamics with the EVP Model: Linearization Issues. *Journal of Computational Physics*, 170(1):18–38. doi:10.1006/jcph.2001.6710.

Hunke, E. C. and Dukowicz, J. K. (1997). An Elastic–Viscous–Plastic Model for Sea Ice Dynamics. *Journal of Physical Oceanography*, 27:1849–1867. doi:10.1175/1520-0485(1997)027<1849:AEVPMF>2.0.CO;2.

Huybers, P. and Wunsch, C. (2005). Obliquity pacing of the late Pleistocene glacial terminations. *Nature*, 434(7032):491–494. doi:10.1038/nature03401.

Ilicak, M., Adcroft, A. J., Griffies, S. M., and Hallberg, R. W. (2012). Spurious dianeutral mixing and the role of momentum closure. *Ocean Modelling*, 45-46:37–58. doi:10.1016/j.ocemod.2011.10.003.

Ilyina, T. and Friedlingstein, P. (2016). WCRP Grand Challenge: Carbon feedbacks in the climate system. Technical report, World Climate Research Programme.

Imbrie, J., Berger, A., Boyle, E. A., Clemens, S. C., Duffy, A., Howard, W. R., Kukla, G., Kutzbach, J., Martinson, D. G., McIntyre, A., Mix, A. C., Molfino, B., Morley, J. J., Peterson, L. C., Pisias, N. G., Prell, W. L., Raymo, M. E., Shackleton, N. J., and Toggweiler, J. R.

(1993). On the structure and origin of major glaciation cycles 2. The 100,000-year cycle. *Paleoceanography*, 8(6):699–735. doi:10.1029/93PA02751.

Imbrie, J. and Imbrie, J. Z. (1980). Modeling the climatic response to orbital variations. *Science*, 207(4434):943–953. doi:10.1126/science.207.4434.943.

Ingleby, B. and Huddleston, M. (2007). Quality control of ocean temperature and salinity profiles Historical and real-time data. *Journal of Marine Systems*, 65(1-4):158–175. doi:10.1016/j.jmarsys.2005.11.019.

IOC, SCOR, and IAPSO (2010). The international thermodynamic equation of seawater - 2010: Calculation and use of thermodynamic properties. Technical report, Intergovernmental Oceanographic Commission, Manuals and Guides No. 56, UNESCO.

IPCC (2013). *Climate Change 2013: The Physical Science Basis. Contribution of Working Group I to the Fifth Assessment Report of the Intergovernmental Panel on Climate Change*. [Stocker, T.F., D. Qin, G.-K. Plattner, M. Tignor, S.K. Allen, J. Boschung, A. Nauels, Y. Xia, V. Bex and P.M. Midgley (eds.)]. Cambridge University Press, Cambridge, United Kingdom and New York, NY, USA.

Ito, T. and Marshall, J. (2008). Control of Lower-Limb Overturning Circulation in the Southern Ocean by Diapycnal Mixing and Mesoscale Eddy Transfer. *Journal of Physical Oceanography*, 38(12):2832–2845. doi:10.1175/2008JPO3878.1.

Iudicone, D., Madec, G., Blanke, B., and Speich, S. (2008). The Role of Southern Ocean Surface Forcings and Mixing in the Global Conveyor. *Journal of Physical Oceanography*, 38(7):1377. doi:10.1175/2008JPO3519.1.

Iudicone, D., Rodgers, K. B., Schopp, R., and Madec, G. (2007). An exchange window for the injection of Antarctic Intermediate Water into the South Pacific. *Journal of Physical Oceanography*, 37(1):31–49. doi:10.1175/JPO2985.1.

Iudicone, D., Rodgers, K. B., Stendardo, I., Aumont, O., Madec, G., Bopp, L., Mangoni, O., and Ribera D'Alcala', M. (2011). Water masses as a unifying framework for understanding the Southern Ocean Carbon Cycle. *Biogeosciences*, 8(5):1031–1052. doi:10.5194/bg-8-1031-2011.

Jaccard, S. L., Hayes, C. T., Martínez-García, A., Hodell, D. A., Anderson, R. F., Sigman, D. M., and Haug, G. H. (2013). Two modes of change in Southern Ocean productivity over the past million years. *Science*, 339(6126):1419–23. doi:10.1126/science.1227545.

Jackett, D. R. and Mcdougall, T. J. (1995). Minimal Adjustment of Hydrographic Profiles to Achieve Static Stability. *Journal of Atmospheric and Oceanic Technology*, 12(2):381–389. doi:10.1175/1520-0426(1995)012<0381:MAOHPT>2.0.CO;2.

Jacobs, S. S. (1991). On the nature and significance of the Antarctic Slope Front. *Marine Chemistry*, 35(1-4):9–24. doi:10.1016/S0304-4203(09)90005-6.

Jacobs, S. S. (2004). Bottom water production and its links with the thermohaline circulation. *Antarctic Science*, 16(4):427–437. doi:10.1017/S095410200400224X.

Jacobs, S. S., Fairbanks, R. G., and Horibe, Y. (1985). Origin and evolution of water masses near the Antarctic continental margin: Evidence from $H_2{}^{18}O/H_2{}^{16}O$ ratios in seawater. In Jacobs, S., editor, *Oceanology of the Antarctic Continental Shelf*, volume 43 of *Antarctic Research Series*, pages 59–85. American Geophysical Union, Washington, D. C. doi:10.1029/AR043.

Jacobs, S. S. and Giulivi, C. F. (2010). Large multidecadal salinity trends near the Pacific-Antarctic continental margin. *Journal of Climate*, 23(17):4508–4524. doi:10.1175/2010JCLI3284.1.

Jacobs, S. S., Giulivi, C. F., and Mele, P. A. (2002). Freshening of the Ross Sea during the late 20th century. *Science*, 297(5580):386–389. doi:10.1126/science.1069574.

Jacobs, S. S., Jenkins, A., Hellmer, H. H., Giulivi, C. F., Nitsche, F., Huber, B., and Guerrero, R. (2012). The Amundsen Sea and the Antarctic Ice Sheet. *Ocenaography*, 25(3):154–163. doi:10.5670/oceanog.2012.90.

Jin, X., Gruber, N., Frenzel, H., Doney, S. C., and McWilliams, J. C. (2008). The impact on atmospheric CO_2 of iron fertilization induced changes in the ocean's biological pump. *Biogeosciences*, 5(2):385–406. doi:10.5194/bg-5-385-2008.

Jones, J. M., Gille, S. T., Goosse, H., Abram, N. J., Canziani, P. O., Charman, D. J., Clem, K. R., Crosta, X., de Lavergne, C., Eisenman, I., England, M. H., Fogt, R. L., Frankcombe, L. M., Marshall, G. J., Masson-Delmotte, V., Morrison, A. K., Orsi, A. J., Raphael, M. N., Renwick, J. A., Schneider, D. P., Simpkins, G. R., Steig, E. J., Stenni, B., Swingedouw, D., and Vance, T. R. (2016). Assessing recent trends in high-latitude Southern Hemisphere surface climate. *Nature Climate Change*, 6(10):917–926. doi:10.1038/nclimate3103.

Joos, F., Plattner, G.-K., Stocker, T. F., Marchal, O., and Schmittner, A. (1999). Global warming and marine carbon cycle feedbacks on future atmospheric CO_2. *Science*, 284(5413):464–467. doi:10.1126/science.284.5413.464.

Jouzel, J., Masson-Delmotte, V., Cattani, O., Dreyfus, G., Falourd, S., Hoffmann, G., Minster, B., Nouet, J., Barnola, J. M., Chappellaz, J., Fischer, H., Gallet, J. C., Johnsen, S., Leuenberger, M., Loulergue, L., Luethi, D., Oerter, H., Parrenin, F., Raisbeck, G., Raynaud, D., Schilt, A., Schwander, J., Selmo, E., Souchez, R., Spahni, R., Stauffer, B., Steffensen, J. P., Stenni, B., Stocker, T. F., Tison, J. L., Werner, M., and Wolff, E. W. (2007). Orbital and millennial Antarctic climate variability over the past 800,000 years. *Science*, 317(5839):793–796. doi:10.1126/science.1141038.

Jullion, L., Naveira Garabato, A. C., Meredith, M. P., Holland, P. R., Courtois, P., and King, B. A. (2013). Decadal Freshening of the Antarctic Bottom Water Exported from the Weddell Sea. *Journal of Climate*, 26(20):8111–8125. doi:10.1175/JCLI-D-12-00765.1.

Jungclaus, J. H., Fischer, N., Haak, H., Lohmann, K., Marotzke, J., Matei, D., Mikolajewicz, U., Notz, D., and Von Storch, J. S. (2013). Characteristics of the ocean simulations in the Max Planck Institute Ocean Model (MPIOM) the ocean component of the MPI-Earth system model. *Journal of Advances in Modeling Earth Systems*, 5(2):422–446. doi:10.1002/jame.20023.

Kanarska, Y., Shchepetkin, A., and McWilliams, J. C. (2007). Algorithm for non-hydrostatic dynamics in the Regional Oceanic Modeling System. *Ocean Modelling*, 18(3-4):143–174. doi:10.1016/j.ocemod.2007.04.001.

Karsten, R. H., Marshall, J., Karsten, R. H., and Marshall, J. (2002). Constructing the Residual Circulation of the ACC from Observations. *Journal of Physical Oceanography*, 32(12):3315–3327. doi:10.1175/1520-0485(2002)032<3315:CTRCOT>2.0.CO;2.

Kern, S., Ozsoy-Çiçek, B., and Worby, A. (2016). Antarctic sea-ice thickness retrieval from ICESat: Inter-comparison of different approaches. *Remote Sensing*, 8(7):538. doi:10.3390/rs8070538.

Kern, S. and Spreen, G. (2015). Uncertainties in Antarctic sea-ice thickness retrieval from ICESat. *Annals of Glaciology*, 56(69):107–119. doi:10.3189/2015AoG69A736.

Kessler, A. and Tjiputra, J. (2016). The Southern Ocean as aconstraint to reduce uncertainty in future ocean carbon sinks. *Earth System Dynamics*, 7(2):295–312. doi:10.5194/esd-7-295-2016.

Key, R. M., Kozyr, A., Sabine, C. L., Lee, K., Wanninkhof, R., Bullister, J. L., Feely, R. A., Millero, F. J., Mordy, C., and Peng, T.-H. (2004). A global ocean carbon climatology: Results from Global Data Analysis Project (GLODAP). *Global Biogeochemical Cycles*, 18(4):GB4031. doi:10.1029/2004GB002247.

Khatiwala, S., Primeau, F., and Hall, T. (2009). Reconstruction of the history of anthropogenic CO_2 concentrations in the ocean. *Nature*, 462(7271):346–349. doi:10.1038/nature08526.

Khatiwala, S., Tanhua, T., Mikaloff Fletcher, S., Gerber, M., Doney, S. C., Graven, H. D., Gruber, N., McKinley, G. A., Murata, A., Ríos, A. F., and Sabine, C. L. (2013). Global ocean storage of anthropogenic carbon. *Biogeosciences*, 10(4):2169–2191. doi:10.5194/bg-10-2169-2013.

Killworth, P. D., Webb, D. J., Stainforth, D., and Paterson, S. M. (1991). The Development of a Free-Surface Bryan-Cox-Semtner Ocean Model. *Journal of Physical Oceanography*, 21(9):1333–1348. doi:10.1175/1520-0485(1991)021<1333:TDOAFS>2.0.CO;2.

Kimura, N. (2004). Sea ice motion in response to surface wind and ocean current in the Southern Ocean. *Journal of the Meteorological Society of Japan*, 82(4):1223–1231. doi:10.2151/jmsj.2004.1223.

Kirkman, C. H. and Bitz, C. M. (2011). The effect of the sea ice freshwater flux on Southern Ocean temperatures in CCSM3: deep-ocean warming and delayed surface warming. *Journal of Climate*, 24(9):2224–2237. doi:10.1175/2010JCLI3625.1.

Kjellsson, J., Holland, P. R., Marshall, G. J., Mathiot, P., Aksenov, Y., Coward, A. C., Bacon, S., Megann, A. P., and Ridley, J. (2015). Model sensitivity of the Weddell and Ross seas, Antarctica, to vertical mixing and freshwater forcing. *Ocean Modelling*, 94:141–152. doi:10.1016/j.ocemod.2015.08.003.

Knox, F. and McElroy, M. B. (1984). Changes in Atmospheric CO_2: Influence of the Marine Biota at High Latitude. *Journal of Geophysical Research*, 89(D3):4629–4637. doi:10.1029/JD089iD03p04629.

Knutti, R. and Sedláček, J. (2013). Robustness and uncertainties in the new CMIP5 climate model projections. *Nature Climate Change*, 3:369–373. doi:10.1038/nclimate1716.

Koenig, Z., Provost, C., Ferrari, R., Sennéchael, N., and Rio, M.-H. (2014). Volume transport of the Antarctic Circumpolar Current: Production and validation of a 20 year long time series obtained from in situ and satellite observations. *Journal of Geophysical Research*, 119(8):5407–5433. doi:10.1002/2014jc009966.

Köhler, P., Bintanja, R., Joos, F., Knutti, R., Lohmann, G., and Masson-Delmotte, V. (2010). What caused Earth's temperature variations during the last 800,000 years? Data-based evidence on radiative forcing and constraints on climate sensitivity. *Quaternary Science Reviews*, 29(1):129–145. doi:10.1016/j.quascirev.2009.09.026.

Komuro, Y. and Hasumi, H. (2003). Effects of surface freshwater flux induced by sea ice transport on the global thermohaline circulation. *Journal of Geophysical Research*, 108(C2):3047. doi:10.1029/2002JC001476.

Kostov, Y., Marshall, J., Hausmann, U., Armour, K. C., Ferreira, D., and Holland, M. M. (2016). Fast and slow responses of Southern Ocean sea surface temperature to SAM in coupled climate models. *Climate Dynamics*, pages 1–15. doi:10.1007/s00382-016-3162-z.

Kottmeier, C., Olf, J., Frieden, W., and Roth, R. (1992). Wind forcing and ice motion in the Weddell Sea region. *Journal of Geophysical Research*, 97(D18):20373–20383. doi:10.1029/92JD02171.

Kottmeier, C. and Sellmann, L. (1996). Atmospheric and oceanic forcing of Weddell Sea ice motion. *Journal of Geophysical Research: Oceans*, 101(C9):20809–20824. doi:10.1029/96JC01293.

Kurtz, N. T. and Markus, T. (2012). Satellite observations of Antarctic sea ice thickness and volume. *Journal of Geophysical Research: Oceans*, 117(C8):C08025. doi:10.1029/2012JC008141.

Kusahara, K. and Hasumi, H. (2014). Pathways of basal meltwater from Antarctic ice shelves: A model study. *Journal of Geophysical Research: Oceans*, 119(9):5690–5704. doi:10.1002/2014JC009915.

Kwok, R. (2005). Ross sea ice motion, area flux, and deformation. *Journal of Climate*, 18(18):3759–3776. doi:10.1175/JCLI3507.1.

Kwok, R. and Maksym, T. (2014). Snow depth of the Weddell and Bellingshausen sea ice covers from IceBridge surveys in 2010 and 2011: An examination. *Journal of Geophysical Research Oceans*, 119(7):4141–4167. doi:10.1002/2014JC009943.

Kwok, R., Schweiger, A., Rothrock, D. A., Pang, S., and Kottmeier, C. (1998). Sea ice motion from satellite passive microwave imagery assessed with ERS SAR and buoy motions. *Journal of Geophysical Research*, 103(C4):8191–8214. doi:10.1029/97JC03334.

Kwon, E. Y. (2013). Temporal variability of transformation, formation, and subduction rates of upper Southern Ocean waters. *Journal of Geophysical Research: Oceans*, 118(11):6285–6302. doi:10.1002/2013JC008823.

Kwon, E. Y., Primeau, F., and Sarmiento, J. L. (2009). The impact of remineralization depth on the air-sea carbon balance. *Nature Geoscience*, 2(9):630–635. doi:10.1038/ngeo612.

Lachkar, Z. and Gruber, N. (2011). What controls biological production in coastal upwelling systems? Insights from a comparative modeling study. *Biogeosciences*, 8(10):2961–2976. doi:10.5194/bg-8-2961-2011.

Lachkar, Z. and Gruber, N. (2013). Response of biological production and air-sea CO_2 fluxes to upwelling intensification in the California and Canary Current Systems. *Journal of Marine Systems*, 109-110(0):149–160. doi:10.1016/j.jmarsys.2012.04.003.

Lachlan-Cope, T. A., Connolley, W. M., and Turner, J. (2001). The Role of the Non-Axisymmetric Antarctic Orography in forcing the Observed Pattern of Variability of the Antarctic Climate. *Geophysical Research Letters*, 28(21):4111–4114. doi:10.1029/2001GL013465.

Landschützer, P., Gruber, N., and Bakker, D. C. E. (2015a). A 30 years observation-based global monthly gridded sea surface pCO_2 product from 1982 through 2011, Oak Ridge, Tennessee. Carbon Dioxide Information Analysis Center, Oak Ridge National Laboratory, US Department of Energy. doi:10.3334/CDIAC/OTG.SPCO2_1982_2011_ETH_SOM-FFN.

Landschützer, P., Gruber, N., Bakker, D. C. E., and Schuster, U. (2014a). An observation-based global monthly gridded sea surface pCO_2 product from 1998 through 2011 and its monthly climatology. Carbon Dioxide Information Analysis Center, Oak Ridge National Laboratory, US Department of Energy, Oak Ridge, Tennessee. doi:10.3334/CDIAC/OTG.SPCO2_1998_2011_ETH_SOM-FFN.

Landschützer, P., Gruber, N., Bakker, D. C. E., and Schuster, U. (2014b). Recent variability of the global ocean carbon sink. *Global Biogeochemical Cycles*, 28(9):927–949. doi:10.1002/2014GB004853.

Landschützer, P., Gruber, N., Haumann, F. A., Rödenbeck, C., Bakker, D. C. E., van Heuven, S., Hoppema, M., Metzl, N., Sweeney, C., and Takahashi, T. (2015b). The reinvigoration of the Southern Ocean carbon sink. *Science*, 349(6253):1221–1224. doi:10.1126/science.aab2620.

Large, W. G., McWilliams, J. C., and Doney, S. C. (1994). Oceanic vertical mixing: A review and a model with a nonlocal boundary layer parameterization. *Reviews of Geophysics*, 32(4):363. doi:10.1029/94RG01872.

Latif, M., Martin, T., Park, W., Latif, M., Martin, T., and Park, W. (2013). Southern Ocean Sector Centennial Climate Variability and Recent Decadal Trends. *Journal of Climate*, 26(19):7767–7782. doi:10.1175/JCLI-D-12-00281.1.

Le Quéré, C., Andrew, R. M., Canadell, J. G., Sitch, S., Korsbakken, J. I., Peters, G. P., Manning, A. C., Boden, T. A., Tans, P. P., Houghton, R. A., Keeling, R. F., Alin, S., Andrews, O. D., Anthoni, P., Barbero, L., Bopp, L., Chevallier, F., Chini, L. P., Ciais, P., Currie, K., Delire, C., Doney, S. C., Friedlingstein, P., Gkritzalis, T., Harris, I., Hauck, J., Haverd, V., Hoppema, M., Klein Goldewijk, K., Jain, A. K., Kato, E., Körtzinger, A., Landschützer, P., Lefèvre, N., Lenton, A., Lienert, S., Lombardozzi, D., Melton, J. R., Metzl, N., Millero, F., Monteiro, P. M. S., Munro, D. R., Nabel, J. E. M. S., Nakaoka, S.-i., O'Brien, K., Olsen, A., Omar, A. M., Ono, T., Pierrot, D., Poulter, B., Rödenbeck, C., Salisbury, J., Schuster, U., Schwinger, J., Séférian, R., Skjelvan, I., Stocker, B. D., Sutton, A. J., Takahashi, T., Tian, H., Tilbrook, B., van der Laan-Luijkx, I. T., van der Werf, G. R., Viovy, N., Walker, A. P., Wiltshire, A. J., and Zaehle, S. (2016). Global Carbon Budget 2016. *Earth System Science Data Discussions*. doi:10.5194/essd-2016-51.

Le Quéré, C., Moriarty, R., Andrew, R. M., Canadell, J. G., Sitch, S., Korsbakken, J. I., Friedlingstein, P., Peters, G. P., Andres, R. J., Boden, T. A., Houghton, R. A., House, J. I., Keeling, R. F., Tans, P., Arneth, A., Bakker, D. C. E., Barbero, L., Bopp, L., Chang, J., Chevallier, F., Chini, L. P., Ciais, P., Fader, M., Feely, R. A., Gkritzalis, T., Harris, I., Hauck, J., Ilyina, T., Jain, A. K., Kato, E., Kitidis, V., Klein Goldewijk, K., Koven, C., Landschützer, P., Lauvset, S. K., Lefèvre, N., Lenton, A., Lima, I. D., Metzl, N., Millero, F., Munro, D. R., Murata, A., Nabel, J. E. M. S., Nakaoka, S., Nojiri, Y., O'Brien, K., Olsen, A., Ono, T., Pérez, F. F., Pfeil, B., Pierrot, D., Poulter, B., Rehder, G., Rödenbeck, C., Saito, S., Schuster, U., Schwinger, J., Séférian, R., Steinhoff, T., Stocker, B. D., Sutton, A. J., Takahashi, T., Tilbrook, B., van der Laan-Luijkx, I. T., van der Werf, G. R., van Heuven, S., Vandemark, D., Viovy, N., Wiltshire, A., Zaehle, S., and Zeng, N. (2015). Global Carbon Budget 2015. *Earth System Science Data*, 7(2):349–396. doi:10.5194/essd-7-349-2015.

Le Quéré, C., Raupach, M. R., Canadell, J. G., and Al., G. M. (2009). Trends in the sources and sinks of carbon dioxide. *Nature Geoscience*, 2(12):831–836. doi:10.1038/ngeo689.

Le Quéré, C., Rödenbeck, C., Buitenhuis, E. T., Conway, T. J., Langenfelds, R., Gomez, A., Labuschagne, C., Ramonet, M., Nakazawa, T., Metzl, N., Gillett, N. P., and Heimann, M. (2007). Saturation of the Southern Ocean CO_2 Sink Due to Recent Climate Change. *Science*, 316(5832):1735–1738. doi:10.1126/science.1136188.

Lecomte, O., Goosse, H., Fichefet, T., Holland, P., Uotila, P., Zunz, V., and Kimura, N. (2016). Impact of surface wind biases on the Antarctic sea ice concentration budget in climate models. *Ocean Modelling*, 105:60–70. doi:10.1016/j.ocemod.2016.08.001.

Lee, K., Tong, L. T., Millero, F. J., Sabine, C. L., Dickson, A. G., Goyet, C., Park, G.-H., Wanninkhof, R., Feely, R. A., and Key, R. M. (2006). Global relationships of total alkalinity with salinity and temperature in surface waters of the world's oceans. *Geophysical Research Letters*, 33(19):L19605. doi:10.1029/2006GL027207.

Lee, S. and Feldstein, S. B. (2013). Detecting ozone- and greenhouse gas-driven wind trends with observational data. *Science*, 339(6119):563–567. doi:10.1126/science.1225154.

Lemarié, F., Debreu, L., Shchepetkin, A. F., and McWilliams, J. C. (2012a). On the stability and accuracy of the harmonic and biharmonic isoneutral mixing operators in ocean models. *Ocean Modelling*, 52-53:9–35. doi:10.1016/j.ocemod.2012.04.007.

Lemarié, F., Kurian, J., Shchepetkin, A. F., Jeroen Molemaker, M., Colas, F., and McWilliams, J. C. (2012b). Are there inescapable issues prohibiting the use of terrain-following coordinates in climate models? *Ocean Modelling*, 42:57–79. doi:10.1016/j.ocemod.2011.11.007.

Lemke, P. (1987). A coupled one-dimensional sea ice-ocean model. *Journal of Geophysical Research*, 92(C12):13164. doi:10.1029/JC092iC12p13164.

Lenaerts, J. T. M., Vizcaino, M., Fyke, J., van Kampenhout, L., and van den Broeke, M. R. (2016). Present-day and future Antarctic ice sheet climate and surface mass balance in the Community Earth System Model. *Climate Dynamics*, 47(5-6):1367–1381. doi:10.1007/s00382-015-2907-4.

Lenton, A., Codron, F., Bopp, L., Metzl, N., Cadule, P., Tagliabue, A., and Le Sommer, J. (2009). Stratospheric ozone depletion reduces ocean carbon uptake and enhances ocean acidification. *Geophysical Research Letters*, 36(12):L12606. doi:10.1029/2009GL038227.

Lenton, A., Tilbrook, B., Law, R. M., Bakker, D., Doney, S. C., Gruber, N., Ishii, M., Hoppema, M., Lovenduski, N. S., Matear, R. J., McNeil, B. I., Metzl, N., Mikaloff Fletcher, S. E., Monteiro, P. M. S., Rödenbeck, C., Sweeney, C., and Takahashi, T. (2013). Sea–air CO_2 fluxes in the Southern Ocean for the period 1990–2009. *Biogeosciences*, 10(6):4037–4054. doi:10.5194/bg-10-4037-2013.

Leonard, K. C., Massom, R., Reid, P., Schlosser, E., Meredith, M. P., Tsukernik, M., Gorodetskaya, I., and Stammerjohn, S. (2016). Quantifying precipitation and its contribution to surface freshening in the Southern Ocean. ACE Project Proposal.

Leppäranta, M. (2011). *The Drift of Sea Ice*. Springer Berlin Heidelberg, Berlin, Heidelberg. doi:10.1007/978-3-642-04683-4.

Levitus, S., Antonov, J. I., Boyer, T. P., Baranova, O. K., Garcia, H. E., Locarnini, R. A., Mishonov, A. V., Reagan, J. R., Seidov, D., Yarosh, E. S., and Zweng, M. M. (2012). World ocean heat content and thermosteric sea level change (0-2000 m), 1955-2010. *Geophysical Research Letters*, 39(10):L10603. doi:10.1029/2012GL051106.

Levitus, S., Antonov, J. I., Wang, J., Delworth, T. L., Dixon, K. W., and Broccoli, A. J. (2001). Anthropogenic warming of Earth's climate system. *Science*, 292(5515):267–270. doi:10.1126/science.1058154.

Li, Q., Webb, A., Fox-Kemper, B., Craig, A., Danabasoglu, G., Large, W. G., and Vertenstein, M. (2016). Langmuir mixing effects on global climate: WAVEWATCH III in CESM. *Ocean Modelling*, 103:145–160. doi:10.1016/j.ocemod.2015.07.020.

Li, X., Holland, D. M., Gerber, E. P., and Yoo, C. (2014). Impacts of the north and tropical Atlantic Ocean on the Antarctic Peninsula and sea ice. *Nature*, 505(7484):538–542. doi:10.1038/nature12945.

Liu, J. and Curry, J. A. (2010). Accelerated warming of the Southern Ocean and its impacts on the hydrological cycle and sea ice. *Proceedings of the National Academy of Sciences of the United States of America*, 107(34):14987–92. doi:10.1073/pnas.1003336107.

Locarnini, R. A., Mishonov, A. V., Antonov, J. I., Boyer, T. P., Garcia, H. E., Baranova, O. K., Zweng, M. M., Paver, C. R., Reagan, J. R., Johnson, D. R., Hamilton, M., and Seidov, D. (2013). World Ocean Atlas 2013, Volume 1: Temperature, p. 40. NOAA Atlas NESDIS 73.

Lorenz, C. and Kunstmann, H. (2012). The hydrological cycle in three state-of-the-art reanalyses: Intercomparison and performance analysis. *Journal of Hydrometeorology*, 13(5):1397–1420. doi:10.1175/JHM-D-11-088.1.

Lovenduski, N. S., Gruber, N., and Doney, S. C. (2008). Toward a mechanistic understanding of the decadal trends in the Southern Ocean carbon sink. *Global Biogeochem. Cycles*, 22(3):GB3016. doi:10.1029/2007GB003139.

Lovenduski, N. S., Gruber, N., Doney, S. C., and Lima, I. D. (2007). Enhanced CO_2 outgassing in the Southern Ocean from a positive phase of the Southern Annular Mode. *Global Biogeochemical Cycles*, 21(2):GB2026. doi:10.1029/2006GB002900.

Lovenduski, N. S. and Ito, T. (2009). The Future evolution of the Southern Ocean CO_2 sink. *Journal of Marine Research*, 67(5):597–617. doi:doi:10.1357/002224009791218832.

Lu, P., Li, Z., and Han, H. (2016). Introduction of parameterized sea ice drag coefficients into ice free-drift modeling. *Acta Oceanologica Sinica*, 35(1):53–59. doi:10.1007/s13131-016-0796-y.

Lumpkin, R. and Speer, K. (2007). Global Ocean Meridional Overturning. *Journal of Physical Oceanography*, 37(10):2550–2562. doi:10.1175/JPO3130.1.

Lüthi, D., Le Floch, M., Bereiter, B., Blunier, T., Barnola, J.-M., Siegenthaler, U., Raynaud, D., Jouzel, J., Fischer, H., Kawamura, K., and Stocker, T. F. (2008). High-resolution carbon dioxide concentration record 650,000-800,000 years before present. *Nature*, 453(7193):379–382. doi:10.1038/nature06949.

Lynch-Stieglitz, J., Adkins, J. F., Curry, W. B., Dokken, T., Hall, I. R., Herguera, J. C., Hirschi, J. J.-M., Ivanova, E. V., Kissel, C., Marchal, O., Marchitto, T. M., McCave, I. N., McManus,

J. F., Mulitza, S., Ninnemann, U., Peeters, F., Yu, E.-F., and Zahn, R. (2007). Atlantic meridional overturning circulation during the Last Glacial Maximum. *Science*, 316(5821):66–69. doi:10.1126/science.1137127.

MacDonald, A. M. and Wunsch, C. (1996). An estimate of global ocean circulation and heat fluxes. *Nature*, 382(6590):436–439. doi:10.1038/382436a0.

Mahlstein, I., Gent, P. R., and Solomon, S. (2013). Historical Antarctic mean sea ice area, sea ice trends, and winds in CMIP5 simulations. *Journal of Geophysical Research Atmospheres*, 118(11):5105–5110. doi:10.1002/jgrd.50443.

Mahowald, N. M., Engelstaedter, S., Luo, C., Sealy, A., Artaxo, P., Benitez-Nelson, C., Bonnet, S., Chen, Y., Chuang, P. Y., Cohen, D. D., Dulac, F., Herut, B., Johansen, A. M., Kubilay, N., Losno, R., Maenhaut, W., Paytan, A., Prospero, J. M., Shank, L. M., and Siefert, R. L. (2009). Atmospheric Iron Deposition: Global Distribution, Variability, and Human Perturbations. *Annual Review of Marine Science*, 1(1):245–278. doi:10.1146/annurev.marine.010908.163727.

Majkut, J. D., Carter, B. R., Frölicher, T. L., Dufour, C. O., Rodgers, K. B., and Sarmiento, J. L. (2014). An observing system simulation for Southern Ocean carbon dioxide uptake. *Philosophical Transactions of the Royal Society A*, 372(2019):20130046. doi:10.1098/rsta.2013.0046.

Maksym, T. (2016). Climate science: Southern Ocean freshened by sea ice. *Nature*, 537(7618):40–41. doi:10.1038/537040a.

Maksym, T. and Markus, T. (2008). Antarctic sea ice thickness and snow-to-ice conversion from atmospheric reanalysis and passive microwave snow depth. *Journal of Geophysical Research*, 113(2):C02S12. doi:10.1029/2006JC004085.

Manabe, S. and Stouffer, R. J. (1993). Century-scale effects of increased atmospheric CO_2 on the ocean-atmosphere system. *Nature*, 364(6434):215–218. doi:10.1038/364215a0.

Marchesiello, P., Debreu, L., and Couvelard, X. (2009). Spurious diapycnal mixing in terrain-following coordinate models: The problem and a solution. *Ocean Modelling*, 26(3-4):156–169. doi:10.1016/j.ocemod.2008.09.004.

Marchesiello, P., McWilliams, J. C., and Shchepetkin, A. (2001). Open boundary conditions for long-term integration of regional oceanic models. *Ocean Modelling*, 3(1-2):1–20. doi:10.1016/S1463-5003(00)00013-5.

Marchesiello, P., McWilliams, J. C., and Shchepetkin, A. F. (2003). Equilibrium Structure and Dynamics of the California Current System. *Journal of Physical Oceanography*, 33(4):753–783. doi:10.1175/1520-0485(2003)33<753:ESADOT>2.0.CO;2.

Marinov, I., Gnanadesikan, A., Toggweiler, J. R., and Sarmiento, J. L. (2006). The Southern Ocean biogeochemical divide. *Nature*, 441(7096):964–967. doi:10.1038/nature04883.

Markus, T. (1999). Results from an ECMWF-SSM/I forced mixed layer model of the Southern Ocean. *Journal of Geophysical Research*, 104(C7):15603. doi:10.1029/1999JC900080.

Marmorino, G. O. and Caldwell, D. R. (1976). Heat and salt transport through a diffusive thermohaline interface. *Deep Sea Research and Oceanographic Abstracts*, 23(1):59–67. doi:10.1016/0011-7471(76)90808-1.

Marsh, R., Ivchenko, V. O., Skliris, N., Alderson, S., Bigg, G. R., Madec, G., Blaker, A. T., Aksenov, Y., Sinha, B., Coward, A. C., Le Sommer, J., Merino, N., and Zalesny, V. B. (2015). NEMOICB (v1.0): interactive icebergs in the NEMO ocean model globally configured at eddy-permitting resolution. *Geoscientific Model Development*, 8(5):1547–1562. doi:10.5194/gmd-8-1547-2015.

Marshall, G. J. (2003). Trends in the Southern Annular Mode from observations and reanalyses. *Journal of Climate*, 16(24):4134–4143. doi:10.1175/1520-0442(2003)016<4134:TITSAM>2.0.CO;2.

Marshall, J. and Radko, T. (2003). Residual-Mean Solutions for the Antarctic Circumpolar Current and Its Associated Overturning Circulation. *Journal of Physical Oceanography*, 33(11):2341–2354. doi:10.1175/1520-0485(2003)033<2341:RSFTAC>2.0.CO;2.

Marshall, J. and Schott, F. (1999). Open-ocean convection: Observations, theory, and models. *Reviews of Geophysics*, 37(1):1–64. doi:10.1029/98RG02739.

Marshall, J. and Speer, K. (2012). Closure of the meridional overturning circulation through Southern Ocean upwelling. *Nature Geoscience*, 5(3):171–180. doi:10.1038/ngeo1391.

Marsland, S. J. and Wolff, J. O. (2001). On the sensitivity of Southern Ocean sea ice to the surface freshwater flux: A model study. *Journal of Geophysical Research*, 106(C2):2723–2741.

Martin, S., Drucker, R. S., and Kwok, R. (2007). The areas and ice production of the western and central Ross Sea polynyas, 1992-2002, and their relation to the B-15 and C-19 iceberg events of 2000 and 2002. *Journal of Marine Systems*, 68(1-2):201–214. doi:10.1016/j.jmarsys.2006.11.008.

Martin, T. and Adcroft, A. (2010). Parameterizing the fresh-water flux from land ice to ocean with interactive icebergs in a coupled climate model. *Ocean Modelling*, 34(3-4):111–124. doi:10.1016/j.ocemod.2010.05.001.

Martin, T., Park, W., and Latif, M. (2013). Multi-centennial variability controlled by Southern Ocean convection in the Kiel Climate Model. *Climate Dynamics*, 40(7-8):2005–2022. doi:10.1007/s00382-012-1586-7.

Martinson, D. G. (1990). Evolution of the Southern Ocean winter mixed layer and sea ice: Open ocean deepwater formation and ventilation. *Journal of Geophysical Research Oceans*, 95(C7):11641–11654. doi:10.1029/JC095iC07p11641.

Martinson, D. G. (1991). Open Ocean Convection in the Southern Ocean. In Chu, P. C. and Gascard, J. C., editors, *Elsevier Oceanography Series*, volume 57, pages 37–52. Elsevier. doi:10.1016/S0422-9894(08)70059-X.

Martinson, D. G., Killworth, P. D., and Gordon, A. L. (1981). A Convective Model for the Weddell Polynya. *Journal of Physical Oceanography*, 11(4):466–488. doi:10.1175/1520-0485(1981)011<0466:ACMFTW>2.0.CO;2.

Martinson, D. G. and McKee, D. C. (2012). Transport of warm Upper Circumpolar Deep Water onto the western Antarctic Peninsula continental shelf. *Ocean Science*, 8(4):433–442. doi:10.5194/os-8-433-2012.

Maslanik, J., Fowler, C., Key, J., Scambos, T., Hutchinson, T., and Emery, W. (1997). AVHRR-based Polar Pathfinder products for modeling applications. *Annals of Glaciology*, 25:388–392.

Massom, R. A., Eicken, H., Haas, C., Jeffries, M. O., Drinkwater, M. R., Sturm, M., Worby, A. P., Wu, X., Lytle, V. I., Ushio, S., Morris, K., Reid, P. A., Warren, S. G., and Allison, I. (2001). Snow on Antarctic sea ice. *Reviews of Geophysics*, 39(3):413–445. doi:10.1029/2000RG000085.

Massonnet, F., Mathiot, P., Fichefet, T., Goosse, H., König Beatty, C., Vancoppenolle, M., and Lavergne, T. (2013). A model reconstruction of the Antarctic sea ice thickness and volume changes over 1980-2008 using data assimilation. *Ocean Modelling*, 64:67–75. doi:10.1016/j.ocemod.2013.01.003.

Matear, R. J. and Lenton, A. (2008). Impact of Historical Climate Change on the Southern Ocean Carbon Cycle. *Journal of Climate*, 21(22):5820–5834. doi:10.1175/2008jcli2194.1.

Mathiot, P., Barnier, B., Gallée, H., Molines, J. M., Sommer, J. L., Juza, M., and Penduff, T. (2010). Introducing katabatic winds in global ERA40 fields to simulate their impacts on the Southern Ocean and sea-ice. *Ocean Modelling*, 35(3):146–160. doi:10.1016/j.ocemod.2010.07.001.

Mathiot, P., Jourdain, N. C., Barnier, B., Gallée, H., Molines, J. M., Le Sommer, J., and Penduff, T. (2012). Sensitivity of coastal polynyas and high-salinity shelf water production in the Ross Sea, Antarctica, to the atmospheric forcing. *Ocean Dynamics*, 62(5):701–723. doi:10.1007/s10236-012-0531-y.

Maykut, G. A. and Untersteiner, N. (1971). Some results from a time-dependent thermodynamic model of sea ice. *Journal of Geophysical Research*, 76(6):1550–1575. doi:10.1029/JC076i006p01550.

Mazloff, M. R., Heimbach, P., and Wunsch, C. (2010). An Eddy-Permitting Southern Ocean State Estimate. *Journal of Physical Oceanography*, 40(5):880–899. doi:10.1175/2009JPO4236.1.

McDougall, T. J. (1987). Thermobaricity, cabbeling, and water-mass conversion. *Journal of Geophysical Research*, 92(C5):5448. doi:10.1029/JC092iC05p05448.

McPhee, M. (2008). *Air-ice-ocean interaction: Turbulent ocean boundary layer exchange processes*. Springer, New York, Dordrecht, Heidelberg, London. doi:10.1007/978-0-387-78335-2.

McPhee, M. G. (1992). Turbulent heat flux in the upper ocean under sea ice. *Journal of Geophysical Research*, 97(C4):5365. doi:10.1029/92JC00239.

McPhee, M. G. (2003). Is thermobaricity a major factor in Southern Ocean ventilation? *Antarctic Science*, 15(1):153–160. doi:10.1017/S0954102003001159.

McWilliams, J. C., Huckle, E., and Shchepetkin, A. F. (2009). Buoyancy Effects in a Stratified Ekman Layer. *Journal of Physical Oceanography*, 39(10):2581–2599. doi:10.1175/2009JPO4130.1.

Meehl, G. A., Arblaster, J. M., Bitz, C. M., Chung, C. T. Y., and Teng, H. (2016). Antarctic sea-ice expansion between 2000 and 2014 driven by tropical Pacific decadal climate variability. *Nature Geoscience*, 9(8):590–595. doi:10.1038/ngeo2751.

Meier, W., Fetterer, F., Savoie, M., Mallory, S., Duerr, R., and Stroeve, J. (2013a). NOAA/NSIDC Climate Data Record of passive microwave sea ice concentration, version 2, 1979–2011, In *Boulder, Colorado USA: National Snow and Ice Data Center*, Boulder, Colorado USA. doi:10.7265/N55M63M1.

Meier, W., Fetterer, F., Savoie, M., Mallory, S., Duerr, R., and Stroeve, J. (2013b). NOAA/NSIDC Climate Data Record of passive microwave sea ice concentration, version 2, 1980–2009, In *Boulder, Colorado USA: National Snow and Ice Data Center*, Boulder, Colorado USA. doi:10.7265/N55M63M1.

Meijers, A. J. S., Bindoff, N. L., and Rintoul, S. R. (2011). Frontal movements and property fluxes: Contributions to heat and freshwater trends in the Southern Ocean. *Journal of Geophysical Research*, 116(8):C08024. doi:10.1029/2010JC006832.

Meijers, A. J. S., Bindoff, N. L., and Roberts, J. L. (2007). On the Total, Mean, and Eddy Heat and Freshwater Transports in the Southern Hemisphere of a 1/8° x 1/8° Global Ocean Model. *Journal of Physical Oceanography*, 37(2):277–295. doi:10.1175/JPO3012.1.

Meijers, A. J. S., Shuckburgh, E., Bruneau, N., Sallée, J.-B., Bracegirdle, T. J., and Wang, Z. (2012). Representation of the Antarctic Circumpolar Current in the CMIP5 climate models and future changes under warming scenarios. *Journal of Geophysical Research: Oceans*, 117(12):C12008. doi:10.1029/2012JC008412.

Mellor, G. L. and Kantha, L. (1989). An ice-ocean coupled model. *Journal of Geophysical Research*, 94(C8):10937. doi:10.1029/JC094iC08p10937.

Meredith, M. P., Gordon, A. L., Naveira Garabato, A. C., Abrahamsen, E. P., Huber, B. A., Jullion, L., and Venables, H. J. (2011a). Synchronous intensification and warming of Antarctic Bottom Water outflow from the Weddell Gyre. *Geophysical Research Letters*, 38(3):L03603. doi:10.1029/2010GL046265.

Meredith, M. P. and Hogg, A. M. (2006). Circumpolar response of Southern Ocean eddy activity to a change in the Southern Annular Mode. *Geophysical Research Letters*, 33(16):L16608. doi:10.1029/2006GL026499.

Meredith, M. P., Naveira Garabato, A. C., Hogg, A. M., and Farneti, R. (2012). Sensitivity of the overturning circulation in the Southern Ocean to decadal changes in wind forcing. *Journal of Climate*, 25(1):99–110. doi:10.1175/2011JCLI4204.1.

Meredith, M. P., Venables, H. J., Clarke, A., Ducklow, H. W., Erickson, M., Leng, M. J., Lenaerts, J. T. M., and Van Den Broeke, M. R. (2013). The freshwater system west of the Antarctic Peninsula: Spatial and temporal changes. *Journal of Climate*, 26(5):1669–1684. doi:10.1175/JCLI-D-12-00246.1.

Meredith, M. P., Wallace, M. I., Stammerjohn, S. E., Renfrew, I. A., Clarke, A., Venables, H. J., Shoosmith, D. R., Souster, T., and Leng, M. J. (2010). Changes in the freshwater composition of the upper ocean west of the Antarctic Peninsula during the first decade of the 21st century. *Progress in Oceanography*, 87(1-4):127–143. doi:10.1016/j.pocean.2010.09.019.

Meredith, M. P., Woodworth, P. L., Chereskin, T. K., Marshall, D. P., Allison, L. C., Bigg, G. R., Donohue, K., Heywood, K. J., Hughes, C. W., Hibbert, A., Hogg, A. M., Johnson, H. L., Jullion, L., King, B. A., Leach, H., Lenn, Y.-D., Morales Maqueda, M. A., Munday, D. R., Naveira Garabato, A. C., Provost, C., Sallée, J.-B., and Sprintall, J. (2011b). Sustained monitoring of the Southern Ocean at Drake Passage: past achievements and future priorities. *Reviews of Geophysics*, 49(4):RG4005. doi:10.1029/2010RG000348.

Meredith, M. P., Woodworth, P. L., Hughes, C. W., and Stepanov, V. (2004). Changes in the ocean transport through Drake Passage during the 1980s and 1990s, forced by changes in the Southern Annular Mode. *Geophysical Research Letters*, 31(21):L21305. doi:10.1029/2004GL021169.

Merino, I., Le Sommer, J., Durand, G. G., Jourdain, N. C., Madec, G., Mathiot, P., and Tournadre, J. (2016). Antarctic icebergs melt over the Southern Ocean: Climatology and impact on sea ice. *Ocean Modelling*, 104:99–110. doi:10.1016/j.ocemod.2016.05.001.

Merrifield, S. T., Laurent, L. S., Owens, B., Thurnherr, A. M., and Toole, J. M. (2016). Enhanced Diapycnal Diffusivity in Intrusive Regions of the Drake Passage. *Journal of Physical Oceanography*, 46(4):1309–1321. doi:10.1175/JPO-D-15-0068.1.

Meyer, A., Sloyan, B. M., Polzin, K. L., Phillips, H. E., and Bindoff, N. L. (2015). Mixing Variability in the Southern Ocean. *Journal of Physical Oceanography*, 45(4):966–987. doi:10.1175/JPO-D-14-0110.1.

Middleton, J. H. and Foster, T. D. (1980). Fine structure measurements in a temperature-compensated halocline. *Journal of Geophysical Research*, 85(C2):1107. doi:10.1029/JC085iC02p01107.

Mikaloff Fletcher, S. E., Gruber, N., Jacobson, A. R., Doney, S. C., Dutkiewicz, S., Gerber, M., Follows, M., Joos, F., Lindsay, K., Menemenlis, D., Mouchet, A., Müller, S. A., and Sarmiento, J. L. (2006). Inverse estimates of anthropogenic CO_2 uptake, transport, and storage by the ocean. *Global Biogeochemical Cycles*, 20(2):GB2002. doi:10.1029/2005GB002530.

Mikaloff Fletcher, S. E., Gruber, N., Jacobson, A. R., Gloor, M., Doney, S. C., Dutkiewicz, S., Gerber, M., Follows, M. J., Joos, F., Lindsay, K., Menemenlis, D., Mouchet, A., Müller, S. A., and Sarmiento, J. L. (2007). Inverse estimates of the oceanic sources and sinks of natural CO_2 and the implied oceanic carbon transport. *Global Biogeochemical Cycles*, 21(1):GB1010. doi:10.1029/2006GB002751.

Moore, J., Doney, S. C., Glover, D. M., and Fung, I. Y. (2001a). Iron cycling and nutrient-limitation patterns in surface waters of the World Ocean. *Deep Sea Research Part II: Topical Studies in Oceanography*, 49(1-3):463–507. doi:10.1016/S0967-0645(01)00109-6.

Moore, J., Doney, S. C., Kleypas, J. A., Glover, D. M., and Fung, I. Y. (2001b). An intermediate complexity marine ecosystem model for the global domain. *Deep Sea Research Part II: Topical Studies in Oceanography*, 49(1-3):403–462. doi:10.1016/S0967-0645(01)00108-4.

Moore, J. K., Doney, S. C., and Lindsay, K. (2004). Upper ocean ecosystem dynamics and iron cycling in a global three-dimensional model. *Global Biogeochemical Cycles*, 18(4):1–21. doi:10.1029/2004GB002220.

Moore, J. K., Lindsay, K., Doney, S. C., Long, M. C., and Misumi, K. (2013). Marine Ecosystem Dynamics and Biogeochemical Cycling in the Community Earth System Model [CESM1(BGC)]: Comparison of the 1990s with the 2090s under the RCP4.5 and RCP8.5 Scenarios. *Journal of Climate*, 26(23):9291–9312. doi:10.1175/JCLI-D-12-00566.1.

Morel, A. and Berthon, J.-F. (1989). Surface pigments, algal biomass profiles, and potential production of the euphotic layer: Relationships reinvestigated in view of remote-sensing applications. *Limnology and Oceanography*, 34(8):1545–1562. doi:10.4319/lo.1989.34.8.1545.

Morrison, A. K., Frölicher, T. L., and Sarmiento, J. L. (2015). Upwelling in the Southern Ocean. *Physics Today*, 68(1):27–32. doi:10.1063/PT.3.2654.

Morrison, A. K., Griffies, S. M., Winton, M., Anderson, W. G., and Sarmiento, J. L. (2016). Mechanisms of Southern Ocean heat uptake and transport in a global eddying climate model. *Journal of Climate*, 29:2059–2075. doi:10.1175/JCLI-D-15-0579.1.

Morrison, A. K. and Hogg, A. M. (2013). On the Relationship between Southern Ocean Overturning and ACC Transport. *Journal of Physical Oceanography*, 43(1):140–148. doi:10.1175/JPO-D-12-057.1.

Morrison, A. K., Hogg, A. M., and Ward, M. L. (2011). Sensitivity of the Southern Ocean overturning circulation to surface buoyancy forcing. *Geophysical Research Letters*, 38(14):L14602. doi:10.1029/2011GL048031.

Muench, R. D., Fernando, H. J. S., and Stegen, G. R. (1990). Temperature and Salinity Staircases in the Northwestern Weddell Sea. *Journal of Physical Oceanography*, 20(2):295–306. doi:10.1175/1520-0485(1990)020<0295:TASSIT>2.0.CO;2.

Munk, W. and Wunsch, C. (1998). Abyssal recipes II: Energetics of tidal and wind mixing. *Deep-Sea Research Part I: Oceanographic Research Papers*, 45(12):1977–2010. doi:10.1016/S0967-0637(98)00070-3.

Munk, W. H. (1966). Abyssal recipes. *Deep Sea Research and Oceanographic Abstracts*, 13(4):707–730. doi:10.1016/0011-7471(66)90602-4.

Munro, D. R., Lovenduski, N. S., Takahashi, T., Stephens, B. B., Newberger, T., and Sweeney, C. (2015). Recent evidence for a strengthening CO_2 sink in the Southern Ocean from carbonate system measurements in the Drake Passage (2002–2015). *Geophysical Research Letters*, 42(18):7623–7630. doi:10.1002/2015GL065194.

Nakayama, Y., Timmermann, R., Rodehacke, C. B., Schröder, M., and Hellmer, H. H. (2014). Modeling the spreading of glacial meltwater from the Amundsen and Bellingshausen Seas. *Geophysical Research Letters*, 41(22):7942–7949. doi:10.1002/2014GL061600.

NASA Aquarius Project (2015). Aquarius Official Release Level 3 Sea Surface Salinity Standard Mapped Image Monthly Data V4.0. PO.DAAC, CA, USA. doi:10.5067/AQR40-3SMCS.

Naveira Garabato, A. C., Jullion, L., Stevens, D. P., Heywood, K. J., and King, B. A. (2009). Variability of Subantarctic Mode Water and Antarctic Intermediate Water in the Drake Passage during the Late-Twentieth and Early-Twenty-First Centuries. *Journal of Climate*, 22(13):3661–3688. doi:10.1175/2009JCLI2621.1.

Naveira Garabato, A. C., Williams, A. P., and Bacon, S. (2014). The three-dimensional overturning circulation of the Southern Ocean during the WOCE era. *Progress in Oceanography*, 120:41–78. doi:10.1016/j.pocean.2013.07.018.

Neff, W., Perlwitz, J., and Hoerling, M. (2008). Observational evidence for asymmetric changes in tropospheric heights over Antarctica on decadal time scales. *Geophysical Research Letters*, 35(18):L18703. doi:10.1029/2008GL035074.

Nevison, C. D., Manizza, M., Keeling, R. F., Stephens, B. B., Bent, J. D., Dunne, J., Ilyina, T., Long, M., Resplandy, L., Tjiputra, J., and Yukimoto, S. (2016). Evaluating CMIP5 ocean biogeochemistry and Southern Ocean carbon uptake using atmospheric potential oxygen: Present-day performance and future projection. *Geophysical Research Letters*, 43(5):2077–2085. doi:10.1002/2015GL067584.

Nguyen, A. T., Menemenlis, D., and Kwok, R. (2009). Improved modeling of the Arctic halocline with a subgrid-scale brine rejection parameterization. *Journal of Geophysical Research: Oceans*, 114(11):C11014. doi:10.1029/2008JC005121.

Nicholson, S.-A., Lévy, M., Llort, J., Swart, S., and Monteiro, P. M. S. (2016). Investigation into the impact of storms on sustaining summer primary productivity in the Sub-Antarctic Ocean. *Geophysical Research Letters*. doi:10.1002/2016GL069973.

Nicolas, J. P. and Bromwich, D. H. (2011). Precipitation Changes in High Southern Latitudes from Global Reanalyses: A Cautionary Tale. *Surveys in Geophysics*, 32(4-5):475–494. doi:10.1007/s10712-011-9114-6.

Niiler, P. P. and Kraus, E. B. (1977). One-dimensional models of the upper ocean. In Kraus, E. B., editor, *Modeling and Prediction of the Upper Layers of the Ocean*, pages 143–172. Pergamon, New York.

Nikurashin, M., Vallis, G. K., and Adcroft, A. (2012). Routes to energy dissipation for geostrophic flows in the Southern Ocean. *Nature Geoscience*, 6(1):48–51. doi:10.1038/ngeo1657.

Notz, D., Haumann, F. A., Haak, H., Jungclaus, J. H., and Marotzke, J. (2013). Arctic sea-ice evolution as modeled by Max Planck Institute for Meteorology's Earth system model. *Journal of Advances in Modeling Earth Systems*, 5(2):173–194. doi:10.1002/jame.20016.

Oerlemans, J. (1980). Model experiments on the 100,000-yr glacial cycle. *Nature*, 287(5781):430–432. doi:10.1038/287430a0.

Ogura, T. (2004). Effects of sea ice dynamics on the Antarctic sea ice distribution in a coupled ocean atmosphere model. *Journal of Geophysical Research*, 109(C4):C04025. doi:10.1029/2003JC002022.

Ohshima, K. I., Fukamachi, Y., Williams, G. D., Nihashi, S., Roquet, F., Kitade, Y., Tamura, T., Hirano, D., Herraiz-Borreguero, L., Field, I., Hindell, M., Aoki, S., and Wakatsuchi, M. (2013). Antarctic Bottom Water production by intense sea-ice formation in the Cape Darnley polynya. *Nature Geoscience*, 6(3):235–240. doi:10.1038/ngeo1738.

Ohshima, K. I., Nakanowatari, T., Riser, S., Volkov, Y., and Wakatsuchi, M. (2014). Freshening and dense shelf water reduction in the Okhotsk Sea linked with sea ice decline. *Progress in Oceanography*, 126:71–79. doi:10.1016/j.pocean.2014.04.020.

Oke, P. R. and England, M. H. (2004). Oceanic response to changes in the latitude of the Southern Hemisphere subpolar westerly winds. *Journal of Climate*, 17(5):1040–1054. doi:10.1175/1520-0442(2004)017<1040:ORTCIT>2.0.CO;2.

Olason, E. and Notz, D. (2014). Drivers of variability in Arctic sea-ice drift speed. *Journal of Geophysical Research*, 119(9):5755–5775. doi:10.1002/2014JC009897.

Olbers, D., Borowski, D., Völker, C., and Wölff, J.-O. (2004). The dynamical balance, transport and circulation of the Antarctic Circumpolar Current. *Antarctic Science*, 16(4):439–470. doi:10.1017/S0954102004002251.

Omstedt, A., Nyberg, L., and Leppäranta, M. (1996). On the ice-ocean response to wind forcing. *Tellus A*, 48(4):593–606. doi:10.1034/j.1600-0870.1996.t01-3-00008.x.

Orlanski, I. (1976). A simple boundary condition for unbounded hyperbolic flows. *Journal of Computational Physics*, 21(3):251–269. doi:10.1016/0021-9991(76)90023-1.

Orr, J. C., Maier-Reimer, E., Mikolajewicz, U., Monfray, P., Sarmiento, J. L., Toggweiler, J. R., Taylor, N. K., Palmer, J., Gruber, N., Sabine, C. L., Le Quéré, C., Key, R. M., and Boutin, J. (2001). Estimates of anthropogenic carbon uptake from four three-dimensional global ocean models. *Global Biogeochemical Cycles*, 15(1):43–60. doi:10.1029/2000GB001273.

Orsi, A. H., Johnson, G. C., and Bullister, J. L. (1999). Circulation, mixing, and production of Antarctic Bottom Water. *Progress in Oceanography*, 43(1):55–109.

Orsi, A. H., Smethie, W. M., and Bullister, J. L. (2002). On the total input of Antarctic waters to the deep ocean: A preliminary estimate from chlorofluorocarbon measurements. *Journal of Geophysical Research*, 107(C8):3122. doi:10.1029/2001JC000976.

Orsi, A. H., Whitworth, T., and Nowlin, W. D. (1995). On the meridional extent and fronts of the Antarctic Circumpolar Current. *Deep-Sea Research Part I*, 42(5):641–673. doi:10.1016/0967-0637(95)00021-W.

Oschlies, A., Dietze, H., and Kähler, P. (2003). Salt-finger driven enhancement of upper ocean nutrient supply. *Geophysical Research Letters*, 30(23):2204. doi:10.1029/2003GL018552.

Otto-Bliesner, B. L., Hewitt, C. D., Marchitto, T. M., Brady, E., Abe-Ouchi, A., Crucifix, M., Murakami, S., and Weber, S. L. (2007). Last Glacial Maximum ocean thermohaline circulation: PMIP2 model intercomparisons and data constraints. *Geophysical Research Letters*, 34(12):L12706. doi:10.1029/2007GL029475.

Paolo, F. S., Fricker, H. A., and Padman, L. (2015). Volume loss from Antarctic ice shelves is accelerating. *Science*, 348(6232):327–331. doi:10.1126/science.aaa0940.

Papritz, L., Pfahl, S., Rudeva, I., Simmonds, I., Sodemann, H., and Wernli, H. (2014). The role of extratropical cyclones and fronts for Southern Ocean freshwater fluxes. *Journal of Climate*, 27(16):6205–6224. doi:10.1175/JCLI-D-13-00409.1.

Papritz, L., Pfahl, S., Sodemann, H., and Wernli, H. (2015). A climatology of cold air outbreaks and their impact on air-sea heat fluxes in the high-latitude South Pacific. *Journal of Climate*, 28(1):342–364. doi:10.1175/JCLI-D-14-00482.1.

Park, W. and Latif, M. (2008). Multidecadal and multicentennial variability of the meridional overturning circulation. *Geophysical Research Letters*, 35(22):L22703. doi:10.1029/2008GL035779.

Parrenin, F., Masson-Delmotte, V., Köhler, P., Raynaud, D., Paillard, D., Schwander, J., Barbante, C., Landais, A., Wegner, A., and Jouzel, J. (2013). Synchronous change of atmospheric CO_2 and Antarctic temperature during the last deglacial warming. *Science*, 339(6123):1060–1063. doi:10.1126/science.1226368.

Patara, L., Böning, C. W., and Biastoch, A. (2016). Variability and trends in Southern Ocean eddy activity in 1/12 ocean model simulations. *Geophysical Research Letters*, 43(9):4517–4523. doi:10.1002/2016GL069026.

Pauling, A. G., Bitz, C. M., Smith, I. J., and Langhorne, P. J. (2016). The Response of the Southern Ocean and Antarctic Sea Ice to Freshwater from Ice Shelves in an Earth System Model. *Journal of Climate*, 29(5):1655–1672. doi:10.1175/JCLI-D-15-0501.1.

Peña-Molino, B., McCartney, M. S., and Rintoul, S. R. (2016). Direct observations of the Antarctic Slope Current transport at 113°E. *Journal of Geophysical Research: Oceans*. doi:10.1002/2015JC011594.

Pérez, F. F., Mercier, H., Vázquez-Rodríguez, M., Lherminier, P., Velo, A., Pardo, P. C., Rosón, G., and Ríos, A. F. (2013). Atlantic Ocean CO_2 uptake reduced by weakening of the meridional overturning circulation. *Nature Geoscience*, 6(2):146–152. doi:10.1038/ngeo1680.

Peterson, T. C., Easterling, D. R., Karl, T. R., Groisman, P., Nicholls, N., Plummer, N., Torok, S., Auer, I., Boehm, R., Gullett, D., Vincent, L., Heino, R., Tuomenvirta, H., Mestre, O., Szentimrey, T., Salinger, J., Førland, E. J., Hanssen-Bauer, I., Alexandersson, H., Jones, P., and Parker, D. (1998). Homogeneity adjustments of in situ atmospheric climate data: a review. *International Journal of Climatology*, 18(13):1493–1517. doi:10.1002/(SICI)1097-0088(19981115)18:13<1493::AID-JOC329>3.0.CO;2-T.

Petit, J. R., Jouzel, J., Raynaud, D., Barkov, N. I., Barnola, J.-M., Basile, I., Bender, M., Chappellaz, J., Davis, M., Delaygue, G., Delmotte, M., Kotlyakov, V. M., Legrand, M., Lipenkov, V. Y., Lorius, C., Pépin, L., Ritz, C., Saltzman, E., and Stievenard, M. (1999). Climate and atmospheric history of the past 420,000 years from the Vostok ice core, Antarctica. *Nature*, 399(6735):429–436. doi:10.1038/20859.

Petrelli, P., Bindoff, N. L., and Bergamasco, A. (2008). The sea ice dynamics of Terra Nova Bay and Ross Ice Shelf Polynyas during a spring and winter simulation. *Journal of Geophysical Research*, 113(C9):C09003. doi:10.1029/2006JC004048.

Pierrehumbert, R. T. (2011). Infrared radiation and planetary temperature. *Physics Today*, 64(1):33. doi:10.1063/1.3541943.

Poisson, A. and Chen, C.-T. A. (1987). Why is there little anthropogenic CO_2 in the Antartic bottom water? *Deep Sea Research Part A. Oceanographic Research Papers*, 34(7):1255–1275. doi:10.1016/0198-0149(87)90075-6.

Pollard, D. and Thompson, S. L. (1994). Sea-ice dynamics and CO_2 sensitivity in a global climate model. *Atmosphere-Ocean*, 32(2):449–467. doi:10.1080/07055900.1994.9649506.

Polvani, L. M. and Smith, K. L. (2013). Can natural variability explain observed Antarctic sea ice trends? New modeling evidence from CMIP5. *Geophysical Research Letters*, 40(12):3195–3199. doi:10.1002/grl.50578.

Primeau, F. (2005). Characterizing Transport between the Surface Mixed Layer and the Ocean Interior with a Forward and Adjoint Global Ocean Transport Model. *Journal of Physical Oceanography*, 35(4):545–564. doi:10.1175/JPO2699.1.

Pritchard, H. D., Ligtenberg, S. R. M., Fricker, H. A., Vaughan, D. G., van den Broeke, M. R., and Padman, L. (2012). Antarctic ice-sheet loss driven by basal melting of ice shelves. *Nature*, 484(7395):502–505. doi:10.1038/nature10968.

Purkey, S. G. and Johnson, G. C. (2013). Antarctic Bottom Water warming and freshening: contributions to sea level rise, ocean freshwater budgets, and global heat gain. *Journal of Climate*, 26(16):6105–6122. doi:10.1175/JCLI-D-12-00834.1.

Qiao, F. and Huang, C. J. (2012). Comparison between vertical shear mixing and surface wave-induced mixing in the extratropical ocean. *Journal of Geophysical Research: Oceans*, 117(C11):C00J16. doi:10.1029/2012JC007930.

Rahmstorf, S. (2002). Ocean circulation and climate during the past 120,000 years. *Nature*, 419(6903):207–214. doi:10.1038/nature01090.

Rahmstorf, S., Box, J. E., Feulner, G., Mann, M. E., Robinson, A., Rutherford, S., and Schaffernicht, E. J. (2015). Exceptional twentieth-century slowdown in Atlantic Ocean overturning circulation. *Nature Climate Change*, 5(5):475–480. doi:10.1038/nclimate2554.

Randerson, J. T., Lindsay, K., Munoz, E., Fu, W., Moore, J. K., Hoffman, F. M., Mahowald, N. M., and Doney, S. C. (2015). Multicentury changes in ocean and land contributions to the climate-carbon feedback. *Global Biogeochemical Cycles*, 29(6):744–759. doi:10.1002/2014GB005079.

Raphael, M. N., Marshall, G. J., Turner, J., Fogt, R. L., Schneider, D., Dixon, D. A., Hosking, J. S., Jones, J. M., and Hobbs, W. R. (2016). The Amundsen Sea Low: Variability, Change, and Impact on Antarctic Climate. *Bulletin of the American Meteorological Society*, 97(1):111–121. doi:10.1175/BAMS-D-14-00018.1.

Raymond, W. H. and Kuo, H. L. (1984). A radiation boundary condition for multi-dimensional flows. *Quarterly Journal of the Royal Meteorological Society*, 110(464):535–551. doi:10.1002/qj.49711046414.

Ren, L., Speer, K., and Chassignet, E. P. (2011). The mixed layer salinity budget and sea ice in the Southern Ocean. *Journal of Geophysical Research: Oceans*, 116(8):C08031. doi:10.1029/2010JC006634.

Reynolds, R. W., Smith, T. M., Liu, C., Chelton, D. B., Casey, K. S., and Schlax, M. G. (2007). Daily high-resolution-blended analyses for sea surface temperature. *Journal of Climate*, 20(22):5473–5496. doi:10.1175/2007JCLI1824.1.

Ridderinkhof, H., van der Werf, P. M., Ullgren, J. E., van Aken, H. M., van Leeuwen, P. J., and de Ruijter, W. P. M. (2010). Seasonal and interannual variability in the Mozambique Channel from moored current observations. *Journal of Geophysical Research*, 115(C6):C06010. doi:10.1029/2009JC005619.

Ridgway, K. R., Dunn, J. R., and Wilkin, J. L. (2002). Ocean Interpolation by Four-Dimensional Weighted Least SquaresApplication to the Waters around Australasia. *Journal of Atmospheric and Oceanic Technology*, 19(9):1357–1375. doi:10.1175/1520-0426(2002)019<1357:OIBFDW>2.0.CO;2.

Rignot, E., Bamber, J. L., van den Broeke, M. R., Davis, C., Li, Y., van de Berg, W. J., and Van Meijgaard, E. (2008). Recent Antarctic ice mass loss from radar interferometry and regional climate modelling. *Nature Geoscience*, 1(2):106–110. doi:10.1038/ngeo102.

Rignot, E., Jacobs, S., Mouginot, J., and Scheuchl, B. (2013). Ice-shelf melting around Antarctica. *Science*, 341(6143):266–70. doi:10.1126/science.1235798.

Rintoul, S. R. and England, M. H. (2002). Ekman Transport Dominates Local Air–Sea Fluxes in Driving Variability of Subantarctic Mode Water. *Journal of Physical Oceanography*, 32(5):1308–1321. doi:10.1175/1520-0485(2002)032<1308:ETDLAS>2.0.CO;2.

Rintoul, S. R. and Naveira Garabato, A. C. (2013). Dynamics of the Southern Ocean Circulation. In *Ocean Circulation and Climate - A 21st Century Perspective*, volume 103 of *International Geophysics*, pages 471–492. Elsevier. doi:10.1016/B978-0-12-391851-2.00018-0.

Riser, S. C., Freeland, H. J., Roemmich, D., Wijffels, S., Troisi, A., Belbéoch, M., Gilbert, D., Xu, J., Pouliquen, S., Thresher, A., Le Traon, P.-Y., Maze, G., Klein, B., Ravichandran, M., Grant, F., Poulain, P.-M., Suga, T., Lim, B., Sterl, A., Sutton, P., Mork, K.-A., Vélez-Belchí, P. J., Ansorge, I., King, B., Turton, J., Baringer, M., and Jayne, S. R. (2016). Fifteen years of ocean observations with the global Argo array. *Nature Climate Change*, 6(2):145–153. doi:10.1038/nclimate2872.

Ritz, C., Edwards, T. L., Durand, G., Payne, A. J., Peyaud, V., and Hindmarsh, R. C. A. (2015). Potential sea-level rise from Antarctic ice-sheet instability constrained by observations. *Nature*, 528(7580):115–118. doi:10.1038/nature16147.

Roberts, M. and Marshall, D. (1998). Do We Require Adiabatic Dissipation Schemes in Eddy-Resolving Ocean Models? *Journal of Physical Oceanography*, 28(10):2050–2063. doi:10.1175/1520-0485(1998)028<2050:DWRADS>2.0.CO;2.

Roche, D. M., Crosta, X., and Renssen, H. (2012). Evaluating Southern Ocean sea-ice for the Last Glacial Maximum and pre-industrial climates: PMIP-2 models and data evidence. *Quaternary Science Reviews*, 56:99–106. doi:10.1016/j.quascirev.2012.09.020.

Rodehacke, C. B., Hellmer, H. H., Beckmann, A., and Roether, W. (2007). Formation and spreading of Antarctic deep and bottom waters inferred from a chlorofluorocarbon (CFC) simulation. *Journal of Geophysical Research: Oceans*, 112(9):C09001. doi:10.1029/2006JC003884.

Roemmich, D., Church, J., Gilson, J., Monselesan, D., Sutton, P., and Wijffels, S. (2015). Unabated planetary warming and its ocean structure since 2006. *Nature Climate Change*, 5(February):2–7. doi:10.1038/nclimate2513.

Roemmich, D., Gould, W. J., and Gilson, J. (2012). 135 years of global ocean warming between the Challenger expedition and the Argo Programme. *Nature Climate Change*, 2(6):425–428. doi:10.1038/nclimate1461.

Rojas, M. (2013). Sensitivity of Southern Hemisphere circulation to LGM and 4x CO2 climates. *Geophysical Research Letters*, 40(5):965–970. doi:10.1002/grl.50195.

Russell, J. L., Dixon, K. W., Gnanadesikan, A., Stouffer, R. J., and Toggweiler, J. R. (2006). The Southern hemisphere westerlies in a warming world: Propping open the door to the deep ocean. *Journal of Climate*, 19(24):6382–6390. doi:10.1175/JCLI3984.1.

Rye, C. D., Naveira Garabato, A. C., Holland, P. R., Meredith, M. P., Nurser, A. J. G., Hughes, C. W., Coward, A. C., and Webb, D. J. (2014). Rapid sea-level rise along the Antarctic margins in response to increased glacial discharge. *Nature Geoscience*, 7(August):2–5. doi:10.1038/ngeo2230.

Sabine, C. L., Feely, R. A., Gruber, N., Key, R. M., Lee, K., Bullister, J. L., Wanninkhof, R., Wong, C. S. S., Wallace, D. W. R., Tilbrook, B., Millero, F. J., Peng, T.-H., Kozyr, A., Ono, T., and Rios, A. F. (2004). The Oceanic Sink for Anthropogenic CO_2. *Science*, 305(5682):367–371. doi:10.1126/science.1097403.

Saenko, O. A., Fyfe, J. C., and England, M. H. (2005). On the response of the oceanic wind-driven circulation to atmospheric CO_2 increase. *Climate Dynamics*, 25(4):415–426. doi:10.1007/s00382-005-0032-5.

Saenko, O. A., Schmittner, A., and Weaver, A. J. (2002). On the role of wind-driven sea ice motion on ocean ventilation. *Journal of Physical Oceanography*, 32(12):3376–3395. doi:10.1175/1520-0485(2002)032<3376:OTROWD>2.0.CO;2.

Saenko, O. A. and Weaver, A. J. (2001). Importance of wind-driven sea ice motion for the formation of Antarctic Intermediate Water in a global climate model. *Geophysical Research Letters*, 28(21):4147–4150. doi:10.1029/2001GL013632.

Saenko, O. A., Weaver, A. J., and England, M. H. (2003). A Region of Enhanced Northward Antarctic Intermediate Water Transport in a Coupled Climate Model. *Journal of Physical Oceanography*, 33(7):1528–1535. doi:10.1175/1520-0485(2003)033<1528:AROENA>2.0.CO;2.

Sallée, J.-B., Shuckburgh, E., Bruneau, N., Meijers, A. J. S., Bracegirdle, T. J., and Wang, Z. (2013a). Assessment of Southern Ocean mixed-layer depths in CMIP5 models: Historical bias and forcing response. *Journal of Geophysical Research: Oceans*, 118(4):1845–1862. doi:10.1002/jgrc.20157.

Sallée, J.-B., Shuckburgh, E., Bruneau, N., Meijers, A. J. S., Bracegirdle, T. J., Wang, Z., and Roy, T. (2013b). Assessment of Southern Ocean water mass circulation and characteristics in CMIP5 models: Historical bias and forcing response. *Journal of Geophysical Research: Oceans*, 118(4):1830–1844. doi:10.1002/jgrc.20135.

Sallée, J.-B., Speer, K., Rintoul, S. R., and Wijffels, S. E. (2010a). Southern Ocean Thermocline Ventilation. *Journal of Physical Oceanography*, 40(3):509–529. doi:10.1175/2009JPO4291.1.

Sallée, J. B., Speer, K. G., and Rintoul, S. R. (2010b). Zonally asymmetric response of the Southern Ocean mixed-layer depth to the Southern Annular Mode. *Nature Geoscience*, 3(4):273–279.

Sallée, J.-B., Speer, K. G., and Rintoul, S. R. (2011). Mean-flow and topographic control on surface eddy-mixing in the Southern Ocean. *Journal of Marine Research*, 69(4-6):753–777. doi:10.1357/002224011799849408.

Saltzman, B., Hansen, A. R., and Maasch, K. A. (1984). The Late Quaternary Glaciations as the Response of a Three-Component Feedback System to Earth-Orbital Forcing. *Journal of the Atmospheric Sciences*, 41(23):3380–3389. doi:10.1175/1520-0469(1984)041<3380:TLQGAT>2.0.CO;2.

Santer, B. D., Wehner, M. F., Wigley, T. M. L., Sausen, R., Meehl, G. A., Taylor, K. E., Ammann, C., Arblaster, J., Washington, W. M., Boyle, J. S., and Brüggemann, W. (2003). Contributions of Anthropogenic and Natural Forcing to Recent Tropopause Height Changes. *Science*, 301(5632):479–483. doi:10.1126/science.1084123.

Santer, B. D., Wigley, T. M. L., Boyle, J. S., Gaffen, D. J., Hnilo, J. J., Nychka, D., Parker, D. E., and Taylor, K. E. (2000). Statistical significance of trends and trend differences in layer-average atmospheric temperature time series. *Journal of Geophysical Research*, 105(D6):7337–7356. doi:10.1029/1999JD901105.

Santoso, A. and England, M. H. (2004). Antarctic Intermediate Water Circulation and Variability in a Coupled Climate Model. *Journal of Physical Oceanography*, 34(10):2160–2179. doi:10.1175/1520-0485(2004)034<2160:AIWCAV>2.0.CO;2.

Sanz Rodrigo, J., Buchlin, J. M., van Beeck, J., Lenaerts, J. T. M., and van den Broeke, M. R. (2013). Evaluation of the antarctic surface wind climate from ERA reanalyses and RACMO2/ANT simulations based on automatic weather stations. *Climate Dynamics*, 40(1-2):353–376. doi:10.1007/s00382-012-1396-y.

Sarmiento, J. L. and Gruber, N. (2006). *Ocean Biogeochemical Dynamics*. Princeton University Press, Princeton, NJ.

Sarmiento, J. L., Gruber, N., Brzezinski, M. A., and Dunne, J. P. (2004). High-latitude controls of thermocline nutrients and low latitude biological productivity. *Nature*, 427(6969):56–60. doi:10.1038/nature10605.

Sarmiento, J. L., Hughes, T. M. C., Stouffer, R. J., and Manabe, S. (1998). Simulated response of the ocean carbon cycle to anthropogenic climate warming. *Nature*, 393(6682):245–249. doi:10.1038/30455.

Sarmiento, J. L. and Le Quéré, C. (1996). Oceanic Carbon Dioxide Uptake in a Model of Century-Scale Global Warming. *Science*, 274(5291):1346–1350. doi:10.1126/science.274.5291.1346.

Sarmiento, J. L., Le Quéré, C., and Pacala, S. W. (1995). Limiting future atmospheric carbon dioxide. *Global Biogeochemical Cycles*, 9(1):121–137. doi:10.1029/94GB01779.

Sarmiento, J. L., Orr, J. C., and Siegenthaler, U. (1992). A perturbation simulation of CO_2 uptake in an ocean general circulation model. *Journal of Geophysical Research*, 97(C3):3621. doi:10.1029/91JC02849.

Sarmiento, J. L. and Toggweiler, J. R. (1984). A new model for the role of the oceans in determining atmospheric PCO_2. *Nature*, 308(5960):621–624. doi:10.1038/308621a0.

Sarmiento, J. L. and Toggweiler, J. R. (1986). A Preliminary Model of the Role of Upper Ocean Chemical Dynamics in Determining Oceanic Oxygen and Atmospheric Carbon Dioxide Levels. In Burton, J. D., Brewer, P. G., and Chesselet, R., editors, *Dynamic Processes in the Chemistry of the Upper Ocean*, chapter 18, pages 233–240. Springer US, Boston, MA. doi:10.1007/978-1-4684-5215-0_18.

Sarmiento, J. L., Toggweiler, J. R., Najjar, R., Webb, D. J., Jenkins, W. J., Wunsch, C., Elderfield, H., Whitfield, M., and Minster, J.-F. (1988). Ocean Carbon-Cycle Dynamics and Atmospheric pCO_2 [and Discussion]. *Philosophical Transactions of the Royal Society A*, 325(1583):3–21. doi:10.1098/rsta.1988.0039.

Schaffer, J., Timmermann, R., Arndt, J. E., Kristensen, S. S., Mayer, C., Morlighem, M., and Steinhage, D. (2016). A global, high-resolution data set of ice sheet topography, cavity geometry, and ocean bathymetry. *Earth System Science Data*, 8:543–557. doi:10.5194/essd-8-543-2016.

Schmidt, G. A., Bigg, G. R., and Rohling, E. J. (1999). Global Seawater Oxygen-18 Database - v1.21. NASA GISS.

Schmidt, H., Rast, S., Bunzel, F., Esch, M., Giorgetta, M., Kinne, S., Krismer, T., Stenchikov, G., Timmreck, C., Tomassini, L., and Walz, M. (2013). Response of the middle atmosphere to anthropogenic and natural forcings in the CMIP5 simulations with the Max Planck Institute Earth system model. *Journal of Advances in Modeling Earth Systems*, 5(1):98–116. doi:10.1002/jame.20014.

Schmidtko, S., Heywood, K. J., Thompson, A. F., and Aoki, S. (2014). Multidecadal warming of Antarctic waters. *Science*, 346(6214):1227–1231. doi:10.1126/science.1256117.

Schmidtko, S. and Johnson, G. C. (2012). Multidecadal warming and shoaling of Antarctic Intermediate Water. *Journal of Climate*, 25(1):207–221. doi:10.1175/JCLI-D-11-00021.1.

Schmidtko, S., Johnson, G. C., and Lyman, J. M. (2013). MIMOC: A global monthly isopycnal upper-ocean climatology with mixed layers. *Journal of Geophysical Research: Oceans*, 118(4):1658–1672. doi:10.1002/jgrc.20122.

Schmitz, W. J. (1995). On the interbasin-scale thermohaline circulation. *Reviews of Geophysics*, 33(2):151. doi:10.1029/95RG00879.

Schmitz, W. J. (1996). On the World Ocean Circulation: Volume I. Some global features / North Atlantic circulation. Technical report, Woods Hole Oceanographic Institution, Woods Hole, MA.

Schneider, D. P., Deser, C., and Okumura, Y. (2012a). An assessment and interpretation of the observed warming of West Antarctica in the austral spring. *Climate Dynamics*, 38(1-2):323–347. doi:10.1007/s00382-010-0985-x.

Schneider, D. P., Okumura, Y., and Deser, C. (2012b). Observed Antarctic Interannual Climate Variability and Tropical Linkages. *J. Climate*, 25(12):4048–4066. doi:10.1175/JCLI-D-11-00273.1.

Schodlok, M. P., Hellmer, H. H., and Beckmann, A. (2002). On the transport, variability and origin of dense water masses crossing the South Scotia Ridge. *Deep-Sea Research Part II: Topical Studies in Oceanography*, 49(21):4807–4825. doi:10.1016/S0967-0645(02)00160-1.

Schröder, M. and Fahrbach, E. (1999). On the structure and the transport of the eastern Weddell Gyre. *Deep Sea Research Part II: Topical Studies in Oceanography*, 46(1-2):501–527. doi:10.1016/S0967-0645(98)00112-X.

Schwegmann, S., Haas, C., Fowler, C., and Gerdes, R. (2011). A comparison of satellite-derived sea-ice motion with drifting-buoy data in the Weddell Sea, Antarctica. *Annals of Glaciology*, 52(57):103–110. doi:10.3189/172756411795931813.

Schwegmann, S., Rinne, E., Ricker, R., Hendricks, S., and Helm, V. (2016). About the consistency between Envisat and CryoSat-2 radar freeboard retrieval over Antarctic sea ice. *The Cryosphere*, 10(4):1415–1425. doi:10.5194/tc-10-1415-2016.

SeaWiFS Project, . (2003). SeaWiFS Global Monthly Mapped 9 km Chlorophyll a. Ver. 1., CA, USA. PO.DAAC.

Sen Gupta, A., Santoso, A., Taschetto, A. S., Ummenhofer, C. C., Trevena, J., and England, M. H. (2009). Projected Changes to the Southern Hemisphere Ocean and Sea Ice in the IPCC AR4 Climate Models. *J. Climate*, 22(11):3047–3078. doi:10.1175/2008JCLI2827.1.

Seviour, W. J. M., Gnanadesikan, A., and Waugh, D. W. (2016). The Transient Response of the Southern Ocean to Stratospheric Ozone Depletion. *Journal of Climate*. doi:10.1175/JCLI-D-16-0198.1.

Shackleton, N. J. (2000). The 100,000-year ice-age cycle identified and found to lag temperature, carbon dioxide, and orbital eccentricity. *Science*, 289(5486):1897–1902. doi:10.1126/science.289.5486.1897.

Shakun, J. D., Clark, P. U., He, F., Marcott, S. A., Mix, A. C., Liu, Z., Otto-Bliesner, B., Schmittner, A., and Bard, E. (2012). Global warming preceded by increasing carbon dioxide concentrations during the last deglaciation. *Nature*, 484(7392):49–54. doi:10.1038/nature10915.

Shchepetkin, A. F. (2005). If-less KPP. *ROMS/TOMS Workshop: Adjoint Modeling and Applications*.

Shchepetkin, A. F. (2015). An adaptive, Courant-number-dependent implicit scheme for vertical advection in oceanic modeling. *Ocean Modelling*, 91:38–69. doi:10.1016/j.ocemod.2015.03.006.

Shchepetkin, A. F. and McWilliams, J. C. (1998). Quasi-Monotone Advection Schemes Based on Explicit Locally Adaptive Dissipation. *Monthly Weather Review*, 126(6):1541–1580. doi:10.1175/1520-0493(1998)126<1541:QMASBO>2.0.CO;2.

Shchepetkin, A. F. and McWilliams, J. C. (2003). A method for computing horizontal pressure-gradient force in an oceanic model with a nonaligned vertical coordinate. *Journal of Geophysical Research*, 108(C3):3090. doi:10.1029/2001JC001047.

Shchepetkin, A. F. and McWilliams, J. C. (2005). The regional oceanic modeling system (ROMS): A split-explicit, free-surface, topography-following-coordinate oceanic model. *Ocean Modelling*, 9(4):347–404. doi:10.1016/j.ocemod.2004.08.002.

Shchepetkin, A. F. and McWilliams, J. C. (2009a). Computational Kernel Algorithms for Fine-Scale, Multiprocess, Longtime Oceanic Simulations. *Handbook of Numerical Analysis*, 14:121–183. doi:10.1016/S1570-8659(08)01202-0.

Shchepetkin, A. F. and McWilliams, J. C. (2009b). Correction and commentary for "Ocean forecasting in terrain-following coordinates: Formulation and skill assessment of the regional ocean modeling system" by Haidvogel et al., J. Comp. Phys. 227, pp. 3595-3624. *Journal of Computational Physics*, 228(24):8985–9000. doi:10.1016/j.jcp.2009.09.002.

Shchepetkin, A. F. and McWilliams, J. C. (2011). Accurate Boussinesq oceanic modeling with a practical, "Stiffened" Equation of State. *Ocean Modelling*, 38(1-2):41–70. doi:10.1016/j.ocemod.2011.01.010.

Shepherd, A., Ivins, E. R., A, G., Barletta, V. R., Bentley, M. J., Bettadpur, S., Briggs, K. H., Bromwich, D. H., Forsberg, R., Galin, N., Horwath, M., Jacobs, S., Joughin, I., King, M. A., Lenaerts, J. T. M., Li, J., Ligtenberg, S. R. M., Luckman, A., Luthcke, S. B., McMillan, M., Meister, R., Milne, G., Mouginot, J., Muir, A., Nicolas, J. P., Paden, J., Payne, A. J., Pritchard, H., Rignot, E., Rott, H., Sorensen, L. S., Scambos, T. A., Scheuchl, B., Schrama, E. J. O., Smith, B., Sundal, A. V., van Angelen, J. H., van de Berg, W. J., van den Broeke, M. R., Vaughan, D. G., Velicogna, I., Wahr, J., Whitehouse, P. L., Wingham, D. J., Yi, D., Young, D., and Zwally, H. J. (2012). A Reconciled Estimate of Ice-Sheet Mass Balance. *Science*, 338(6111):1183–1189. doi:10.1126/science.1228102.

Siegenthaler, U. and Wenk, T. (1984). Rapid atmospheric CO_2 variations and ocean circulation. *Nature*, 308(5960):624–626. doi:10.1038/308624a0.

Sigman, D. M. and Boyle, E. A. (2000). Glacial/interglacial variations in atmospheric carbon dioxide. *Nature*, 407(6806):859–869. doi:10.1038/35038000.

Sigman, D. M., Hain, M. P., and Haug, G. H. (2010). The polar ocean and glacial cycles in atmospheric CO_2 concentration. *Nature*, 466(7302):47–55. doi:10.1038/nature09149.

Sigman, D. M., Jaccard, S. L., and Haug, G. H. (2004). Polar ocean stratification in a cold climate. *Nature*, 428(6978):59–63. doi:10.1038/nature02378.1.

Sigmond, M. and Fyfe, J. C. (2014). The Antarctic Sea Ice Response to the Ozone Hole in Climate Models. *Journal of Climate*, 27(3):1336–1342. doi:10.1175/JCLI-D-13-00590.1.

Sigmond, M., Reader, M. C., Fyfe, J. C., and Gillett, N. P. (2011). Drivers of past and future Southern Ocean change: Stratospheric ozone versus greenhouse gas impacts. *Geophysical Research Letters*, 38(12):L12601. doi:10.1029/2011GL047120.

Silva, T. A. M., Bigg, G. R., and Nicholls, K. W. (2006). Contribution of giant icebergs to the Southern Ocean freshwater flux. *Journal of Geophysical Research: Oceans*, 111(3):C03004. doi:10.1029/2004JC002843.

Simpkins, G. R., Ciasto, L. M., Thompson, D. W. J., and England, M. H. (2012). Seasonal relationships between large-scale climate variability and antarctic sea ice concentration. *Journal of Climate*, 25(16):5451–5469. doi:10.1175/JCLI-D-11-00367.1.

Simpkins, G. R., McGregor, S., Taschetto, A. S., Ciasto, L. M., and England, M. H. (2014). Tropical Connections to Climatic Change in the Extratropical Southern Hemisphere: The Role of Atlantic SST Trends. *Journal of Climate*, 27(13):4923–4936. doi:10.1175/JCLI-D-13-00615.1.

Skinner, L. C., Fallon, S., Waelbroeck, C., Michel, E., and Barker, S. (2010). Ventilation of the deep Southern Ocean and deglacial CO_2 rise. *Science*, 328(5982):1147–1151. doi:10.1126/science.1183627.

Sloyan, B. M. and Rintoul, S. R. (2001a). Circulation, renewal, and modification of Antarctic Mode and Intermediate Water. *Journal of Physical Oceanography*, 31(4):1005–1030. doi:10.1175/1520-0485(2001)031<1005:CRAMOA>2.0.CO;2.

Sloyan, B. M. and Rintoul, S. R. (2001b). The Southern Ocean Limb of the Global Deep Overturning Circulation. *Journal of Physical Oceanography*, 31(1):143–173. doi:10.1175/1520-0485(2001)031<0143:TSOLOT>2.0.CO;2.

Smith, K. L. and Polvani, L. M. (2016). Spatial patterns of recent Antarctic surface temperature trends and the importance of natural variability: lessons from multiple reconstructions and the CMIP5 models. *Climate Dynamics*, 48(7-8):2653–2670. doi:10.1007/s00382-016-3230-4.

Smith, R. D. and Gent, P. R. (2004). Anisotropic Gent-McWilliams parameterization for ocean models. *Journal of Physical Oceanography*, 34(11):2541–2564. doi:10.1175/JPO2613.1.

Snow, K., Hogg, A. M., Downes, S. M., Sloyan, B. M., Bates, M. L., and Griffies, S. M. (2015). Sensitivity of abyssal water masses to overflow parameterisations. *Ocean Modelling*, 89:84–103. doi:10.1016/j.ocemod.2015.03.004.

Snow, K., Sloyan, B. M., Rintoul, S. R., Hogg, A. M., and Downes, S. M. (2016). Controls on circulation, cross-shelf exchange, and dense water formation in an Antarctic polynya. *Geophysical Research Letters*, 43(13):7089–7096. doi:10.1002/2016GL069479.

Sokolov, S. and Rintoul, S. R. (2009a). Circumpolar structure and distribution of the Antarctic Circumpolar Current fronts: 1. Mean circumpolar paths. *Journal of Geophysical Research*, 114(11):C11018. doi:10.1029/2008JC005108.

Sokolov, S. and Rintoul, S. R. (2009b). Circumpolar structure and distribution of the Antarctic Circumpolar Current fronts: 2. Variability and relationship to sea surface height. *Journal of Geophysical Research*, 114(11):C11019. doi:10.1029/2008JC005248.

Son, S.-W., Gerber, E. P., Perlwitz, J., Polvani, L. M., Gillett, N. P., Seo, K.-H., Eyring, V., Shepherd, T. G., Waugh, D., Akiyoshi, H., Austin, J., Baumgaertner, A., Bekki, S., Braesicke, P., Brühl, C., Butchart, N., Chipperfield, M. P., Cugnet, D., Dameris, M., Dhomse, S., Frith, S., Garny, H., Garcia, R., Hardiman, S. C., Jöckel, P., Lamarque, J. F., Mancini, E., Marchand, M., Michou, M., Nakamura, T., Morgenstern, O., Pitari, G., Plummer, D. A., Pyle, J., Rozanov, E., Scinocca, J. F., Shibata, K., Smale, D., Teyssèdre, H., Tian, W., and Yamashita, Y. (2010). Impact of stratospheric ozone on Southern Hemisphere circulation change: A multimodel assessment. *Journal of Geophysical Research*, 115(D3):D00M07. doi:10.1029/2010JD014271.

Son, S.-W., Polvani, L. M., Waugh, D. W., Akiyoshi, H., Garcia, R., Kinnison, D., Pawson, S., Rozanov, E., Shepherd, T. G., and Shibata, K. (2008). The impact of stratospheric ozone recovery on the Southern Hemisphere westerly jet. *Science*, 320(5882):1486–1489. doi:10.1126/science.1155939.

Song, Y. and Haidvogel, D. (1994). A Semi-implicit Ocean Circulation Model Using a Generalized Topography-Following Coordinate System. *Journal of Computational Physics*, 115(1):228–244. doi:10.1006/jcph.1994.1189.

Speer, K., Lovenduski, N., England, M., Thompson, D. J., and Beswick, C. (2012). Developing a vision for climate variability research in the Southern Ocean-Ice-Atmosphere system, In *CLIVAR Exchanges*, 17(58), pages 43–45.

Speer, K., Rintoul, S. R., and Sloyan, B. (2000). The Diabatic Deacon Cell. *Journal of Physical Oceanography*, 30(12):3212–3222. doi:10.1175/1520-0485(2000)030<3212:TDDC>2.0.CO;2.

Spence, P., Griffies, S. M., England, M. H., Hogg, A. M., Saenko, O. A., and Jourdain, N. C. (2014). Rapid subsurface warming and circulation changes of Antarctic coastal waters by poleward shifting winds. *Geophysical Research Letters*, 41(13):4601–4610. doi:10.1002/2014GL060613.

Stammer, D., Ueyoshi, K., Köhl, A., Large, W. G., Josey, S. A., and Wunsch, C. (2004). Estimating air-sea fluxes of heat, freshwater, and momentum through global ocean data assimilation. *Journal of Geophysical Research*, 109(C5):C05023. doi:10.1029/2003JC002082.

Stammer, D., Wunsch, C., Giering, R., Eckert, C., Heimbach, P., Marotzke, J., Adcroft, A., Hill, C. N., and Marshall, J. (2003). Volume, heat, and freshwater transports of the global ocean circulation 1993-2000, estimated from a general circulation model constrained by World Ocean Circulation Experiment (WOCE) data. *Journal of Geophysical Research*, 108(C1):3007. doi:10.1029/2001JC001115.

Stammerjohn, S., Massom, R., Rind, D., and Martinson, D. (2012). Regions of rapid sea ice change: An inter-hemispheric seasonal comparison. *Geophysical Research Letters*, 39(6):L06501. doi:10.1029/2012GL050874.

Stammerjohn, S. E., Martinson, D. G., Smith, R. C., Yuan, X., and Rind, D. (2008). Trends in Antarctic annual sea ice retreat and advance and their relation to El Nino-Southern Oscillation and Southern Annular Mode variability. *Journal of Geophysical Research*, 113:C03S90. doi:10.1029/2007JC004269.

Steele, M., Mellor, G. L., and McPhee, M. G. (1989). Role of the Molecular Sublayer in the Melting or Freezing of Sea Ice. *Journal of Physical Oceanography*, 19(1):139–147. doi:10.1175/1520-0485(1989)019<0139:ROTMSI>2.0.CO;2.

Stevens, B., Giorgetta, M., Esch, M., Mauritsen, T., Crueger, T., Rast, S., Salzmann, M., Schmidt, H., Bader, J., Block, K., Brokopf, R., Fast, I., Kinne, S., Kornblueh, L., Lohmann, U., Pincus, R., Reichler, T., and Roeckner, E. (2013). Atmospheric component of the MPI-M Earth System Model: ECHAM6. *Journal of Advances in Modeling Earth Systems*, 5(2):146–172. doi:10.1002/jame.20015.

Stewart, A. L. and Thompson, A. F. (2013). Connecting Antarctic Cross-Slope Exchange with Southern Ocean Overturning. *Journal of Physical Oceanography*, 43(7):1453–1471. doi:10.1175/JPO-D-12-0205.1.

Stewart, K. D., Haine, T. W. N., Stewart, K. D., and Haine, T. W. N. (2016). Thermobaricity in the Transition Zones between Alpha and Beta Oceans. *Journal of Physical Oceanography*, 46(6):1805–1821. doi:10.1175/JPO-D-16-0017.1.

Stocker, B. D., Roth, R., Joos, F., Spahni, R., Steinacher, M., Zaehle, S., Bouwman, L., Xu-Ri, and Prentice, I. C. (2013). Multiple greenhouse-gas feedbacks from the land biosphere under future climate change scenarios. *Nature Climate Change*, 3(7):666–672. doi:10.1038/nclimate1864.

Stocker, T. F. (2015). The silent services of the world ocean. *Science*, 350(6262):764–766. doi:10.1126/science.aac8720.

Stocker, T. F. and Schmittner, A. (1997). Influence of CO_2 emission rates on the stability of the thermohaline circulation. *Nature*, 388(6645):862–865. doi:10.1038/42224.

Stössel, A., Notz, D., Haumann, F. A., Haak, H., Jungclaus, J., and Mikolajewicz, U. (2015). Controlling high-latitude Southern Ocean convection in climate models. *Ocean Modelling*, 86:58–75. doi:10.1016/j.ocemod.2014.11.008.

Stössel, A., Yang, K., and Kim, S.-J. (2002). On the Role of Sea Ice and Convection in a Global Ocean Model. *Journal of Physical Oceanography*, 32(4):1194–1208. doi:10.1175/1520-0485(2002)032<1194:OTROSI>2.0.CO;2.

Stössel, A., Zhang, Z., and Vihma, T. (2011). The effect of alternative real-time wind forcing on Southern Ocean sea ice simulations. *Journal of Geophysical Research: Oceans*, 116(11):C11021. doi:10.1029/2011JC007328.

Stull, R. B. (1988). *An Introduction to Boundary Layer Meteorology*, volume 13 of *Atmospheric Sciences Library*. Kluwer Academic Publishers, Dordrecht, Boston, London. doi:10.1007/978-94-009-3027-8.

Suess, E. (1980). Particulate organic carbon flux in the oceanssurface productivity and oxygen utilization. *Nature*, 288(5788):260–263. doi:10.1038/288260a0.

Sumata, H., Lavergne, T., Girard-Ardhuin, F., Kimura, N., Tschudi, M. A., Kauker, F., Karcher, M., and Gerdes, R. (2014). An intercomparison of Arctic ice drift products to deduce uncertainty estimates. *Journal of Geophysical Research: Oceans*, 119(8):4887–4921. doi:10.1002/2013JC009724.

Sun, S., Eisenman, I., and Stewart, A. L. (2016). The influence of Southern Ocean surface buoyancy forcing on glacial-interglacial changes in the global deep ocean stratification. *Geophysical Research Letters*, 43(15):8124–8132. doi:10.1002/2016GL070058.

Sutterley, T. C., Velicogna, I., Rignot, E., Mouginot, J., Flament, T., van den Broeke, M. R., van Wessem, J. M., and Reijmer, C. H. (2014). Mass loss of the Amundsen Sea Embayment of West Antarctica from four independent techniques. *Geophysical Research Letters*, 41(23):8421–8428. doi:10.1002/2014GL061940.

Sverdrup, H. U. (1933). On vertical circulation in the ocean due to the action of the wind with application to conditions within the Antarctic Circumpolar Current, In *Discovery reports*, pages 139–170. Cambridge University Press.

Swart, N. C. and Fyfe, J. C. (2012). Observed and simulated changes in the Southern Hemisphere surface westerly wind-stress. *Geophysical Research Letters*, 39(16):L16711. doi:10.1029/2012GL052810.

Tagliabue, A. and Arrigo, K. R. (2016). Decadal trends in air-sea CO_2 exchange in the Ross Sea (Antarctica). *Geophysical Research Letters*, 43(10):5271–5278. doi:10.1002/2016GL069071.

Takahashi, T., Sutherland, S. C., Sweeney, C., Poisson, A., Metzl, N., Tilbrook, B., Bates, N., Wanninkhof, R., Feely, R. A., Sabine, C., Olafsson, J., and Nojiri, Y. (2002). Global sea–air CO_2 flux based on climatological surface ocean pCO_2, and seasonal biological and temperature effects. *Deep Sea Research Part II: Topical Studies in Oceanography*, 49(9):1601–1622. doi:10.1016/S0967-0645(02)00003-6.

Takahashi, T., Sutherland, S. C., Wanninkhof, R., Sweeney, C., Feely, R. A., Chipman, D. W., Hales, B., Friederich, G., Chavez, F., Sabine, C., Watson, A., Bakker, D. C. E., Schuster, U., Metzl, N., Yoshikawa-Inoue, H., Ishii, M., Midorikawa, T., Nojiri, Y., Körtzinger, A., Steinhoff, T., Hoppema, M., Olafsson, J., Arnarson, T. S., Tilbrook, B., Johannessen, T., Olsen, A., Bellerby, R., Wong, C. S., Delille, B., Bates, N. R., and de Baar, H. J. W. (2009). Climatological mean and decadal change in surface ocean pCO_2, and net sea–air CO_2 flux over the global oceans. *Deep Sea Research Part II: Topical Studies in Oceanography*, 56(8-10):554–577. doi:10.1016/j.dsr2.2008.12.009.

Talley, L. D. (1996). Antarctic Intermediate Water in the South Atlantic. In Wefer, G., Berger, W., Siedler, G., and Webb, D., editors, *The South Atlantic: present and past circulation*, pages 219–238. Springer, Berlin, Heidelberg. doi:10.1007/978-3-642-80353-6_11.

Talley, L. D. (2003). Shallow, Intermediate, and Deep Overturning Components of the Global Heat Budget. *Journal of Physical Oceanography*, 33(3):530–560. doi:10.1175/1520-0485(2003)033<0530:SIADOC>2.0.CO;2.

Talley, L. D. (2008). Freshwater transport estimates and the global overturning circulation: Shallow, deep and throughflow components. *Progress in Oceanography*, 78(4):257–303. doi:10.1016/j.pocean.2008.05.001.

Talley, L. D. (2013). Closure of the global overturning circulation through the Indian, Pacific, and Southern Oceans: Schematics and transports. *Oceanography*, 26(1):80–97. doi:10.5670/oceanog.2013.07.

Tamura, T., Ohshima, K. I., and Nihashi, S. (2008). Mapping of sea ice production for Antarctic coastal polynyas. *Geophysical Research Letters*, 35(7):L07606. doi:10.1029/2007GL032903.

Tamura, T., Ohshima, K. I., Nihashi, S., and Hasumi, H. (2011). Estimation of surface heat/salt fluxes associated with sea ice growth/melt in the Southern Ocean. *SOLA*, 7:17–20. doi:10.2151/sola.2011-005.

Thomas, E. R. and Abram, N. J. (2016). Ice core reconstruction of sea ice change in the Amundsen-Ross Seas since 1702 A.D. *Geophysical Research Letters*, 43(10):5309–5317. doi:10.1002/2016GL068130.

Thompson, A. F., Heywood, K. J., Schmidtko, S., and Stewart, A. L. (2014). Eddy transport as a key component of the Antarctic overturning circulation. *Nature Geoscience*, 7(12):879–884. doi:10.1038/ngeo2289.

Thompson, D. W. J., Solomon, S., Kushner, P. J., England, M. H., Grise, K. M., and Karoly, D. J. (2011). Signatures of the Antarctic ozone hole in Southern Hemisphere surface climate change. *Nature Geoscience*, 4(11):741–749. doi:10.1038/ngeo1296.

Thorndike, A. S. and Colony, R. (1982). Sea ice motion in response to geostrophic winds. *Journal of Geophysical Research*, 87(C8):5845–5852. doi:10.1029/JC087iC08p05845.

Tietäväinen, H. and Vihma, T. (2008). Atmospheric moisture budget over Antarctica and the Southern Ocean based on the ERA-40 reanalysis. *International Journal of Climatology*, 28(15):1977–1995. doi:10.1002/joc.1684.

Timco, G. W. and Frederking, R. M. W. (1996). A review of sea ice density. *Cold Regions Science and Technology*, 24(1):1–6. doi:10.1016/0165-232X(95)00007-X.

Timmermann, R. and Beckmann, A. (2004). Parameterization of vertical mixing in the Weddell Sea. *Ocean Modelling*, 6(1):83–100. doi:10.1016/S1463-5003(02)00061-6.

Timmermann, R., Beckmann, A., and Hellmer, H. H. (2001). The role of sea ice in the fresh-water budget of the Weddell Sea, Antarctica. *Annals of Glaciology*, 33(1):419–424. doi:10.3189/172756401781818121.

Timmermann, R., Beckmann, A., and Hellmer, H. H. (2002). Simulations of ice-ocean dynamics in the Weddell Sea 1. Model configuration and validation. *Journal of Geophysical Research*, 107(C3):3024. doi:10.1029/2000JC000741.

Timmermann, R. and Hellmer, H. H. (2013). Southern Ocean warming and increased ice shelf basal melting in the twenty-first and twenty-second centuries based on coupled ice-ocean finite-element modelling. *Ocean Dynamics*, 63(9-10):1011–1026. doi:10.1007/s10236-013-0642-0.

Timmermann, R., Le Brocq, A., Deen, T., Domack, E., Dutrieux, P., Galton-Fenzi, B., Hellmer, H., Humbert, A., Jansen, D., Jenkins, A., Lambrecht, A., Makinson, K., Niederjasper, F., Nitsche, F., Nøst, O. A., Smedsrud, L. H., and Smith, W. H. F. (2010). A consistent data set of Antarctic ice sheet topography, cavity geometry, and global bathymetry. *Earth System Science Data*, 2(2):261–273. doi:10.5194/essd-2-261-2010.

Timmermann, R., Wang, Q., and Hellmer, H. H. (2012). Ice-shelf basal melting in a global finite-element sea-ice/ice-shelf/ocean model. *Annals of Glaciology*, 53(60):303–314. doi:10.3189/2012AoG60A156.

Toggweiler, J. and Samuels, B. (1995). Effect of drake passage on the global thermohaline circulation. *Deep Sea Research Part I: Oceanographic Research Papers*, 42(4):477–500. doi:10.1016/0967-0637(95)00012-U.

Toggweiler, J. R. (1999). Variation of atmospheric CO_2 by ventilation of the ocean's deepest water. *Paleoceanography*, 14(5):571. doi:10.1029/1999PA900033.

Toggweiler, J. R. and Russell, J. (2008). Ocean circulation in a warming climate. *Nature*, 451(7176):286–288. doi:10.1038/nature06590.

Toggweiler, J. R., Russell, J. L., and Carson, S. R. (2006). Midlatitude westerlies, atmospheric CO_2 , and climate change during the ice ages. *Paleoceanography*, 21(2):PA2005. doi:10.1029/2005PA001154.

Toggweiler, J. R. and Samuels, B. (1993). Is the Magnitude of the Deep Outflow from the Atlantic Ocean Actually Governed by Southern Hemisphere Winds? In *The Global Carbon Cycle*, pages 303–331. Springer Berlin Heidelberg, Berlin, Heidelberg. doi:10.1007/978-3-642-84608-3_13.

Tournadre, J., Bouhier, N., Girard-Ardhuin, F., and Rémy, F. (2016). Antarctic icebergs distributions 1992-2014. *Journal of Geophysical Research: Oceans*, 121:327–349. doi:10.1002/2015JC011178.

Treguier, A. M., Le Sommer, J., Molines, J. M., and de Cuevas, B. (2010). Response of the Southern Ocean to the Southern Annular Mode: Interannual Variability and Multidecadal Trend. *Journal of Physical Oceanography*, 40(7):1659–1668. doi:10.1175/2010JPO4364.1.

Trenberth, K. E., Caron, J. M., Trenberth, K. E., and Caron, J. M. (2001). Estimates of Meridional Atmosphere and Ocean Heat Transports. *Journal of Climate*, 14(16):3433–3443. doi:10.1175/1520-0442(2001)014<3433:EOMAAO>2.0.CO;2.

Trenberth, K. E., Fasullo, J. T., and Mackaro, J. (2011). Atmospheric moisture transports from ocean to land and global energy flows in reanalyses. *Journal of Climate*, 24(18):4907–4924. doi:10.1175/2011JCLI4171.1.

Turi, G., Lachkar, Z., and Gruber, N. (2014). Spatiotemporal variability and drivers of pCO_2 and air-sea CO_2 fluxes in the California Current System: An eddy-resolving modeling study. *Biogeosciences*, 11(3):671–690. doi:10.5194/bg-11-671-2014.

Turi, G., Lachkar, Z., Gruber, N., and Münnich, M. (2016). Climatic modulation of recent trends in ocean acidification in the California Current System. *Environmental Research Letters*, 11(1):014007. doi:10.1088/1748-9326/11/1/014007.

Turner, J., Bracegirdle, T. J., Phillips, T., Marshall, G. J., Hosking, J. S., and Scott Hosking, J. (2013). An Initial Assessment of Antarctic Sea Ice Extent in the CMIP5 Models. *Journal of Climate*, 26(5):1473–1484. doi:10.1175/JCLI-D-12-00068.1.

Turner, J., Comiso, J. C., Marshall, G. J., Lachlan-Cope, T. A., Bracegirdle, T., Maksym, T., Meredith, M. P., Wang, Z., and Orr, A. (2009). Non-annular atmospheric circulation change induced by stratospheric ozone depletion and its role in the recent increase of Antarctic sea ice extent. *Geophysical Research Letters*, 36(8):L08502. doi:10.1029/2009GL037524.

Turner, J., Lu, H., White, I., King, J. C., Phillips, T., Hosking, J. S., Bracegirdle, T. J., Marshall, G. J., Mulvaney, R., and Deb, P. (2016). Absence of 21st century warming on Antarctic Peninsula consistent with natural variability. *Nature*, 535(7612):411–415. doi:10.1038/nature18645.

Turner, J. S. (1973). *Buoyancy Effects in Fluids*. Cambridge University Press, Cambridge. doi:10.1017/CBO9780511608827.

Uotila, P., Holland, P. R., Vihma, T., Marsland, S. J., and Kimura, N. (2014). Is realistic Antarctic sea-ice extent in climate models the result of excessive ice drift? *Ocean Modelling*, 79:33–42. doi:10.1016/j.ocemod.2014.04.004.

Urakawa, L. S. and Hasumi, H. (2012). Eddy-Resolving Model Estimate of the Cabbeling Effect on the Water Mass Transformation in the Southern Ocean. *Journal of Physical Oceanography*, 42(8):1288–1302. doi:10.1175/JPO-D-11-0173.1.

van Loon, H. and Jenne, R. L. (1972). The zonal harmonic standing waves in the southern hemisphere. *Journal of Geophysical Research*, 77(6):992–1003. doi:10.1029/JC077i006p00992.

Vancoppenolle, M., Fichefet, T., and Goosse, H. (2009). Simulating the mass balance and salinity of Arctic and Antarctic sea ice. 2. Importance of sea ice salinity variations. *Ocean Modelling*, 27(1-2):54–69. doi:10.1016/j.ocemod.2008.11.003.

Viglione, G. A. and Thompson, A. F. (2016). Lagrangian pathways of upwelling in the Southern Ocean. *Journal of Geophysical Research*. doi:10.1002/2016JC011773.

Wang, S. and Moore, J. K. (2012). Variability of primary production and air–sea CO_2 flux in the Southern Ocean. *Global Biogeochemical Cycles*, 26(1):GB1008. doi:10.1029/2010GB003981.

Wanninkhof, R. and McGillis, W. R. (1999). A cubic relationship between air-sea CO_2 exchange and wind speed. *Geophysical Research Letters*, 26(13):1889–1892. doi:10.1029/1999GL900363.

Watson, A. J., Ledwell, J. R., Messias, M.-J., King, B. a., Mackay, N., Meredith, M. P., Mills, B., and Naveira Garabato, A. C. (2013). Rapid cross-density ocean mixing at mid-depths in the Drake Passage measured by tracer release. *Nature*, 501(7467):408–411. doi:10.1038/nature12432.

Watson, A. J. and Naveira Garabato, A. C. (2006). The role of Southern Ocean mixing and upwelling in glacial-interglacial atmospheric CO_2 change. *Tellus, Series B: Chemical and Physical Meteorology*, 58(1):73–87. doi:10.1111/j.1600-0889.2005.00167.x.

Watson, A. J., Vallis, G. K., and Nikurashin, M. (2015). Southern Ocean buoyancy forcing of ocean ventilation and glacial atmospheric CO_2. *Nature Geoscience*, 8(11):861–864. doi:10.1038/ngeo2538.

Waugh, D. W. (2014). Changes in the ventilation of the southern oceans. *Philosophical transactions. Series A*, 372(2019):20130269. doi:10.1098/rsta.2013.0269.

Waugh, D. W., Primeau, F., DeVries, T., and Holzer, M. (2013). Recent Changes in the Ventilation of the Southern Oceans. *Science*, 339(6119):568–570. doi:10.1126/science.1225411.

Weaver, A. J., Sarachik, E. S., and Marotze, J. (1991). Freshwater flux forcing of decadal and interdecadal oceanic variability. *Nature*, 353(6347):836–838. doi:10.1038/353836a0.

Wentz, F. J. (1991). User's manual: SSM/I antenna temperature tapes (revision 1), report number 120191. Technical report, Remote Sensing Systems, Santa Rosa, CA, USA.

Wijffels, S. (2001). Freshwater Transport and Climate. In Steele, J. H., editor, *Encyclopedia of Ocean Sciences*, pages 1104–1111. Academic Press, Oxford. doi:10.1006/rwos.2001.0265.

Willebrand, J., Barnier, B., Böning, C., Dieterich, C., Killworth, P. D., Le Provost, C., Jia, Y., Molines, J. M., and New, A. L. (2001). Circulation characteristics in three eddy-permitting models of the North Atlantic. *Progress in Oceanography*, 48(2-3):123–161. doi:10.1016/S0079-6611(01)00003-9.

Williams, G., Maksym, T., Wilkinson, J., Kunz, C., Murphy, C., Kimball, P., and Singh, H. (2015). Thick and deformed Antarctic sea ice mapped with autonomous underwater vehicles. *Nature Geoscience*, 8(1):61–67. doi:10.1038/ngeo2299.

Williams, G. D., Aoki, S., Jacobs, S. S., Rintoul, S. R., Tamura, T., and Bindoff, N. L. (2010). Antarctic Bottom Water from the Adélie and George V Land coast, East Antarctica (140-149°E). *Journal of Geophysical Research*, 115(C4):C04027. doi:10.1029/2009JC005812.

Williams, G. D., Herraiz-Borreguero, L., Roquet, F., Tamura, T., Ohshima, K. I., Fukamachi, Y., Fraser, A. D., Gao, L., Chen, H., McMahon, C. R., Harcourt, R., and Hindell, M. (2016). The suppression of Antarctic bottom water formation by melting ice shelves in Prydz Bay. *Nature Communications*, 7:12577. doi:10.1038/ncomms12577.

Wolff, E. W., Fischer, H., Fundel, F., Ruth, U., Twarloh, B., and Littot, G. C. (2006). Southern Ocean sea-ice extent, productivity and iron flux over the past eight glacial cycles. *Nature*, 449(October):6271. doi:10.1038/nature06271.

Wong, A. P. S., Bindoff, N. L., and Church, J. A. (1999). Large-scale freshening of intermediate waters in the Pacific and Indian oceans. *Nature*, 400(6743):440–443. doi:10.1038/22733.

Worby, A. P., Geiger, C. A., Paget, M. J., van Woert, M. L., Ackley, S. F., and DeLiberty, T. L. (2008). Thickness distribution of Antarctic sea ice. *Journal of Geophysical Research*, 113(C5):C05S92. doi:10.1029/2007JC004254.

Wunsch, C. and Ferrari, R. (2004). Vertical mixing, energy, and the general circulation of the oceans. *Annual Review of Fluid Mechanics*, 36(1):281–314. doi:10.1146/annurev.fluid.36.050802.122121.

Wunsch, C. and Stammer, D. (1998). Satellite altimetry, the marine geoid, and the oceanic general circulation. *Annual Review of Earth and Planetary Sciences*, 26(1):219–253. doi:10.1146/annurev.earth.26.1.219.

Xiao, W., Esper, O., and Gersonde, R. (2016). Last Glacial - Holocene climate variability in the Atlantic sector of the Southern Ocean. *Quaternary Science Reviews*, 135:115–137. doi:10.1016/j.quascirev.2016.01.023.

Yang, S. and Gruber, N. (2016). The anthropogenic perturbation of the marine nitrogen cycle by atmospheric deposition: Nitrogen cycle feedbacks and the [15]N Haber-Bosch effect. *Global Biogeochemical Cycles*, 30:1418–1440. doi:10.1002/2016GB005421.

Yang, S., Gruber, N., Long, M. C., and Vogt, M. (2017). ENSO driven variability of denitrification and suboxia in the Eastern Pacific Ocean. *In preparation*.

Yeo, S.-R. and Kim, K.-Y. (2015). Decadal changes in the Southern Hemisphere sea surface temperature in association with El NiñoSouthern Oscillation and Southern Annular Mode. *Climate Dynamics*, 45(11-12):3227–3242. doi:10.1007/s00382-015-2535-z.

Yi, D., Zwally, H. J., and Robbins, J. W. (2011). ICESat observations of seasonal and inter-annual variations of sea-ice freeboard and estimated thickness in the Weddell Sea, Antarctica (2003-2009), In *Annals of Glaciology*, 52(57), pages 43–51. International Glaciological Society. doi:10.3189/172756411795931480.

Yuan, X. and Martinson, D. G. (2001). The Antarctic dipole and its predictability. *Geophysical Research Letters*, 28(18):3609–3612. doi:10.1029/2001GL012969.

Yuan, X. and Yonekura, E. (2011). Decadal variability in the Southern Hemisphere. *Journal of Geophysical Research*, 116(D19):D19115. doi:10.1029/2011JD015673.

Zachos, J., Pagani, M., Sloan, L., Thomas, E., and Billups, K. (2001). Trends, rhythms, and aberrations in global climate 65 Ma to present. *Science*, 292(5517):686–693. doi:10.1126/science.1059412.

Zeebe, R. E., Ridgwell, A., and Zachos, J. C. (2016). Anthropogenic carbon release rate unprecedented during the past 66 million years. *Nature Geoscience*, 9(4):325–329. doi:10.1038/ngeo2681.

Zeng, N., Mariotti, A., and Wetzel, P. (2005). Terrestrial mechanisms of interannual CO_2 variability. *Global Biogeochemical Cycles*, 19(1):GB1016. doi:10.1029/2004GB002273.

Zhai, X., Greatbatch, R. J., and Zhao, J. (2005). Enhanced vertical propagation of storm-induced near-inertial energy in an eddying ocean channel model. *Geophysical Research Letters*, 32(18):L18602. doi:10.1029/2005GL023643.

Zhang, J. (2007). Increasing Antarctic sea ice under warming atmospheric and oceanic conditions. *Journal of Climate*, 20(11):2515–2529. doi:10.1175/JCLI4136.1.

Zhang, J. (2014). Modeling the impact of wind intensification on Antarctic sea ice volume. *Journal of Climate*, 27(1):202–214. doi:10.1175/JCLI-D-12-00139.1.

Zhang, J., Schmitt, R. W., and Huang, R. X. (1998). Sensitivity of the GFDL Modular Ocean Model to Parameterization of Double-Diffusive Processes. *Journal of Physical Oceanography*, 28(4):589–605. doi:10.1175/1520-0485(1998)028<0589:SOTGMO>2.0.CO;2.

Zhang, Z., Vihma, T., Stössel, A., and Uotila, P. (2015). The role of wind forcing from operational analyses for the model representation of Antarctic coastal sea ice. *Ocean Modelling*, 94:95–111. doi:10.1016/j.ocemod.2015.07.019.

Zika, J. D., England, M. H., Sijp, W. P., Zika, J. D., England, M. H., and Sijp, W. P. (2012). The Ocean Circulation in Thermohaline Coordinates. *Journal of Physical Oceanography*, 42(5):708–724. doi:10.1175/JPO-D-11-0139.1.

Zunz, V., Goosse, H., and Massonnet, F. (2013). How does internal variability influence the ability of CMIP5 models to reproduce the recent trend in Southern Ocean sea ice extent? *The Cryosphere*, 7(2):451–468. doi:10.5194/tc-7-451-2013.

Zwally, H. J., Comiso, J. C., and Gordon, A. L. (1985). Antarctic offshore leads and polynyas and oceanographic effects. In Jacobs, S. S., editor, *Oceanology of the Antarctic Continental Shelf*, pages 203–226. American Geophysical Union, Washington, D. C. doi:10.1029/AR043p0203.

Zweng, M. M., Reagan, J. R., Antonov, J. I., Locarnini, R. A., Mishonov, A. V., Boyer, T. P., Garcia, H. E., Baranova, O. K., Johnson, D. R., Seidov, D., and Biddle, M. M. (2013). World Ocean Atlas 2013, Volume 2: Salinity, p. 39. NOAA Atlas NESDIS 74.

Acknowledgements

us to solve existing issues in the model. I would like to thank Julien Le Sommer, Paul Holland, and Judith Hauck for inviting me to their institutes and for sharing their thoughts and ideas. These visits and discussions have greatly improved my research and helped me to understand my results and resolve issues. I would also like to thank Mike Dinniman for sharing his experience in modeling the Southern Ocean with ROMS. I thank Julienne Stroeve and the National Academies of Science as well as Stefan Kern and the International Space Science Institute for inviting me to two great and inspiring workshops on Antarctic sea ice. I especially thank Stefan for his valuable input regarding uncertainties in observational sea-ice data.

I am thankful to Dirk Notz, Michiel van den Broeke, Jan Lenaerts, Jan van Angelen, Thomas Röckmann, and Anneke Batenburg for providing me with initial skills and ideas that led to the success of this Ph. D. project.

I have had many great scientific discussions throughout this Ph. D. project that helped me to shape my research. I especially would like to thank François Massonnet, Achim Stössel, Daniel Sigman, Jorge Sarmiento, Lynne Talley, Kay Ohshima, Ted Maksym, Clara Deser, Nicole Lovenduski, Marika Holland, David Schneider, Raffaele Bernadello, Ivana Cerovečki, Corinne Le Quéré, Samuel Jaccard, Adam Hasenfratz, Heini Wernli, Lukas Papritz, Nacho Merino, Gildas Mainsant, and Hugues Goosse for discussions, ideas, and asking the right questions.

I am hugely grateful to my family Carmen, Jürgen, Kai, Simon, and Fabian for their loving and caring support, providing me with motivation, and teaching me persistence and curiosity. Thank you for filling my breaks from science with uncountable great times, laughs, and memories.

I am endlessly thankful to Heike for her loving and caring mental and emotional support throughout the years, for giving me confidence, perspective, and for always understanding me and believing in me. Thank you for improving my writing and for cross-reading this thesis. And more importantly, I am grateful to you for being part of this entire journey through my Ph. D. project, for providing me with countless wonderful thoughts, and teaching me how to pursue balance and happiness. Thank you.

Curriculum Vitae

Fabian Alexander Haumann
born in Herdecke, Germany on May 28th, 1984

Education

2012 – 2016	Dr. Sc., Environmental Systems Science, ETH Zürich, Switzerland
2009 – 2011	M. Sc., Physics and Climate Science (Cum Laude), Universiteit Utrecht, The Netherlands
2005 – 2009	B. Sc., Geosciences (Major in Geography), Universität Basel, Switzerland
2000 – 2004	Matura, Kantonsschule Wettingen, Switzerland

Professional experience

Since 2012	Research assistant, Environmental Physics, ETH Zürich, Switzerland
2011 – 2012	Research associate, Sea Ice in the Earth System, Max Planck Institute for Meteorology, Germany
2010 – 2011	Student assistant, Institute for Marine and Atmospheric Research, University of Utrecht, The Netherlands
2008 – 2009	Research associate, Regional Climate Modelling, Max Planck Institute for Meteorology, Germany
2008	Research internship, Potsdam Institute for Climate Impact Research, Germany
2007	Student assistant, Institute of Physical Geography and Environmental Change, University of Basel, Switzerland

Teaching experience

2014 – 2015	M. Sc. thesis adviser of Samuel Eberenz, ETH Zürich, Switzerland
2013 – 2015	Tutor for *Introduction to Physical Oceanography*, ETH Zürich, Switzerland
2013	Tutor for *Term Paper Writing*, ETH Zürich, Switzerland

Other qualifications and training

2015   Workshop on *Presentation Techniques*, ETH Zürich

2013   12th International Swiss Climate Summer School: *From Climate Reconstructions to Climate Predictions*

2012   Workshop on *Advanced Scientific Writing*, IMPRS-ESM

2011   Summer school on the *Role of Sea Ice in Climate System*, ResClim

2010   *Fokuz Marine Master Course*, NIOZ

2009   Summer school on the *Physics of the Climate System*, Utrecht University

2006 – 2009   Certificate studies in Astronomy, Basel Advanced Study Centre

Awards

2014   Poster award at the 15th Swiss Global Change Day

Peer-reviewing

Journal of Climate, Geophysical Research Letters, Journal of Geophysical Research, The Cryosphere

Peer-reviewed publications

Haumann, F. A., N. Gruber, M. Münnich, I. Frenger, and S. Kern (2016): Sea-ice transport driving Southern Ocean salinity and its recent trends. Nature, 537 (7618), 89–92. doi:10.1038/nature19101.

Landschützer, P., N. Gruber, **F. A. Haumann**, C. Rödenbeck, D. C. E. Bakker, S. van Heuven, M. Hoppema, N. Metzl, C. Sweeney, T. Takahashi, B. Tilbrook, and R. Wanninkhof (2015): The reinvigoration of the Southern Ocean carbon sink. Science, 349 (6253), 1221–1224. doi:10.1126/science.aab2620.

Stössel, A., D. Notz, **F. A. Haumann**, H. Haak, J. Jungclaus, and U. Mikolajewicz (2015): Controlling High-Latitude Southern Ocean Convection in Climate Models. Ocean Modelling, 86, 58–75. doi:10.1016/j.ocemod.2014.11.008.

Haumann, F. A., D. Notz, and H. Schmidt (2014): Anthropogenic influence on recent circulation-driven Antarctic sea-ice changes. Geophysical Research Letters, 41 (23), 8429–8437. doi:10.1002/2014GL061659.

Haumann, F. A., A. M. Batenburg, G. Pieterse, C. Gerbig, M. C. Krol, and T. Röckmann (2013): Emission ratio and isotopic signatures of molecular hydrogen emissions from tropical biomass burning. Atmospheric Chemistry and Physics, 13 (18), 9401–9413. doi:10.5194/acp-13-9401-2013.

Notz, D., **F. A. Haumann**, H. Haak, J. Jungclaus, and J. Marotzke (2013): Arctic sea-ice evolution as modeled by Max Planck Institute for Meteorology's Earth system model. Journal of Advances in Modeling Earth Systems, 5 (2), 173–194. doi:10.1002/jame.20016.

Tomassini, L., S. Hagemann, C. Moseley, **A. Haumann**, R. Podzun, and D. Jacob (2011): Extremes and predictability in the European pre-industrial climate of a regional climate model. Climate Dynamics, 36 (11), 2371–2397. doi:10.1007/s00382-010-0814-2.

Thesis

Haumann, F. A. (2011): Dynamical Interaction between Atmosphere and Sea Ice in Antarctica. Master's thesis. Utrecht University. Available online: http://dspace.library.uu.nl/handle/1874/285256.

Other publications

Haumann, F. A., N. Gruber, M. Münnich, I. Frenger, and S. Kern (2016): Antarctic sea-ice freshwater fluxes associated with freezing, transport, and melting. ETH Zurich. doi:10.16904/8.

Gruber, N., D. Clement, T. Frölicher, **A. Haumann**, and P. Landschützer (2015): The Global Ocean Carbon Sink: Recent Trends and Variability. Nova Acta Leopoldina, 121 (408), 85–88.

Conference and workshop presentations

Haumann, F. A., N. Gruber, M. Münnich, S. Eberenz, C. Nissen, and P. Landschützer (2016): Strengthening of the Southern Ocean Carbon Sink through Recent Changes in Freshwater Forcing. 2016 Ocean Sciences Meeting, New Orleans, USA.

Haumann, F. A. (2016): Dependence of Antarctic Sea-Ice Trends on Zonally Asymmetric Atmospheric Circulation Changes and Ocean Stratification. Antarctic Sea Ice Workshop, National Academies of Science, Boulder, USA. (Invited panelist)

Haumann, F. A., N. Gruber, M. Münnich, S. Eberenz, C. Nissen, and P. Landschützer (2015): Cryospheric drivers of changes in Southern Ocean stratification and carbon uptake. 26th General Assembly of the International Union of Geodesy and Geophysics (IUGG), Prague, Czech Republic.

Haumann, F. A., M. Münnich, I. Frenger, and N. Gruber (2014): Freshening of the Southern Ocean through enhanced sea-ice transport. 7th IBP PhD Congress, Switzerland.

Haumann, F. A., M. Münnich, I. Frenger, and N. Gruber (2014): Sea-ice freshwater flux: An important driver of recent Southern Ocean salinity changes. 2014 Ocean Sciences Meeting, Hawaii Convention Center, Honolulu, USA.

Haumann, F. A., M. Münnich, I. Frenger, and N. Gruber (2013): On the role of sea-ice transport for Southern Ocean stratification in the past, present, and future. Davos Atmosphere and Cryosphere Assembly 2013, Davos, Switzerland.

Haumann, F. A., D. Notz, H. Schmidt, and M. R. van den Broeke (2012): Response of Wind-Driven Antarctic Sea Ice Transport to External Anthropogenic Forcings. EGU General Assembly, Vienna, Austria.

Poster presentations

Haumann, F. A., N. Gruber, M. Münnich, and S. Eberenz (2016): Strengthening of the Southern Ocean carbon sink through freshwater forcing. 9th IBP PhD Congress, Switzerland.

Haumann, F. A., D. Notz, and H. Schmidt (2015): Anthropogenic influence on recent Antarctic sea-ice changes: Why do models and observations disagree?. 26th General Assembly of the International Union of Geodesy and Geophysics (IUGG), Prague, Czech Republic.

Haumann, F. A., N. Gruber, M. Münnich, I. Frenger, and S. Eberenz (2015): Influence of sea-ice freshwater fluxes on Southern Ocean salinity, stratification and overturning. Nova Acta Leopoldina, Halle, Germany.

Haumann, F. A., S. Eberenz, M. Münnich, and N. Gruber (2015): Cryospheric influence on recent Southern Ocean stratification changes. 8th IBP PhD Congress, Switzerland.

Haumann, F. A., M. Münnich, I. Frenger, and N. Gruber (2014): Freshening of the Southern Ocean through enhanced sea-ice transport. 15th Swiss Global Change Day, Bern, Switzerland.

Haumann, F. A., D. Notz, and H. Schmidt (2014): Circulation-driven response of Antarctic sea ice to external anthropogenic forcings: Why do models and observations disagree? IGS 2014 Sea-Ice Symposium, C3 Convention Centre, Hobart, Australia.

Haumann, F. A., I. Frenger, M. Münnich, and N. Gruber (2013): Sea ice freshwater fluxes: An underestimated driver of the Southern Ocean water cycle and its recent changes.The Royal Society meeting on New models and observations of the Southern Ocean, its role in global climate and the carbon cycle, Chicheley Hall, Buckinghamshire, United Kingdom.

Haumann, F. A., I. Frenger, M. Münnich, and N. Gruber (2013): Sea ice freshwater fluxes: An underestimated driver of the Southern Ocean water cycle and its recent changes. C2SM Symposium 2013: The Water Cycle in a Changing Climate, ETH Zurich, Switzerland.

Haumann, F. A., M. Münnich, I. Frenger, and N. Gruber (2013): On the role of sea ice for Southern Ocean stratification. EGU General Assembly, Vienna, Austria.

Haumann, F. A., A. M. Batenburg, G. Pieterse, C. Gerbig, and T. Röckmann (2013): Signature of molecular hydrogen emissions from tropical biomass burning. EGU General Assembly, Vienna, Austria.

Haumann, F. A., M. Münnich, I. Frenger, and N. Gruber (2013): On the role of sea ice for Southern Ocean stratification. 6th IBP PhD Congress, Switzerland.